Investigating the Mechanisms of Silver Nanoparticle Toxicity in *Daphnia magna*: A Multi-Omics Approach

By

Alex Gavin

A thesis submitted to

The University of Birmingham

for the degree of

DOCTOR OF PHILOSOPHY

School of Biosciences

College of Life and Environmental Sciences

University of Birmingham

September 2014

Abstract

Silver nanoparticles (AgNPs), one of the most common nanomaterials in use today, have been shown to enter the aquatic environment through use of commercially obtained products. Although toxicity to aquatic organisms has been demonstrated, there is still uncertainty surrounding the molecular mechanism of AgNP-induced toxicity. The work presented in this thesis investigates the hypothesis that AgNP toxicity is induced indirectly through the release of ionic silver (Ag^+) upon dissolution. The mechanism of AgNP toxicity would therefore be identical to that induced by dissolved silver. This hypothesis was tested through the comparison of the molecular-level changes in *Daphnia magna*, a global keystone species of freshwater ecosystems, induced by AgNP and $AgNO_3$ exposure. Through use of Agilent microarray transcriptomics and direct-infusion mass spectrometry metabolomics, the same molecular profile changes were observed in *D. magna* exposed to AgNPs and to the dissolved Ag fraction alone. However, a greater magnitude of effect was observed in AgNP exposures. The measurement of the uptake and depuration of both forms of silver suggested the increased magnitude of molecular response to AgNP exposure fit a Trojan-horse type mechanism. Therefore, AgNPs absorbed by *D. magna*, resulted in higher internal concentration of toxic Ag^+. Further investigation into the mechanism of AgNP toxicity revealed significant changes to constituents of the purine metabolism pathway. Additionally, measurement of the expression of glutathione-S-transferase and heme-oxygenase 1 (traditional markers for oxidative stress) by quantitative RT-PCR showed no significant changes. This suggested that if oxidative stress was a primary mechanism of AgNP toxicity in *D. magna*, the transcriptional response may not be through well-conserved anti-oxidant enzymes. Overall, this research advances the mechanistic understanding of AgNP toxicity to aquatic organisms, and highlights the ability of omics technologies to provide unique insights into mechanisms of toxicity.

Acknowledgements

I've learnt a lot over the past four years:

- I have met a woman with two birthdays and a man with incessant hiccups
- I now know that Cornwall has its own style of tartan
- Despite possibly being the most eaten thing on the entire planet, the resting eggs of *Daphnia* can survive dormant for 700 years. And then hatch. Alive.
- And finally, it is fundamentally impossible to complete a PhD and the resulting thesis without the support of those around you

It is on this final point I wish to focus. A lot of people have helped me throughout the term of my PhD and it is in this section that I would like to acknowledge their help and contributions to this thesis.

Firstly, I would like to thank both Professor Mark Viant and Professor Kevin Chipman for their guidance and support. Thanks are also due to Dr Tim Willams, Dr Leda Mirbahai and Lorna Thorne for their patience and tuition on all things microarray and PCR. Thanks to Dr Andy Southam for his lessons on mass spectrometry, and also to Dr Nadine Taylor and Dr Thomas White for the *Daphnia magna* culturing 101. This work revolves around silver nanoparticles which were manufactured in-house, and without the help of Dr Isabella Romer, Dr Mila Tejamaya, and soon to be Doctors Laura Ellis and Marie-France Belinga-Desaunay-Nault, this thesis would be a lot shorter.

I would like to thank members of the fourth floor, past and present, for their help, advice, tea-breaks, cake-breaks and the proverbial one or two in staff house. So thanks to Tom, Rosie, Kate, Martin, Leda, Chib, Nadine, Louise, Lorna, Will, Ralf, Greg, Jinkang, Ricardo, Andy, Rob, Cronin and Tim; you've all made lab-life a lot more bearable.

I must also thank my parents, Tony and Lyn Gavin, for raising me the way they have and always telling me off for saying “that’ll do” – either something’s done to the best of your ability or it’s not good enough. Finally, this thesis simply would not exist without the unending support of my fantastic and wonderful wife Rebecca Gavin. She kept me motivated, positive and never let me be too hard on myself. And when things got really stressful she put the kettle on.

Table of Contents

List of Figures

Chapter 1

Chapter 3

Chapter 4

Chapter 5

Chapter 6

List of Tables

Chapter 1

Chapter 2

Chapter 3

Chapter 4

Chapter 5

Chapter 6

Chapter 9 (Appendix)

Abbreviations

AgNPs	Silver nanoparticles
BSI	British standards institution
ISO	International organization for standardization
SCHENIR	Scientific committee on emerging and newly identified health risks
EC	European commission
REACH	Registration, evaluation, authorisation and restriction of chemicals
Ag^{+}	Silver ion
ROS	Reactive oxygen species
OECD	The organisation for economic co-operation and development
MoA	Mode of action
RNA	Ribonucleic acid
rRNA	Ribosomal ribonucleic acid
mRNA	Messenger ribonucleic acid
tRNA	Transfer ribonucleic acid
NMR	Nuclear magnetic resonance
MS	Mass spectrometry
m/z	Mass to charge ratio
DIMS	Direct infusion mass spectrometry
GC-MS	Gas chromatography mass spectrometry
LC-MS	Liquid chromatography mass spectrometry
FT-ICR	Fourier transform ion cyclotron resonance
LTQ	Linear trap quadropole
nESI	Nano electrospray ionisation
PCA	Principal Component's analysis
PC	Principal Component
MS/MS	Tandem mass spectrometry
SPS	Single peak search
MI-Pack	Metabolite identification package

TM	Transformation mapping
KEGG	Kyoto encyclopaedia of genes and genomes
FDR	False discovery rate
ORA	Over representation analysis
FCSA	Functional class scoring analysis
PTA	Pathway topology analysis
PAK	Serine/threonine-protein kinase
MAPK	Mitogen-activated protein kinases
PP2A	Protein phosphatase 2A
DLVO	Derjaguin, Landau, Verwey, and Overbeek theory
VDW	Van der Waals
Cit-AgNPs	Citrate stabilised silver nanoparticles
PVP-AgNPs	Polyvinylpyrrolidone stabilised silver nanoparticles
UF	Ultrafiltration
UC	Ultracentrifugation
FlFFF	Flow field flow fractionation
DLS	Dynamic light scattering
TEM	Transmission electron microscopy
AFM	Atomic force microscopy
BBM	Bold's basal medium
SEM	Standard error of the mean
HPLC	High-performance liquid chromatography
QC	Quality control
PCR	Polymerase chain reaction
SIM	Selective ion monitoring
PQN	Probable quotient normalisation
KNN	K nearest neighbour
ANOVA	Analysis of variance
EC_{50}	Median effective concentration

ICP-MS	Inductively coupled plasma mass spectrometry
SIMS	Secondary ion mass spectrometry
DAVID	Database for annotation visualisation and integrated discovery
IMPaLA	Integrated molecular pathway level analyses
RT-qPCR	Reverse transcriptase quantitative polymerase chain reaction
BBID	Biological biochemical image database
EHMN	Edinburgh human metabolic network
cAMP	Cyclic adenosine monophosphate
ADSSL1	Adenylosuccinate synthetase like 1
POLR2G	Polymerase (RNA) II (DNA directed) polypeptide G
NT5C2	5'-nucleotidase, cytosolic II
PAPSS2	3'-phosphoadenosine 5'-phosphosulfate synthase 2
AMP	adenosine monophosphate
dGMP	deoxyguanosine monophosphate
NIBB	National institute for basic biology
SOD	Super oxide dismutase
GSH	Glutathione
GSSG	Glutathione disulfide
GST	Glutathone-S-transferase
HMOX	Heme oxygenase 1
MicroPIXE	Microscopic proton-induced X-ray emission

Chapter 1: General Introduction

1.1 Nanotechnologies and the emergence of Nanotoxicology

Nanotechnology has become of huge interest, both industrially and politically, over the past decade and has amassed billions of dollars in investment (Wardak et al., 2007). This has led to a wide range of available nanomaterials and an equally wide range of applications that make use of their unique size-related properties. For example, the use of TiO_2 nanoparticles as UV filters in sunscreens (Johnson et al., 2011) and as photocatalytic degrading agents in self-cleaning windows (Parkin and Palgrave, 2005), carbon nanotubes as high tensile strength fibres, cerium dioxide nanoparticles as a diesel fuel additive and constituent of catalytic converters (Bekyarova et al., 1998), and an increasing number of products which benefit from the antimicrobial properties of silver nanoparticles (AgNPs) (Chaloupka et al., 2010). This is just a handful of examples of the products known to contain nanomaterials; 1827 products are currently listed on the nanotechnology consumer product inventory (http://www.nanotechproject.org/cpi/) (Vance et al., 2015) and that number is certain to rise.

Despite an increasing body of literature in nanotechnology and nanotoxicology, there is still, as of yet, no single internationally agreed definition of a nanomaterial with individual organisations each providing their own interpretation of a definition. These definitions have gradually expanded and developed over time. Early definitions of nanomaterials were based principally on size parameters alone (Kreyling et al., 2010), for example, the British Standards Institution (BSI) (British Standards Institution, 2007) and the International Organisation for Standardisation (ISO) (ISO, 2010) define nanomaterials simply as materials with one or more external dimensions in the nanoscale (British Standards Institution, 2007). The ISO also includes materials with internal structures or

surface structures within the nanoscale (ISO, 2010). Both of these institutions define the nanoscale as a size range from approximately 1 nm to 100 nm (British Standards Institution 2007; ISO, 2010), a definition which was first held by the Scientific Committee on Emerging and Newly Identified Health Risks (SCENIHR). To put things in perspective, the smallest particles in this scale would be of similar size to a molecule of glucose, whereas the largest molecules would be of similar size to coated vesicles and some virus molecules. In practice however, this range is arbitrary and there is no scientific evidence to date that clearly defines a size cut-off where the characteristic effects of nanomaterials begin to appear (Bleeker et al., 2013; Horbach et al., 2014).

These simplistic definitions of nanomaterials have since been deemed inadequate by some institutions. Recent recommendations given by both SCENIHR (2010) and the EC (2011), include the number size distribution of the material as an additional tool to aid classification. The number size distribution represents the number of particles within a given size range, and is used to account for the poly-disperse nature of nanomaterials. SCENIHR recommends that if greater than 0.15 % of a material contains dimensions within the nanoscale, then it may be classified as a nanomaterial (SCENIHR, 2010). The EU definition published in 2011 (EU, 2011) recommends that this threshold be increased to 50 %. Particle aggregates and agglomerates are often not considered as nanomaterials, however the EU recommended definition recognises that agglomerates and aggregates may exhibit the same properties as disperse particles and therefore includes them if constituent particles are in the nanoscale.

The necessity for a definition arises from the growing recognition that some nanomaterials may be hazardous to human and environmental health (Bleeker et al., 2013). As such a definition will be necessary should legislation be required for their regulation. It has been found that nanomaterials often display physical and chemical properties which can be

substantially different from those of their bulk counterparts. These unique properties are thought to arise from the increased available surface area that a given mass of nanoparticles has when compared to the same mass of bulk-scale particles. Currently, there is no specific legislation surrounding the regulation of nanomaterials. The main concern regarding this lack of regulation is that as well as beneficial effects, the nanoscale could also bestow a "nanostructure-dependant biological activity" (Oberdörster et al., 2005b), which could result in the amplification of any inherent toxic properties that are otherwise unseen in the substance at larger scales. There is also concern surrounding the potential of particles at the lower end of the scale being able to cross biological membranes with relative ease. This property has been shown in multiple particle types (Geiser et al., 2005; Ryman-Rasmussen et al., 2009; Bhabra et al., 2009), and in some cases has been used to our benefit in the areas of nanomedicine and drug delivery (Roy and Vij, 2010; Couvreur, 2013).

Although engineered nanomaterials are relatively new, the idea that a substance can become toxic simply by being at a reduced scale is not; particle toxicology is a well-established discipline, and it is two paradigms of this science, quartz and asbestos, that formed the basis of research into nanomaterial toxicity (Seaton et al., 2010). In their larger crystalline forms, these two substances are inert, however, if inhaled in powder form these two substances become toxic, with asbestos responsible for over 4,000 deaths in the UK in 2011 alone (http://www.hse.gov.uk/statistics/causdis/asbestos.htm). They also serve as a reminder that in the advancement of technology, thorough assessment of potential risks and hazards that any new technology may present should not be forfeit (Seaton et al., 2010). The discipline of nanotoxicology was therefore created to investigate the potential threats that widespread use of nanoparticles may present to humans and the wider

environment (Donaldson et al., 2004) with the aim of better risk assessment and regulation for nanomaterials.

1.2 Silver nanoparticles: The most commercially prominent nanomaterial

AgNPs have become one of the most commercially available varieties of nanomaterial due to their ease of manufacture and potent antimicrobial properties. They are found in a growing list of medical (Chen and Schluesener, 2008; Rai et al., 2009; Chaloupka et al., 2010) and consumer-based (Chaudhry et al., 2008) products with 442 products currently listed as containing AgNPs on the nanotechnology consumer product inventory (http://www.nanotechproject.org/cpi/) (Vance et al., 2015). Products containing silver salts (such as silver nitrate) have been recognised for their medicinal properties since ancient times and until the widespread use of antibiotics in the 1940s, were the antiseptic treatment of choice for burns and open wounds. AgNPs are a much more recent addition though arguably have been used as antimicrobial agents in the form of colloidal silver for over 100 years (Nowack et al., 2011). In the past decade the use of AgNPs has increased dramatically, partially in response to increasing numbers of antibiotic-resistant strains of bacteria (Rai et al., 2012). As well as being potent bactericides (reviewed in Rai et al., 2012 and Mijnendonckx et al., 2013), they have shown anti-fungal (Chladek et al., 2011) as well as anti-viral properties (Rogers et al., 2008; De Gusseme et al., 2011). As a direct consequence of their growing use there is an increased likelihood of AgNPs entering the aquatic environment. Prior to the development and use of AgNPs, the primary source of Ag contamination was from the photographic industry, as well as from mining and leaching from natural sources (Purcell and Peters, 1998). The environmental concentrations of Ag in natural waters have been measured in the ng/L range (Luoma, 2008; Gottschalk et al., 2013). The points of AgNP environmental contamination are most likely during synthesis, during the incorporation of AgNPs into products and through the

use and disposal of these products (Fabrega et al., 2011). Experimental evidence has identified their release from the washing of commercially available sock fabrics into waste water (Benn and Westerhoff, 2008; Geranio et al., 2009), as well as from outdoor facades coated in nano-silver paints in rainwater runoff (Kaegi et al., 2010). Despite evidence of their release, there is a lack of experimental data on the exact environmental concentrations due to a lack of analytical methods available for quantification of trace concentrations of nanoparticles (Mueller and Nowack, 2008). This has subsequently led to a number of modelling studies in an attempt to predict environmental conditions from limited measurements or effluent data (reviewed in Gottshalk et al., 2013).

These studies suggest that freshwater ecosystems are likely to act as terminal sinks for AgNP products, which raises concerns for the potential effects that these products may have on organisms within these ecosystems. Although the toxicity of AgNPs to aquatic organisms is not fully understood, dissolved Ag is a well-known, highly potent aquatic toxicant. If we use this prior knowledge as a baseline for our assessment of AgNPs, then obtaining a detailed understanding of the exact risks posed by AgNPs to the environment should become a priority.

1.2.1 The toxicity of dissolved silver

The toxicity of a substance is ultimately determined by the level of exposure an organism has to that particular toxicant and the amount that is available for internalisation over time. The availability of metals in the aqueous environment is primarily dependant on their speciation – the distribution of a metal between its ionic or ligand-bound forms (Luoma, 2008). As a rule of thumb, it is usually the free metal ion which is the most toxic form, with reductions in toxicity observed for ion-complexes with dissolved organic matter and inorganic cations. For example, the free ion form of silver (Ag^{+}) is easily adsorbed into an organism's cells through ion transport proteins which normally transport the essential ions

sodium (Na^{+}) and copper (transported as Cu^{1+}) (Bury and Wood, 1999; Fabrega et al., 2011).

It is the relative ease with which Ag^{+} are internalised into the cells of organisms which results in their high toxicity. If the uptake of these ions is prevented, then their bioavailability and hence their toxicity is reduced. The free Ag^{+} ion can form strong complexes with organic and inorganic ligands such as the chloride anion (Cl^{-}) and sulfhydryl groups (-SH), which can either be free in solution or incorporated within dissolved organic materials (Adams and Kramer, 1998; Luoma, 2008). In environments where these ligands are present in greater concentrations than Ag^{+}, it is possible for all silver to complex with these materials and precipitate out of solution, rendering them non-toxic and unavailable for uptake by organisms (Leblanc et al., 1984; Erikson et al., 1997; Bianchini and Wood, 2008). In these instances silver cannot enter cells through ion-transport proteins leaving them less available for adsorption than the free ionic form. However it is still possible for these forms of silver to enter an organism's cells by alternative pathways such as endocytosis. As a consequence of this decreased bioavailability, complexed silver ions are less toxic than their free counterparts (Bianchini and Wood, 2008).

Following internalisation, Ag^{+} ions are free to induce toxicity through interaction with cellular components (Figure 1.1) such as -SH groups of cysteine residues (Liau et al., 1997; Jung et al., 2008). These residues are often important in maintaining conformation of cytosolic or membrane-associated proteins; interaction of silver with these groups leads to the production of strong S-Ag bonds which prevent disulphide bond formation. This ultimately results in the disruption of protein structure and loss of function (Ratte, 1999; Luoma, 2008).

This protein-function disruption through interaction with sulfhydryl groups has long been associated with the primary antibacterial mechanism of Ag^+ (Yudkin, 1937; Chambers et al., 1962; Russell and Hugo, 1994), namely the interruption of the bacterial respiratory chain by proton-pump inhibition which has been observed in *Escherichia coli* and *Staphylococcus aureus* (Bragg et al., 1974; Jung et al., 2008; Mijnendonckx et al., 2013). This impairment has been shown to induce the generation of the superoxide radical (O_2^-) in both organisms (Park et al., 2009) leading to cell death. A similar mechanism has been observed in rat liver mitochondria; Ag has been shown to induce the permeability of the inner mitochondrial membrane through disruption and opening of the permeability transition pore (Almofti et al., 2003). This was shown to result in a loss of proton potential (the driving force of oxidative phosphorylation) and the release of cytochrome c; an apoptosis-inducing factor (Almofti et al., 2003). The authors summarised that Ag induced the opening of this pore through interaction with sulfhydryl groups within its structure (Almofti et al., 2003).

The primary mechanism of acute, aquatic Ag^+ toxicity is well established in rainbow trout (*Oncorhynchus mykiss*) (for reviews see (Hogstrand and Wood, 1998; Wood, 1999); near-total reduction of the active transport of Na^+ and Cl^- at the gill. This reduction was shown to occur primarily through the inhibition of Na^+/K^+-ATPase activity in the basolateral membrane of the gill epithelium following absorption into the cell (Morgan et al., 1997). This occurs through a direct interaction of Ag with cytoplasmic side of this enzyme, specifically a competitive inhibition of the Mg^{2+} binding site, preventing the binding and hydrolysis of ATP (Ferguson et al., 1996). This inhibition reduces the transport capacity of this enzyme, leading to a net loss of Na^+ and Cl^- from blood plasma. This results in an osmotic imbalance between the plasma and surrounding tissues, causing a net shift of water from the blood to the intracellular compartment. Death is finally thought to occur

from circulatory failure induced by low blood volume and high blood viscosity (Hogstrand and Wood, 1998; Wood, 1999; Bianchini and Wood, 2003). This is also thought to be the primary mechanism of Ag toxicity in *D. magna*; exposure to Ag in the form of $AgNO_3$ induced a reduction of whole-body Na concentration as well as a rapid inhibition of Na^+/K^+-ATPase activity (Bianchini and Wood, 2003).

Ag is also known to induce the formation of reactive oxygen species (ROS). This has been observed in *E. coli*, *S. aureus* (Park et al., 2009), and human skin fibroblasts (Cortese-Krott et al., 2009) in response to $AgNO_3$ exposure. Ag is thought to induce ROS formation by two mechanisms; either through the disruption of the respiratory chain via interaction with thiol groups of mitochondrial proteins (Mijnendonckx et al., 2013), or through the catalysis of the production of superoxide radicals, hydroxyl radicals and hydrogen peroxide from O_2. If the production of ROS becomes excessive, cellular anti-oxidant systems can become overwhelmed resulting in a state of oxidative stress (Finkel and Holbrook, 2000). Common consequences of oxidative stress include damage to DNA, the oxidation of polyunsaturated fatty acids in lipids (lipid peroxidation) and oxidation of amino acids in cellular proteins. This can result in genotoxicity and mutations, as well as membrane and enzyme dysfunction potentially leading to cytotoxicity and cell death. Ag^+ has also been observed to complex directly with DNA and RNA molecules, specifically at the N7 site of the purine bases guanine and adenine (Arakawa et al., 2001) which has been shown to interrupt DNA replication leading to mutagenesis and genotoxicity.

The reason that metallic silver is essentially non-toxic to humans and other mammalian species is removal of Ag occurs much more proficiently than in aquatic organisms (Fabrega et al., 2011). Protection against, and sequestration of, Ag occurs either through precipitation with chloride, sulfide or phosphate ions within the cytoplasm, or through binding with antioxidants (such as cysteine and glutathione), or with sulfhydryl-rich metal-

specific binding proteins like the metallothionein family of proteins (Ferguson et al., 1996). Precipitated forms of silver (chloride, sulfide and phosphate complexes) are deposited outside cells in connective tissue, whereas silver sequestered by antioxidants and proteins aggregate together and are encased by lysosomes. These methods of Ag sequestration have been hinted to occur in aquatic organisms, but do not do so with the efficiency of some other organisms. A summary of the cellular mechanisms of toxicity of dissolved Ag and also AgNPs, is depicted in Figure 1.1.

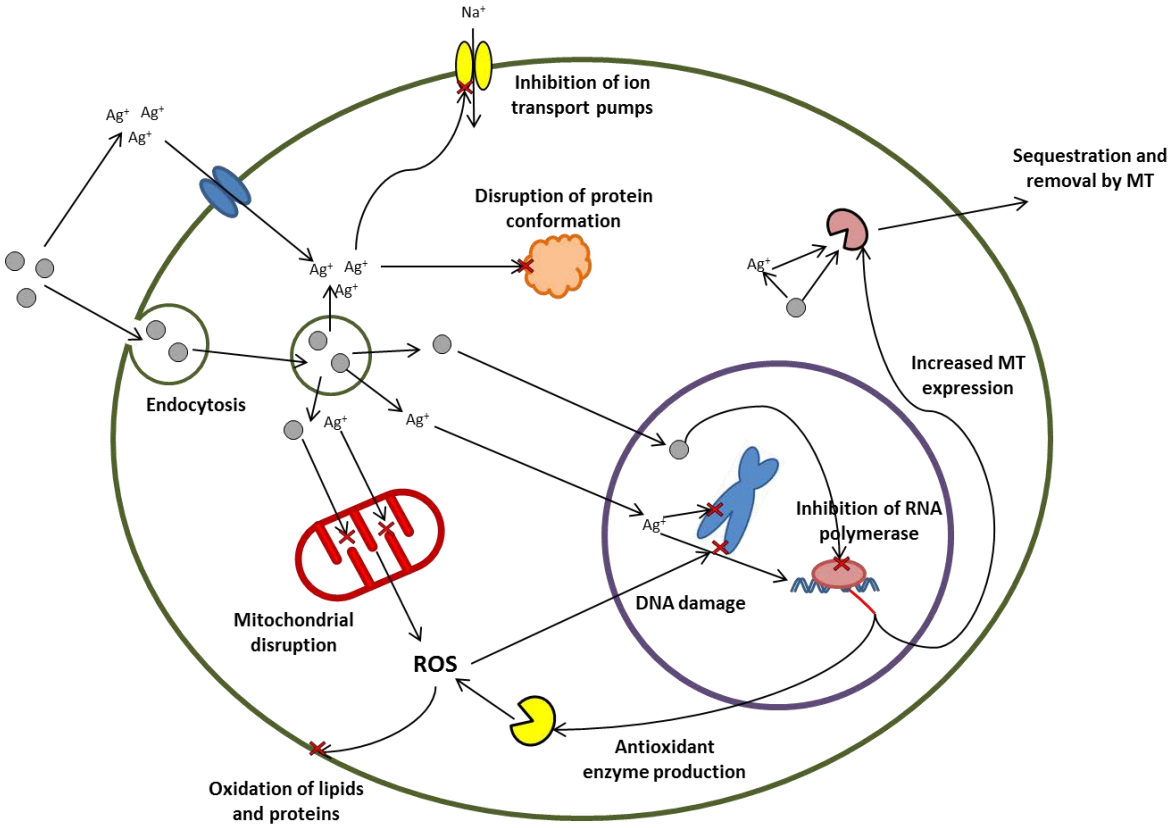

Figure 1.1: Summary of some of the major molecular interactions of Ag^+ and AgNPs reported in the literature. AgNPs have been shown to enter eukaryotic cells via endocytosis whereas Ag^+ enter through ion transport channels. AgNPs are then thought to enact toxicity primarily through the release of Ag^+ within the cell, but they have been shown to directly affect transcription through RNA polymerase inhibition. Once within the cell, silver ions interact with –SH groups on cellular proteins, such as ion-transport pumps, which can lead to disruption of conformation and loss of function. Ag^+ can induce DNA damage and ROS production through direct interaction with genomic DNA and mitochondria respectively. Unchecked production of ROS can lead to oxidative stress, resulting in DNA damage and the oxidation of cellular lipids and proteins. The presence of Ag and AgNP is primarily combated through the increased production of antioxidant enzymes and metallothionein. Metallothionein sequesters Ag^+ and removes it from the cell.

1.2.2 The molecular toxicity of silver nanoparticles

The efficiency with which a metal can exert toxicity depends on its bioavailability; how readily it can be internalised within the cells of an organism. Metal bioavailability is itself dependent upon speciation, with the free ion form of a metal typically being the most toxic due to their mimicry of major essential ions such as Na^+ and subsequent uptake via ion-transport pumps (Bury and Wood, 1999). These methods of uptake are rapid, and are unavailable to the larger, nanoparticle forms of metals thus reducing the rate at which they are internalised by cells and organisms. Metallic nanoparticles are therefore less bioavailable than their free ion counterparts, an observation which is reflected in the reported LC_{50} and EC_{50} data. A recent review has compared terrestrial and aquatic ecotoxicity data for three metal and metal oxide nanoparticles; silver, zinc oxide and copper oxide (Notter et al., 2014). Through calculation of a ratio comparing nanomaterial and metal LC_{50}, LD_{50} and EC_{50} data, it was determined that in almost all cases the nanoparticle forms of these compounds were less toxic than their ionic counterparts (Notter et al., 2014). Although the authors themselves did not provide an explanation for this observation, it is possible that this is the result of reduced availability for the nanoparticle form of the metal in question.

It is unlikely that metallic nanoparticles cross cellular membranes via the same mechanism as metal ions, however a large variety of nanomaterials have been shown to be taken into cells by endocytosis (Zhao et al., 2011). Using selective inhibitors of the different endocytotic pathways, it was determined that AgNPs are adsorbed primarily by both clathrin-mediated endocytosis and macropinocytosis in human lung fibroblasts and glioblastoma cells (Asharani et al., 2009), as well as in human mesenchymal stem cells (Greulich et al., 2011). Endocytosis was also confirmed as the primary mechanism of AgNP transport in the ragworm, *Nereis diversicolor,* using Transmission Electron

Microscopy (TEM) and Energy Dispersive X-ray analysis, but the exact form of endocytosis was not detailed in this study (García-Alonso et al., 2011). AgNPs have been identified as being localised to the lysosomes of mouse macrophage cells using confocal laser microscopy following a 24 h exposure to 10 μg/ml of AgNPs with a 20 nm core diameter (Arai et al., 2015). This observation has also been made using fluorescence microscopy in human mesenchymal stem cells; AgNPs were found to co-localise to endo-lysosomes after a 24 h exposure to AgNPs (Greulich et al., 2011). Lysosomes are an endpoint of endocytosis; they are specifically designed for the degradation of foreign material. The detection of AgNPs within these structures was considered by the authors of both papers to be evidence of uptake via endocytosis. Nanoparticles of other forms have been reported to escape these structures should the internal concentration of particles become high enough (Nam et al., 2009). A summary of the cellular interactions of AgNP is depicted in Figure 1.1.

Investigations into the molecular mechanisms of AgNP toxicity are mostly inconclusive but one thing which is frequently investigated is the potential indirect induction of toxicity through the release of the free silver ion, Ag^+.

1.2.3 The potential role of dissolved Ag^+ in AgNP toxicity

Several studies have suggested that toxicity induced by AgNPs can be fully accounted for by the Ag^+ fraction of AgNP dispersions (Kennedy et al., 2010; Zhao and Wang, 2011; Newton et al., 2013). Kennedy et al. (2010) assessed the acute toxicity of AgNPs to *P. subcapitata D. magna*, and *P. promelas*. They discovered that when expressed in terms of "fractionated nanosilver" (their terminology for the free silver ion) and/or <4nm particles), the LC_{50} values of AgNPs were comparable to those of $AgNO_3$ within 95% confidence intervals (Kennedy et al., 2010). A separate study by Newton et al. in 2013 characterised the dose-response relationship of $AgNO_3$ and AgNPs with three different

capping agents to *D. magna*. When the dissolved Ag content was measured at the 48 h LC_{50} values for each of these, they were found to be similar for all nanoparticles and $AgNO_3$. This led the authors to conclude that toxicity of AgNPs was a function of dissolved silver released by AgNP dissolution.

Chelating agents have been used frequently alongside AgNP exposures in order to sequester dissolved Ag ions and test their role in toxicity (Zhao and Wang, 2011; Kim et al., 2011; Zhao and Wang, 2013; Groh et al., 2014). The toxicity of $AgNO_3$ and carbonate-coated AgNPs to zebrafish embryos was shown to be prevented by the addition of cysteine (Groh et al., 2014). Addition of cysteine was also seen to protect against PVP-coated AgNP and $AgNO_3$ toxicity to *D. magna* (Zhao and Wang, 2011) as well as the disruptive effects of both $AgNO_3$ and AgNPs to Na and Ca regulation in *D. magna* (Zhao and Wang, 2013). In each of these studies the authors surmised that the reduction or removal of toxicity was the direct result of the successful sequestration of dissolved Ag from all exposures. They followed by concluding that all toxicity observed in these exposures could be fully accounted for by the dissolved Ag fraction, and that AgNP would have no independent toxicity.

One shortfall of the work referenced above is that the comparison of the ultimate outcome of toxicant exposure, namely mortality, gives no information as to the underlying molecular perturbations which are induced following exposure to AgNPs and $AgNO_3$. Comparison of these profiles will allow a more detailed assessment of which form is responsible for toxicity, or if unique mechanisms are induced by either species of Ag. There has been an increase in the number of robust investigations into the molecular mechanism of AgNP toxicity in recent years, utilising large combinations of traditional biochemical techniques (Yang et al., 2012; Stensberg et al., 2013; Wang et al., 2013; Ahn et al., 2014; De Matteis et al., 2015) or high-throughput omics technologies (Scown et al.,

2010; Poynton et al., 2012; Aerle et al., 2013; Rainville et al., 2014; Li et al., 2015a, 2015b) to address the role of Ag^+ in AgNP toxicity. A number of these studies have shown agreement between the molecular responses induced by nanoparticle and ionic Ag (Scown et al., 2010; Poynton et al., 2012; Aerle et al., 2013; Rainville et al., 2014; Li et al., 2015a, 2015b). A comparison of the transcriptional changes observed in zebrafish embryos (*Danio rerio*) following exposure to 5 µg/L of 10 nm commercial AgNPs, 5 µg/L of Bulk Ag (600 -1600 nm) and 0.25 µg/L of $AgNO_3$ showed significant over-representation of mitochondrial disruption pathways across all treatments (Aerle et al., 2013). This was primarily caused by down-regulation of genes encoding complexes I, II, III and IV of the oxidative phosphorylation machinery (Aerle et al., 2013). This study aligns with other work demonstrating the disruption of mitochondrial membrane potential by AgNPs (Stensberg et al., 2013) and also with a previous study demonstrating mitochondrial disruption by $AgNO_3$ (Almofti et al., 2003). A ^1H NMR-based metabolomics investigation in *D. magna* saw similar profiles induced in response to AgNP and $AgNO_3$ (Li et al., 2015a). This investigation also saw disturbances in energy metabolism and oxidative stress. Western blot analysis and immunofluorescence showed a significant increase in expression of the metallothionein family of proteins in human lung carcinoma and human cervix carcinoma cells exposed to 20 nM AgNPs over 48 h (De Matteis et al., 2015). The metallothionein family of proteins, as metal-specific, thiol-rich proteins appear to be a primary response to Ag exposure in many organisms (Ferguson et al., 1996; Chae et al., 2009; Meyer et al., 2010; García-Alonso et al., 2011; Johari et al., 2015). This further supports the notion that both nanoparticle and dissolved forms of silver induce a similar response.

Other studies have proposed that AgNPs may have a particle-specific mechanism, which may either be the sole cause of toxicity, or may act alongside effects initiated by Ag^+

release. In 2013, Stensberg and colleagues measured the impact of AgNP and Ag^+ exposure to *D. magna* on Na^+ transport and mitochondrial activity – processes known to be affected by Ag^+ (Stensberg et al., 2013). They discovered that AgNPs were not as effective at disrupting Na^+ transportation as their ionic counterparts, but induced greater H^+ efflux from mitochondria. This led the authors to conclude that AgNP and Ag^+ have different mechanisms of toxicity, though they may act in a synergistic mechanism to produce a greater overall response (Stensberg et al., 2013). The inhibition of RNA polymerase has been previously observed as an adverse effect induced specifically by the nanoparticle form of Ag (Wang et al., 2013). Wang and colleagues demonstrated that exposure of erythroid progenitor cells to 8 µg/l AgNP resulted in >50 % inhibition of RNA synthesis (Wang et al., 2013). The study also used a pull down assay to demonstrate the association of AgNPs with Sp6 RNA polymerase.

A transcriptomics investigation by Poynton et al. showed the induction of different gene expression profiles by AgNP and Ag^+ (Poynton et al., 2012). They showed that Ag^+ resulted in a down-regulation of developmental processes, whereas AgNPs increased expression of metallothionein and genes involved in the repair of DNA (Poynton et al., 2012). A proteomic study by Rainville et al. revealed that both forms of silver induced an increase of protein-thiol content, but only AgNPs caused an increase of protein carbonyls (Rainville et al., 2014). The authors suggest that the increase in protein-thiol content is in response to the presence of Ag^+ ions within the organisms; to directly chelate the ions and decrease their toxicity, or to reduce toxicity by ROS. The increased carbonyl content induced by AgNPs is thought to be an indication of AgNP-induced oxidative stress. The authors surmise that signs of different MoAs were discovered suggesting AgNP can induce toxicity independently of Ag^+ (Rainville et al., 2014).

From the data discussed above, it seems highly likely that Ag^+ play a role in AgNP toxicity, but there is great uncertainty on whether they are solely responsible. Importantly, studies taking a mechanistic approach report discrepancies in the mechanisms induced by the two compounds, which may suggest independent but synergistic MoAs (Poynton et al., 2012; Stensberg et al., 2013; Rainville et al., 2014). One of the more popular hypotheses to arise in recent years is the 'Trojan horse' hypothesis. It addresses the conflicting evidence, some of which is discussed above, stating that AgNPs act as a vehicle for Ag^+ toxicity. The hypothesis states that AgNPs are taken into an organism, tissue, or cell, resulting in a concentrated, internalised dissolution of AgNPs resulting in toxicity induced by the released free Ag^+ ion (Moore, 2006; Luoma, 2008; Lubick, 2008). This MoA has been suggested to occur in a mouse macrophage cell line (Park et al., 2010) and has also been implied within the digestive tract of *D. magna* (Zhao and Wang, 2010). The gradual dissolution of internalised AgNPs has been observed previously using a fluorescent chemosensor specific for the observation of Ag^+ in living cells (RC-1) by confocal microscopy (De Matteis et al., 2015). Following a 3 h exposure to 0.6 nM of 20 nm AgNPs, human lung carcinoma cells were observed for 96 h. A significant increase in fluorescence was observed after 24 h and again 48 h and 96 h after the initial exposure distributed across the cytoplasm, organelles and nuclei. The authors concluded that this internal release of Ag^+ was a direct result of adsorption of AgNP by the endocytosis pathway leading to an accumulation of AgNP in the lysosomes. The acidic environment of these structures was thought to then accelerate the dissolution of the particles, resulting in toxicity via Ag^+ (De Matteis et al., 2015) which is consistent with the Trojan-horse hypothesis. However it is not evident, from this study, which species of silver is responsible for toxicity following AgNP absorption, only that dissolution of can occur

following internalisation. To better compare the exact role each form of silver plays in AgNP toxicity, a more detailed comparison of the global molecular response is required.

1.3 Omics-technologies and their application to silver nanotoxicology

The majority of investigations into the molecular mechanism of AgNP toxicity have primarily centred on the traditional biochemical targets of dissolved Ag toxicity (reviewed in section 1.2.3). This has potentially led to a narrow perspective on the molecular perturbations induced by AgNPs, leaving potential novel changes undiscovered. In order to give greater insight into the entire molecular mechanisms of toxicity an increasing number of studies, including those investigation AgNP toxicity, are utilising high-throughput omics technologies. Omics technologies enable us to employ a non-targeted or hypothesis-forming approach as a platform from which to direct further investigations. The global molecular perturbations induced by toxicant-exposure can be assessed at the level of: gene expression (transcriptomics), protein synthesis and modification (proteomics), and the entire profile of small molecular metabolites (metabolomics) (Figure 1.2). The use of transcriptomics techniques in tandem with metabolomics for example, will allow for the mapping of the initial transcriptional changes onto the phenotypic response of the organism. Through use of these techniques it is possible to observe the molecular responses that occur as a result of exposure to a particular toxicant, such as AgNPs (Figure 1.2), and from this one can infer the MoA (Fiehn, 2002; Taylor et al., 2010; Piña and Barata, 2011).

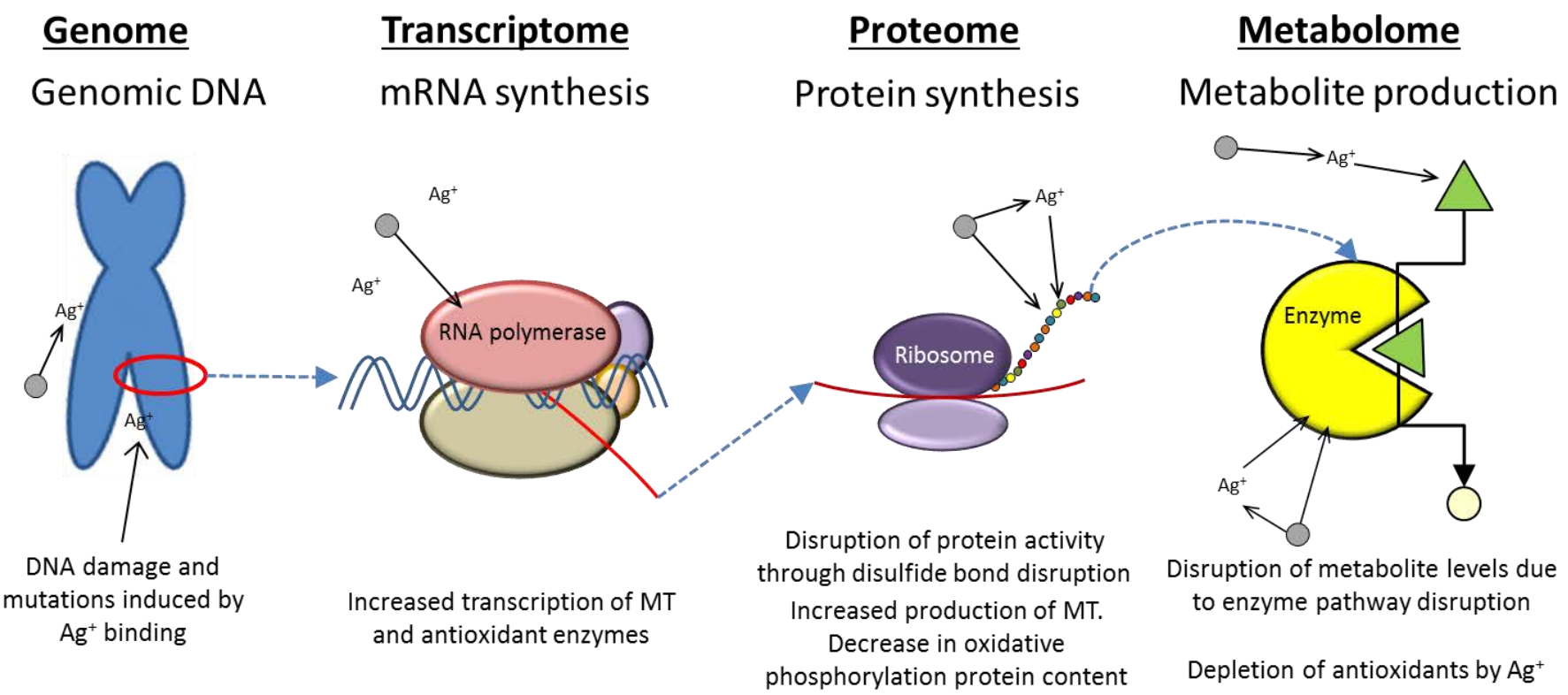

Figure 1.2: Representation of the different molecular processes measured by 'omics technologies and the potential interactions of Ag at each level. Shown are the connections between the chromosomal DNA sequences (genomics), followed by the entire profile of mRNA transcripts (transcriptomics), the proteins and modified proteins produced by those transcripts (proteomics), to the metabolites that those proteins act upon (metabolomics).

1.3.1 Analytical platforms for Transcriptomics

Transcriptomics represents one of the most developed and utilised high-throughput 'omics approaches, which aims to measure the entire gene transcription profile of an organism or tissue i.e. the entire complement of ribonucleic acid (RNA) molecules . There are three major forms of RNA: ribosomal RNA (rRNA), which forms the bulk of the translational machinery; messenger RNA (mRNA) which is a transcription of the protein-coding regions of a particular gene, and transfer RNA (tRNA) which provides the physical link between mRNA and the encoded amino acid sequence during translation. The aim of transcriptomics is to gain an insight into all genes being expressed at any given time, and it is the mRNA fraction which contains this information. The expression of certain genes changes during toxicity, either as a direct or indirect result of exposure (Nuwaysir et al., 1999). By measuring these changes in comparison with untreated conditions we can begin to infer which molecular pathways or processes are involved in the toxicant response.

The most commonly utilised transcriptomics technology when applied to toxicology is the gene expression microarray (Nuwaysir et al., 1999; Schirmer et al., 2010; Piña and Barata, 2011) which allows for rapid analysis of genome-wide expression profiles. Various microarray technologies have been developed but currently oligonucleotide microarrays are most commonly used. These microarrays consist of short single-stranded 60-mer DNA oligonucleotide probes, synthesised *in situ* on glass arrays, corresponding to transcribed regions and hence RNA transcripts, of known genes. The total RNA content of control and treated samples is extracted then simultaneously amplified and labelled with a fluorescent dye by reverse transcription (Piña and Barata, 2011). Samples are then hybridised to individual arrays, and the fluorescence measured from each probe corresponds to relative concentration, and hence expression, of that particular mRNA molecule (Nguyen et al., 2002). The major disadvantage to DNA microarrays is that they require some prior

knowledge of the test organism's genome or transcriptome, as this information is necessary to synthesise the DNA probes.

1.3.2 Analytical platforms for metabolomics

Metabolomics is the measurement of the entire profile of low molecular weight products within a cell-line, tissue or whole organism (Viant, 2008). An organism's metabolic profile is the direct result of gene expression and cellular metabolism (Figure 1.2) and as such can be considered the phenotype of alterations in gene-expression (Fiehn, 2002). Metabolomics has been readily applied to ecotoxicology studies through comparison of the metabolic profiles of treated and untreated samples. To detect and identify as many components of an organism's metabolome as possible, the discipline requires highly sensitive and highly selective analytical techniques (Lenz and Wilson, 2006). Two technologies come close to meeting this paradigm; Nuclear Magnetic Resonance (NMR) and Mass Spectrometry (MS).

NMR has been used in metabolomics-based toxicology and ecotoxicology studies for years and is still used extensively for this purpose. NMR is rapid, highly-reproducible between procedures and laboratories (Viant et al., 2009), and does not alter the original sample i.e. it is non-destructive (Lenz and Wilson, 2007). As a major limitation however, NMR is not as sensitive as MS and as such struggles to detect the naturally low-concentration metabolites that make up a majority of the metabolome. For this reason NMR was not appropriate for this thesis.

Unlike NMR, MS is a destructive technique that depends upon the ionisation of metabolites in order to separate and detect them based on their molecular mass/charge (*m/z*) ratios. The end result of MS analysis is a spectrum of *m/z* values plotted against their respective relative intensities which correspond to metabolite abundance. MS techniques

are often as rapid as NMR but have much greater sensitivity, enabling the detection of the large number of low-concentration metabolites that exist in biological mixtures (Lenz and Wilson, 2007). This enhanced sensitivity has resulted in an increased use of MS techniques in environmental metabolomics due to a need for greater exploration of organism metabolomes (Viant and Sommer, 2012).

MS analysis usually occurs either through an initial separation of metabolites by chromatography or electrophoresis techniques (hyphenated MS), or through the direct-infusion of mixtures with the ionisation source (Direct Infusion MS (DIMS)) (Robertson et al., 2007). Prior separation using Gas-Chromatography (GC-MS), Liquid-Chromatography (LC-MS) or capillary electrophoresis is often employed to enable better separation of peaks thus enhancing identification and quantification of metabolites (Allwood and Goodacre, 2010). However the price for this enhanced level of identification is longer preparation and analysis time which reduces the efficiency of this technique as a high-throughput technology.

DIMS allows rapid sample throughput, with each analysis potentially acquired within minutes. However, without the addition of one of the techniques above the separation of peaks is based on *m/z* values only. To address this problem mass spectrometers with high mass resolution and high mass accuracy are required to accurately differentiate peaks with similar *m/z* values (Dettmer et al., 2007). Of the various forms of MS technique, Fourier Transform Ion Cyclotron Resonance (FT-ICR) and Orbitrap MS are the most favoured for DIMS (Junot et al., 2010). In this thesis, data is acquired using a FT-ICR MS, hybridised with a Linear Trap Quadropole (LTQ) ion trap MS (LTQ-FT Ultra). Metabolites within samples are first ionised using a nano-Electrospray Ionisation (nESI) source. This utilises electrical energy to ionise samples as either positively or negatively charged droplets which are transferred into the LTQ-MS (Bruins, 1998). The LTQ is used as an ion-trap;

this allows collection of a specific number of ions of a particular m/z range prior to injection into the ICR cell. Contrary to conventional mass spectrometers, the ICR is not dependent upon the collision of ions with a detector plate. Instead, ions are trapped within a strong magnetic field and excited by electrodes to rotate at a frequency which is dependent upon their *m/z*. This rotation of ions allows them to be detected as they pass the surrounding detector plates.

1.3.3 Statistical analysis of 'omics datasets

Transcriptomics and metabolomics data are intrinsically multivariate and as such multivariate statistical methods are commonly used. Principal Components Analysis (PCA) allows perception of inherent similarities between transcriptional or metabolic profiles of samples based upon the relative proportions of the constituent genes or metabolites. PCA does not use sample class information in the construction of models, but rather attempts to describe the dataset based on the overall variation in the data (Wise et al., 2006). Patterns of variation are described as principal components (PCs). Each subsequent PC in a PCA model describes a decreasing amount of variance within the data; that is PC1 accounts for the greatest patterns variance, followed by PC2 then PC3 and so on (Robertson, 2005). Each sample is assigned a score value based upon how it reflects the variation described by a PC. Score plots (typically PC1 against PC2) are used to visually determine if there are any natural similarities in the profiles of samples through clustering of scores values (Robertson et al., 2007). These clusters allow for rapid identification of similar and dissimilar samples, indicating a common effect or mechanism (Keun, 2006).

1.3.4 Annotation of genes and metabolites and methods of pathway analysis

Assigning functional or chemical identities to genes and compounds is referred to as annotation. For transcriptomics data, online databases allow the comparison of transcript

sequences with those of other documented genes (Piña and Barata, 2011). Examples of such databases include the Gene Ontology consortium (http://geneontology.org/) and the National Centre for Biotechnology Information (http://blast.st-va.ncbi.nlm.nih.gov/Blast.cgi). This allows the user to identify genes with the greatest sequence homology/similarity to their target genes across multiple species in an effort to assign an appropriate annotation (such as gene- function).

For metabolomics techniques, the process of metabolite identification is still a major limiting factor. Metabolite identification is possible through tandem mass spectrometry (MS/MS) which fragments metabolites allowing the elucidation of structures. However, this approach is time-consuming, and is unfeasible for the thousands of peaks that can be detected by FT-ICR MS. Theoretically, through the accurate mass values obtained by the FT-ICR, putative identification of metabolites is possible following a database search for each peak in turn (Kind and Fiehn, 2006). This process is known as a Single Peak Search (SPS). The Metabolite Identification Package (MI-Pack) is a software package which enables the automated putative annotation of *m/z* peaks by SPS and by the Transformation Mapping (TM) algorithm. TM utilises prior information of the metabolic interactions mapped in the Kyoto Encyclopaedia of Genes and Genomes (KEGG) to improve putative annotation of *m/z* peaks. The TM algorithm has been shown to reduce the false positive rate (FPR) of metabolite annotation from 68% (by SPS) to 15.9 % while maintaining a minimal false negative rate of 5.6% (Weber and Viant, 2010). However the number of known metabolites is comparatively small to the numbers of peaks possible to detect in an FT-ICR spectrum. Additionally, many metabolites are present at concentrations or for periods of time which make them very difficult to detect.

Pathway analysis allows us to make sense of large lists of putative genes or metabolites by putting them into context of known molecular interactions. As our understanding of

molecular pathways grow, the available methods for pathway analysis have also grown to incorporate more and more variables (Khatri et al., 2012). There are three major categories of pathway analysis; Over-Representation Analysis (ORA), Function Class Scoring Analysis (FCSA) and Pathway Topology Analysis (PTA) (Khatri et al., 2012). The general principles surrounding each category are outlined below.

ORA is a qualitative form of pathway analysis that determines the fraction of detected genes or metabolites within a pathway that change in expression or concentration (Khatri et al., 2012). An input list is formed consisting of genes or metabolites deemed to be of interest, normally by statistical significance tests or through use of an arbitrary fold-change threshold. The number of these compounds within each tested pathway-definition is then counted, and the same process is repeated for an appropriate background list. Traditionally for microarray analyses this background consists of all detected genes on the microarray, regardless of expression or significance. When applied to metabolomics, determining this background list has proven problematic due to the minute fraction of detected metabolites which are successfully identified (Bouhifd et al., 2013). Statistical tests for ORA are based around the hypergeometric or binomial distributions such as the Fisher's exact test. The major disadvantage of ORA is that it purely accounts for the presence or absence of 'interesting' pathway components and does not take into account associated intensity values (Khatri et al., 2012).

FCSA is based on the notion that small, but co-ordinated pathway-wide increases or decreases in gene expression or metabolite production are equally as important as large changes in individual genes or metabolites. As such FCSA takes into account the changes in expression or production of all pathway constituents and not just a selection (Khatri et al., 2012). Most methods of FCSA follow the same three steps (Ackermann and Strimmer, 2009). Firstly differential expression of individual pathway components is calculated

through univariate statistics. Secondly the component-level statistics are combined to create pathway-level statistics which are then ranked in order of importance. Finally, the significance of the pathway-level statistic is assessed.

Pathway topology analysis is the most recent development in pathway analysis techniques. This method follows the same three steps as FCSA but instead use information on pathway topology, interactions of constituent genes and metabolites, to compute component-level statistics (Khatri et al., 2012). One major challenged faced by this method that the topology of many pathways is entirely dependent on the cells or organisms used and largely unavailable.

In the field of transcriptomics, pathway analysis has proven invaluable for years and as a result large numbers of analysis tools are available (reviewed in Khatri et al., 2012). For the relatively new discipline of metabolomics, the connection of metabolomics results to the genome has long been predicted (Fiehn, 2002) and only recently enabled (Xia and Wishart, 2010; Xia et al., 2012). Online tools have also become available for combined transcriptomics and metabolomics pathway analysis (Kamburov et al., 2011). This enables an objective, statistical approach which avoids speculation as to how statistically significant genes and metabolites interact (Cavill et al., 2011). One massive disadvantage of all categories of pathway analysis is that they rely upon absolute confidence in the assigned, imputed identities. For microarray transcriptomics, where the identity of each probe is known prior to analysis, this is less of a problem. However for DIMS, where high-throughput identification of detected metabolites is limited, it presents an additional limitation.

1.3.5 The application of omics-technologies for the elution of the AgNP MoA

As stated above, the non-targeted approach of mechanistic investigation that omics technologies provide us with, allows us to bypass the potential limitations of traditional hypothesis-driven research. Several omics-investigations into AgNP toxicity have highlighted mechanisms known also to be shared by dissolved silver, such as disruption of mitochondrial activity (Aerle et al., 2013), energy metabolism (Li et al., 2015a; 2015b) and the induction of oxidative stress following production of ROS (Poynton et al., 2012; Rainville et al., 2014). However some studies have highlighted potential mechanisms of AgNP toxicity that have not been investigated as extensively. A summary of omics investigations into AgNP toxicity is given in Table 1.1.

Table 1.1 – Summary of the key findings of omics-investigations into AgNP toxicity to date.

Technique	Organism	Summary of principal findings	Reference
Microarray transcriptomics	*Daphnia magna*	PVP-AgNPs induce a significant ($p<0.05$) increase in metallothionien and the DNA-damage repair gene REV1 (2-fold and 1.5-fold respectively) expression, and cause an increase in expression of genes involved in protein degradation and signal transduction. $AgNO_3$ induces a down-regulation of genes involved in developmental processes.	Poynton *et al* 2012
2DE proteomics	*Daphnia magna*	Both AgNP and $AgNO_3$ exposure significantly ($p<0.01$ in both cases) increases protein-thiol content approximately 1.5 fold- a potential response to oxidative stress or metal toxicity. AgNP alone induce a significant ($p<0.001$) 1.5-fold increase in protein carbonyl content, a potential sign of oxidative stress.	Rainville *et al* 2014
^{1}H NMR metabolomics	*Daphnia magna*	AgNPs and Ag ions induce significant ($p<0.05$) separations along PC1 compared to control groups. the same metabolic profiles. Authors conclude that released Ag^{+} from AgNPs disrupt energy metabolism and induces oxidative stress.	Li *et al* 2015
SuperSAGE RNA sequencing	*Danio rerio*	AgNP toxicity is thought to be induced by bioavailable Ag ions. Toxicity is induced through disruption of mitochondrial activity and oxidative phosphorylation. Disruption of genes within oxidative phosphorylation complexes I, II, III and IV with expression decreasing between 2 and 10 fold in response to both $AgNO_3$ and AgNP exposure.	Van Aerle *et al* 2013
LC-MS/MS proteomics	LoVo cells	Treatment with 20nm and 100nm AgNPs lead to significant changes in regulation of 620 and 717 proteins respectively. Of these, 252 and 458 proteins in the proteome of 20 nm and 100 nm AgNP exposed animals respectively, were determined to be induced by Ag^{+} through comparison to exposures with the AgNP supernatant (Ag^{+}). Potential impact of AgNP size observed. 100 nm AgNP exposure resulted in upregulation of proteins involved in apoptotic signalling cascades (PAK, MAPK, PP2A). Exposure to 20 nm AgNPs caused generation of ROS and carbonylation of proteins and an increase in protein SUMOlation	Verano-Braga *et al* 2014

HPLC-QTOF metabolomics	Wistar rat	Significantly elevated production of uric acid and allantoin ($p<0.0001$ for both metabolites) found in urine of rats exposed to 9 mg/kg body weight of AgNP. Suspected disruption of purine metabolism.	Hadrup *et al* 2012
^{1}H NMR metabolomics	*Eisenia fetida*	Induction of oxidative stress following exposure to both AgNP and Ag ions. PCA loadings depict depletion of malate, glucose, ATP and inosine and increase in leucine and arginine in response to AgNP exposure. Elevation of succinate and depletion of fumerate in response to dissolved Ag. A significant ($p<0.05$) 1.4-fold increase in SOD activity and 1.3-fold increase in catalase activity in worms exposed to $AgNO_3$. No change in these enzymes observed following AgNP exposures.	Li *et al* 2015

A quantitative proteomics investigation identified up-regulation of serine/threonine protein kinase (PAK), mitogen-activated protein kinase (MAPK) and protein phosphatase 2A (PP2A) subunits following exposure of human colon carcinoma cells to 100 nm citrate-coated AgNPs (Verano-Braga et al., 2014). PAK and MAPK are both involved in signalling cascades that result in caspase-dependent and caspase-independent apoptosis respectively, and PP2A is involved in the regulation of the cell cycle. This study also detected an increase in protein ubiquitination, as well as an upregulation of proteins involved in the ribosome and proteasome complexes. This implies an increase in degradation of proteins by the ubiquitin-proteasome system, possibly damage proteins, followed by the synthesis of replacement proteins (Verano-Braga et al., 2014). In addition to concluding that both AgNPs and dissolved silver impact oxidative phosphorylation and mitochondrial activity, Van Aerle et al (2013) identified significant down-regulation (6.3 fold over 24 h) in cryptochrome 1a transcription, a protein involved in the repressor of clock function. Additional observations included down-regulation of proteasome subunit beta type-1 and up-regulation of ribosomal protein S6 modification-like protein B, the authors suggested that together these alterations imply an increased level of protein turnover due to oxidative damage (Aerle et al., 2013). AgNP-exposed rats were identified as having an increase in the concentration of uric acid and allantoin excreted in their urine suggested a disruption of purine metabolism (Hadrup et al., 2012). These pathways are unlikely to have been targeted through use of a traditional approach, as the background knowledge of AgNP toxicity is still relatively low. AgNPs are therefore ideal candidates for a non-targeted omics approach to investigating their mechanism of toxicity in environmentally relevant test organisms.

1.4 Ecotoxicogenomics and the importance of relevant test organisms

Ecotoxicology, the combination of ecology and toxicology, is the discipline of observing toxicant effects upon ecological systems. Although heavily influenced by toxicology with regards to experimental methods, the influence of ecology is most notable in the selection of ecologically relevant test species and test conditions (Chapman, 2002). Environmental risk assessment differs from standard toxicological risk assessment, in that it not only aims to look at the effects of toxicants on individual organisms, but also the consequences of these effects upon the wider ecosystem (Breitholtz et al., 2006). In an ideal situation all species in a particular ecosystem would be tested to fully investigate the potential impact of a toxicant (Breitholtz et al., 2006). However, as this is impossible, it is vital to select an organism that is representative of the ecosystem under investigation (Chapman, 2002; Breitholtz et al., 2006). Examples of such organisms recommended by the OECD are summarised in Table 1.2 along with examples of recommended testing guidelines.

Table 1.2: The OECD recommended species for aquatic ecotoxicology tests alongside the biological endpoints for testing. This list covers a broad range of species including algae, cyanobacteria, water fleas, non-biting midges and many species of fish.

Test species	Common name	OECD Test No.	Biological endpoints
Anabaena flos-aquae	Cyanobacteria	201	Acute growth inhibition
Desmodesmus subspicatus	Pond algae		
Navicula pelliculosa	Diatom algae		
Pseudokirchneriella subcapitata	Micro-algae		
Synechococcus leopoliensis	Cyanobacteria		
Lemna gibba	Duckweed	221	Acute growth inhibition
Lemna minor	Duckweed		
Daphnia magna	Water flea	202, 211	Neonate immobilisation, Reproductive output
Daphnia pulex	Water flea		
Cyprinodon variegatus	Sheepshead minnow	210	Embryonic development abnormalities
Xenopus laevis	Clawed frog	231	Chronic metamorphosis
Gasterostreus aculeatus	Three-spined stickleback	234	Sexual development
Chironomus dilutus	Non-biting midge	235	Acute larval immobilisation
Chironomus riparius	Non-biting midge		
Chironomus yoshimatsui	Non-biting midge		
Lepomis macrochirus	Bluegill	203, 204	Acute adult mortality, Chronic adult mortality
Poecilia reticulata	Fathead minnow		

Oncorhynchus mykiss	Rainbow trout	203, 204, 210, 212, 215	Acute adult mortality, Chronic adult mortality, Chronic embryonic development, Acute embryonic development, Juvenile growth
Oryzias latipes	Japanese medaka	203, 204, 210, 212, 215, 229, 230, 234	Acute adult mortality, Chronic adult mortality, Chronic embryonic development, Acute embryonic development, Juvenile growth, Acute endochrine disruption, Chronic endochrine disruption, Sexual development
Danio rerio	Zebra fish	203, 204, 210, 212, 215, 229, 230, 234, 236	Acute adult mortality, Chronic adult mortality, Chronic embryonic development, Acute embryonic development, Juvenile growth, Acute endochrine disruption, Chronic endochrine disruption, Sexual development, Acute embryo mortality
Pimephales promelas	Fathead minnow	203, 204, 210, 212, 229, 230	Acute adult mortality, Chronic adult mortality, Chronic embryonic development, Acute embryonic development, Acute endochrine disruption, Chronic endochrine disruption
Cyprinus carpio	Common carp	203, 204, 212	Acute adult mortality, Chronic adult mortality, Embryonic development abnormalities

Daphnia magna (Figure 1.3), a species of small crustacean of the order *Cladocera* commonly known as water fleas, are found in freshwater ecosystems across the globe (Lampert, 2011). They represent a keystone species in aquatic environments serving as an important link between primary producers (in this case phytoplankton) and many species of fish (Tatarazako and Oda, 2007). They have been used extensively as a model organism for aquatic toxicology for many years (Martins et al., 2007; Altshuler et al., 2011) and they are being used increasingly in environmental nanotoxicology (Gaiser et al., 2011; Skjolding et al., 2014; Adam et al., 2014).

All species of *Daphnia* share a cyclical parthenogenetic reproductive cycle (Figure 1.4). In the absence of environmental stressors such as shortened photoperiod, starvation, and overcrowding, adult female Daphnids reproduce asexually yielding genetically-identical daughters. The life cycle of Daphnid species is short with individuals reaching asexual maturity within 6-9 days. This rapid production of genetically identical keystone animals, coupled with low maintenance costs and a presence in freshwater ecosystems the world over make *D. magna* an ideal choice for aquatic ecotoxicology tests.

Figure 1.3: Image of a *D. magna* adult female with a brood chamber full of developing parthenogenetic eggs.

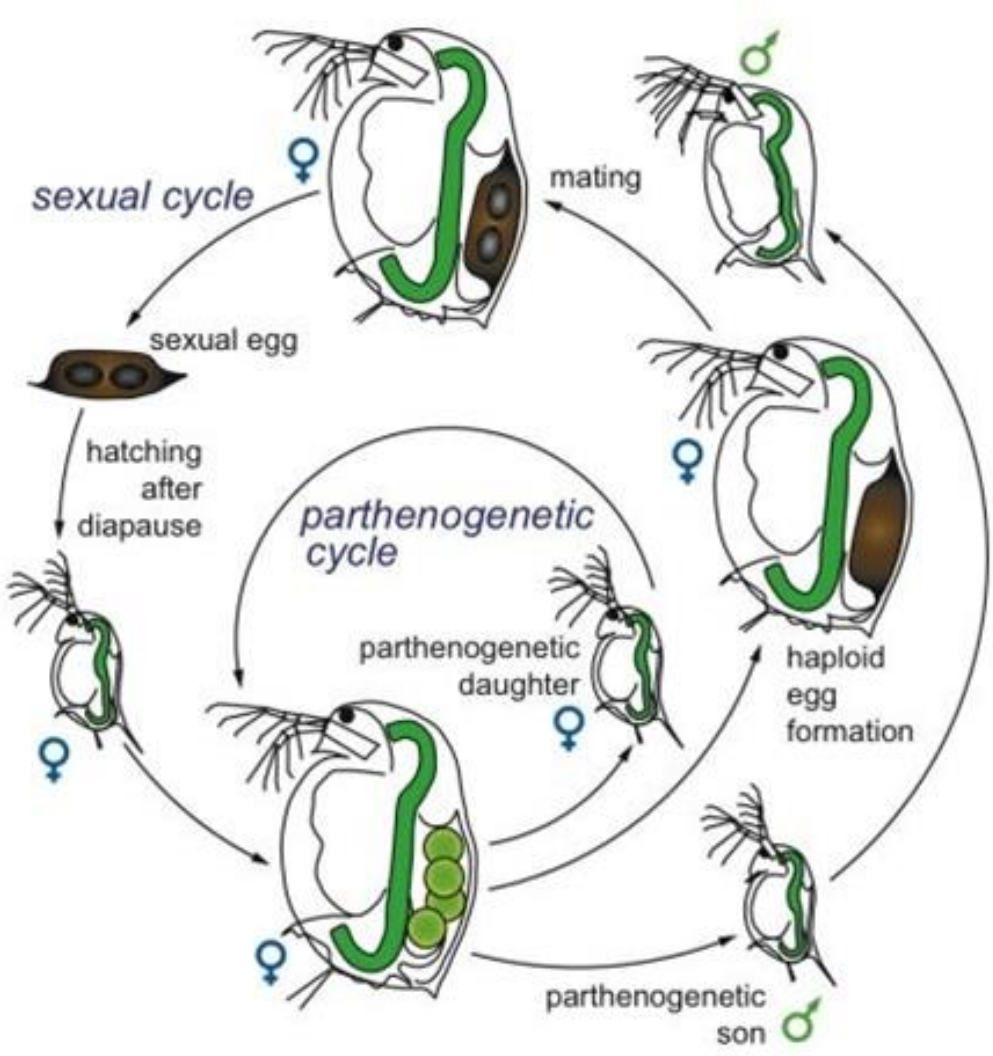

Figure 1.4: The *Daphnia* reproductive cycle. Outlined in this image is the asexual, parthenogenetic cycle which is able to switch to the sexual cycle under unfavourable or stressful conditions (Ebert, 2005)

1.4.1 Ecotoxicogenomics and *Daphnia magna*

In recent years, the number of studies which have applied omics technologies to *D. magna* toxicology studies has grown, with applications of transcriptomics (Garcia-Reyero et al., 2009; David et al., 2011; Poynton et al., 2012; Campos et al., 2013; Rivetti et al., 2014), proteomics (Le et al., 2013; Otte et al., 2014; Rainville et al., 2014), and metabolomics (Taylor et al., 2009; Bunescu et al., 2010; Poynton et al., 2011b; Nagato et al., 2013) being reported. With the publication of the *Daphnia pulex* genome in 2011 (Colbourne et al., 2011), it was not long before gene-expression microarrays were constructed for the sister species *D. magna* from EST libraries (Watanabe et al., 2007; Heckmann et al., 2008; Garcia-Reyero et al., 2009). The transcriptomics analysis in this thesis uses a custom *D. magna* microarray developed in 2009 (Garcia-Reyero et al., 2009) and used previously for nanoparticle toxicology (Poynton et al., 2011a, 2012; Scanlan et al., 2013). Despite its value as a toxicity test species, only a few metabolomic toxicity studies using *D. magna* have been reported (Taylor et al., 2009, 2010; Bunescu et al., 2010; Poynton et al., 2011b; Nagato et al., 2013). The first recorded metabolomics study using *D. magna* was in 2009, where Taylor et al. validated the use of FT-ICR MS in metabolomic studies of *D. magna*, using copper as a model toxicant. This model has already been used previously with AgNPs for mechanistic investigations using transcriptomics (Poynton et al., 2012), proteomics (Rainville et al., 2014) and NMR-metabolomics (Li et al., 2015a). This organism therefore represents an ideal model for a dual-omic assessment of molecular mechanisms of toxicity of AgNPs. Omics-technologies present a unique opportunity in the on-going debate over the role of Ag^+ in AgNP toxicity through direct comparison of the pathways perturbed by both forms of silver. These technologies can also be used to direct further research into the elution of the changes induced in *D. magna* by exposure to Ag.

1.5 Research hypothesis, aims and objectives

The primary objective of this research was to investigate the molecular mechanisms of AgNP toxicity to the freshwater *Cladocera*, *D. magna*, using a combined analysis platform of microarray transcriptomics and FT-ICR MS metabolomics. The work within this thesis tested the hypothesis that toxicity by AgNPs to *D. magna* is induced through the actions of dissolved Ag released upon nanoparticle dissolution. Specifically that, if the nanoparticle fraction plays no part in toxicity, AgNP toxicity is induced through mechanisms known to be induced by dissolved Ag; such as oxidative stress, disruption of mitochondrial function and inhibition of ion-transport proteins.

The primary aims were:

1. To compare the transcriptional and metabolic perturbations induced by AgNPs and dissolved Ag, to determine whether AgNP toxicity is induced solely by the dissolved Ag component.
2. To use the non-targeted approach offered by omics technologies to identify the prominent molecular pathways impacted by AgNP exposure. This platform would then be used to develop and test hypotheses with the aim of elucidating the AgNP mechanism of toxicity.

Chapter 2: Materials and Methods

2.1 Standard chemicals and reagents

Unless otherwise stated, all standard chemicals and reagents were purchased from Sigma-Aldrich.

2.2 Acid-wash cleaning procedures

All glassware and plastic-ware used for exposures, ultrafiltration, or in the preparation of samples for ICP-MS were rinsed and then soaked in a bath of 10 % nitric acid (analytical grade, Fisher Scientific) made with ultrapure water (18.2 MΩ, Purelab) for 24 h. Following this, items were rinsed thoroughly and left to soak in ultrapure water for a further 24 h. All equipment was then left to dry overnight and wrapped in cling-film prior to use.

2.3 Nanoparticle synthesis and characterisation

2.3.1 Silver nanoparticle synthesis – conducted by Dr. Isabella Römer and Dr. Mila Tejamaya (University of Birmingham)

AgNPs stabilised with citrate (cit-AgNPs) were synthesised by Dr. Isabella Römer through the reduction of $AgNO_3$ (100 ml, 0.25 mM) by sodium borohydride ($NaBH_4$, 6 ml, 10 mM) in the presence of sodium citrate (100 ml, 0.31 mM) using a method outlined previously (Römer et al. 2011). AgNPs stabilised with polyvinyl pyrrolidone (PVP-AgNPs) were synthesised by Dr. Mila Tejamaya using a similar method, again through the reduction of $AgNO_3$ (60 ml, 1 mM) with $NaBH_4$ (180 ml, 2 mM) however this time in the presence of PVP_{10} (Tejamaya et al. 2012). Newly synthesised nanoparticles were 'cleaned' to remove excess reagents using ultrafiltration (UF) through a 1 kDa regenerated cellulose membrane (Millipore, USA) in a stirred UF cell under N_2. The volume was

maintained with capping agent solution (sodium citrate or PVP) using a diafiltration method to keep particles in solution. Particles underwent cleaning 3 times following preparation and a further 3 times prior to all exposure work, with the final clean always finishing less than 1 h before the initiation of particle exposures. All UF equipment was washed in 2% nitric acid and rinsed thoroughly in ultrapure water prior to use.

2.3.2 Particle characterisation – conducted by Dr. Isabella Römer and Dr. Mila Tejamaya (University of Birmingham)

The cit-AgNPs and PVP-AgNPs used in this research were characterised in ultrapure water, by Dr Isabella Romer and Dr Mila Tejamaya respectively, using flow field flow fractionation (Fl-FFF), dynamic light scattering (DLS), transmission electron microscopy (TEM) and in the case of cit-AgNPs only, atomic force microscopy (AFM) as outlined previously (Römer et al. 2011; Roche 2012; Tejamaya et al. 2012) and summarised in Table 2.1. Briefly, both particles were dispersed in ultrapure water and deemed spherical in shape by TEM analysis. The cit-AgNPs had mean diameters measured as 7.2 ± 0.2, 7.0 ± 2.0 and 6.0 ± 3.0 nm by Fl-FFF, TEM and AFM respectively and 16 ± 1.0 nm by DLS. The discrepancy in the measurement made by DLS when compared to the other techniques is indicative of the particles hydrated radius (Baalousha and Lead, 2012). The PVP-AgNPs had mean diameter measurements of 25.6, 10.8 ± 3.3 and 28.3 ± 0.8 nm by Fl-FFF, TEM and DLS. The discrepancy between measurements of the PVP-AgNPs by TEM and Fl-FFF is due to the inability of TEM to visualise the increased diameter of the particles caused by the PVP polymer coating (Domingos et al., 2009). Observational techniques such as TEM and AFM therefore give an assessment of the particles' core diameter whereas Fl-FFF also measures the PVP shell (Baalousha and Lead, 2012). As it is the technique which directly measures the core of the nanoparticles, the measurements made by TEM will be used when referring to nanoparticle size in this thesis.

Table 2.1: Average hydrodynamic and core particle diameter ± standard deviation (nm) of citrate and PVP-coated AgNPs measured by DLS, Fl-FFF, TEM and AFM. Measurements made by DLS and Fl-FFF represent the hydrodynamic diameter of the particles whereas measurements by TEM and AFM give the core particle diameter.

Measurement	Technique	Average diameter (nm) ± SD	
		Citrate-AgNPs	PVP-AgNPs
Hydrodynamic diameter	DLS	16 ± 1.0	28.3 ± 0.8
	Fl-FFF	7.2 ± 0.2	25.6 ± 0.3
Core diameter	TEM	7.0 ± 2.0	10.8 ± 3.3
	AFM	6 .0 ± 3.0	N/A

2.3.3 Measurement of total Ag concentration of stock solutions by Inductively Coupled Plasma Mass Spectrometry (ICP-MS)

Concentrations of AgNP and $AgNO_3$ stocks prepared in ultrapure water for use throughout this thesis were measured by Inductively Coupled Plamsa Mass Spectrometry (ICP-MS). Prior to measurement of particle concentration, AgNP solutions were acidified to 20 % HNO_3 for 24 h to promote digestion and dissolution of the particles. All acidified samples were diluted 10-fold to a final HNO_3 concentration of approximately 2% and were subsequently analysed for total silver concentration by ICP-MS. The analysis was conducted using an Agilent 7500c with an Octopole Reaction System calibrated for use between 0.1 and 200 µg/l. Silver standards were prepared from a 1000 mg/l stock solution (VWR) in 2% nitric acid. A calibration graph of counts (ppb) against concentration (µg/l) gave an R^2 correlation coefficient of 1.000. An average was taken from 4 technical replicate measurements (in ppb) for each sample of dosed media; these readings were then converted into a concentration (in µg/l) from the calibration graph. The recovery of known concentrations of Ag via this method was tested and confirmed in section 6.2.3.

2.4 *Daphnia magna* culturing

2.4.1 Preparation and composition of media

Three different preparations of ISO test water (1) (Annex 3, OECD 202, 2004) with additional sodium selenite (Keating and Dagbusan, 1984; Taylor et al., 2009) were used throughout this thesis (Table 2.2). These consisted of the standard strength media (media1) as well as a 2-fold (media2) and 10-fold (media10) dilution as reported previously (Römer et al., 2011; Tejamaya et al., 2012; Römer et al., 2013). Media were prepared through the addition of concentrated stocks of the composite salts to deionised water (15 MΩ). The composition of media1, media2 and media10 is outlined below (Table 2.2). Following preparation, media was aerated for a minimum of 24 h after which the pH and dissolved oxygen concentration were measured before use. Media was used only with a pH between 6.0 and 9.0 and a dissolved oxygen concentration above 60 % relative saturation as outlined in the OECD guidelines (OECD 202, 2004).

Table 2.2: Chemical composition of modified OECD ISO media used within this thesis for *D. magna* culturing and chemical exposures. All solutions were made using deionised water (15 MΩ), concentrations given are nominal values.

		Final concentration (mM)		
Compound name	**Empirical Formula**	**Media 1**	**Media2**	**Media10**
Calcium chloride	$CaCl_2.2H_2O$	2.00	1.00	0.20
Magnesium sulfate	$MgSO_4.7H_20$	0.50	0.25	0.05
Sodium bicarbonate	$NaHCO_3$	0.77	0.39	0.08
Potassium chloride	KCl	0.77	0.39	0.08
Sodium selenite	Na_2SeO_3	116 nM	58 nM	12 nM

2.4.2 *Chlorella vulgaris* maintenance and preparation of feeding solution

Chlorella vulgaris was cultured in semi-static conditions for use as feed for *D. magna* cultures. Algal cells were suspended in Bold's basal medium (BBM, pH 6.7 ± 0.3), constantly aerated and kept under constant light at room temperature. The composition of BBM is outlined below in Table 2.3.

Table 2.3: Chemical composition of Bold's basal medium (BBM) used in the culture of *C. vulgaris* algal feed. All solutions were made using deionised water (15 MΩ), concentrations given are nominal values.

Stock No.	Compound	Empirical formula	Final conc (mM)
1	di-Potassium hydrogen orthophosphate	K_2HPO_4	0.43
2	Potassium di-hydrogen orthophosphate	KH_2PO_4	1.29
3	Magnesium sulfate	$MgSO_4.7H_2O$	0.33
4	Sodium nitrate	$NaNO_3$	3.62
5	Calcium chloride	$CaCl_2.2H_2O$	0.17
6	Sodium chloride	NaCl	0.43
7	EDTA tetrasodium salt &	$EDTA\text{-}Na_4$	0.13
	Potassium hydroxide	KOH	0.55
8	Iron(II) sulfate in Sulfuric acid (0.1 %)	$FeSO_4.7H_2O$	0.02
9	Boric acid	H_3BO_3	0.18
Stock No.	**Compound**	**Empirical formula**	**Final conc (μM)**
10	Zinc sulfate	$ZnSO_4.7H_2O$	4.91
11	Manganese chloride	$MnCl_2.4H_2O$	1.17
12	Cupric sulfate	$CuSO_4.5H_2O$	1.01
13	Cobaltous nitrate	$Co(NO_3)_2.6H_2O$	0.27
14	Sodium molybdate	$Na2MoO_4.2H_2O$	0.79

For feeding, an aliquot of algae was removed from the main culture and the optical density of a 1 in 10 dilution was assessed at 440 nm by spectophotometry. The sample was then centrifuged at 3000 rpm for 30 minutes (Falcon 6/300 centrifuge, 4x750 ml Windshield rotor, MSE, UK), the supernatant was discarded and the pellet re-suspended in de-ionised water so that a 1 in 10 dilution would have an optical density of 0.8 at 440 nm. The re-suspension volume was calculated using Equation 2.1. This food stock was then used in *D. magna* culture.

Equation 2.1: Calculation of the re-suspension volume (V_2) is required to produce algal feed with an optical density of 0.8 at 440 nm. The original volume and optical density of collected algae are represented by V_1 and A_{440} respectively.

$$V_2 = \frac{V_1 \times A_{440}}{0.8}$$

2.4.3 Preparation of dietary supplements for *D. magna* culture

Saccharomyces cerevisiae (Baker's yeast, Sigma-Aldrich) and *Ascophyllum nodosum* (Marinure, Wilfrid-Smith Ltd, UK) were used as dietary supplements for the feeding of *D. magna* cultures. Dried Baker's yeast was suspended at a concentration of 10 mg/ 100 ml of deionised water and stirred magnetically until fully suspended, and added to *D. magna* cultures as described in Section 2.4.5. A fresh batch of this solution was made every 14 days. A working stock of *A. nodosum* (Marinure, Wilfrid-Smith Ltd, UK) is obtained through the dilution of a concentrated aliquot with deionised water to yield an optical density of 0.8 ± 5 % at a wavelength of 400 nm. Volumes of this working stock were added to culture beakers as described in Section 2.4.5.

2.4.4 *Daphnia magna* strain origin

The *D. magna* strain used in this study originated from the National Institute for Applied Chemical Research, France, and was obtained from the University of Reading in 2007. These animals have been cultured continuously since this date according to OECD guidelines.

2.4.5 *Daphnia magna* culture maintenance

D. magna cultures were maintained as described previously in media1 (Taylor et al., 2009), and media10 (Römer et al., 2011). *D. magna* were cultured at a density of 20 animals per 1200 ml of media, with a 16:8 h light:dark cycle and an ambient temperature

of 19 °C. *D. magna* were fed daily with 0.5 ml baker's yeast solution (Section 2.4.3), and a set volume of the *C. vulgaris* food stock depending on the age of the organisms within the culture. Animals aged between 0-2 d were fed 1 ml, 3-7 d daphnids were fed 1.5 ml, and daphnids aged 8 d and older were fed 2 ml. Marinure (Section 2.4.3) was added upon culture initiation and bi-weekly media change; 3 ml was added aged 1-7 d, and 4 ml for daphnids aged 8 d and over. Cultures were maintained for 14 days allowing the production of at least three broods of neonates before exposures were set up or colonies restarted with < 24 h old neonates.

2.5 *Daphnia magna* toxicity exposure conditions

Before their neonates could be collected for use, animals were cultured for at least one full generation (ca. 14 days) in the appropriate medium as outlined in section 2.4.5. *D. magna* neonates (< 24 h) from at least the third reproductive brood of a culture were used in all toxicity exposures described in this thesis. The concentration of all AgNP and $AgNO_3$ exposure stocks was measured by ICP-MS prior to use in toxicity exposures. A spike-in method was used for exposure; groups of *D. magna* neonates (<24 h) were added to vessels (250 ml glass beaker, Fisher Scientific) containing between approximately 50% and 80% of the total desired exposure volume. A pre-calculated volume of AgNP or $AgNO_3$ exposure stock was then used to spike the study medium followed immediately by the remaining volume of exposure medium to mix. The exact volumes of medium and exposure stock concentrations used in each exposure, as well as exposure durations, are reported in greater detail in the respective chapters of this thesis. Once prepared, exposure vessels were kept at 19 ± 1 °C and on a 16h:8h light:dark cycle with no additional administration of food or supplements. Tests were only considered valid if no more than 10% of control animals were immobilised during the exposure.

Chapter 3: Optimisation of aqueous nanoparticle toxicity exposure conditions and characterisation of AgNPs*

3.1 Introduction

One of the major setbacks of many published nanoparticle toxicology studies is improper characterisation of the particles or experimental conditions that are used. As stated earlier, the unique effects of the nano-scale are directly related to the area of the particles' surface available for interaction (Section 1.1). The composition of the medium in which nanoparticles are dispersed can impact their stability; either allowing for an even dispersal or the formation of particle aggregates (Badawy et al., 2010; Römer et al., 2011; Tejamaya et al., 2012). According to Derjaguin, Landau, Verwey, and Overbeek (DLVO) theory, the colloidal stability of nanoparticles in solution is dictated by the balance between attractive forces such as van der Waal's (VDW), which promote aggregation, and electrostatic repulsion forces which oppose aggregation (Badawy et al., 2010). In high purity water and at neutral pH two particles of the same type in suspension will have the same surface charge and will therefore repel one another. This electrostatic repulsion will prevent the two particles from getting close enough for VDW forces to promote aggregation. The dispersion of particles within an aqueous medium can be impacted by the ionic strength and the pH of the medium (Stebounova et al., 2011). Free-ions present in the aqueous medium such as Ca^{2+}, Cl^{-}, H^{+} and OH^{-}, will be attracted to disperse particles if they are of the opposing charge to the particle's surface. Interactions between these ions within the medium and dispersed particles may result in a shielding of the particle's surface charge. This reduces the level of electrostatic repulsion between colloidal particles allowing for

* Contents of this chapter, including the figures, have been published in *Toxicology Letters:*
Römer, I., Gavin, A. J., White, T. A., Merrifield, R. C., Chipman, J. K., Viant, M. R., & Lead, J. R. (2013). The critical importance of defined media conditions in *Daphnia magna* nanotoxicity studies. *Toxicology letters*, *223*(1), 103-108.

VDW forces to induce formation of particle aggregates. To reduce the likelihood of aggregation, particles are often coated in substances which either increase the electrostatic repulsion between particles, such as citrate or that prevent VDW interactions through steric hindrance of particle interactions such as polyvinylpyrrolidone (PVP) (Christian et al., 2008).

When particles are aggregated, the quantity of surface area available for interaction is reduced, potentially suppressing toxicity (Jiang et al., 2008). The bioavailaility of aggregates is also seen to be less than dispersed particles, as large aggregates are more likely to be deposited in sediments removing them from the water column (Bradford et al., 2009). If we are to account for any potential impact that aggregation may have on AgNP toxicity, particle stability must be fully characterised in the appropriate exposure conditions. It has been shown previously that AgNPs stabilised with various capping agents (citrate, PVP and PEG) form aggregates in standard OECD ISO test media (media1) for *D. magna* acute toxicity tests (Römer et al., 2011; Tejamaya et al., 2012). By diluting the standard media 10-fold, aggregation is reduced substantially without inducing immobilisation or a significant reduction in daphnid reproductive output (Römer et al., 2011). What has not yet been observed is whether the aggregation induced by media composition has a significant impact upon the results of a *D. magna* acute immobilisation test.

The primary aim of this chapter is to assess the impact that dilution of standard exposure media, and hence particle stability, has on acute nanoparticle toxicity. To that end, the dose-response relationships of cit-AgNPs and a non-nanoparticle control ($AgNO_3$) were characterised in standard strength OECD ISO test water (media1) and a 10-fold dilution of this medium (media10). To investigate the potential role of particle stability in any observed effect, stability assessed in media1, and a two-fold (media2) and ten-fold

(media10) dilution of media1 using AFM and TEM. The results of this and previous studies determined the optimum combination of exposure medium and AgNPs that yield dispersed particles.

To study the molecular level changes that occur in response to AgNP exposure, the use of exposure concentrations which do not induce organism death are required. The large number of transcriptional and metabolic changes associated with death may mask the more subtle changes associated purely with adaptive responses to toxicant exposure. To accurately select an appropriate concentration for omics exposures, the full dose-response relationship of both toxicants must be characterised. As stated above (Section 1.2.3), the mechanism of AgNP toxicity is widely thought to be mediated by Ag^+ ions which are released from the particles' surface. It is therefore imperative to control for the dissolved Ag^+ component of nanoparticle exposures if we are to attempt to elucidate its role in AgNP toxicity (Allen et al., 2010; Kennedy et al., 2010; Zhao and Wang, 2012a). Therefore the secondary aim of this chapter was to characterise the full dose-response relationship of both the AgNPs and Ag^+ ions in the optimum test media, and to assess the amount of Ag^+ released from AgNPs over the standard exposure period. This enables the calculation of EC_{50} values for each toxicant and an accurate selection of sub-lethal exposure concentrations. Through use of ultracentrifugation (UC) and ultrafiltration (UF) followed by inductively coupled plasma mass spectrometry (ICP-MS), the release of Ag^+ from AgNPs in the selected exposure conditions can be assessed.

3.2 Materials and Methods

3.2.1 Nanoparticle synthesis and characterisation - conducted by Dr. Isabella Römer & Dr. Mila Tejamaya (University of Birmingham)

AgNPs stabilised with citrate and PVP were synthesised and characterised according to the methods outlined in Section 2.3.

3.2.2 Determining the impact of media composition on cit-AgNP toxicity

The impact of media composition on AgNP toxicity to *D. magna* was investigated through the exposure of *D. magna* neonates to increasing concentrations of 0.1, 0.5, 1.0, 2.5, 5.0, 7.5, 10, 11.25 and 20 µg/l cit-AgNPs in media1 and media10 (compositions outlined in section 2.4.1). To control for any potential change in toxicity due to sequestration of dissolved Ag by Cl^- ions, *D. magna* neonates were also exposed to increasing concentrations of 0.1, 0.25, 0.5, 0.75, 1.00, 5.00 and 10.00 µg/l $AgNO_3$ in media1 and media10 (equating to total silver concentrations of 0.06, 0.13, 0.31, 0.47, 0.63, 3.15 and 6.30 µg/l). Additional concentrations of 1.78, 2.37, 3.16 and 4.22 µg/l $AgNO_3$ (equating to total silver concentrations of 1.12, 1.49, 1.99 and 2.66 µg/l respectively) were required to induce partial death in media1 to better characterise the dose-response curve. The concentration ranges used for each form of silver were based upon the results of range-finding exposures (unreported) that identified the EC_{50} for each AgNPs and $AgNO_3$ as being between 1 - 10 µg/l and between 0.1 - 1 µg/l respectively. Capping agent and untreated (water, 18.5 MΩ) controls were used to assess the potential adverse effects of the capping agent and background mortality.

To initiate exposures, groups of 10 *D. magna* neonates (<24 h old) were added to exposure vessels (250 ml glass beaker, Fisher Scientific) containing either 200 ml of media1 or 200 ml of media10 (adjusted to pH 7.5 as in section 2.4.1). Volumes of a 12 mg/l stock of

cit-AgNP (prepared and concentration measured as in Sections 2.3 and 2.3.3 respectively) were added, in groups of 3 replicates per media composition, to prepare each of the nine nominal cit-AgNP exposure concentrations. An analogous protocol was used with a 1.79 mg/l stock of $AgNO_3$ to prepare each of the 7 and 11 intended exposure concentrations in media 10 and media1 respectively. Once spiked, an additional 50 ml of appropriate media was added to each vessel to mix. The exact volumes used in the production of these control groups and nominal exposure concentrations are outlined in Table 3.1. Exposure conditions were otherwise as outlined in section 2.5.

Animals were exposed for 24 h after which the total number of dead or immobilised neonates was counted. Immobilisation is defined by the OECD, as "those animals not able to swim within 15 seconds after gentle agitation of the test container" (OECD, 2004). EC_{50}s were calculated using the logistic analysis algorithms in Prism6 statistical analysis software (version 6.03, GraphPad Software Inc., California). Briefly, the mean % immobilisation (± SEM) values were calculated from the raw data and plotted against their respective log_{10}-transformed nominal concentration values using a sigmoidal (four-parametric logistic) curve with lower and upper constraints of 0 and 100 % respectively. Where possible the resulting EC_{50} values were compared between exposures in media1 and media10 for each toxicant by a sum-of-squares F-test in Prism6.

Table 3.1: Spiking volumes of a 1.79 mg/l $AgNO_3$ stock needed to make the desired exposure concentrations upon addition to a total volume of 250 ml media1 or media10

Desired Exposure conc. (µg/l)	Spike volume (µl)
0.10	14
0.25	35
0.50	70
0.75	105
1.00	140
1.78	249
2.37	331
3.16	441
4.22	589
5.00	698
10.00	1397

Table 3.2: Spiking volumes of a 12.0 mg/l AgNP stock needed to make the desired exposure concentrations upon addition to a total volume of 250 ml media1 or media10

Desired Exposure conc. (µg/l)	Spike volume (µl)
0.10	2
0.50	10
1.00	21
2.50	52
5.00	104
7.50	156
10.00	208
11.25	234
20.00	417

3.2.3 Determining the impact of media composition on cit-AgNP stability

In parallel to the toxicity assessment of cit-AgNPs described above (section 3.2.2) the impact of media composition (outlined for all media types in Table 2.1) on particle stability was assessed through TEM and AFM measurement of particle size distributions and TEM measurement of particle circularity. To assess stability, 46 ml aliquots (n=3 per media type) of a 12 mg/l stock solution of cit-AgNPs were added to 250 ml of media1, as well as media2 and media10, to a final concentration of 2.2 mg/l. The final pH of solutions was adjusted to 7.5 through addition of 1 M HNO_3 or NaOH to lower or raise the pH respectively. Suspensions were maintained at room temperature for 24 h to match the duration of an acute toxicity exposure before imaging with TEM and AFM.

These suspensions of AgNPs were then prepared for TEM analysis by using the "drop method" as outlined previously (Domingos et al., 2009; Römer et al., 2013). Briefly, a single droplet of AgNP suspension was partially dried at room temperature on a carbon-coated copper mesh (Agar Scientific). Once dry, samples were washed with ultrapure water (18.2 MΩ) and images were obtained with a transmission electron microscope (Tecnai F20, Phillips, Netherlands), and recorded and analysed using digital micrograph software (Gatan, Abingdon, UK) to measure size distribution and Image J to measure particle circularity. Circularity is defined as the ratio of a particle's area to its perimeter (Stevenson et al., 2012), and ranges from 0 (elongated or irregular shape) to 1 (circular shape). Where possible, mean circularity values as well as mean particle size distributions were compared between particle suspensions in each media composition by a 1-way ANOVA followed by a Tukey post-hoc test for multiple comparisons.

Samples for AFM measurements were prepared by ultracentrifugation. Briefly, 10 ml aliquots of AgNP suspensions were transferred into ultracentrifuge tubes containing a cleaved mica sheet on a flat polytetrafluoroethylene support. Samples were then ultra-

centrifuged (Beckman L7-65 Ultracentrifuge with SW40 swinging bucket rotor) at 10,000 rpm, for 60 minutes at 15°C. After centrifugation, the tubes were emptied, the PTFE supports removed and the mica sheets washed in high purity water (18.2 MΩ) and dried at ambient conditions prior to AFM analysis. Images were obtained with an AFM (XE 100, Park Systems) in non-contact mode, as described previously (Römer et al., 2013). Non-contact mode silicon AFM Cantilevers PPP-NCHR were used (spring constant 42 N m^{-1}), X–Y scan sizes were 5 μm × 5 μm with resolution of 250 pixels per line. Scanning rates were optimised to acquire a stable and clear image without damaging the tip or detaching particles during scanning, usually 0.3–1 Hz. Images were recorded using XEP data acquisition software and analysed with XEI data analysis software (Park systems). Where possible, mean particle size distributions were compared between particle suspensions in each media composition by a 1-way ANOVA followed by a Tukey post-hoc test for multiple comparisons. Both TEM and AFM analysis were done in equal collaboration with Dr Isabella Romer (University of Birmingham).

3.2.4 Full characterisation of dose-response curves of PVP-AgNPs and dissolved Ag (from $AgNO_3$) to *D. magna* neonates in media10

Initial range-finding exposures (not reported) in media10 identified the EC_{50} for each form of Ag as being between 1 and 10 μg/l for AgNPs and between 0.1 and 1 μg/l of total Ag for $AgNO_3$. Following these range-finding exposures, nominal exposure concentrations of 3.08, 3.54, 4.07, 4.70, 6.29, 8.38, 9.69, and 11.17 μg/l of PVP-AgNPs and 0.10, 0.18, 0.32, 0.56, 0.75, 1.00 and 1.78 μg/l of $AgNO_3$ (equating to 0.07, 0.12, 0.20, 0.37, 0.41, 0.62 and 1.07 μg/l theoretical total Ag) were assembled to map the dose-response relationship for each form of Ag. Capping agent (0.03 % v/v. PVP) and no-added silver controls were used to account for any potential impact of the nanoparticle capping agent and background mortality respectively.

PVP-coated AgNPs were prepared as outlined in section 2.3 and the final concentration was measured as 14.70 mg/l by ICP-MS using methods outlined in section 2.3.3. This AgNP Master-Stock was then used directly to prepare Spiking-Stocks for each of the 8 desired nominal AgNP exposure concentrations mentioned above using volumes outlined in Table 3.3. A Master Stock of $AgNO_3$ was prepared through the addition of 100.0 mg of $AgNO_3$ (Sigma Aldrich) to 100 ml MilliQ water giving a nominal concentration of 1000 mg/l. A 1 in 100 dilution of this master stock, followed by a further 1 in 10 dilution was made to yield a Working Stock with a nominal concentration of 1 mg/l $AgNO_3$. This $AgNO_3$ Working-Stock was then used directly to prepare Spiking-Stocks for each of the 7 desired nominal $AgNO_3$ exposure concentrations using volumes outlined in Table 3.4.

Table 3.3: Preparation of the AgNP spiking stocks from the 14.7 mg/l master stock. The table gives the volumes of the 14.7 mg/l AgNP master stock used to prepare each of the spiking stocks. Each spiking stock was designed to be 250 times more concentrated than the desired exposure concentration.

Nominal conc. of AgNP (µg/l)		
Desired exposure conc.	Spiking stock conc.	Volume of 14.7 mg/l Master stock (µl)
3.08	769	52
3.54	884	60
4.07	1016	69
4.70	1176	80
6.29	1573	107
8.38	2095	143
9.69	2422	165
11.17	2793	190

Table 3.4: Preparation of the $AgNO_3$ spiking stocks from the 1 mg/l working stock. The table gives the volumes of working stock used to prepare each spiking stock in a total volume of 10 ml. Each spiking stock was designed to be 250 times more concentrated than the desired exposure concentration.

Nominal conc. of $AgNO_3$ (µg/l)		
Desired exposure conc.	Spiking stock conc.	Volume of 1.0 mg/l Working stock (ml)
0.10	25	0.25
0.18	45	0.45
0.32	80	0.80
0.56	140	1.40
0.75	188	1.88
1.00	250	2.50
1.78	445	4.45

To initiate toxicant exposures, groups of 10 neonates (<24 h old) were added using a plastic Pasteur pipette to 200 ml of media10 in 72 x 250 ml glass beakers. In groups of four, these vessels were spiked with 1 ml of a Spiking-Stock immediately followed by a further 49 ml of media10 to mix. This produced the 8 desired AgNP concentrations along with the 7 desired $AgNO_3$ concentrations complete with one PVP control and two no-added silver control groups. Exposure conditions were otherwise as outlined in section 2.5. Animals were exposed for 48 h in total, with the number of dead or immobilised neonates counted after 24 h and 48 h. Immobilisation is defined by the OECD, as "those animals not able to swim within 15 seconds after gentle agitation of the test container" (OECD, 2004). EC_{50}s were calculated using the logistic analysis algorithms in Prism6 statistical analysis software (version 6.03, GraphPad Software Inc., California). Briefly, the mean % immobilisation (± SEM) values were calculated from the raw data for each group and plotted against their respective log_{10}-transformed nominal total Ag concentrations using a sigmoidal (four-parametric logistic) curve using lower and upper constraints of 0 and 100 % respectively. The resulting EC_{50} values of PVP-AgNPs and $AgNO_3$ were compared at each time point by a sum of squares F-test in Prism6.

3.2.5 Measurement of PVP-AgNP dissolution in media10

Three individual suspensions of PVP-AgNPs were made through the addition of 140 µl from a 8.839 mg/l stock solution (approximately 8 mg/l) in triplicate to 200 ml of media10. The final volume was made up to 250 ml to mix yielding a final nominal AgNP concentration of approximately 5 µg/l. No daphnids were present during the 48 h period. Kept alongside the three nanoparticle suspensions were three control beakers consisting of 250 ml of media10 and no additional nanoparticles. The separation of the nanoparticle and ionic fractions of PVP-AgNP suspensions was attempted using ultacentrifugation (UC)

and ultrafiltration (UF) prior to measurement of their respective concentrations by ICP-MS (section 3.2.8).

3.2.6 Assessment of particle dissolution by ultracentrifugation

Aliquots (5 ml) of the PVP-AgNP suspensions and control samples were removed at 0, 24 and 48 h after particle dispersal into UC tubes (14 ml, Ultra-Clear, Beckman Coulter, USA). These aliquots were then made up to a total volume of 10 ml with ultrapure water (18.2 MΩ, Purelab), and vortex mixed before centrifugation at 30000 rpm for 1 h at 10 °C in a (L7-65 ultracentrifuge using a SW 40 swinging-bucket rotor, Beckman Coulter, USA). In theory, ultracentrifugation of AgNP suspensions should result in the concentration of AgNPs at the bottom of the test tube, while any dissolved Ag should remain in solution dispersed evenly throughout the solution. Following UC separation, 4.9 ml of solution was removed from the top of each sample. This 4.9 ml top aliquot, along with the remaining 5.1 ml bottom aliquot for each sample, was subsequently acidified by the addition of 2.0 ml and 1.8 ml concentrated (69 % v/v) nitric acid (HNO_3, trace metal grade, Fisher Scientific) respectively. The acidification of samples to 20 % HNO_3 followed by vortex mixing until colourless ensured the total Ag content of each sample was fully dissolved ready for analysis.

3.2.7 Assessment of particle dissolution by ultrafiltration

Triplicate aliquots (10 ml) of the 5 µg/l PVP-AgNP dilutions were taken at 0, 24 and 48 h after particle dispersal and transferred directly into separate UF cells (10 ml, Millipore UK). Each cell was fitted with a 1 kDa NMWL filter with a 2nm pore (25 mm, Ultracel regenerated cellulose) and a magnetic stir-bar. Cells were pressurised with nitrogen gas (N_2, 1 bar) for approximately 1 h, with constant stirring, until the volume of solution had reduced by half. The 2 nm pore filter used in this study should trap AgNPs (which are 10.8 ± 3.3 nm in diameter) inside the ultrafiltration cell allowing only water and dissolved

substances through the pores. Any form of Ag that passes through the 2nm pore should, in theory, be dissolved silver. However in actuality this will include the free silver ion, Ag salt complexes and any Ag compounds < 2 nm. All nanoparticles used in this study have been filtered and washed by ultrafiltration previously so only particles which are 10.8 ± 3.3 nm in diameter remain within the sample. Stirring was stopped and pressure relieved before 4 ml aliquots of both the filtrate and filtrand were transferred to acid-washed scintillation vials. Nanoparticle aliquots were acidified to 20 % HNO_3 by the addition of 1.9 ml of concentrated HNO_3 (trace metal grade, Fisher Scientific) and vortex-mixed to ensure complete dissolution of total silver prior to measurement by ICP-MS. Aliquots expected to contain dissolved silver (the top fraction of UC samples and the filtrand of UF samples) were acidified to 10 % HNO_3 by the addition of 0.95 ml of concentrated HNO_3 (trace metal grade, Fisher Scientific) and vortex-mixed to ensure complete dissolution of total silver. The dissolved Ag fractions were expected to contain concentrations of silver close to the detection limit of the ICP-MS instrumentation so the lower concentration of HNO_3 used was to minimise dilution of samples.

3.2.8 Measurement of silver dissolution samples by ICP-MS

All acidified samples from sections 3.2.6 and 3.2.7 were diluted 10-fold to a final HNO_3 concentration of approximately 2% and were subsequently analysed for total silver concentration by ICP-MS as outlined in Section 2.3.3. The analyses were conducted using an Agilent 7500c with an Octopole Reaction System calibrated for use between 0 and 200 µg/l and with a lower detection limit of 0.02 µg/l. An average reading was taken from 4 technical replicate measurements for each sample of dosed media; these readings were then converted into a concentration (in µg/l) from the calibration graph. To investigate the potential interference of media10 with the measurement of dissolved total silver, two spike recovery tests were performed using a sample of the same batch of media10 used in

exposures. The first test using a final spike concentration of 1 ppb gave a return reading of 1.02 ppb and the second using a final concentration of 10 ppb gave a return reading of 10.03 ppb, indicating that the media component had no impact on the measurements. All submitted control samples resulted in a total silver content below the limit of detection signifying the background Ag content of exposures to be, at the very least, <0.02 µg/l. ICP-MS measurements were conducted by Dr Steve Baker (University of Birmingham).

The concentration of dissolved silver in the exposure vessels at 0 h, 24 h and 48 h was calculated using Equation 3.1. Briefly, the concentration of total silver measured in the top fraction of UC samples or the filtrate of UF samples $[Ag]_{dm}$ was multiplied by the total factor of dilution (D) that occurred during sample preparation (14.75 fold dilution in total). Theoretically, as described above (sections 3.2.6 and 3.2.7), these fractions should contain only dissolved Ag species and as such should be representative of the total dissolved silver fraction of exposures once dilutions during preparation are taken into account. The concentration of the AgNP fraction is calculated using Equation 3.2. The total silver concentration of the lower UC fraction and UF filtrand should theoretically contain both dissolved and concentrated nanoparticle silver. As such is representative of the total silver concentration of the media once dilutions during preparation and concentration of AgNP fraction has been taken into account. The initial concentration of AgNPs $[Ag]_{NP}$ is therefore calculated through the multiplication of the measured total silver fraction $[Ag]_{tm}$ by the dilution factor (D) of sample preparation. This resulting figure then has the $[Ag]_{ds}$ value calculated earlier subtracted from it before dividing the result by the concentration factor (C); the factor by which the nanoparticles have become concentrated from the original aliquot. The mean total Ag concentrations measured following UC and UF separation are given in the Appendix (Table 9.1 and Table 9.2 respectively).

The percentage dissolution was then calculated by dividing the concentration of the dissolved Ag fraction $[Ag]_d$ by the total silver concentration of the exposure media ($[Ag]_{NP}+[Ag]_I$) and multiplying the resulting fraction by 100 (Equation 3.3). The resulting data were compared for each technique across treatment type and dissolution duration by a 2-way ANOVA followed by a Sidak's comparison test.

Equation 3.1 – Calculation of dissolved silver content in spiked exposure media. Where $[Ag]_{ds}$ is the concentration of dissolved silver in the exposure sample, $[Ag]_I$ is the measured concentration of total silver in the top fraction following UC or the filtrate of UF and D is the total dilution factor used in sample preparation.

$$[Ag]_{\mathrm{d}} = [Ag]_{\mathrm{dm}} \times D$$

Equation 3.2 - Calculation of nano-silver content in spiked exposure media. Where $[Ag]_{NP}$ is the concentration of the AgNP fraction within the exposure vessel, $[Ag]_{Tm}$ is the measured concentration of the UC bottom fraction or the UF filtrand, D is the dilution factor from sample preparation and C is the nanoparticle concentration factor from UC or UF.

$$[Ag]_{\mathrm{NP}} = (([Ag]_{\mathrm{tm}} \times D) - [Ag]_{\mathrm{d}}) \div C$$

Equation 3.3 - Calculation of nanoparticle dissolution. The dissolution of each sample (% total Ag) is the concentration of the dissolved fraction of the spiked exposure media ($[Ag]_d$) as a percentage of the concentration of both the nanoparticle and dissolved silver fractions.

$$\%\ \text{dissolution} = \left(\frac{[Ag]_{\mathrm{d}}}{[Ag]_{\mathrm{d}} + [Ag]_{\mathrm{NP}}}\right) \times 100$$

3.3 Results and Discussion

3.3.1 Importance of media composition in nanoparticle toxicity testing

The potential impact of the concentration of *D. magna* culture media on cit-AgNP acute immobilisation exposures was assessed in media1 and media10. Groups of *D. magna* neonates were exposed to increasing concentrations of cit-AgNPs, as well as Ag^+ ions to control for any non-nanoparticle specific effects in media1 and media10 only. Under all conditions, immobilisation followed a concentration-dependent pattern with an absence of adverse effect in both the negative and capping agent controls. For cit-AgNPs in media10 a lowest observed adverse effect concentration (LOAEC) of 2.5 µg/l was observed, with total immobilisation occurring at 10 µg/l (Figure 3.1). The corresponding LOAEC in media1 was 11.25 µg/l and, despite an increased exposure range of up to 20 µg/l, complete immobilisation was not achieved (Figure 3.1). The EC_{50} for AgNPs was calculated as 7.70 µg/l in media10 and nominally stated as being 20.00 µg/l in media1. Due to the incomplete dose-response curve in media1, a comparison by sum of squares F-test was not possible. However, in media1 the lowest observed effect is induced at a concentration shown to cause total immobilisation in media10. The non-nanoparticle control exposures of $AgNO_3$ in media10 began inducing immobilisation from 0.31 µg/l until total immobilisation was observed at 3.15 µg/l. In media1, immobilisation was induced between 0.63 and 1.12 µg/l until total immobilisation was observed at 1.49 µg/l. Through use of the logistic approach EC_{50}s were calculated as being 0.61 µg/l in media10 and 1.10 in media1. These two EC_{50}s were deemed as not being significantly different through use of a sum-of-squares F-test, nevertheless the EC_{50} of $AgNO_3$ in media1 is greater than in media10.

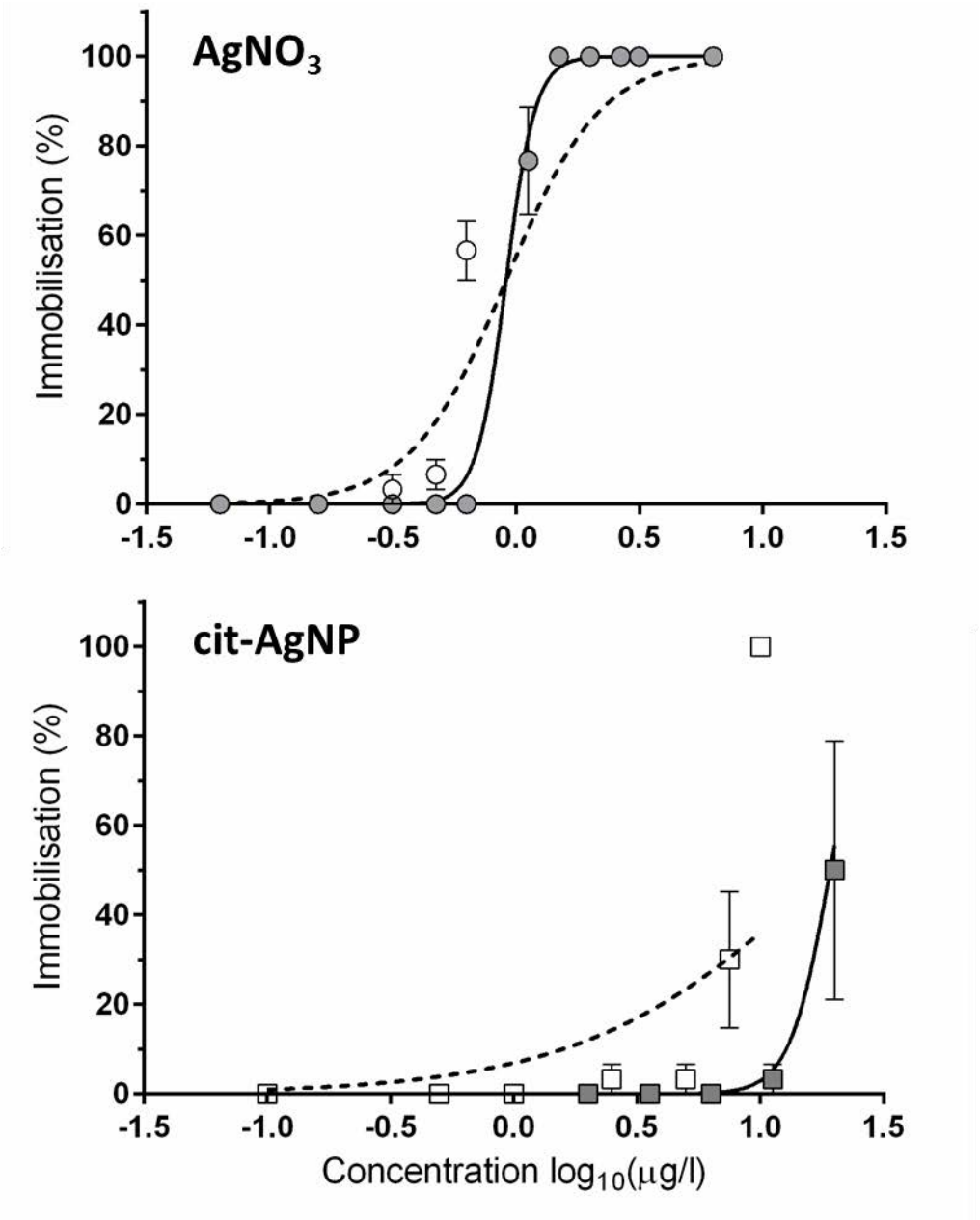

Figure 3.1 - Sigmoidal dose-response curves showing the mean percentage immobilisation of *D. magna* neonates (n=3) ± SEM in response to increasing concentrations of Ag^+ ions (a) and cit-AgNPs (b) in media1 (grey) and media10 (clear). The concentration of total Ag has been log_{10}-transformed for the application of the logistic model. Media1 and media10 dose-response curves for each toxicant were compared by a sum-of-squares F-test. Log EC_{50} values of $AgNO_3$ exposures in media1 and media10 were determined as the same for each data set ($p>0.05$) whereas comparison of AgNP exposures was not possible due to incomplete characterisation in media1.

These results suggest that the toxicity of the cit-AgNPs used in this study is impacted by the composition of exposure media. This potential media-dependant reduction in toxicity could occur for two reasons. Firstly, if AgNP toxicity is mediated by the free silver ion as previously hypothesised, the decreased concentration of chloride ions in media10 could allow for greater availability of the free silver ion which could also potentially result in an increase in AgNP toxicity. The non-nanoparticle control of $AgNO_3$ does show a slight, yet insignificant reduction in toxicity to *D. magna* when dispersed in media1 compared to media10. This slight change may be due to the higher concentration of Cl^- in media1 driving an increased formation of insoluble AgCl thus reducing the bioavailability of Ag to *D. magna*. However if the formation of AgCl does reduce the toxicity of $AgNO_3$ it does not do so significantly between these two compositions of media (Figure 3.1).

Secondly, as would be expected from DVLO theory, the reduced concentration of ions in media10 could allow for greater dispersal of the citrate-capped nanoparticles, which could result in greater nanoparticle toxicity. This second potential explanation was investigated through measurement of the size distribution and circularity of the particles in these media as well as an additional dilution (media2). The size distributions of particles were measured by TEM and AFM, and the circularity ratio of particles – a measurement of particle shape – was measured by TEM. In media1 and media2, it was not possible to determine an accurate distribution of primary particle size due to the presence of large polydisperse particles and aggregates (Figure 3.2). In media10, particle aggregates were not observed and as such it was possible to measure an accurate size distribution by both TEM (10 ± 5nm) and AFM (7 ± 3nm) of the mono-disperse particles in suspension (summarised in Table 3.5). A statistical comparison of primary particle size distributions between media was therefore not possible, but aggregation of particles in media1 and media 2 is apparent through observation by TEM (Figure 3.2).

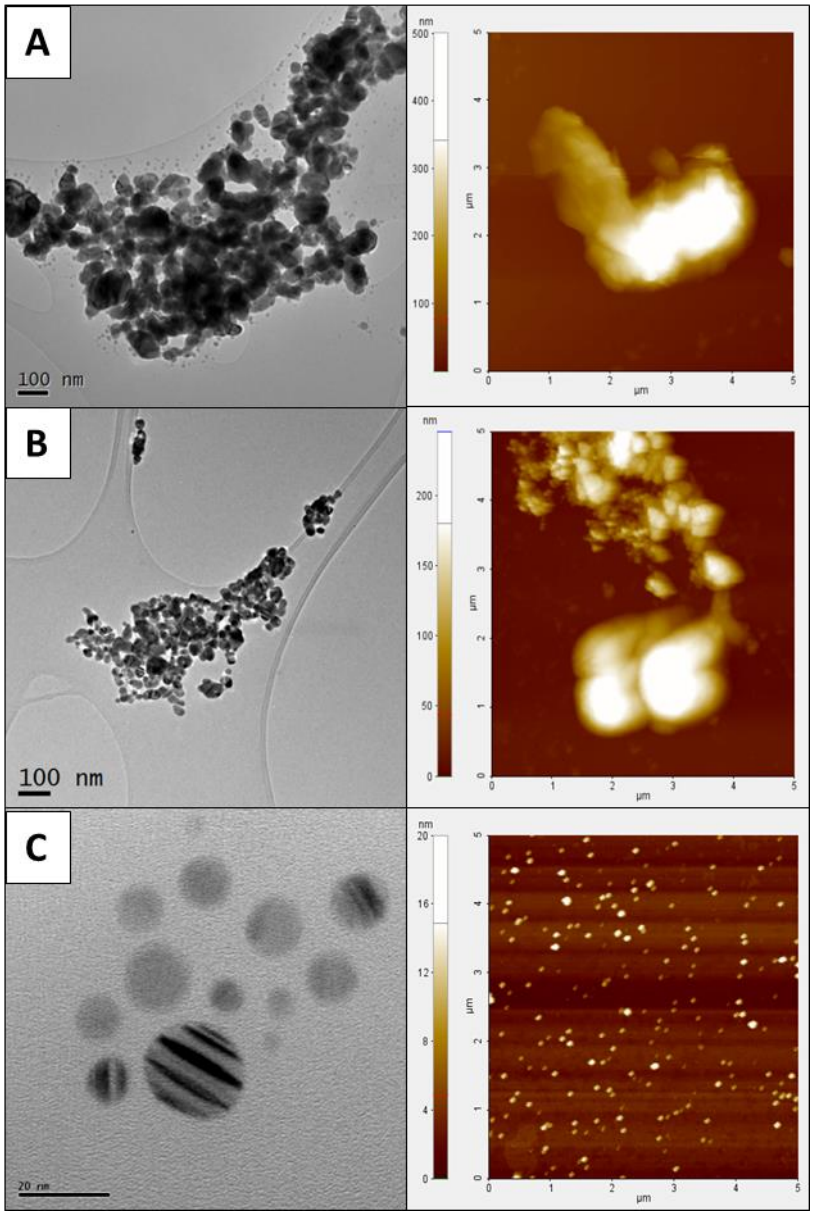

Figure 3.2: TEM (left) and AFM (right) images of cit-AgNPs suspended in standard OECD ISO test water (media1 (A)), as well as a 2-fold (media 2 (B)) and 10-fold dilution of the media (media10 (C)). The TEM scale bar represents 100 nm in images A and B, but 20 nm in image C. In the two most concentrated media (images A and B), large particle aggregates can be seen whereas in media10 (C) particles are evenly dispersed with little observed aggregation. Images are representative of 3 separate dispersions in each media type (adapted from Romer et al 2013).

Table 3.5 - The size-ranges (nm) of single particles, particle aggregates and circularity ratios of cit-AgNPs suspended in media1, media2 and media10 as measured by TEM and AFM. The mean particle size measurements are calculated from a minimum of 100 observations across 3 replicate dispersions in each media type. Accurate particle size distributions could not be made in media1 or media2 due to the presence of large polydisperse aggregates. In these cases the approximate range of single particle sizes is included. Table adapted from Romer et al., 2013. A 1-way ANOVA indicated the circularity of particles in media1 and media2 were not significantly different ($p=0.9388$), but that particle circularity of particles in media 10 were significantly different compared to in media1 and media 2 ($p<0.001$ in both cases).

Measurement	Range of aggregate sizes TEM (nm)	Single particle size TEM (nm)	Single particle size AFM (nm)	Circularity (from TEM)
Media1	50 - 3300	2 - 40	N/A	0.28 ± 0.13
Media2	60 - 1100	3 - 60	N/A	0.25 ± 0.12
Media10	N/A	10 ± 5	7 ± 3	0.95 ± 0.06

The circularity ratios obtained for media1 and media2 were 0.28 ± 0.13 and 0.25 ± 0.12 respectively (Table 3.5) suggesting the presence of irregular-shaped particle aggregates (Stevenson et al., 2012). Values for circularity of cit-AgNP suspension in media10 were much closer to 1 (0.95 ± 0.06) suggesting the presence of circular structures which were confirmed as disperse particles by TEM (Figure 3.2). Following a 1-way ANOVA and Tukey post-hoc test, the circularity of particles suspended in media1 and media2 were not shown to be significantly different ($p=0.9388$). Conversely, circularity of cit-AgNPs suspended in media 10 were seen to be significantly different to suspensions in both media1 and media2 ($p<0.001$).

These results suggest that dilution of media1 to media10 has resulted in reduced aggregation of cit-AgNPs and increased particle dispersion and stability. This results corresponds with data published previously where these same particles were measured in media1, media2 and media10 using DLS and Fl-FFF (Römer et al., 2011). This increased stability could be a result of the reduced overall ionic strength of the media. It has been previously noted that the overall concentrations of salts within exposure media can affect the stability of AgNPs (Badawy et al., 2010) and induce the formation of aggregates (Römer et al., 2011; Tejamaya et al., 2012). Likewise this increased stability could be the result of a reduction in any of the individual ions that are present in the media. It has been shown, for example, that millimolar concentrations of Ca have been shown to induce aggregation of AgNPs (Badawy et al., 2010; Piccapietra et al., 2012; Behra et al., 2013). The nominal concentration of $CaCl_2$ in media1 is 2mM compared to 0.2 mM in media10 which could explain the decreased aggregation of AgNPs.

When the cit-AgNP stability data in media1 and media 10 are coupled with the corresponding toxicity data, it is possible to infer that when media1 is diluted to media10, cit-AgNPs are more dispersed leading to a truer assessment of AgNP toxicity to *D. magna*.

The overall ionic strength of the two dilutions of media were not measured, neither were the individual concentrations of the constituent salts. Therefore the exact route cause of this increased stability it cannot be categorically concluded. Regardless of the initial cause, it is apparent that the stability of particles within this media is increased, and previous work in this medium has identified an absence of acute and chronic effects on *D. magna* cultured in this media (Römer et al., 2011). This therefore makes media10 an adequate candidate for AgNP exposures.

3.3.2 Characterisation of PVP-AgNP and Ag^+ toxicity to *D. magna* in media10

In addition to media composition it is possible to reduce the likelihood of particle aggregation further by using AgNPs capped with a more stable capping agent. PVP-AgNPs have been shown previously to be very stable in the three dilutions of media used here (Tejamaya et al., 2012). In order to ensure that all following exposures are with fully dispersed AgNPs, a combination of PVP-AgNPs and media10 was used. The results of initial range-finding studies revealed that the EC_{50}s of PVP-AgNPs at 24 and 48 h lie between 1 µg/l and 10 µg/l, respectively, and the $AgNO_3$ EC_{50}s lie between 0.1 µg/l and 1 µg/l. Following the results of these studies, exposures were designed within these concentration ranges in an attempt to fully characterise the dose-response relationship between the exposure concentration of these toxicants and the endpoint of daphniid immobilisation (Figure 3.3). The EC_{50}s for both AgNPs and Ag^+ were calculated at 24 h and 48 h post-exposure with the EC_{50} for Ag^+ calculated from the corrected weight of $AgNO_3$ to account for relative weight of Ag^+. At 24 h, the EC_{50} values for AgNP and Ag^+ are 7.24 µg/l and 0.48 µg/l respectively. At 48 h the toxicity of both toxicants appears to increase slightly, with EC_{50} values of 4.82 µg/l and 0.40 µg/l for PVP-AgNPs and Ag^+ ions respectively. EC_{50}s for PVP-AgNPs and Ag^+ ions were found to be significantly different at 24 h ($p < 0.0001$) and again at 48 h ($p < 0.0001$). A full account of EC_{50}s and 95 %

confidence intervals for PVP-AgNPs, $AgNO_3$ and the corrected values accounting for relative weight of Ag^+ from $AgNO_3$ are tabulated in Table 3.6. It is apparent from these results that dissolved silver ions are significantly more toxic to *D. magna* neonates than the nanoparticles used in this study. The EC_{50} values obtained here are similar to those reported in previous published material (Hoheisel et al., 2012; Asghari et al., 2012; Newton et al., 2013; Ribeiro et al., 2014), which all observed dissolved Ag (from $AgNO_3$) as being significantly more toxic than AgNP.

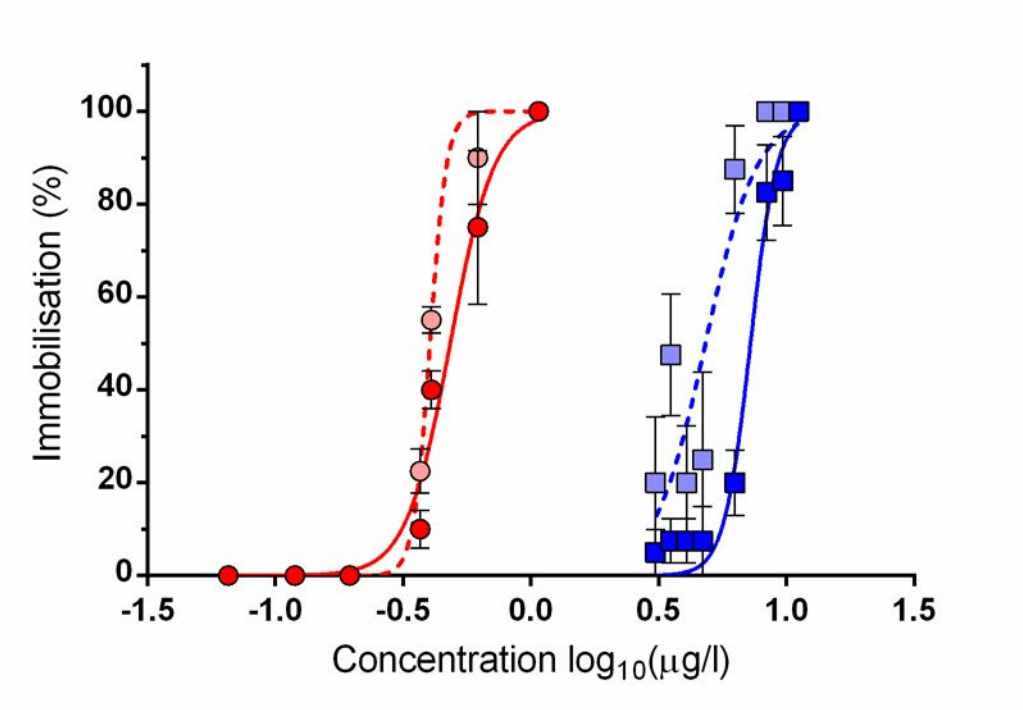

Figure 3.3: Sigmoidal dose-response curves showing the immobilisation of *D. magna* neonates in response to increasing concentrations of PVP AgNPs (blue squares) and $AgNO_3$ (red circles) over 24 h (darker coloured symbols, solid line) and 48 h (lighter coloured symbols, dashed line) exposure durations. Concentrations are given as log10 transformations of the theoretical total Ag concentration of each exposure group. Points represent average number of immobilised organisms (n=4) ± standard error of the mean.

Table 3.6: Median effect concentrations (EC_{50}) in µg/l of PVP-AgNPs, and $AgNO_3$ after 24 h and 48 h exposures to *D. magna* neonates. $AgNO_3$ concentrations are given as theoretical total Ag concentration. Lower (LCI) and upper (UCI) 95% confidence intervals are also shown.

		Concentration (µg/l)		
Toxicant	**Time-point**	**EC_{50}**	**95 % LCI**	**95 % UCI**
PVP-AgNP	24 h	7.24	6.80	7.71
	48 h	4.82	4.21	5.53
Ag	24 h	0.48	0.44	0.53
	48 h	0.40	0.39	0.41

3.3.3 Measuring dissolution of AgNPs in *D. magna* exposure media

The two techniques used to separate the nanoparticle and ionic components of PVP-AgNPs yielded differing results which are compared in Figure 3.4. When using UC, it is suggested that the majority of total measured silver was in the dissolved form prior to acidification. At 0, 24 and 48 h post-exposure, Ag^+ accounted for 89.75 ± 3.49, 82.48 ± 4.49 and 87.40 ± 3.17 % of the total silver concentration respectively (Figure 3.4 (a)) suggesting the nanoparticles almost completely dissolve upon addition to the exposure media. As can be seen from the dose-response characterisations in this chapter (Figure 3.3, Table 3.6), the dose response curves and EC_{50} values for PVP-AgNP and Ag^+ (both at 24 and 48 h) are significantly different from one another. If the results of the UC study are a true reflection of PVP-AgNP dissolution, then this should be reflected in the toxicity data; i.e. the nanoparticle EC_{50} should be much closer to the dissolved Ag EC_{50} due to the presence of high concentrations of dissolved Ag. Although the two fractions themselves

were not checked for the presence of particles by an observational technique, if 80 - 90 % of the particles were to dissolve upon addition to media, it would have made characterisation by TEM difficult. This leads me to surmise that these results are inaccurate, and that either UC simply does not affect particles of this size (10 nm) or that the pellet formed was very unstable and re-suspended before the layers were separated. In contrast to UC, the dissolution study using UF suggests a much lower level of dissolution that does not appear to change significantly over the 48 h exposure period (Figure 3.4 (b)). It is also apparent that despite repetitive cleaning washes, a minor background of dissolved Ag^+ is inevitable. Immediately after addition to exposure media, Ag^+ ions accounted for 4.05 ± 1.15 % (mean ± SD) of the total Ag concentration. After 24 and 48 h in exposure media, the average concentration of the dissolved silver component was 5.68 ± 2.87 and 8.15 ± 3.60 % of the total concentration of Ag respectively (Figure 3.5). These values are similar to previously reported % dissolution values for PVP-coated AgNPs (Zhao and Wang, 2012a; Yang et al., 2012; Groh et al., 2014). The results of the UF dissolution study will therefore be used to control for Ag^+ release from the AgNP exposures over the defined exposure period.

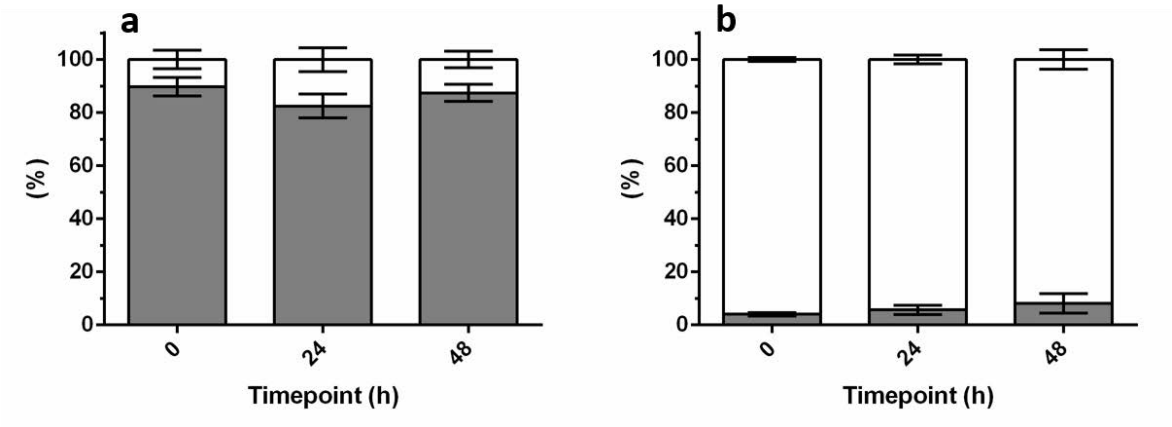

Figure 3.4: Relative mean percentage ± SEM of nanoparticle (white) and dissolved (dark grey) silver in terms of total silver as determined by ultracentrifugation (A) and ultrafiltration (B) taken at 0, 24 and 48 h post-exposure. Error bars are representative of the standard deviation, n=3 per time point. A 2-way ANOVA followed by Sidak's multiple comparison test determined no significant change in concentration of either form of silver over time. In both cases the technique was deemed to have a significant impact upon the proportions of nanoparticle and dissolved silver ($p<0.0001$)

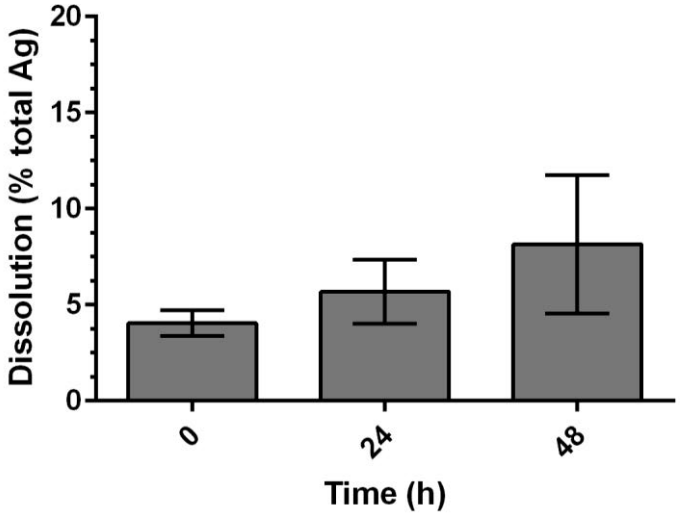

Figure 3.5: Relative mean percentage ± SEM (n=3 per time point) of ionic silver in terms of total silver as determined by ultrafiltration 0, 24 and 48 h post-exposure. The apparent increase over time was determined to be not-significant by 1-way ANOVA (p=0.4226).

3.4 Conclusions

TEM and AFM confirm that cit-AgNPs suspended in media10 are dispersed, whereas in media1 the formation of aggregates is observed. This observed increase in stability with reduced nominal concentration of salts within culture/exposure media is in accordance with DLVO theory, whereby an increased ion concentration shields the surface-charges of nanoparticles allowing them to come into sufficiently close contact for aggregation to occur. The observed significant reduction in toxicity of AgNPs dispersed in media1 is not seen for $AgNO_3$ in media10 suggesting that this is a consequence of nanoparticle aggregation and not increased sequestration of the dissolved component by Cl^- ions. To fully assess the toxicity of AgNPs we need them in their dispersed form (Stevenson et al., 2012). From the results of this and previous studies (Römer et al., 2011; Tejamaya et al., 2012) it is clear that media10 presents an ideal medium in which to achieve increased particle dispersal for toxicity assessment. In addition to this, the likelihood of particle aggregation can be reduced further through use of capping agents that induce stability through steric hindrance and not charge-based repulsion. PVP-AgNPs have been shown previously to be very stable in the three dilutions of media used here (Tejamaya et al., 2012). In order to ensure that all following exposures, specifically those intended to induce a sub-lethal toxic response, are with fully dispersed AgNPs, a combination of PVP-AgNPs and media10 was used.

The fully characterised dose-response curves and EC_{50} values for PVP-AgNPs and $AgNO_3$ reflect the same comparisons in previously reported studies (Hoheisel et al., 2012; Asghari et al., 2012; Newton et al., 2013; Ribeiro et al., 2014) that conclude dissolved silver (from $AgNO_3$) is more toxic to *D. magna* than AgNPs. This is an observation that has also been made in the comparison of other metal or metal-oxide nanoparticles with the EC_{50}'s of their respective dissolved forms (Notter et al., 2014). The dissolution of PVP-AgNPs over

24 h and 48 h, measured by ICP-MS following UF, were found to be similar to previously reported values (Zhao and Wang, 2012a; Yang et al., 2012; Groh et al., 2014).

For the planned exposures for omics analyses, the planned concentration of the dissolved-Ag groups would be 5.68 ± 2.87 % over 24 h or 8.15 ± 3.60 % over 48 h of the AgNP w/v concentration. This would be to ensure animals in the dissolved-Ag control groups were exposed to the same concentration of dissolved Ag as animals in the respective AgNP groups. The 48 h exposure duration suggested by the OECD is designed to observe a final outcome of immobilisation or organism death whereas the initial transcriptional response to toxicant exposure and likewise the resulting impact on metabolism will occur much earlier, within the first 24 h. Therefore, an exposure duration of 24 h was selected as the optimum window to capture the transcriptional and metabolic response. This exposure duration has been used previously in –omic analyses of *D. magna* toxicity tests (Poynton et al., 2012). To detect the subtle molecular responses of *D. magna* to AgNP and AgNP exposure, a range of concentrations was selected – thus enabling identification of potential concentration dependant responses – which are high enough to induce a subtle response but low enough avoid lethality. The lowest observed adverse effect concentration (LOAEC) of PVP-AgNPs was observed to be approximately 4.70 µg/l over 24 h and 3.08 µg/l over 48 h. Only three neonates were immobilised at this concentration at 24 h suggesting a threshold point between maximum tolerance and immobilisation. The LOAEC for the chosen exposure period was therefore selected as the maximum PVP-AgNP exposure concentration. Following the results of the UF dissolution test, the Ag control concentrations would be 5.68 ± 2.87 % of the AgNP w/v concentration.

Chapter 4: Determining the role of Ag^+ ions in AgNP toxicity

4.1 Introduction

Studies investigating AgNP toxicity often centre on whether dissolved Ag released from the nanoparticle surface is the sole cause of nanoparticle toxicity (Lubick, 2008). From the literature (reviewed in section 1.2.3) it is possible to conclude three potential MoAs relating to the role of dissolved Ag in AgNP toxicity to *D. magna* (Figure 4.1). Firstly, AgNPs dissolve within the exposure medium and the resulting dissolved Ag is absorbed by *D. magna*, primarily at the site of ion-exchange, resulting in a toxic response. Secondly, both the AgNP and any dissolved Ag are absorbed by *D. magna* and induce independent but potentially synergistic mechanisms of toxicity. The third possibility is a 'Trojan Horse' mechanism, whereby AgNP dissolve internally following absorption by *D. magna*; this results in a highly-concentrated, localised release of Ag. Toxicity in the Trojan horse mechanism is thought to be induced primarily by the dissolved silver, with AgNPs being the vehicle for delivery.

The primary aim of this chapter was to determine which of these potential mechanisms are true for AgNP. To that end, using optimal exposure conditions determined in Chapter 3, *D. magna* neonates were simultaneously exposed to AgNPs and to the concentration of the dissolved Ag fraction (from $AgNO_3$) measured to be released from these particles into media10 over a 24 h exposure period (section 3.3.3). The impact of these exposures was then assessed by a custom Agilent *D. magna* microarray, and by direct infusion FT-ICR MS; the resulting data were analysed by multivariate and univariate statistical analyses.

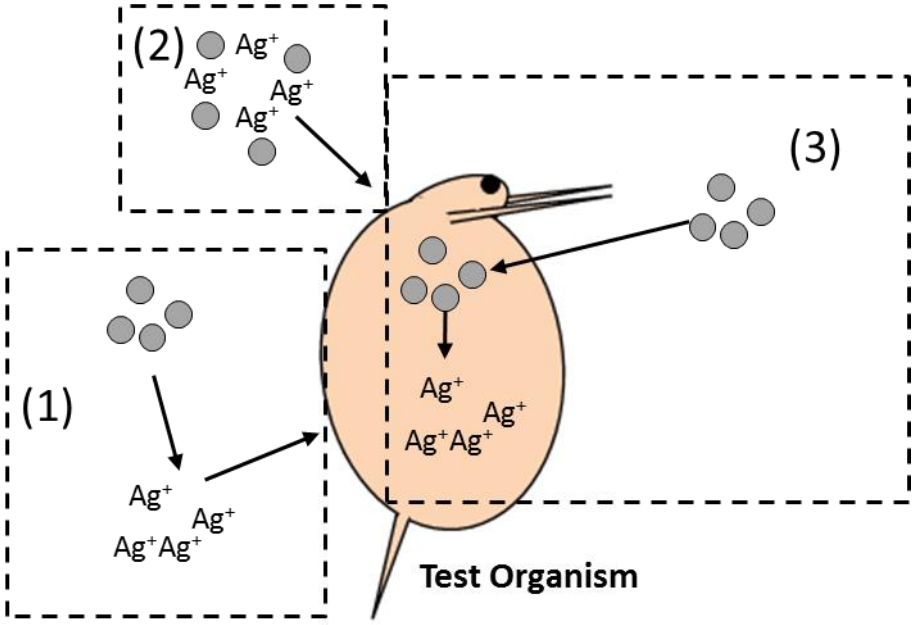

Figure 4.1 The three hypothesised roles of Ag^+ in AgNP toxicity to *D. magna*. (1) AgNPs dissolve completely externally to the organism and toxicity is induced by the dissolved silver alone. (2) AgNPs are absorbed by the organism and exert toxicity by an independent and potentially synergistic mechanism to dissolved Ag. (3) AgNPs are absorbed and dissolve internally, resulting in a concentrated release of Ag^+ which are then the sole mediators of toxicity.

Similarities or discrepancies between these exposure profiles measured by this dual-omics approach will give an enhanced insight into the role of dissolved Ag in AgNP-induced toxicity through a direct comparison of the induced molecular level changes. Certain molecular responses have been shown to occur following exposure to both Ag and AgNP. For example, Ag^+ is known to impact Na^+/Cl^- transport and Na^+/K^+-ATPases, an effect which may be reflected in the transcription of their respective genes. AgNP have been also observed to disrupt the transport of Na^+ by these enzymes but at a reduced level (Stensberg et al., 2013). Both forms of silver have also been identified as causing an increase in protein-thiols (Rainville et al., 2014), such as glutathione, cysteine residues and metallothioneins. Impacts on amino acids and sugars have been measured as being similar for both forms of silver (Li et al., 2015a), as has their impact on genes for oxidative phosphorylation complexes I, II, III and IV (Aerle et al., 2013). If AgNP toxicity is due solely to the dissolved fraction, which would be the case in both mechanism 1 and 3 above (Figure 4.1), we would expect to see similar changes in the molecular response of *D. magna* exposed to AgNPs and to the respective dissolved fraction alone.

Likewise any discrepancies in the MoAs of AgNP and Ag^+ ions will be observed. For example, as well as the reduced efficiency for Na^+ transport disruption of AgNPs mentioned above (Stensberg et al., 2013), other molecular effects have been identified which are specific to either AgNP or dissolved Ag exposure. It is known, for example, that AgNPs and Ag^+ ions enter cells by differing methods; Ag^+ ions through ion-transport pumps (Bury and Wood, 1999) and AgNPs primarily by clathryn-mediated endocytosis (Asharani et al., 2009). There may be differing levels of expression in the genes associated with these processes upon exposure to either dissolved silver or AgNPs. High-throughput superSAGE (serial analysis of gene expression) in zebrafish embryos identified 13 *D. magna* genes unique to the response to AgNP exposure and 32 genes unique to

dissolved Ag treatment including cyclic AMP-dependent transcription factor ATF-4 (Aerle et al., 2013). If AgNPs induce an independent molecular response, the patterns of gene-expression and metabolite production will be noticeably different to those induced by $AgNO_3$ exposure.

In this chapter a dual-omics approach is taken to compare the perturbations induced in the overall transcriptional and metabolic profiles of *D. magna,* following exposure to increasing concentrations of AgNPs and $AgNO_3$. As an additional stage of investigation, the uptake and elimination of Ag in *D. magna* at these concentrations was assessed. By confirming the presence of Ag within or on the organisms it will allow the differentiation between some of the hypothesised mechanisms. If only dissolved silver is available to *D. magna* neonates then these exposures will result in similar concentrations of Ag associated with the exposed neonates. If the nanoparticle form of silver is ingested, then a greater Ag body burden would be expected in those animals exposed to AgNPs. The pattern of Ag elimination from the organisms can give an insight into the extent of Ag accumulated within tissues and cells.

4.2 Materials and Methods

4.2.1 Sub-lethal omics exposure studies

Nominal exposure concentrations of 4.70, 2.35, 1.18 and 0.59 µg/l AgNPs (AgNP High, Mid, Low and V. Low respectively) were used alongside nominal concentrations of 0.44, 0.22, 0.11 and 0.06 µg/l $AgNO_3$ (Ag^+ High, Mid, Low and V. Low respectively). These exposure concentrations of $AgNO_3$ equate to 0.28, 0.14, 0.07 and 0.04 µg/l of total Ag corresponding to approximately 6 % of the respective AgNP exposures. Untreated (deionised water; no-added silver), capping agent (0.03 % v/v. PVP) and bulk silver (4.7 µg/l, 3µm average diameter, Sigma Aldrich) controls were used to account for background mortality, any potential impact of the capping agent, and to control for potential aggregation effects respectively. The Ag filtered from the AgNP stock prior to use was included as an additional filtrate control. Each group contained 6 biological replicates and all exposures were performed in media10. For each desired control, AgNP and $AgNO_3$ exposure concentration to be used, a 250-fold concentrated stock was made. A master sock of PVP-AgNPs was prepared as outlined in section 2.3 and measured by ICP-MS (section 2.3.3) to have a concentration of 14.7 mg/l. Separately, 117.5, 58.8, 29.4 and 14.7 µl of this stock were diluted with MilliQ water to a volume of 10 ml to produce spiking stocks for the AgNP High, Mid, Low and V Low groups respectively. A $AgNO_3$ Master-Stock was produced as before (section 3.2.4) by weighing 100.5 mg $AgNO_3$ into 100 mL MilliQ water to give a nominal concentration of 1 g/l. This stock was subsequently diluted 1 in 100 followed by a subsequent 1 in 10 dilution to produce a working stock with a nominal concentration of 1 mg/l. Seperately, 1100, 550, 275 and 150 µl of this stock were diluted to 10 ml with MilliQ water to produce spiking stocks for the Ag^+ High, Mid, Low and V Low groups respectively. The exposure groups used and the desired nominal exposure concentrations are outlined in (Table 4.1).

Table 4.1 Outline of the nominal exposure concentrations for AgNP and $AgNO_3$ exposures for omics analysis. All concentrations are in terms of total Ag content with the exception of the PVP-control which is % volume/volume.

	Nominal concentrations (µg/l)			
	High	Mid	Low	V.Low
AgNP	4.70	2.35	1.18	0.59
$AgNO_3$ (total Ag)	0.28	0.14	0.07	0.04
No-silver control	0.00			
PVP-control	0.03% v/v			
Bulk silver control	4.70			

Each biological replicate consisted of 30 *D. magna* neonates (<24 h) with 6 biological replicates per treatment group. The AgNP High group had an additional 2 replicates (n = 8 in total) to account for potential mortalities induced by the higher concentration. Groups of 30 *D. magna* neonates (<24 h) were added to individual exposure vessels (250 ml glass beaker, Fisher Scientific) containing 200 ml of media10. The appropriate spiking stock (1 ml) was then used to spike the study medium followed immediately by 49 ml of additional media10 to mix. Exposure vessels were kept as described in section 2.5. Tests were only considered valid if no more than 10% of control animals were immobilised during the exposure. Following exposure, animals were filtered from media into a precellys homogenization tube (Stretton Scientific Ltd., UK), flash frozen in liquid nitrogen and stored at -80 °C prior to extraction.

4.2.2 Dual-omics extraction protocol

Frozen animals (30 neonates per sample) were homogenised using a Precellys-24 ceramic bead-based homogeniser (Stretton Scientific Ltd., UK) in 448 µl of a 5:2 mix of methanol

(HPLC grade): water (nuclease free, QIAGEN) for two 10 s bursts at 6400 rpm with a 15 s intermission then returned to ice. A 112 µl aliquot of homogenate was then removed into a nuclease-free microfuge tube (1.7 ml, Axygen) for RNA extraction and replaced with the same volume of 5:2 methanol:water. This aliquot was centrifuged for 5 minutes at 15,000 rcf in a bench-top microcentrifuge (5415D, Eppendorf) and the supernatant was removed. The pellet was then immediately re-suspended vigorously in 350 µl of guanidine-thiocyanate containing buffer (RLT buffer, QIAGEN) with added β-mercaptoethanol (1 µl per ml of buffer) and stored at -80 C for future extraction.

4.2.3 Bi-phasic extraction of polar metabolites

Polar metabolites were extracted using a two-step, biphasic method as detailed previously (Wu et al., 2008). Briefly, homogenate was transferred into 1.8 ml glass vials on ice and further volumes of nuclease free water (160 µl) and chloroform (320 µl) were added to produce a final solvent ratio of 2:2:1.8 methanol:chloroform: water (Wu et al., 2008). This mixture was then vortex-mixed for 30 s and left on ice for 10 minutes before being centrifuged (4000 rcf, 4 °C, 10 min) (Biofuge Primo R, Thermo Scientific) yielding a biphasic mixture separated by a layer of protein debris. The upper, polar layer of each sample was removed into a single 1.5 ml microfuge tube (Starstedt, Leicester, UK) via Hamilton syringe. The lower, non-polar layer was removed and prepared for FT-ICR lipidomic analysis which is not reported in this thesis (White, 2013). Polar extracts were dried under vacuum (Savant Refrigerated Vapour Trap, Thermo Scientific) using a centrifugal concentrator (Savant SpeedVac concentrator, Thermo Scientific) without application of heat and stored at -80 °C prior to FT-ICR analysis. Two extract blanks were created using the above homogenisation and extraction protocols in the absence of biological material.

4.2.4 Polar extract re-suspension for MS analysis

All frozen, dried, polar extracts were re-suspended by addition of 30µl 4:1 mixture of methanol:water with 20 mM ammonium acetate followed by vortex-mixing for 30 s for negative ion mode analysis. All re-suspended samples were centrifuged at 22,000 rcf, 4 °C for 10 minutes to remove particulate matter. The supernatant of each sample was then loaded alongside quality control (QC) samples in a randomly generated order on 384 well polymerase chain reaction (PCR) plates (Agilent technologies). QC samples were created from a pool of *D. magna* polar extract collected from a separately collected group of neonates. Once samples were loaded, wells were immediately covered with self-adhesive foil to temporarily prevent contamination or sample evaporation. Once an entire plate was loaded, it was permanently sealed using a single, heat-sealed, foil sheet (ALPS 50V, Thermo Fisher Scientific, US).

4.2.5 Acquisition of mass spectra

All extracts were analysed in quadruplicate using an LTQ-FT Ultra (Thermo Fisher Scientific, Bremen, Germany) hybrid LTQ FT-ICR mass spectrometer with a direct infusion, chip-based nano-electrospray ionisation source (Triversa, Advion Biosciences, Ithaca, NY). Nanoelectrospray conditions consisted of a 200 nl/min flow rate, 0.3 psi backing pressure and an electrospray voltage of either +1.7 kV or -1.7 kV in positive or negative ion mode respectively controlled by Chipsoft software (Advion, Ithaca, NY, USA). An automatic gain control setting of $1x10^6$ was used in combination with a mass resolution of 100,000 (FWHM at 400 *m/z*). Each technical replicate was analysed using Xcalibur software (Version, Thermo Scientific). Data were acquired as transients from *m/z* 70-590 using the selected ion monitoring (SIM) stitching methodology (Southam et al., 2007; Payne et al., 2009; Weber et al., 2011) in 7 SIM windows of 100 *m/z* width and

30 *m/z* overlap. Samples were analysed in a randomly generated order with QC samples spaced evenly throughout to disentangle MS technical drift from biological differences.

4.2.6 Mass spectral data processing

Transient data from the FT-ICR were processed, and the SIM stitch algorithm was applied as described previously (Southam et al., 2007; Payne et al., 2009). Briefly, transients were averaged and then transformed into spectra with Fast Fourier Transform (Comisarow and Melka, 1979) and calibrated using a list of defined peaks for each SIM window (Section 0). SIM window spectra were then 'stitched' together through the alignment of peaks in overlapping regions (30 Da) using the SIM-stitching algorithm (Southam et al., 2007). All peaks with intensities with a signal to noise ratio of less than 3.5 were removed, as were areas of 'mechanical noise' or 'high noise regions' in the *m/z* ranges of (*m/z* = (74.05-74.2); (90.50-90.58), (101.32-101.42); (101.6-102.1); (105.1-105.5); and (116.37 116.5)). This process resulted in four stitched spectra per biological sample; the three best quality replicates were then selected for further filtering. Replicate quality was primarily based on the variation of relative intensity within SIM windows. The spectra of the three selected technical replicates were then aligned and merged, with peaks being retained only if present in at least two of the remaining three replicates, thus resulting in one spectrum per biological sample. When aligning replicate spectra, peaks were considered to be the same if they occurred within a 1.5 ppm error of one another along the *m/z* axis. The spectra of all samples were then aligned and filtered with *m/z* peaks only being retained if they were present in at least 80 % of all experimental samples. Due to the differing origin of the QC samples, they were excluded from this process to avoid skewing the filter. When aligning sample spectra, peaks were considered to be the same if they occurred within a 2.5 ppm error of one another along the *m/z* axis. A blank filter was also applied; any of the remaining sample peaks which were also detected within the extract blanks were removed

from all spectra. All spectral processing steps were completed in MATLAB (student version 7, The Math-Works, Natick, MA). These processing steps yield a matrix of raw peak intensity values, with columns corresponding to *m/z* values and rows corresponding to samples, which require further processing before statistical analysis.

4.2.7 Probable Quotient Normalisation of *m/z* intensity matrices

To account for variation arising from differences in sample concentration, the resulting filtered matrix was normalised via Probable Quotient Normalisation (PQN) (Dieterle et al., 2006) using an in-house MATLAB script. Quotients of dilution were calculated by dividing the intensity of each peak in a spectrum by the mean intensity for that peak across all samples. The median quotient of the entire spectrum is then selected as the scaling factor (most probable quotient) for that spectrum. Quotients were only calculated for peaks that occurred in 100 % of all samples except QCs.

4.2.8 Missing value imputation by the k-nearest neighbour method

Due to the nature of the sample filter, some samples within the intensity matrix may not have intensity values for peaks which are otherwise detected in the remaining samples. To prevent miscalculation of fold changes, missing values were imputed using the k-nearest neighbour (KNN) algorithm using an in-house MATLAB script (Hrydziuszko and Viant, 2011). Briefly, the top k (in this study k = 5) peaks with the most similar intensity profiles across all samples were used to calculate a weighted average (the most similar peaks being favoured) for that sample. This value was then imputed in the place of the missing value. This normalised matrix with imputed missing values was used for the assessment of fold changes in peak intensities across groups and for univariate analysis to determine significantly changing peaks.

4.2.9 Generalised logarithm transformation for multivariate analysis

Peaks of naturally higher intensities are intrinsically prone to greater technical variation, in terms of absolute values, than those which are naturally lower in intensity. This can skew the results of multivariate statistical analysis. To counteract this, the normalised matrix was transformed using the generalised logarithm transformation (Parsons et al., 2007). This process uses a scaling factor (λ) derived from the QC samples i.e., samples between which, theoretically, the only variation is technical and not biological. This process stabilises technical variation and reduces dominance of large intensity peaks, allows for better observation of biological differences in subsequent multivariate statistical analyses such as PCA (Parsons et al., 2007).

4.2.10 Generation of calibration lists

In order to complete the processing workflow, a calibration list of robust peaks is required. This list is generated from a preliminary run of the steps outlined above but with the following exceptions. A signal:noise ratio of 10 was used instead of 3.5, only peaks occurring within all three technical replicates of a sample were kept, and finally only peaks which occurred in 100 % of samples were retained. This stringent filtering process ensured the retention of robust *m/z* features within the *D. magna* or *D. pulex* metabolome. Features retained from this process were putatively annotated using MI-Pack as outlined below using the single peak search function. The final calibration lists were created using a minimum of one successfully annotated *m/z* feature within each of the SIM windows. The calibrants used in this chapter are listed in the Appendix (Table 9.3).

4.2.11 Assessment of MS data quality

The quality of mass spectral data was assessed using two methods. First the analytical reproducibility (or precision) of the data was assessed through calculation of the median Relative Standard Deviation (RSD) of QC spectra. Briefly, the RSD was calculated for

each peak remaining from MS spectral processing from the respective intensity values within the QC sample population. The median RSD value was then taken as indication of analytical reproducibility as outlined previously (Parsons et al., 2009). A median RSD of <20% is deemed to be an acceptable level of reproducibility (Kirwan et al., 2014). The median RSD was also calculated for each control and exposure group as well as for all biological samples (not QCs) used within the study. Comparison of these values showed a much lower median RSD between the QC samples in comparison to the RSD of all biological samples; 12.0 % compared to 33.5 % respectively (Table 4.2) indicating that the analytical variation observed in the dataset is much lower than the background biological variation between unique replicates.. Next, the quality of the final processed dataset was assessed through a multivariate quality assessment as described previously (Sangster et al., 2006; Kirwan et al., 2014). Following the method outlined below (section 4.2.17), PCA was conducted on all biological samples and QC samples. The degree to which QC samples cluster relative to the variation in biological samples was then visualised as first outlined by Sangster et al., 2006. The tight clustering of QC samples observed in Figure 4.2 relative to the wide spread of the biological samples clearly indicates that the analytical variation within the dataset is small relative to the biological variation.

Table 4.2. Median Relative Standard Deviation (% RSD) of *m/z* peak intensities for QC samples compared to all control and exposure groups combined (Test samples) and seperately.

Exposure Group	Median % RSD
QC samples	12.0
Test Samples	33.5
PVP Control	33.7
Untreated Control	26.1
Bulk Ag Control	28.6
Ag^+ Filtrate	29.1
AgNP Very Low	22.2
AgNP Low	26.5
AgNP Mid	25.8
AgNP High	30.5
$AgNO_3$ Very Low	25.8
$AgNO_3$ Low	26.9
$AgNO_3$ Mid	26.7
$AgNO_3$ High	25.0

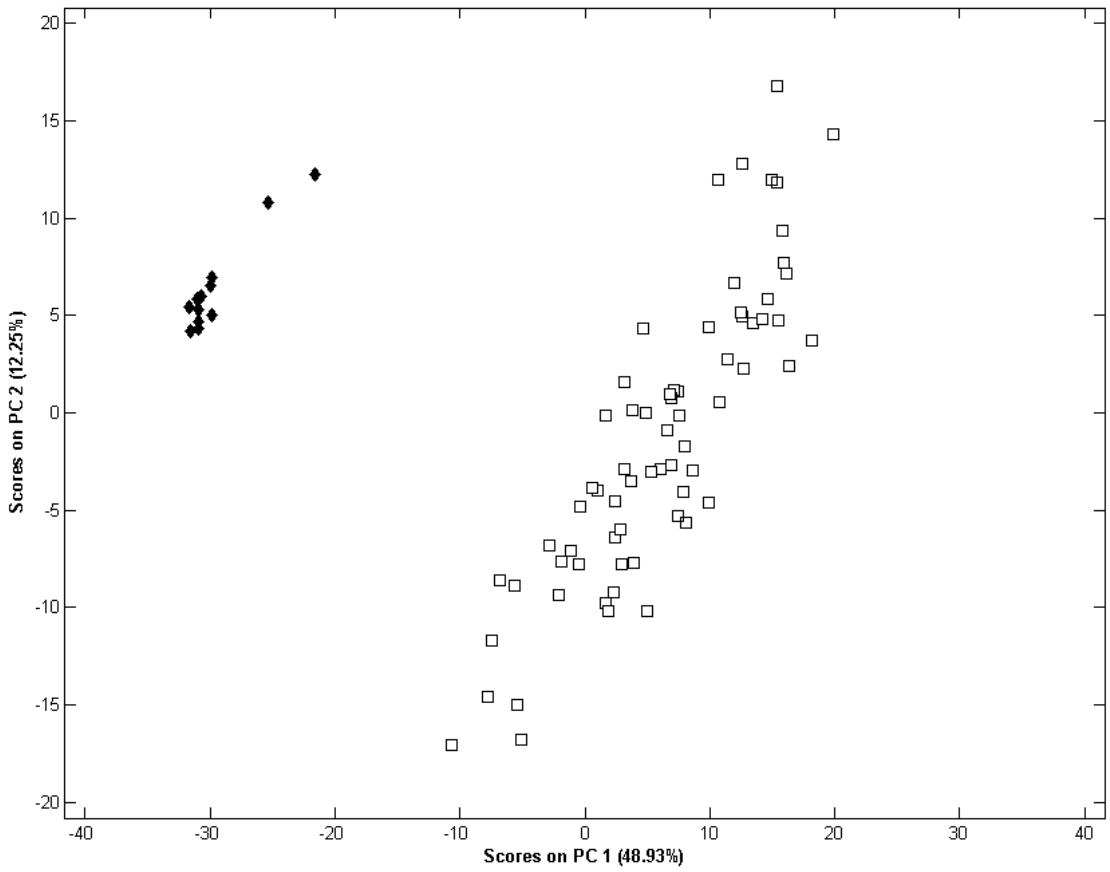

Figure 4.2: Principal components analysis comparing scores values on PC1 and PC2 of the model for all test organisms (□) and quality control (QC) samples (♦). The tight clustering of QC samples in comparison to the wide spread of the biological replicates indicates and absence of technical drift.

4.2.12 Extraction of total RNA

The homogenate aliquot in RLT buffer was thawed on ice and RNA extraction continued using a column-based extraction kit (RNeasy Mini Kit, QIAGEN) following manufacturer's instructions, including DNase1 treatment (RNase-Free DNase kit, QIAGEN). Briefly, 350 µl 70 % v/v ethanol was mixed with thawed aliquots and then spun through silica-based spin-columns (30 s, 8000 rcf) to allow RNA binding. Samples were then washed three times in low salt, ethanol buffers before elution in 40 µl nuclease free water. The quantity and quality of RNA was assessed using a spectrophotometer (NanoDrop 1000, Thermo Scientific, Waltham, MA) using an analysis constant of 40 for RNA. The integrity of all samples was measured using an Agilent RNA 6000 Nano Kit and an Agilent 2100 Bioanalyser (Agilent Technologies, Santa Clara, CA).

4.2.13 Ethanol/Acetate precipitation of RNA

Any RNA extracts with an A_{260}/A_{230} ratio (measured by nanodrop (Section 4.2.12) lower than 1.5 were cleaned using the ethanol/acetate precipitation method and then re-measured. Ethanol (100 %, 2 volumes, -20 °C) and sodium acetate (3 M, 0.1 volumes, pH 5.2) were mixed with each extract before incubation at -80 °C for 1 h. Samples were then centrifuged for 30 min at 4 °C and the supernatant was removed. The pellet was washed with ethanol (70 % v/v) and centrifuged before being air dried for 30 min. Once dry the RNA pellet was re-suspended in nuclease free water.

4.2.14 Amplification and Cy3-labelling of selected RNA samples

Only samples within the untreated, PVP and bulk control groups, the Ag^+ High and Ag^+ Low exposure groups and the AgNP High and AgNP Low exposure groups were selected for microarray analysis. The One-Color RNA Spike-In Kit (Agilent Technologies) was used to account for variation between the arrays as quality control. This kit contains a mixture of 10 positive control transcripts at known concentrations which anneal to

complementary probes on the microarray. This kit is an invaluable form of quality assurance, controlling for any abnormalities in the labelling and hybridisation procedure including the potential interference AgNPs may have with fluorescent dyes in use. The results of the QC probes were comparable across all groups, no differences were observed between control groups, AgNP or $AgNO_3$-exposed animals. One AgNP High failed QC as a result of non-specific hybridisation and was removed from future analyses. Briefly, the stock Agilent One Colour RNA Spike Mix concentrate was serially diluted four times (1:20, 1:25, 1:20 and finally 1:4) then 2 µl of the final dilution was added to 50 ng of each sample of total RNA. The labelling reaction was prepared using the one-colour Low Input QuickAmp Labelling kit (Agilent Technologies), according to manufacturer's instructions using an input of 50 ng of spiked-RNA. This kit employs a double amplification strategy in which the total RNA is first reverse-transcribed to cDNA which is then used to produce the fluorescent Cy3-CTP labelled cRNA. The labelled, amplified cRNA was made up to 100 µl with nuclease free water and was purified using an RNeasy Mini Kit (QIAGEN). Once purified, the labelled cRNA was quantified using the microarray measurement function on the NanoDrop with an analysis constant of 40 for RNA. From these measurements, the yield of cRNA (µg) and the specific activities of Cy3 per µg cRNA were calculated. All samples were found to have a specific activity above the recommended minimum value of 6 pmol Cy3 per µg cRNA.

4.2.15 Hybridisation and scanning of a custom *D. magna* microarray

The hybridisation and scanning of the microarray slides were conducted with supervision from the Genomics Facility, University of Birmingham. Following purification, Cy3-labelled cRNA samples (600 ng) were fragmented through addition of Agilent gene expression blocking agent (5 µl) and fragmentation buffer (1 µl) (Agilent Technologies) in a total reaction volume of 25 µl (made up waith nuclease free water) and incubated for

30 min at 60 °C. Fragmented cRNA was then immediately cooled on ice and mixed with 25 µl hybridisation buffer to stop fragmentation. Samples were hybridised to a custom *D. magna* gene expression microarray (Design ID: 023710, Agilent Technologies) as used previously (Poynton et al., 2012; Antczak et al., 2013; Scanlan et al., 2013). The array is constructed from 15,000 unique, best-responding probes from a preliminary microarray constructed from a *D. magna* expressed sequence tag database (Garcia-Reyero et al., 2009). The hybridized microarrays were scanned with an Agilent Technologies Scanner G2505B at 535 nm for Cy3. Scanned images were processed and results were extracted using Feature Extraction software (Agilent Technologies).

4.2.16 Microarray data processing

Microarray data processing and analyses were performed within Genespring analytical software (version GX7.3.1, Agilent Technologies). Prior to normalisation, low intensity values (< 0.01) were set to a minimum value of 0.01 intensity units. Each measurement was then normalised by the 50th percentile of all measurements within each individual sample-array. Each gene-probe was normalised by the median of its measurements across all sample-arrays. Genes with particularly low expression levels (< 40) were removed with background noise, as were genes whose standard deviation exceeded 1.4 in greater than 4 of the 7 exposure groups. The normalized microarray dataset were $\log_2$ transformed prior to multivariate statistical analysis.

4.2.17 Principal components analysis of multivariate data

PCA was used to assess the variation of glog-transformed metabolic and log-transformed transcriptional matrices in an unbiased manner. Prior to PCA model creation, glog or log-transformed intensity values for each variable (*m/z* peak or gene probe respectively) were mean centred. PCA models were then generated from mean-centred transformed matrices with 4 PCs for each model using the PLS_Toolbox (version 6.0.1, Eigenvector Research,

Manson, WA) within MATLAB. The significance of differences between scores values for each group was assessed along each PC by analysis of variance (ANOVA) using an in-house script in MATLAB. The p-values generated by this test were corrected using a FDR of 5 % to account for the multiple-testing of all PC scores (Benjamini and Hochberg, 1995). All QC samples were excluded from multivariate analyses.

4.2.18 Analysis of variance of individual peak intensities between exposure groups

One-way ANOVAs were used to determine those genes and *m/z* peaks that changed significantly in intensity between exposure groups. Multivariate and univariate statistical analyses indicated no significant differences between the untreated, PVP and bulk control groups as outlined in section 4.3.1. For this analysis samples in the untreated, PVP and bulk control groups were treated as a single group to identify only those variables which changed significantly in response to Ag exposure. Briefly, mean intensity values of the combined control and all exposure groups were compared by one-way ANOVAs for each individual m/z peak or gene. Due to the large size of metabolomics and transcriptomics datasets, the comparison of multiple variables in this manner is likely to induce a large number of false positives. For example, using a significance value of 0.05 for each test could potentially mean that of the multiple comparisons taking place, 5 % could be incorrectly assigned a significant p-value. This false discovery rate is accounted for by calculating a corrected (or adjusted) p-value (Benjamini and Hochberg, 1995). The p-values generated from these tests were corrected using an FDR of 5 % to account for the multiple testing hypothesis (Benjamini and Hochberg, 1995). QC samples were not included in these tests.

4.2.19 AgNP and $AgNO_3$ uptake and elimination studies

In a separate set of exposures to the omics-analyses outlined above, *D. magna* neonates were exposed to nominal concentrations of 4.70 and 1.18 µg/l AgNPs as well as 0.44 and

0.11 µg/l $AgNO_3$ (theoretically equating to 0.28 and 0.07 µg/l total Ag) as well as untreated (no-added silver) conditions in media10. Spiking stocks were made using the AgNP master stock and $AgNO_3$ working stock previously described in section 4.2.1. Briefly, 1.6 ml and 100 µl of AgNP master stock (14.7 mg/l) were made to total volumes of 20 ml and 5 ml with MilliQ water to produce the AgNP High and AgNP Low spiking stocks respectively. Similarly, 2.2 ml and 140 µl of $AgNO_3$ master stock (1 mg/l), were made to total volumes of 20 ml and 5 ml in MilliQ water to produce the AgHigh and AgLow spiking stocks respectively. The concentrations of these spiking stocks were measured by ICP-MS as described in section 4.2.20 and are tabulated below along with their intended nominal concentrations (Table 4.3). Due to the limitations of ICP-MS, the concentrations of the individual water exposures were not measured.

Table 4.3: The nominal spiking stock and final exposure concentrations for all AgNP and $AgNO_3$ exposure groups alongside the measured stock concentrations and the estimated exposure concentrations derived from these values.

	Stock conc. (µg/l)		Exposure conc. (µg/l)	
Group	**Nominal**	**Measured**	**Nominal**	**Estimated**
Ag Low	17.5	30.8	0.07	0.12
Ag High	70	89.4	0.28	0.36
AgNP Low	295	293.2	1.18	1.17
AgNP High	1175	1108.3	4.70	4.43

Each biological replicate consisted of 30 *D. magna* neonates (<24 h) with 9 biological replicates per treatment group with the exception of the lower AgNP and $AgNO_3$ concentrations which only contained 3 biological replicates. Groups of 30 *D. magna* neonates (<24 h) were added to individual exposure vessels (250 ml glass beaker, Fisher Scientific) containing 200 ml of media10. The appropriate exposure stock (1 ml) was then used to spike the study medium followed immediately by 49 ml of additional medium10 to mix. Exposure vessels were kept under conditions outlined in section 2.5. Tests were only

considered valid if no more than 10 % of control animals were immobilised during the exposure.

After the 24 h exposure period, neonates were filtered and rinsed with Milli-Q water to remove any externally bound Ag (Khan et al., 2015). Three biological replicates from all treatment conditions (Control, AgNP Low, AgNP High, $AgNO_3$ Low and $AgNO_3$ High) were then blotted dry and transferred to pre-weighed, acid-washed 1.5 ml microfuge tubes. Tissue wet-weight was then determined by difference before samples were flash frozen in liquid nitrogen and stored at -80 °C prior to acid-digestion for ICP-MS analysis to determine initial Ag burden.

The remaining replicates were transferred via an intermediate "wash" beaker of Milli-Q water to a clean vessel of media10 with 0.5 ml algal feed to begin clearance of the gut contents thus ending internal exposure (Khan et al., 2015). After 18 h depuration, 3 biological replicates from the three exposure conditions were filtered, rinsed with Milli-Q water and then transferred into pre-weighed, acid-washed 1.5 ml Eppendorf tubes. Tissue wet-weight was determined by difference. Samples were flash-frozen in liquid nitrogen and then stored at -80 until needed for ICP-MS analysis. The exposure media of the remaining exposures was replaced at 18 h and then every subsequent 24 h until the end of the exposure. Fresh algal feed was added with every media change. After a total of 96 h, the remaining three replicates of the control, AgNP High and $AgNO_3$ High treatments were harvested as described for 0 h and 18 h post-exposure.

4.2.20 Preparation of samples for ICP-MS analysis of internalised silver

Frozen neonates (2.4 – 3.5 mg tissue at T=0, 2.9 – 4.8 mg of tissue at T= 18 h and 12.0 – 17.8 mg tissue at T=96 h) were submerged in 100 µl of concentrated (69 %) trace-metal grade nitric acid (Fisher Scientific), mixed by vortexing, and then allowed to digest

overnight. Once fully digested, samples were transferred to an acid-washed scintillation vial and diluted to approx 1 % acid by addition of ultrapure water to a total volume of 6.9 ml. A digestion blank was prepared following the same method but with no *Daphnia* included. The exposure stocks from section 4.2.19 were prepared for measurement in a similar way; 100 µl of stock was digested in 100 µl of trace-metal HNO_3 as described for *Daphnia* samples. Once digested these stocks were diluted to a total volume of 6.9 ml. All samples intended for measurement were shipped to the Swiss Federal Institute of Aquatic Science and Technology (EAWAG) for ICP-MS analysis by Dr Smitha Pillai (EAWAG, Dubendorf, Switzerland). The concentration of total Ag in all submitted samples was measured by high-resolution ICP-MS (ELEMENT 2, Thermo Scientific) with a lower limit of detection for Ag of 1 ng/l. Each sample was measured ten times from which an average measurement was taken. Blanks were measured after every ten samples alongside two references containing known concentrations of Ag. All blanks returned values below the 1 ng/l of total Ag detection limit. The results from the reference samples were used in the normalisation of sample concentrations. The measured concentrations of the reference samples were within acceptable ranges. The measured internal concentrations of silver of individual samples were normalised by their individually measured sample wet-weight. A 1-way ANOVA was used on the same data followed by a Tukey post-hoc test to compare the differences in Ag body-burdens between treatment groups. The uptake and data was also analysed by 2-way ANOVA followed by Sidak's multiple comparison test to compare the effects of concentration and treatment type on Daphnid Ag body-burden. Depuration data was analysed using a 2-way ANOVA followed by Sidak's multiple comparison test to compare the impact of total depuration time and treatment type on the body burden of Ag-exposed Daphnia in terms of % initial body burden.

4.3 Result and Discussion

4.3.1 Exposure to the capping agent and bulk-Ag controls does not induce an adverse transcriptional or metabolic response.

All neonates from the no-added silver, PVP and bulk silver (3 μm average diameter) control survived the 24 h exposures indicating a valid experiment (Appendix Table 9.4). Prior to analysis of toxicant exposures, the metabolic and transcriptional profiles of these control groups were compared using PCA (Figure 4.3). In total, the 4 PCs that constituted either model described approximately 61.24 % of the transcriptomics data and 71.85 % of the metabolomics data, representing the greatest trends/patterns in the data. Scores generated for the samples within each condition were compared by a 1-way ANOVA to identify potential statistical differences between the groups. These comparisons were performed for each of the 4 PCs within the multivariate model. Following adjustment for multiple testing (Benjamini and Hochberg, 1995) all of the calculated p-values were greater than 0.05 indicating no significant separation between the three controls groups along any PC (Table 4.4). A univariate comparison of the relative intensities of genes-spots or *m/z* peaks within the three groups of profiles indicated no significant changes in expression or concentration. The results of these analyses indicate no difference between the transcriptome and metabolome of these animals, implying that no adverse effects had been induced in response to PVP or bulk-Ag exposure. With this in mind these three groups will therefore be classed as a single "combined control" group for statistical analyses of Ag exposed profiles to identify only those changes occurring as a result of AgNP or $AgNO_3$ exposure.

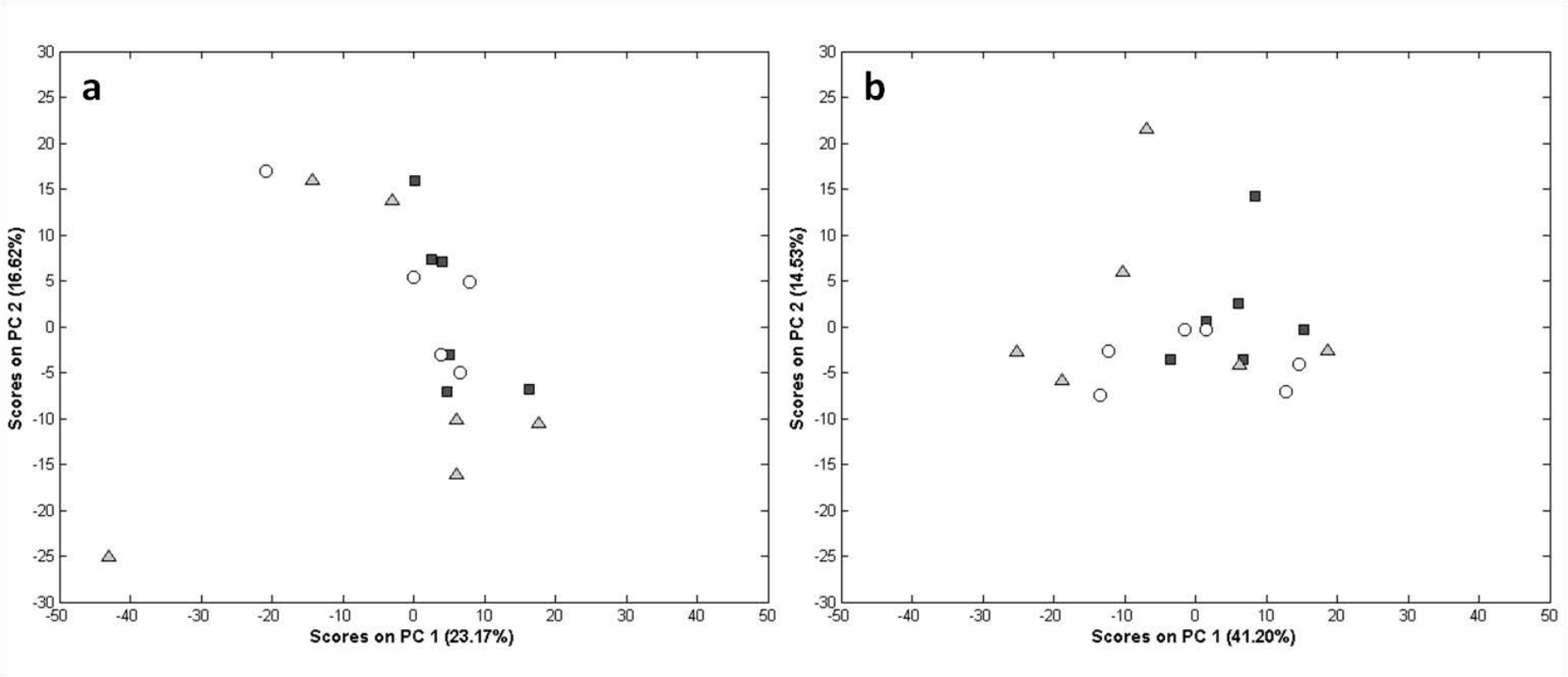

Figure 4.3: PCA scores plot comparing the transcriptional (a) and metabolic (b) profiles of the untreated (○), PVP (▲) and bulk (■) control groups along the first two principal components.

Table 4.4: p-values following adjustment for multiple testing generated by a 1-way ANOVA comparing the scores values for the untreated, PVP and bulk control groups along the four principal components of the transcriptomic and metabolomic PCA models.

	Adjusted p-values			
Method	**PC1**	**PC2**	**PC3**	**PC4**
Transcriptomics	0.47387	0.42181	0.84116	0.50450
Metabolomics	0.27220	0.35346	0.34275	0.99008
	Variance covered (%)			
Metabolomics	41.20	14.53	8.88	7.24
Transcriptomics	23.17	16.62	11.50	9.94

4.3.2 AgNP and Ag^{+} exposures and sample processing

The highest AgNP exposure concentration used in this study was the 24 h LOAEC of 4.7 µg/l (section 3.3.2) and as such some immobilisation of neonates was expected. However the actual number of neonate deaths in this group and in the AgNP Mid group was unexpectedly high. This reduced the number of biological replicates in these groups to 4 and 5 respectively (Appendix Table 9.4).

Additionally, one biological replicate was lost from the Ag High exposure group due to a loose tube cap during sample homogenisation. During the processing of transcriptomics data, two arrays were removed from the study; an untreated control replicate produced a "black hole", whereby only the outer wells hybridised and one AgNP High replicate showed substantial variation from the remaining samples in the group resulting from non-specific hybridisation as indicated by the spike-in QC oligonucleotides. Both samples were removed as the data they provided was considered unreliable and not a true representation of the exposed animals' transcripome. No samples were removed from the metabolomics data during processing.

4.3.3 Ag NPs induce a dose-dependent perturbation to *Daphnia* gene transcription and metabolism which is not fully accounted for by the Ag^{+} content of AgNP exposures

After data acquisition and processing, PCA was used to assess the variation of the transcriptional and metabolic profiles of all animals used in this study. Models consisting of 4 PCs were created and scores values for PC1 and PC2, the PCs covering the greatest variation, were plotted for both transcriptional (Figure 4.4) and metabolic (Figure 4.5) profiles. The untreated, PVP and Bulk controls groups are indicated separately on the plots but were treated as a combined control for all statistics. The raw and transformed microarray data matrices produced from this work is available in the ArrayExpress database (www.ebi.ac.uk/arrayexpress) using the accession number: E-MTAB-4041. Likewise the FT-ICR data is obtainable from the MetaboLights database (http://www.ebi.ac.uk/metabolights) using the accession number: MTBLS259.

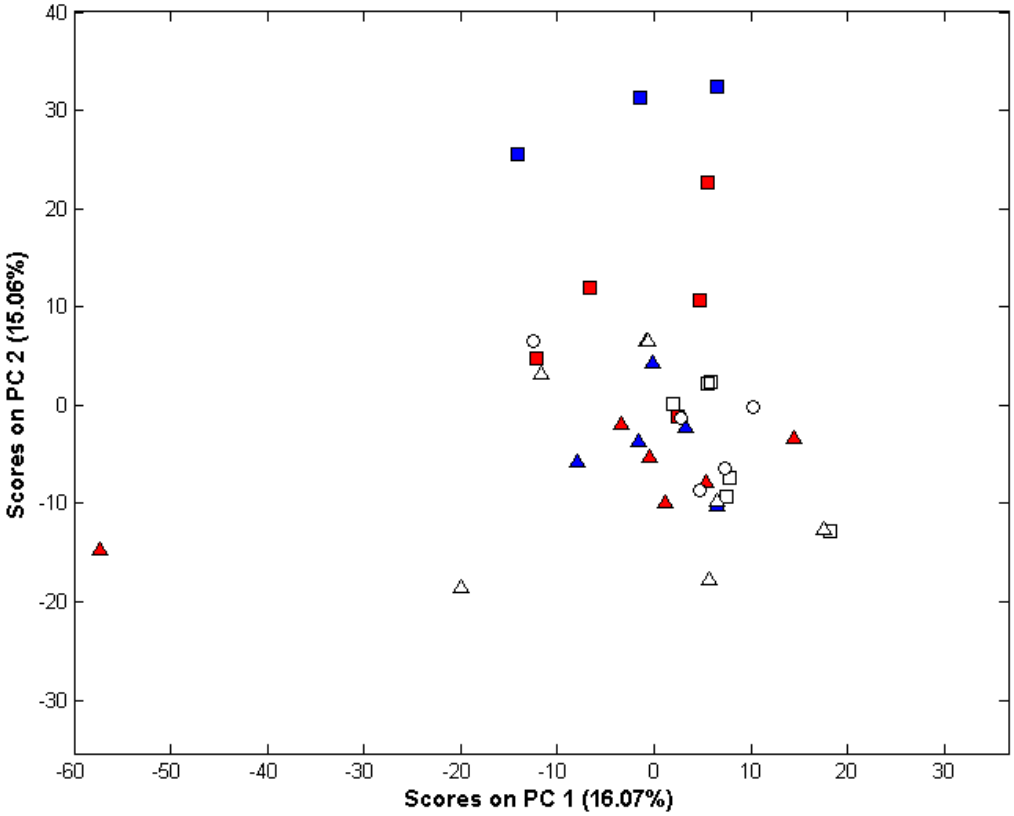

Figure 4.4: PCA scores plot (PC1 Vs PC2) from the 4 PC transcriptomics PCA model generated from intensity values of all 8128 detected genes. Clear symbols represent the untreated (○), PVP (Δ) and Bulk (□) control groups. Blue and red symbols represent AgNP and Ag^{+} exposures respectively with symbols representing the High (■) and Low (▲) concentrations. Separation of the AgNP High and Ag^{+} High groups is apparent along PC2.

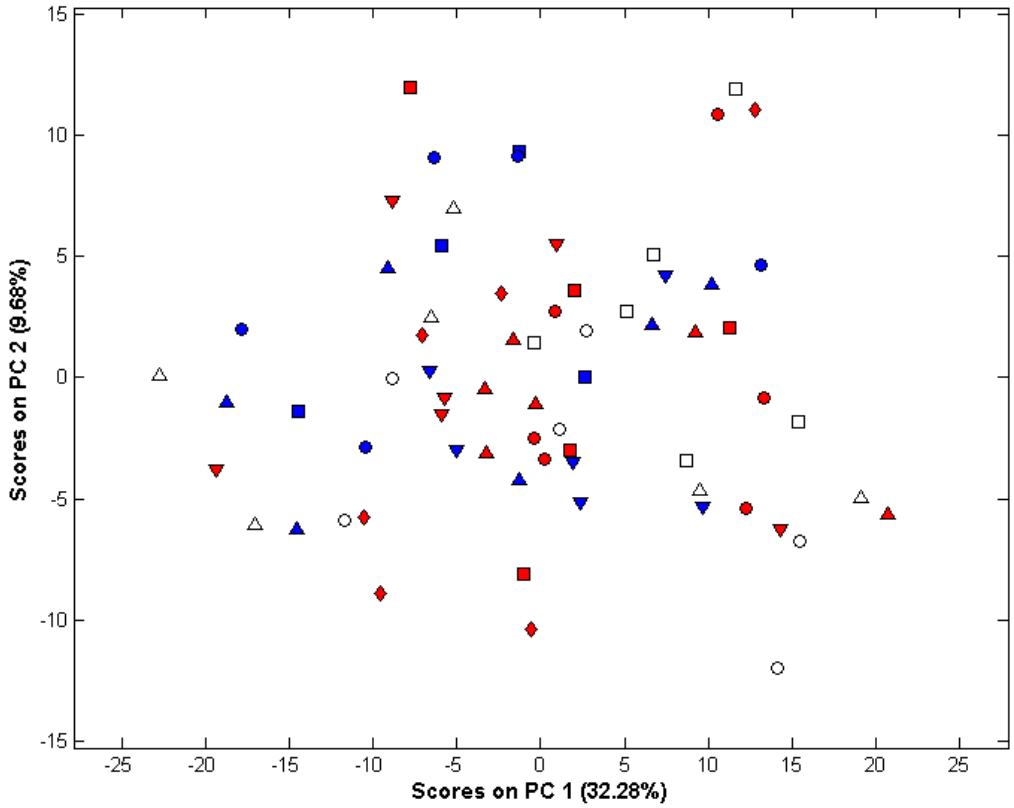

Figure 4.5: PCA scores plot (PC1 Vs PC2) from the 4 PC metabolomics PCA model generated from intensity values of all 1330 detected *m/z* peaks. Clear symbols represent the untreated (○), PVP (Δ) and Bulk (□) control groups. Blue and red symbols represent AgNP and Ag^{+} exposures respectively with symbols representing the High (■), Mid (●), Low (▲), and V. Low (▼) concentrations. No separation is observed between any of the groups along PC1 or PC2.

As observed from the PCA scores plots, the transcriptional profiles exposed to AgNP High and Ag High groups appear to separate along PC2 from the control groups and lower exposure concentrations (Figure 4.4). In contrast, no separation is observed between the metabolic profiles of any group along PC1, nor PC2 (Figure 4.5). To identify the key PCs of each model, a one-way ANOVA was implemented between scores values of all samples across all 4 PCs. This test identified significant differences between the scores values of groups present in the transcriptomics model on PC2 ($p = 4.12x10^{-7}$) and the metabolomics model on PC3 ($p = 3.83x10^{-4}$) (Table 4.5). To allow clearer visualisation of the changes described by these significant PCs, each sample is plotted against their respective scores value for transcriptomics on PC2 (Figure 4.6) and metabolomics on PC3 (Figure 4.7). Tukey-Kramer post-hoc tests identified the metabolic profiles of animals exposed to the highest concentration of AgNP as being significantly different from the combined controls, and all other groups except the AgNP Mid, the Ag High, and the Ag Filtrate (Figure 4.8). This is again true on a transcriptional level, but here animals exposed to the highest concentration of Ag ions also show significant separation along the same principal component (Figure 4.9)

Table 4.5: FDR-corrected p-values generated for transcriptomics and metabolomics data, by a 1-way ANOVA comparing scores of each exposure group across all four PCs. PCs along which significant separations occur are highlighted in red.

	Adjusted p-values			
Method	**PC1**	**PC2**	**PC3**	**PC4**
Transcriptomics	0.58031	**0.00000**	0.04767	0.18786
Metabolomics	0.48872	0.66794	**0.00008**	0.93627

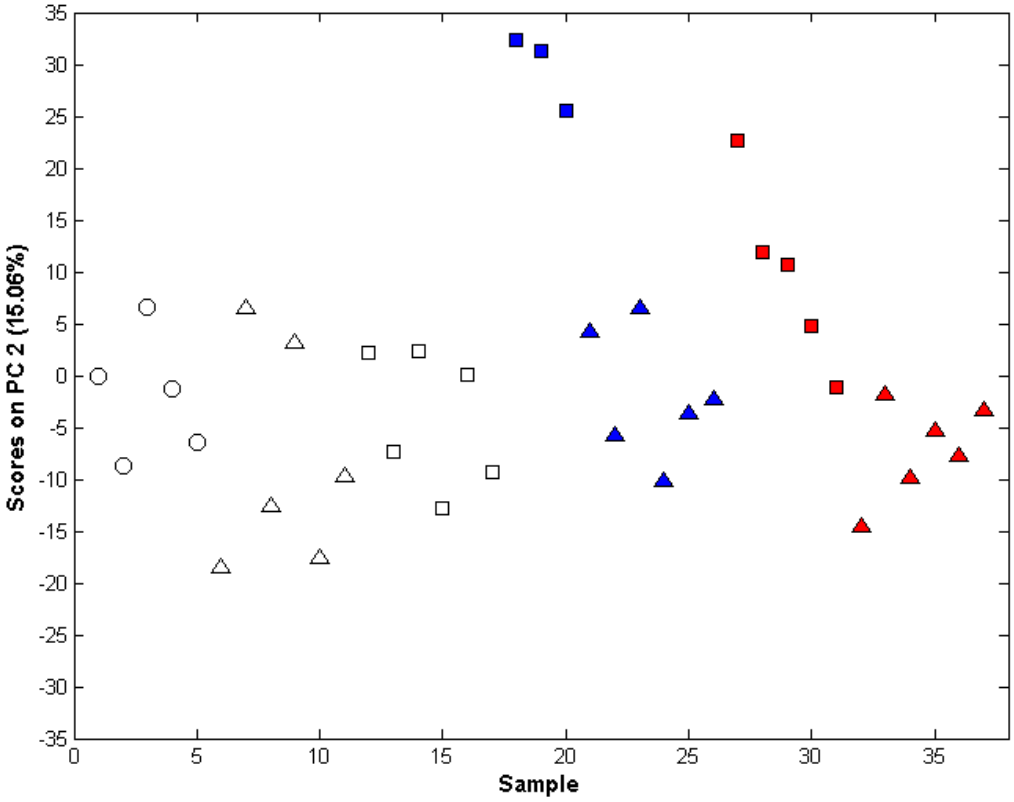

Figure 4.6: Plot of PC2 scores from the 4 PC transcriptomics PCA model for each sample generated from intensity values of all 8128 detected genes. Clear symbols represent the untreated (○), PVP (Δ) and Bulk (□) control groups, and although they are shown separately on the plot, they were combined for statistical analysis. Blue and red symbols represent AgNP and Ag exposures respectively with symbols representing the High (■) and Low (▲) concentrations.

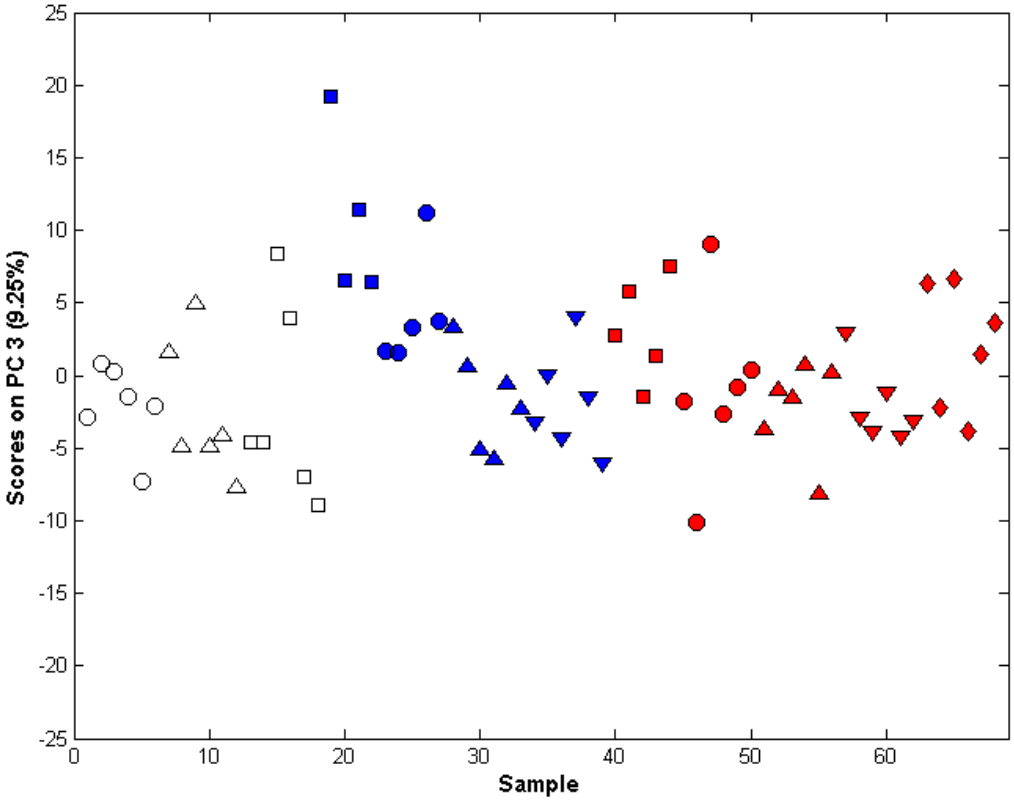

Figure 4.7: Plot of PC3 scores from the 4 PC metabolomics PCA model for each exposure sample generated from intensity values of all 1330 detected *m/z* peaks. Clear symbols represent the untreated (○), PVP (Δ) and Bulk (□) control groups, and although they are shown separately on the plot, they were combined for statistical analysis. Blue and red symbols represent AgNP and Ag exposures respectively with symbols representing the High (■), Mid (●), Low (▲), and V. Low (▼) concentrations.

Exposure groups	AgNP High	AgNP Mid	AgNP Low	AgNP Vlow	Ag^+ High	Ag^+Mid	Ag^+ Low	Ag^+ Vlow	Ag^+ Filtrate	Control
Control										N/A
Ag Filtrate									N/A	
Ag Vlow								N/A		
Ag Low							N/A			
Ag Mid						N/A				
Ag High					N/A					
AgNP Vlow				N/A						
AgNP Low			N/A							
AgNP Mid		N/A								
AgNP High	N/A									

Figure 4.8: Tukey-Kramer post-hoc results following an ANOVA of PC3 scores generated from metabolomics data ($p = 3.83x10^{-4}$). Green squares indicate a sgnificant difference between the two groups in question. The metabolic profiles of animals exposed to the highest concentration of AgNP are significantly different from all groups, with the exception of the Ag High, the AgNP Mid and the Ag Filtrate.

Exposure groups	AgNP High	AgNP Low	Ag High	Ag Low	Control
Control					N/A
Ag Low				N/A	
Ag High			N/A		
AgNP Low		N/A			
AgNP High	N/A				

Figure 4.9: Tukey-Kramer post-hoc results following an ANOVA of PC2 scores generated from transcriptomics data ($p = 4.12x10^{-7}$). Green squares indicate a sgnificant difference between the two groups in question. The high dose groups (for both Ag and AgNP) are significantly different from all other groups. Furthermore, the high dose Ag and high dose AgNP groups are themselves significantly different.

In this study, 8128 gene-spots and 1330 *m/z* peaks were retained following extensive data processing prior to the statistical analyses. To discover which genes and metabolites were responsible for the separation observed by PCA, a 1-way ANOVA was used to determine those which changed significantly in intensity across exposure groups. Statistical analysis, following correction for multiple testing (Benjamini and Hochberg, 1995), identified 711 significantly changing genes and 190 significantly changing peaks ($p \leq 0.05$) across all groups.

To visualise this molecular change further, matrices of peak intensity or gene-spot fluorescence relating specifically to these significantly changing peaks or genes, were compiled and PCA scores models were generated (Figure 4.10). By concentrating solely on these variables, the dose-response effect of AgNP exposure to the *D. magna* metabolome is more apparent; both the AgNP Mid and AgNP Low groups begin to separate along PC1 with the AgNP High group. This concentration-dependant separation strongly implies that the representative molecular changes are a direct response to AgNP exposure. What is also depicted, in both the metabolic and transcriptional datasets, is that these features are perturbed in a similar way in animals exposed to the highest concentration of $AgNO_3$ (Figure 4.10). PC1 scores values for samples in this group are positive, separating from controls in the same direction as the AgNP groups along the same PC. This reinforces what was seen previously with the unrefined datasets at a transcriptional level (Figure 4.6) and suggests that the list of significantly changing variables accurately reflects the impact of both AgNP and $AgNO_3$ exposures.

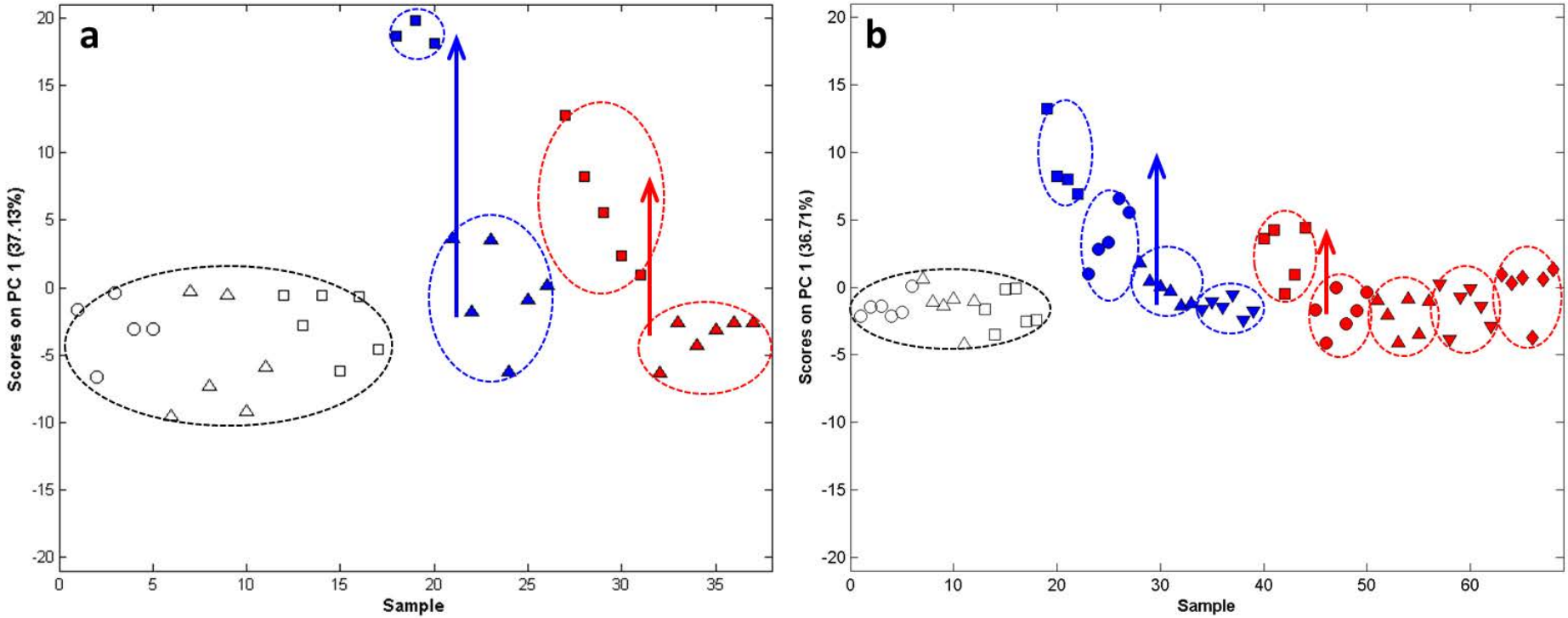

Figure 4.10: PCA scores plots of models generated from significantly changing gene-spots (A) or *m/z* peaks (B) only. The scores for PC1 only are plotted for each biological sample in the model to allow for the comparison of magnitude of affect along this PC between all groups. Clear symbols represent the untreated (○), PVP (Δ) and Bulk (□) control groups, treated as a combined control for statistical tests. Blue and red symbols represent AgNP and $AgNO_3$ exposures respectively with symbols representing the High (■), Mid (●), Low (▲), and V. Low (▼) concentrations. Ellipses and arrows are present to aid in the visualisation of separations between groups along PC1 only.

In the case of this study, PCA is analysing all possible related patterns of variance in the transcriptional or metabolic profiles of animals; and then ranking these patterns as PCs in order of total variance described. Each PC therefore represents a particular pattern of changes in gene expression or metabolite concentration. Samples that generate similar scores values on a particular PC are likely to have similar profiles. If members of two exposure groups separate from the control in the same direction along a principal component then it suggests that a similar response is being induced. This is what is observed in the significant molecular response of animals exposed to the highest concentrations of both forms of silver (Figure 4.10). When observing the significant changes induced upon the transcriptome and the metabolome, the profiles of animals exposed to the highest concentration of either AgNP or $AgNO_3$ in both cases separate from controls in the same positive direction along PC1. This implies that both AgNP and dissolved Ag induce a similar transcriptional profile and also a similar metabolic profile, though it is not possible at this stage to say if the two omics profiles are related. Along with this shared exposure profile, there is a significant difference in the magnitude of response between the transcriptional profiles of the AgNP High samples and their dissolved Ag counterparts (Figure 4.9). This implies that at these concentrations, AgNPs induce a greater level of response than exposures to the dissolved Ag fraction alone, though the molecular responses induced by each form appear to be similar.

It is therefore unlikely that AgNPs and Ag^+ induce toxicity by different mechanisms, as this would have been represented by separation of the AgNP and $AgNO_3$ exposure groups along different PCs (e.g. AgNP on PC1 and $AgNO_3$ on PC2) in PCA scores plots. The similarities in the induced profiles could suggest that Ag^+ is the mediator of toxicity for AgNP. This would be consistent with previous studies that have shown a complete reduction of AgNP toxicity following chelation of the free-ion form of Ag (Zhao and

Wang, 2011). If this was the case the greater magnitude of response observed for AgNP-exposed animals could be the result of the Trojan-horse mechanism. This would mean that the absorption and subsequent internal dissolution of AgNPs (either in the lumen of the gut or within tissues) could result in a large internal concentration of toxic Ag^+, with the AgNPs themselves remaining relatively non-toxic. Alternatively this result could mean that both AgNP and dissolved Ag induce toxicity independently, but that both forms of Ag induce the same molecular profile changes. This would account for the greater magnitude of response observed in AgNP-exposed animals, as the theoretical total Ag concentration of AgNP exposures is greater than that of their counterpart $AgNO_3$ exposures. Both explanations would conform to the results of previous mechanistic investigations of the two forms of silver which concluded that both species of Ag induced a similar molecular response (Aerle et al., 2013; Ahn et al., 2014; De Matteis et al., 2015), including an NMR-based metabolomics investigation in *D. magna* which showed agreement between the overall molecular profiles induced by both forms of silver by PCA (Li et al., 2015a). However, it has been observed previously that chelation of Ag^+ in AgNP suspensions results in a complete reduction of AgNP toxicity to *D. magna* (Kennedy et al., 2010; Zhao and Wang, 2011; Newton et al., 2013) suggesting that AgNPs themselves have little-to-no inherent toxicity compared to dissolved Ag. It is more likely that if AgNPs induced toxicity independent of any released Ag^+, the changes observed would be unique to those induced by Ag^+ which would be reflected in the transcriptional and metabolic profiles observed by PCA. These differences were not observed, suggested that dissolved Ag is the form responsible for AgNP toxicity.

4.3.4 AgNP likely enact toxicity via the digestive tract

The concentration of total Ag associated with *D. magna* following AgNP and $AgNO_3$ exposures was investigated using ICP-MS to gain greater insight into the role of Ag uptake

in the mechanism of toxicity. AgNP and $AgNO_3$ stocks used in sub-lethal uptake exposures were measured by ICP-MS and the $AgNO_3$ stocks were found to be slightly higher than originally intended (Table 4.3). The Ag^+ High stock is 8.06 % of the AgNP High stock which is within 1 SD of the mean percentage dissolution at 24 h (5.68 % ± 2.87). The Ag^+ Low stock is 10.50 % of its AgNP counterpart which is above the originally intended range; this must be taken into account when interpreting results.

After a 24 h exposure, the concentration of associated silver was measured by ICP-MS, and body burden was calculated in terms of µg of Ag per g of *daphnid* wet weight. Animals exposed to the lowest concentrations of AgNP (1.17 µg/l) and dissolved Ag (0.12 µg/l) were measured to have average body burdens of 0.4316 ± 0.7475 µg/l and 0.5443 ± 0.0605 µg/l respectively. Exposure to 4.43 µg/l of AgNP and 0.36 µg/l of dissolved silver yielded respective *D. magna* body-burdens of 3.8402 ± 0.2695 µg/l and 1.9632 ± 0.3099 µg/l. The Ag body burden of animals exposed to the lowest concentrations of $AgNO_3$ and AgNP (0.12 µg/l and 1.17 µg/l respectively) were deemed as not being significantly different to controls by a 1-way ANOVA followed by Dunnett's multiple comparison test. It is worth noting that two of the three AgNP Low biological replicates failed to measure any silver associated with the exposed animals, whereas the third measured 1.27 µg/g; this resulted in a SD value larger than the mean. At the highest concentration $AgNO_3$ (0.12 µg/l) AgNP (1.17 µg/l) exposures there is significantly more ($p < 0.0001$) Ag associated with the animals upon exposure compared to control animals. The relationship between total Ag exposure concentration and body-burden for AgNP and $AgNO_3$ exposed *Daphnia* is shown in Figure 4.11. With respect to the total concentration of Ag in the exposure media, $AgNO_3$ exposures result in a higher body burden of Ag within the exposed animals than AgNPs, highlighting the difference in uptake rate and bioavailability between the two species of silver.

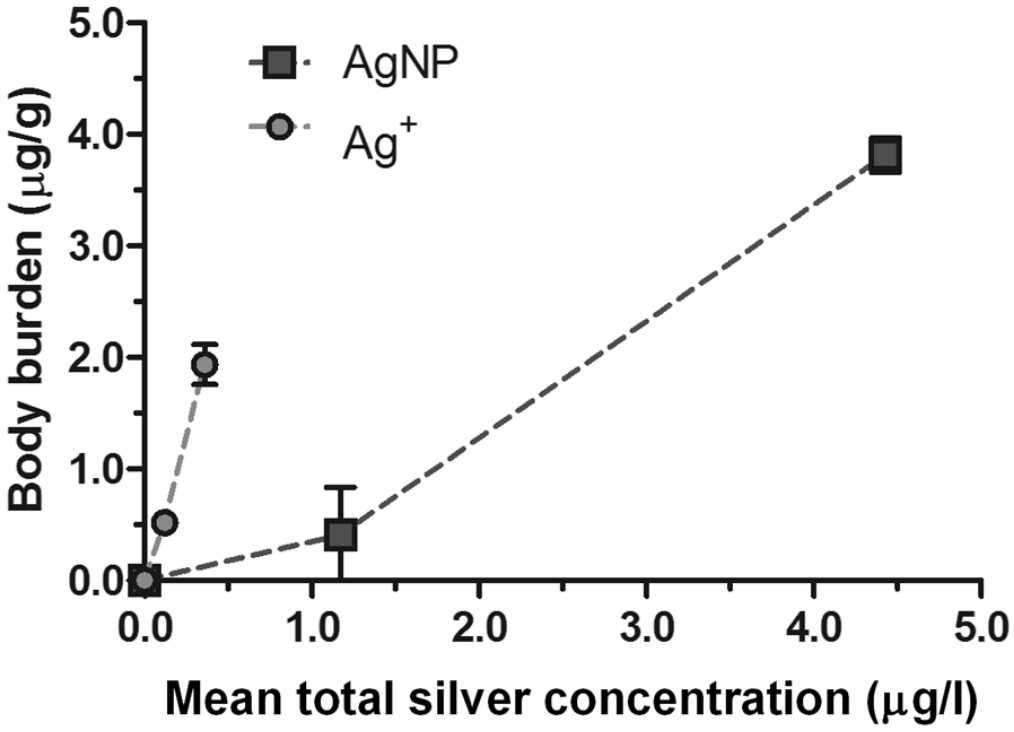

Figure 4.11: Comparison of the relationship between body burden of Ag following AgNP and $AgNO_3$ exposure, and the total Ag concentration of the exposure media. A 1-way ANOVA identified significantly higher body burden in animals exposed to the highest concentration of AgNPs when compared with its $AgNO_3$ counterpart ($p < 0.0001$). No difference in Ag body burden was observed between the low concentration exposures. N = 3 replicates for each group, error bars represent standard error of the mean.

The total Ag concentrations of $AgNO_3$ in this experiment were chosen to represent the concentration of the dissolved Ag fraction of their respective AgNP exposures. In theory, the $AgNO_3$ Low and AgNP Low should contain the same concentrations of dissolved Ag. Likewise this should be the case for the $AgNO_3$ High and AgNP High groups. When analysed by a 2-way ANOVA comparing these nominal treatment and concentration goups, it was deemed that concentration of toxicant had a significant impact on the resulting body-burden ($p = 0.0063$) and that animals exposed to AgNP yielded significantly greater body-burdens than *D. magna* exposed to the respective dissolved silver fraction alone ($p < 0.0001$) as depicted in Figure 4.12. This latter result suggests that AgNPs must account for some of the total Ag measured within these organisms, if only dissolved Ag was absorbed into or onto the animals (i.e., if the neonates did not or could not ingest the nanoparticles), it would be more likely that there would be no significant difference between the AgNP High and $AgNO_3$ High exposures.

The methodology of this experiment included a "rinse" step with Milli-Q water prior to measurement by ICP-MS in order to remove any Ag attached to the external surface of the organisms. Because of this, it is likely that any Ag measured within the acid-digested *Daphnia* samples was contained within the organism; however there is still a chance that some Ag was attached to the carapace. The ingestion of AgNP by *D. magna* has been observed previously through measurement of AgNP uptake and efflux using ICP-MS (Zhao and Wang, 2010; Khan et al., 2015), and through secondary ion mass spectrometry (SIMS), a MS-based imaging technique that successfully detected the presence of silver, following AgNP exposure in the digestive tract of *D. magna* (Audinot et al., 2013). However, this data cannot distinguish between the presence of Ag within the gut or attached to the carapace of exposed *Daphnia*, and Ag that has accumulated within the animal's tissues.

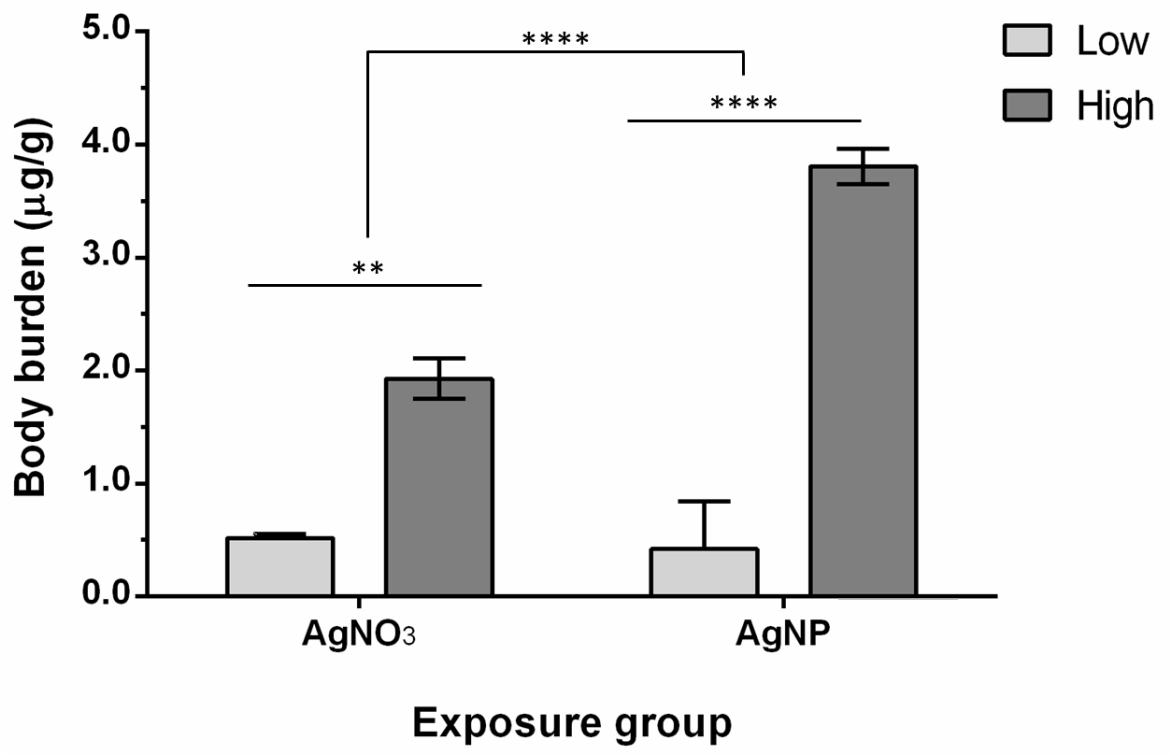

Figure 4.12: Comparison of body burden of Ag following exposure to Low and High concentrations of $AgNO_3$ and AgNPs. A 2-way ANOVA followed by Sidak's multiple comparison test determined significantly higher body burdens observed in animals exposed to AgNPs in comparison to their corresponding dissolved Ag fractions alone ($p < 0.0001$). The concentration of toxicant was also deemed to have a significant impact on Ag body burden ($p = 0.0063$). N = 3 replicates for each group, error bars represent standard deviation.

As an addition to the assessment of AgNP uptake into *D. magna* the elimination of both AgNPs and $AgNO_3$ were also measured (Figure 4.13). Following an exposure to AgNP High and to the respective dissolved Ag fraction for 24 h, animals were immediately transferred to clean media10 with algal feed to promote gut-clearance. The concentration of silver within animals was measured at 18 h and again at 96 h (4 d) after exposures had finished. Elimination was plotted as a percentage of absorbed total silver (0 h) against time (Figure 4.13). The Ag body burden of animals at 0 h was measured to be 3.8402 ± 0.2695 µg/l for AgNPs and 1.9632 ± 0.3099 µg/l for $AgNO_3$. After an 18 h depuration period, the body burden of animals that were exposed to AgNPs has reduced to 0.8805 ± 0.5645 µg/l, equating to 23.1 % of the 0 h concentration. Likewise after 18 h the body burden of animals that were exposed to $AgNO_3$ has reduced to 2.8 %. At the final 96 h time point, AgNP-exposed animals have a body burden of 0.0423 ± 0.0081, which is approximately 2.2 % of the original body burden. The Ag body burden of Daphnia exposed to $AgNO_3$ is below the detection limit of the instrument, potentially indicating a complete removal of all internal silver at this point.

The burden of silver within animals exposed to both AgNP and Ag^+ ions reduces significantly ($p < 0.0001$) 18 h following the end of exposure, and by 96 h post-exposure the internalised silver is nearly completely removed. Due to the lack of data points, fitting the data to a single-step or two-step depuration model was not possible, and the data should be considered as preliminary. However, the resulting plot (Figure 4.13) is similar in profile to those plotted previously by studies investigating the influx and efflux of AgNP (Zhao and Wang, 2010; Khan et al., 2015) and gold nanoparticles (Khan et al., 2014) in *Daphnia magna*. These previous efflux patterns are typically biphasic, with the initial rapid phase describing the passage of NPs through the digestive tract and the second, slower phase relating to the elimination of NPs which had either been absorbed

from the gut into the surrounding tissue or simply remain in the lumen (Khan et al., 2015). In this study, the initial rapid removal of silver observed over the initial 18 h matches previously published data (Khan et al., 2015), but 96 h after the end of exposure almost all of the silver within the organism over the 24 h exposure period was completely cleared. This differs to previous work which see approximately 10 % of the initial Ag content remaining within exposed *D. magna* even as long as 5 days following exposure. This suggests that in this study the silver may not be retained to a substantial degree within the tissues of *D. magna*, but instead passes relatively rapidly through the organism.

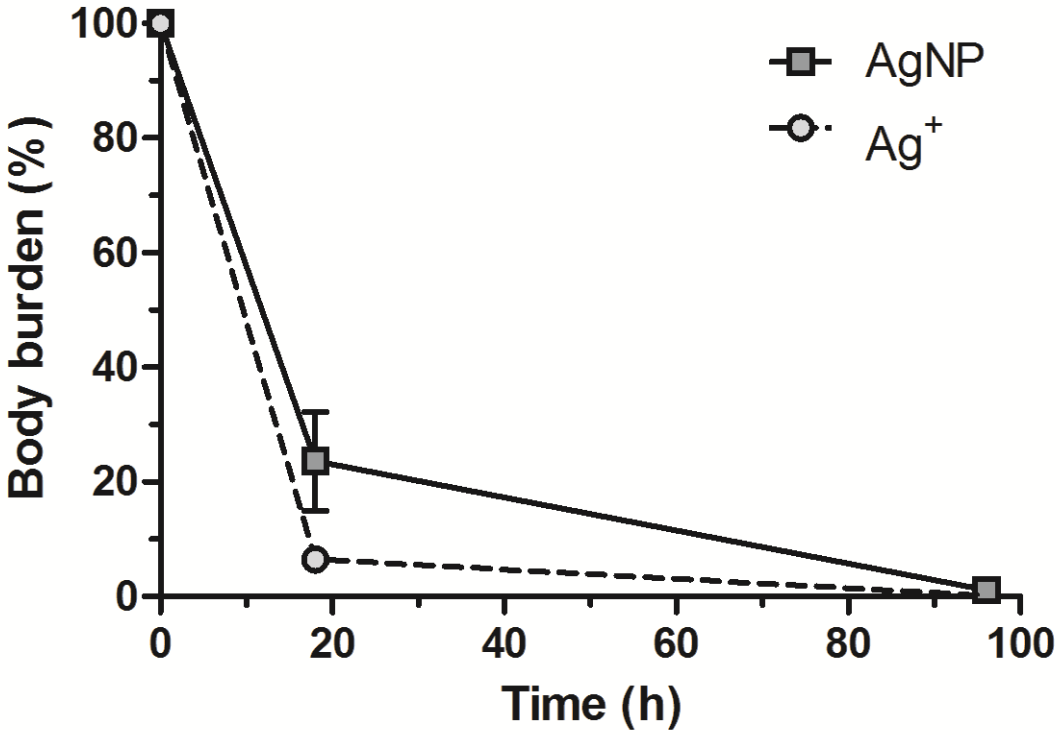

Figure 4.13: The depuration of absorbed AgNPs (■) and Ag^+ (○) from exposed *D. magna* over a 96 h period. N = 3 replicates per time point, error bars represent the standard error of the mean. Connective lines are for visualisation purposes as fit of the data to a two-step depuration model was not possible. Following a 2-way ANOVA and Sidak's multiple comparison test, it was determined that the body burden of animals decreased significantly over time ($p < 0.0001$) for both AgNP and dissolved Ag. Mean body burden values for AgNP and dissolved Ag at 18 h are significantly different ($p = 0.0186$).

4.4 Conclusion

The primary aim of this chapter was to determine which of three hypothetical mechanisms proposed in the introduction to this chapter (Figure 4.1), if any, best described the role of dissolved Ag in AgNP toxicity. From comparison of the transcriptional and metabolic profiles of *D. magna* neonates exposed to AgNPs and dissolved Ag, the data suggests that both forms of Ag induce similar overall molecular responses. These similarities in profiles suggest that exposure to AgNPs induce the same molecular perturbations as exposure to $AgNO_3$, which would be consistent with dissolved Ag as the mediator of toxicity for AgNP. This conclusion would be consistent with previous studies that have shown a complete reduction of AgNP toxicity following chelation of the free-ion form of Ag (Zhao and Wang, 2011). It is therefore likely that the dissolved silver fraction is responsible for AgNP-induced toxicity as in mechanism 1 and 3 (Figure 4.1). However, the elevated Ag body-burden and omics response observed for AgNP exposed animals compared to that of animals exposed to the dissolved fraction alone suggests that although the dissolved silver fraction is responsible for AgNP-induced toxicity, it is unlikely to do so following dissolution external to the organisms. This data would therefore disprove hypothesised mechanism 1.

The data presented in this chapter also does not fit fully with the second hypothetical mechanism which suggested simultaneous, different, but potentially synergistic mechanisms for AgNPs and dissolved Ag (Figure 4.1). Mechanism 2 hypothesises that AgNPs and dissolved Ag ions both induce toxicity upon exposure through separate and potentially synergistic mechanism. If the responses induced by the two forms of Ag were different this would have been reflected in PCA of transcriptional and metabolic profiles; the two forms of silver would have been seen to separate along separate PCs rather than to differing magnitudes on the same PC. Unlike mechanism 1 above however, mechanism 2

cannot be ruled out completely. The limited annotation of the *D. magna* microarray and the limitations in detecting many naturally low-level metabolites means it is still possible that some significant differences between the two mechanisms exist but remain largely undetected.

The combination of results from omics analyses and determination of total Ag body burden would therefore better suit a Trojan-horse type mechanism (mechanism 3, Figure 4.1); whereby AgNPs are ingested by *D. magna*, resulting in a concentrated delivery of Ag^{+} ions following AgNP dissolution within tissues or the lumen of the gut and an elevated molecular response.

Chapter 5: Elucidating the molecular mode of action of silver nanoparticles to *Daphnia magna*

5.1 Introduction

The molecular perturbations induced by Ag and AgNPs are still mostly uncharacterised but a number of mechanistic studies in recent years have highlighted some key responses and areas for further investigation. A potential limitation of these studies is their use of a targeted, hypothesis-driven approach. An advantage of omics-technologies is the ability to use a non-targeted approach for mechanistic investigation (Keun, 2006); measuring hundreds of endpoints rather than focusing on a select few (Viant, 2009). This alternative approach to study-design potentially allows for the generation of new hypotheses and the identification of otherwise unconsidered mechanisms for investigation in cases where the prior knowledge for the traditional targeted approach is still lacking; as is the case for AgNPs. There are currently three high-thoughput "omics" analyses of AgNP and $AgNO_3$ toxicity in *D. magna*; a microarray investigation into the impact of exposure on the transcriptome (Poynton et al., 2012), a redox-proteomic approach using two-dimensional electrophoresis (2DE) (Rainville et al., 2014), and a ^{1}H-NMR-based analysis comparing the overall impact on the metabolic profiles (Li et al., 2015a).

To investigate the transcriptional impact of AgNP exposures, the transcriptional profiles of 10 day old *D. magna* adults exposed to the $^{1}/_{10}$ LC_{50} and the LC_{25} of citrate and PVP-stabilised AgNPs, as well as the ¼ LC_{25} and ½ LC_{25} of $AgNO_3$ were compared following a 24 h exposure (Poynton et al., 2012). Enrichment analysis of these profiles highlighted several gene ontology (GO) terms as being enriched or over represented. AgNP were seen to induce in increase in protein ubiquitination and proteolysis and in cellular signalling processes, whereas $AgNO_3$ exposure resulted in an increase in transcription of genes

related to energy production and cellular respiration as well as a decrease in those involved in embryonic morphogenesis and segmentation, eye photoreceptor development and reproduction and oogenesis (Poynton et al., 2012).

The proteomic investigation by Rainville et al. analysed the impact of a 24 h exposure to 5, 15, 20 and 30 μg/L of AgNPs and 0.4, 1.2 and 2.5 μg/L $AgNO_3$ on the proteome of *D. magna* by 2DE (Rainville et al., 2014). This exposure revealed that both forms of silver induced an increase of protein-thiol content, but only AgNPs caused an increase of protein carbonyls. The authors suggest that the increase in protein-thiol content is in response to the presence of Ag^+ ions within the organisms; to directly chelate the ions and decrease their toxicity, or alternatively as a response to reduce toxicity by ROS. The increased carbonyl content induced by AgNPs is thought to be an indication of AgNP-induced oxidative stress and oxidation of cellular proteins (Rainville et al., 2014). Additionally, MS/MS following 2D electrophoresis identified 4 of 8 features of interest as vitellogenin fused with superoxide dismutase; a key enzyme in the response to reactive oxygen species (ROS).

An NMR investigation into the impact of AgNP and $AgNO_3$ exposure on the metabolic profile of *D. magna* suggested that both forms of Ag induced the same metabolic perturbations (Li et al., 2015a). Exposure to 2 and 10 μg/l of 10 nm AgNP showed elevated levels of lactate and phosphocholine and depleted levels of 3-hydroxybutyrate, arginine, lysine and choline (Li et al., 2015a).

By analysing samples using a combination of omics technologies, we can achieve an understanding of the genes and metabolites involved in the global response to AgNP and Ag^+ exposure. However, lists of genes and metabolites tell us very little without wider consideration for how they interact with one another. Pathway analysis allows a statistical

approach to decipher large lists of putative responsive genes or metabolites by putting them into the context of known molecular interactions. Online tools are available for the analysis of transcriptomics (http://david.abcc.ncifcrf.gov/) and metabolomics (Xia et al., 2012) datasets individually as well as for integrated analysis (Kamburov et al., 2011). This enables an objective, statistical approach to interpret interactions between genes and metabolites of interest without having to resort to speculation (Cavill et al., 2011) or dependence on prior knowledge. The results of these analyses can then be used to form hypotheses on the response being observed. However, all current methods of pathway analysis are not without their limitations and some prior knowledge is still needed for successful interpretation of results.

The literature surrounding the genes, proteins and metabolites involved in response to AgNP toxicity is expanding, following an increase in mechanistic investigations across multiple cell lines and test organisms. (Comfort et al., 2014; Verano-Braga et al., 2014; McQuillan and Shaw, 2014; Carrola et al., 2015). Mitotoxicity has been observed through use of fluorescent dye-based assays in HeLa and A549 cells (De Matteis et al., 2015) and through measurement of the impact of Ag exposure on H^+ flux across the mitochondrial membrane in *D. magna* (Stensberg et al., 2013). A quantitative proteomic analysis of AgNP-exposed human colon carcinoma cells observed a down-regulation of mitochondrial proteins, including those involved with the electron transport chain (Verano-Braga et al., 2014). On a transcriptional level, significant down-regulation of genes encoding complexes I, II, III and IV of the oxidative phosphorylation machinery have been observed in zebrafish (Aerle et al., 2013). Studies in cell lines have measured the presence of ROS following AgNP and $AgNO_3$ exposure (Arora et al., 2009; Asharani et al., 2009; Domingos et al., 2009; Chairuangkitti et al., 2013), potentially suggesting the direct induction of oxidative stress by these two forms of silver. In some cases this production of

ROS has been linked to the aforementioned disruption of mitochondrial activity (Asharani et al., 2009) as well as being linked to the induction of DNA damage and genotoxicity (AshaRani et al., 2009). It has been observed that the principal response to Ag toxicity across multiple model organsims is an increase in the production of metallothioneins and other thiol-containing peptides (Ferguson et al., 1996; Chae et al., 2009; Meyer et al., 2010; García-Alonso et al., 2011; Johari et al., 2015). The inhibition of RNA polymerase by AgNP has been measured; Wang and colleagues demonstrated that exposure of erythroid progenitor cells to AgNP resulted in the inhibition of RNA polymerase activity and RNA transcription through the direct binding of AgNPs to the enzyme (Wang et al., 2013). Ag exposure has also been seen to disrupt key cellular processes such as an increase in calcium transients (Asharani et al., 2009), cell cycle arrest (De Matteis et al., 2015) and impacts on transcription factors (Aerle et al., 2013). An NMR-based metabolomics study has suggested Ag-induced perturbation to the purine metabolism pathway (Hadrup et al., 2012) following detection of an increase in uric acid and allantoin excretion in mice. AgNPs have been seen to exert indirect effects via serine/threonine protein kinase (PAK), mitogen-activated protein kinase (MAPK), and phosphatase 2A pathways (Verano-Braga et al., 2014).

In this Chapter, the markers of AgNP and $AgNO_3$ exposure discovered in Chapter 4 underwent extensive annotation yielding robust putative identities. To statistically interpret interactions between putative annotations, ORA was rigorously applied using three online platforms: the Database for Annotation, Visualization and Integrated Discovery (DAVID) (Huang et al., 2009), MetaboAnalyst (Xia et al., 2012) and Integrated Molecular Pathway-Level Analyses (IMPaLA) (Kamburov et al., 2011) all of which search different databases. This allowed the assessment of key putative interactions or pathways that were perturbed in response to AgNP and Ag^+ exposures. Significantly changing

putative identities involved in these interactions were then investigated further by RT-qPCR and MS/MS to confirm gene expression levels and peak identity respectively.

5.2 Materials and Methods

5.2.1 Putative annotation of filtered genes and m/z peaks

The *D. magna* microarray was originally designed using a large expressed sequence tag (EST) database and annotated by Poynton et al (2012). An initial BLASTX search of these EST sequences (http://blast.ncbi.nlm.nih.gov/Blast.cgi) against the entire NCBI non-redundant protein database gave the closest protein homologues to the microarray targets using an e-value filter of 10^{-6}. Further annotation was acquired through a BLASTX search against the *Daphnia pulex* genome v1.0 (Colbourne et al., 2005). *D. pulex* protein sequences corresponding with hits from this search were compared with human peptide sequences, downloaded from Ensembl (Flicek et al., 2014) using BLASTp to find putative human orthologues for pathway analysis. Gene ontology annotation was achieved using Blast2GO (Götz et al., 2008). This method of annotation was adapted from previously published methods (Williams et al., 2011; David et al., 2011; Poynton et al., 2012).

For FT-ICR mass spectrometry data, all filtered *m/z* values with corresponding average raw intensities (non-normalised) were imputed into MI-Pack (Weber and Viant, 2010) to generate possible empirical formulae and putative metabolite names for each *m/z* peak using KEGG. Briefly, MI-Pack calculates accurate *m/z* values for common negative ions ($[M-H]^-$, $[M+^{35}Cl]^-$, $[M+^{37}Cl]^-$, [M+Acetate (Ac)]$^-$, $[M+K-2H]^-$ and $[M+Na-2H]^-$) and positive ions ($[M+H]^+$, $[M+Na]^+$, $[M+^{39}K]^+$, $[M+^{41}K]^+$) of all compounds within the KEGG compounds database. It then attempts to match these values with the accurate mass *m/z* values detected during the experiment using an error window of 1 ppm. The transformation mapping algorithm (Weber and Viant, 2010) was used to increase confidence in assigned putative metabolite names.

5.2.2 Over-representation analysis of transcriptomics datasets using DAVID

ORA was performed with putative orthologous human Ensembl gene IDs using the DAVID (version 6.7). The input list consisted of all Ensemble IDs assigned the gene-spots that were deemed to change significantly via 1-way ANOVA in the previous chapter (Section 4.3.3). A list of all detected gene-spots with orthologous human Ensemble gene IDs, regardless of significance, was used as a background comparison list. Fisher's exact test was used with a FDR of 0.05 to correct for the multiple-testing hypothesis (Benjamini and Hochberg, 1995). Four pathway databases were used for their respective pathway definitions: KEGG-Pathway, Reactome-Pathway, BIOCARTA and the Biological Biochemical Image Database (BBID). Pathways relating to diseased states and first-tier Reactome definitions that encompass many smaller pathways (e.g. 'Metabolism' or 'Signal transduction') were excluded. Only pathway definitions with a minimum of 3 hits from the input list were retained.

5.2.3 Over-representation analysis of metabolomics datasets using MetaboAnalyst

ORA was applied using MetaboAnalyst (Version 2.0 (Xia et al. 2012)) to putatively assigned KEGG IDs from the metabolomics dataset. An input list was formed from all KEGG IDs that were assigned to m/z peaks deemed to change significantly via 1-way ANOVA in the previous chapter (Section 4.3.3). A list of all putative KEGG IDs assigned to any peak regardless of significance was assembled for use as a background reference list. If a particular KEGG ID was assigned to multiple peaks only a single iteration of the ID was used. Fisher's exact test was used with a FDR of 0.05 to correct for the multiple-testing hypothesis (Benjamini and Hochberg, 1995). Pathway definitions used were obtained from KEGG. Only pathway definitions with a minimum of 3 hits from the input list were retained.

5.2.4 Integrated over-representation pathway analysis of metabolomics and transcriptomics datasets using IMPaLA

IMPaLA is an online analytical software tool that allows the combined pathway analysis of transcriptomics and metabolomics datasets (Kamburov et al., 2011). ORA was performed using input lists of the significantly changing Ensembl gene and KEGG compound IDs generated in the previous chapter (Section 4.3.3). Background lists of all detected Ensemble and KEGG IDs were used to avoid bias as above. IMPaLA applies Fisher's exact test independently for transcriptomics and metabolic datasets and then integrates the resulting p-values using Fisher's combined probability test (Cavill et al., 2011). These 'joint-p' values are then corrected using a FDR of 0.05 to account for the multiple testing hypothesis (Benjamini and Hochberg, 1995). Pathways relating to diseased states and first-tier Reactome definitions that encompass many smaller pathways (e.g. 'Metabolism' or 'Signal transduction') were excluded. Only pathway definitions with a minimum of 3 hits from each input list were retained.

5.2.5 Confirmation of gene changes in purine metabolism pathway by quantitative, reverse transcriptase PCR

To validate the microarray data, Reverse-Transcriptase quantitative PCR (RT-qPCR) was conducted on the four genes from the purine metabolism pathway whose expression was discovered to have been altered significantly in response to AgNP exposure. The same samples used for microarray analysis were used for validation by RT-qPCR.

5.2.6 Synthesis of cDNA

Prior to primer validation and RT-qPCR, cDNA was synthesised using a Tetro cDNA synthesis kit (Bioline Reagents Limited, London, UK) according to manufacturer's instructions. RNA was first incubated with a mix of random hexamers (1 µl) for 2 minutes at 65 °C to denature template RNA. For primer validation 500 ng of template RNA was

used. For cDNA synthesis from omics-samples, the maximum available volume of 12 µl was used due to very low sample concentrations. Once incubation was completed, 5x RT Buffer (4 µl), a 10 mM dNTP mix (1 µl), Ribosafe RNase inhibitor (1 µl), and 1 µl Tetro reverse transcriptase (200 units/µl) was added to each tube. For primer validation, nuclease free water was added to make a final reaction volume of 20 µl. Each reaction was incubated using a thermocycler (Eppendorf Mastercycler Gradient; Eppendorf, Cambridge, UK) according to the temperature cycle outlined below (Table 5.1). The concentration of cDNA was measured after synthesis using a Nanodrop spectrophotometer, with an analysis constant of 33 for single-stranded DNA, and stored at -20°C.

Table 5.1: The temperature cycle for synthesis of cDNA using Tetro reverse transcriptase

Temperature	Duration	Notes
25 °C	10 min	Annealing
42 °C	90 min	cDNA synthesis
70 °C	15 min	Denaturation

5.2.7 Primer design and validation

Primers were designed using Primer3 (Rozen and Skaletsky, 1999) and synthesised by Sigma-Aldrich (Sigma-Aldrich, UK). Primer sequences are presented in Table 5.2

.

Table 5.2: qPCR primer sequences and target information

Gene ID	Ensemble ID	Human Gene Symbol	Direction	Primer Sequence (5' to 3')
DM00042	ENSG00000185100	ADSSL1	Forward	TAATGGAATCCGCGTTGCTG
			Reverse	CCAAGACCATTTTCCCTGCC
DM00720	ENSG00000185100	ADSSL1	Forward	CTACCGCCATCGCTTATTGG
			Reverse	ATCCACAACGTCTTTTCCGC
DM00278	ENSG00000168002	POLR2G	Forward	ACGAAATTCTGTTGCACCCA
			Reverse	TGTCCAGGCTGTATGATTCCA
DM00814	ENSG00000076685	NT5C2	Forward	CACCTGTGTTCATGGCATCC
			Reverse	TGTAGTCCATGTCGAAGCCA
DM02745	ENSG00000198682	PAPSS2	Forward	AAATCCTCTTTGCGTTCCGG
			Reverse	ACATCGTAGGCAGAGATCCG

Primers were validated using BIOTAQ polymerase (Bioline Reagents Limited, London, UK). For each reaction, 100 ng of template cDNA was mixed with forward and reverse primers (each at 2 μM final concentration), 3 mM Mg^{2+} (from $MgCl_2$), 0.2 mM dNTPs and 1 unit of BIOTAQ polymerase. Once reactions were mixed, samples were incubated in a thermocycler (Eppendorf Mastercycler Gradient; Eppendorf, Cambridge, UK) to the temperature cycle outlined in Table 5.3, then prepared for gel electrophoresis to confirm the presence of a PCR product.

Table 5.3: Primer validation temperature cycle using BIOTAQ polymerase. Each stage proceeds in order from top to bottom with the middle three stages repeated (in order) 37 times before the final elongation stage

Temperature	Duration	Cycles	Notes
95 °C	5 min	1	Activation of TAQ
95 °C	30 s		Primer activation
60 °C	30 s	38	Annealing
72 °C	30 s		Elongation
72 °C	15 min	1	Final elongation

5.2.8 Agarose gel electrophoresis of PCR products

Agarose powder (Bioline Ltd, UK) was added to 1x TBE buffer (89 mM Tris base, 89 mM boric acid and 2 mM EDTA, adjusted to pH 8.0) with added SYBR Safe DNA gel stain (1 µl per 10 ml of dissolved gel, Invitrogen, Life Technologies, CA, USA) and dissolved by heating. Once poured and set in the electrophoresis tank, the gel was submerged in 1x TBE Buffer. DNA samples and DNA molecular weight markers (100 bp, New England Biolabs, USA) were mixed with loading dye (6x gel loading dye, orange; New England Biolabs, USA) and loaded into the wells. Electrophoresis was performed at 80 V for 20-45 minutes and the gel was visualised by UV trans-illumination (Machine, model, manufacturer). PCR products were confirmed by sequencing, as described in section 5.2.9.

5.2.9 Purification and sequencing of PCR products

Prior to sequencing, PCR products were purified using a kit (QIAquick PCR purification kit, QIAGEN) according to the manufacturer's guidelines. Briefly, 5 µl of sodium acetate and 250 ml buffer PB were added to the product and filtered through the QIAquick column for 1 min at 13,000 rpm in a desk-top microfuge (5415D, Eppendorf). The column was washed with 750 µl of buffer PF, the product was then eluted from the column in 50 µl nuclease free water. Purified samples were sequenced by the Functional Genomics and Proteomics Unit, (School of Biosciences, University of Birmingham, Birmingham, UK) using an ABI3730 DNA analyser (Applied Biosystems, UK). Each sequencing reaction was set up using 10 ng of the purified DNA samples and 0.4 µl of either reverse or forward primers (10 pmol). The final volume was adjusted to 10 µl using sterile water. To determine whether the custom primers had amplified the gene of interest, the sequences of the amplified DNA fragments were imputed into BLAST (http://blast.ncbi.nlm.nih.gov/Blast.cgi).

5.2.10 RT-qPCR using omics samples

Following cDNA synthesis from all selected groups, the three biological replicates with the highest concentration and best quality cDNA were selected for RT-qPCR. Approximately 100 ng of each sample was mixed with a final concentration of 1 µM forward and reverse primers and 10 µl of SensiFAST SYBR Lo-ROX mix (Bioline Reagents Limited, London, UK) and made to a total volume of 20 µl per individual reaction. Each of the 21 biological samples was plated in triplicate on a 96-well PCR plate (Agilent Technologies). A separate plate was used for each of the selected genes with a functioning pair of primers including 4 $\log_{10}$-fold dilutions of template cDNA as a concentration curve, a non-template control and a non-reverse-transcriptase control which utilised template RNA instead of cDNA. Forward and reverse primers for the *D. magna* Actin gene were utilised as a reference gene. Each plate was scanned for SYBR Green 1 intensity on an Mx3005P RT-PCR machine and MxPro analysis software (Agilent technologies) using a 3-step cycle (Table 5.4) followed melt-profile analysis. Amplification efficiencies were calculated from the concentration curve.

Table 5.4: RT-qPCR temperature cycle. Each stage proceeds in order from top to bottom with the middle three stages repeated (in order) 39 times before melt-curve determination

Temperature (°C)	Duration	No. cycles
95	2 min	1
95	5 s	
60	10 s	40
72	5 s	
Melt curve		1

5.2.11 Relative quantification using the Pfaffl method

The amplification efficiencies of the reference and target genes were not equal; therefore the Pfaffl method (Pfaffl, 2001) was used to calculate relative expression levels of target genes. The Pfaffl method follows the equation outlined in Equation 5.1.

Equation 5.1: The Pfaffl method for relative quantification and calculation of the relative expression ratio (*R*). Where *E* represents the amplification efficiency of the target or reference gene and ΔCq is the Cq deviation of control – sample of the target of reference gene.

$$R = \frac{(E_{\text{target}})^{\Delta Cq_{\text{target}}(control-sample)}}{(E_{\text{reference}})^{\Delta Cq_{\text{ref}}(control-sample)}}$$

5.2.12 Confirming the identities of significantly changing metabolites

A *D. magna* QC aliquot was re-suspended in 100 µl of a 4:1 mixture of methanol:water with 20 mM ammonium acetate for FT-ICR MS analysis in negative ion mode according to protocol outlined earlier (Section 4.2.4). The use of a smaller re-suspension volume was to enhance sensitivity for easier detection of the lower intensity peaks of interest. Once re-suspended, 5 µl aliquots were loaded onto a 384 well plate as before, and sealed using a single, heat-sealed, foil sheet. Samples were directly and continuously infused into the MS using parameters outlined earlier (Section 4.2.5). Using the FT-ICR-MS, attempts were made to manually isolate (1 *m/z* isolation window) ions at 266.08954 *m/z*, 267.07354 *m/z* 282.08439 *m/z* and 328.04510 *m/z* believed to correspond to deoxyadenosine/guanosine, inosine, guanosine and cAMP respectively. Isolated ions were fragmented through collision induced dissociation under nitrogen gas at a normalised collision energy of 35%, with detection of resulting product ions performed using the LTQ-MS. Where possible, the highest intensity product ion was subsequently isolated (1 *m/z*) and further fragmented (normalised collision energy of 35 %), as above. The fragmentation patterns of the

isolated peaks were compared to those reported in the available literature for purified standards (Struck-Lewicka et al., 2014; Stentoft et al., 2014).

5.3 Result and Discussion

5.3.1 Putative annotation of molecular markers of AgNP exposure

After implementing the annotation processes outlined above (section 5.2.1), 4121 of the 8128 detected gene spots were identified as putative orthologues of human genes, and were assigned human Ensembl gene IDs. Of these, 313 changed significantly in expression upon exposure to AgNPs and a detailed list is available in the Appendix (Table 9.6). Despite the genome of *D. magna* being sequenced the data is not yet published or available for public use. This situation will be partially responsible for the relatively low level of annotation observed in this study; the other will be due to the many 'species specific' genes that have no homologue in other model organisms (Colbourne et al., 2011).

Of the 1330 detected m/z peaks, only 145 were successfully assigned at least 1 empirical formula with a minimum of 1 putative KEGG Compound ID. Of these, 26 had been deemed to change significantly in intensity upon exposure to AgNPs. A full list of all putatively annotated significantly changing *m/z* peaks can be found in the appendix (Table 9.7). Although the transformation mapping algorithm improves assignment of putative IDs, many of the 145 successfully annotated m/z peaks had been assigned multiple potential KEGG IDs. 361 KEGG IDs had been assigned in total, with 68 assigned to significantly changing *m/z* values. Due to the nature of the data the true identity cannot be assigned at this point so, for computational pathway analysis, all putative identities have to be assumed to be equally possible.

5.3.2 Interpreting annotation: over-representation analysis of annotated variables

All 313 putative Ensemble IDs were imputed into DAVID for ORA against a background of all detected putative Ensemble IDs using Fisher's exact test. Pathway definitions from KEGG-Pathway, Reactome-Pathway, BIOCARTA and BBID were used in the analysis. Similarly, each of the 68 individual putative KEGG IDs assigned to each of the 31 generated empirical formulae were compiled and imputed into MetaboAnalyst for over-representation pathway analysis again using Fisher's exact test (Xia et al., 2012). Following correction for multiple testing using a FDR of 0.05 (Benjamini and Hochberg, 1995), it was determined that none of the tested transcriptional or metabolic pathway definitions were significantly enriched. It is worth noting however, that the galactose metabolism pathway as defined by KEGG had an adjusted p-value of 0.0622 following ORA via MetaboAnalyst.

The result of Fisher's exact test directly depends upon the size of the background list used for comparison. Due to the bottle-neck of metabolite identification, the number of detected metabolites that can be putatively annotated is limited, resulting in a truncated background list of hundreds of metabolites compared to the potential thousands that exist in eukaryotic cells (Bouhifd et al., 2013). This, along with the limited annotation of the *D. magna* microarray in use, could potentially reduce the efficiency of analysis making it less likely for any one pathway to be statistically over-represented. Despite a lack of significant over-representation, the data still holds information as to which pathways are impacted by Ag exposure. To isolate potential pathways of interest, disease-related pathways and first-tier Reactome pathways were removed, as were any pathway definitions with < 4 hits from the input list. This shortlisted 22 transcriptional pathway definitions (Table 5.5) and 6 metabolic pathway definitions (Table 5.6) which were involved in the response to Ag toxicity.

Table 5.5: Pathways of interest following over-representation analysis of the transcriptomics dataset via DAVID. For each pathway the number of significant and background hits is included as well as the raw and FDR-correct p-values.

Pathway Name	Pathway Source	Input List		Background		Statistics	
		Hits	Total	Hits	Total	p-value	adj p-value
Amino sugar and nucleotide sugar metabolism	KEGG	6	110	20	989	0.0595	0.9998
Retinol metabolism	KEGG	4	110	12	989	0.1371	1.0000
Cysteine and methionine metabolism	KEGG	4	110	13	989	0.1646	0.9998
Chemokine signaling pathway	KEGG	6	110	28	989	0.1871	0.9994
Processing of Capped Intron-Containing Pre-mRNA	REACTOME	7	73	40	730	0.1924	0.9947
Tyrosine metabolism	KEGG	4	110	14	989	0.1936	0.9978
Signaling by Rho GTPases	REACTOME	4	73	21	730	0.3433	0.9838
Metabolism of amino acids	REACTOME	9	73	69	730	0.3682	0.9765
Biological oxidations	REACTOME	4	73	23	730	0.3999	0.9720
Lysosome	KEGG	6	110	38	989	0.4101	0.9981
Glutathione metabolism	KEGG	4	110	21	989	0.4131	0.9970
Transcription	REACTOME	5	73	34	730	0.4368	0.9703
Pathways in cancer	KEGG	7	110	51	989	0.5002	0.9979
Neurotrophin signaling pathway	KEGG	4	110	24	989	0.5039	0.9971
Focal adhesion	KEGG	6	110	43	989	0.5233	0.9948
Metabolism of carbohydrates	REACTOME	5	73	44	730	0.6495	0.9941
Wnt signaling pathway	KEGG	4	110	30	989	0.6610	0.9966
Metabolism of lipids and lipoproteins	REACTOME	5	73	49	730	0.7343	0.9955
Signalling by NGF	REACTOME	4	73	39	730	0.7614	0.9955
Purine metabolism	KEGG	4	110	38	989	0.8104	0.9988
MAPK signaling pathway	KEGG	4	110	42	989	0.8618	0.9993
Spliceosome	KEGG	4	110	43	989	0.8725	0.9992

Table 5.6: Pathways of interest following over-representation analysis of the metabolomics dataset via MetaboAnalyst. For each pathway the number of significant and background hits is included as well as the raw and FDR-correct p-values.

		Input List		Background		Statistics	
Pathway	Pathway Source	Hits	Total	Hits	Total	p-value	adj p-value
Galactose metabolism	KEGG	8	47	12	276	0.0008	0.0622
Starch and sucrose metabolism	KEGG	4	47	5	276	0.0088	0.3511
Fructose and mannose metabolism	KEGG	7	47	15	276	0.0248	0.6617
Butanoate metabolism	KEGG	4	47	9	276	0.1092	1.0000
Purine metabolism	KEGG	6	47	16	276	0.1095	1.0000
Amino sugar and nucleotide sugar metabolism	KEGG	4	47	13	276	0.3119	1.0000

As outlined in Table 5.5, the genes that were identified as being significantly up or down regulated in response to Ag exposure are involved in many varied processes. These include the metabolism and transport of small molecules such as hexose sugars and amino acids, and signalling cascades involving MAP kinases, nerve growth factor, neurotrophin and Rho-GTPases. The glutathione metabolism and cysteine and methionine metabolism pathways both contain four gene products which alter significantly in response to Ag exposure. Both glutathione and cysteine contain thiol groups and can act to both sequester free metal ions including Ag^{+} and to protect against oxidative stress through the reduction of ROS. The metabolic pathways outlined in Table 5.6 are involved in the metabolism of dietary sugars as well as purines and amino-sugars and nucleotide sugars. This may suggest an impact on energy metabolism and the production of ATP, processes which have been seen to be impacted by Ag exposure previously.

While robust and informative, these two independent ORA alone do not give a definitive image of the extent of overlap and interaction between the transcriptome and metabolome of Ag-exposed *Daphnia*. It is possible to gain knowledge of these interactions through conceptual integration of these lists based on published data, however this approach is subjective and may result in potentially novel mechanisms being overlooked (Cavill et al., 2011). As a more objective, statistical approach, integrated pathway analysis was used to take the interactions between metabolites and genes into account. The KEGG Compound IDs and the Ensembl Gene IDs putatively assigned to the significant, annotated MS peaks and gene-probes respectively were compiled for ORA using IMPaLA (Kamburov et al., 2011). ORA was implemented using Fisher's exact test with a reference background of all detected Ensembl Gene IDs and KEGG Compound IDs. After correcting for the multiple testing hypothesis (Benjamini and Hochberg, 1995), it was again found that none of the molecular-level pathways from the 12 tested databases were significantly over-represented

(Table 5.7). As with the results of DAVID and MetaboAnalyst, the result of ORA via IMPaLA is restricted by the limitations in metabolite identification and the current level of annotation of the *D. magna* microarray.

Despite the lack of significant over-representation, the results are informative as to the pathways in which significantly altered metabolites and gene products are involved. To isolate potential pathways of interest, those with ≥ 3 putative metabolites and ≥ 3 putative genes were shortlisted. These parameters yielded 2 pathway definitions from KEGG, 1 from the Edinburgh Human Metabolic Network (EHMN), and 10 from the Reactome database. To restrict the search further, pathways relating to diseased states were excluded as well as first-tier Reactome definitions that encompass many smaller pathways (e.g. 'Metabolism' or 'Signal transduction'). This second stage filter resulted in 11 pathway definitions which are listed in Table 5.7. These suggest perturbations to the metabolism of lipids, lipoproteins and fatty acids, the transport of small organic molecules, the metabolism carbohydrates, signalling via G-protein coupled receptors and the metabolism of purines.

Table 5.7: Pathways of interest following over-representation analysis. For each pathway the number of significant and background hits is included for transcriptomics and metabolomics analyses. The p-values and adjusted p-values from the integrated analyses are also included. Pathway definitions are from Reactome, KEGG, and the Edinburgh Human Metabolic Network (EHMN).

		Transcriptomics		Metabolomics		Integrated Statistics	
Pathway Name	Pathway Source	Input Hits	Background Hits	Input Hits	Background Hits	p-value	adj p-value
Metabolism of lipids and lipoproteins	Reactome	19	123 (490)	6	15 (443)	0.0234	1
Amino sugar and nucleotide sugar metabolism - Homo sapiens (human)	KEGG	6	21 (47)	4	13 (99)	0.0314	1
Fatty acid, triacylglycerol, and ketone body metabolism	Reactome	6	42 (92)	3	6 (90)	0.125	1
SLC-mediated transmembrane transport	Reactome	5	35 (254)	10	35 (164)	0.142	1
Purine metabolism - Homo sapiens (human)	KEGG	4	41 (172)	6	16 (92)	0.167	1
Transport of sugars, bile salts, organic acids, metal ions and amine compounds	Reactome	3	14 (97)	6	23 (83)	0.199	1
Metabolism of carbohydrates	Reactome	9	67 (255)	4	12 (120)	0.219	1
Purine metabolism	EHMN	4	55 (224)	5	16 (94)	0.419	1
Signaling by GPCR	Reactome	5	41 (1071)	4	15 (151)	0.436	1
GPCR downstream signaling	Reactome	4	29 (960)	3	14 (124)	0.538	1
Metabolism of nucleotides	Reactome	3	31 (80)	5	20 (135)	0.551	1

5.3.3 AgNPs and Ag^+ ions induce a significant change in metabolites and gene-products involved in purine metabolism

Of the shortlisted pathways, purine metabolism as defined by KEGG showed the greatest interaction between the constituent significant gene-products and putative metabolites. All significantly changing gene-probes and *m/z* peaks found within this pathway are listed in Table 5.8..

Table 5.8: Putative identities of significantly changing metabolites and gene-products in the purine metabolism pathway.

m/z peak	KEGG Compound ID	Putative name	adj p-value
266.08954	C00330	Deoxyguanosine	0.01044
266.08954	C00212	Adenosine	0.01044
267.07354	C00294	Inosine	0.00770
282.08439	C00387	Guanosine	0.00022
328.0451	C02353	2',3'-Cyclic AMP	0.01881
328.0451	C00575	3',5'-Cyclic AMP	0.01881

Gene ID	Ensemble gene ID	Predicted function	Human Symbol	adj p-value
DM00042	ENSG00000185100	adenylosuccinate synthase like 1	ADSSL1	0.03860
DM00278	ENSG00000168002	polymerase (RNA) II (DNA directed) polypeptide G	POLR2G	0.00167
DM00720	ENSG00000185100	adenylosuccinate synthase like 1	ADSSL1	0.00130
DM00814	ENSG00000076685	5'-nucleotidase, cytosolic II	NT5C2	0.00822
DM02745	ENSG00000198682	3'-phosphoadenosine 5'-phosphosulfate synthase 2	PAPSS2	0.01880
DM09437	ENSG00000185100	adenylosuccinate synthase like 1	ADSSL1	0.04520

AgNP exposure has been suggested previously to affect the metabolism of purines. Specifically, Wistar rats exposed to AgNPs showed elevated excretion of uric acid and allantoin which are products of purine breakdown (Hadrup et al., 2012). What is observed in this study is a significant increase in the four peaks putatively annotated as cyclic adenosine monophosphate (cAMP), inosine, guanosine and adenosine/deoxyguanosine. The relative fold changes of these peaks are at their highest in response to AgNP High (Figure 5.2). Interestingly, these four m/z peaks are all within the top 50 loadings values from PCA analysis, indicating their importance in the concentration-dependant response observed in the last chapter (Figure 4.10). The six significantly changing gene-probes within this pathway have four predicted functions: adenylosuccinate synthase (ADSSL1), polypeptide G of RNA polymerase II (POLR2G), cytosolic II 5'-nucleotidase (NT5C2) and 3'-phosphoadenosine 5'-phosphosulfate synthase 2 (PAPSS2). NT5C2 in particular interacts with the four putative purine nucleosides inosine, guanosine, adenosine, and deoxyguanosine catalysing the dephosphorylation of their respective monophosphates (Figure 5.1). Two of these nucleoside-monophosphates, AMP and dGMP, are putatively detected but do not change significantly in intensity. With the exception of POLR2G whose expression putatively decreases in response to AgNP High exposure, the remaining target genes show an increase in expression with increasing AgNP or Ag^{+} concentration (Figure 5.3).

The definitions of metabolic pathways or gene ontology functions used in ORA do not accurately reflect the intricate web of interactions that comprise cellular metabolism (Khatri et al., 2012). Many of the constituent genes and metabolites of these definitions function in multiple pathways, meaning that there is often overlap between the pathways themselves. This level of interaction and inter-dependence is not reflected in ORA or other forms of pathway analysis. Consequently this may mean that if a particular pathway

is affected by Ag exposure, the result following ORA may show multiple pathways to be over-represented due to overlapping genes or metabolites between the pathways. An example within this study may be seen following ORA of putative metabolites. Three of the pathways in Table 5.6; galactose metabolism, fructose and mannose metabolism and starch and sucrose metabolism, contain a large number of overlapping metabolites. It is therefore not possible to say that any one of these pathways is or is not over-represented, they are therefore treated as being equally likely.

Likewise any significant constituent of an over-represented pathway may be altered due to perturbations in a different pathway. The putative significantly changing metabolites involved in the purine metabolism pathway are also involved in multiple cellular processes. As well as being essential for the production of nucleoside triphosphates and therefore the synthesis of RNA, the three nucleosides inosine, guanosine and adenosine have alternative roles. Adenosine is essential for the production of ATP, the primary source of energy for all active processes. Guanosine is necessary for the production of GDP and GTP which are key for the function of G-protein coupled receptors. These membrane proteins trigger cellular signalling through, among others, the cAMP signalling pathway which is involved in the regulation of glycogen, sugar and lipid metabolism.

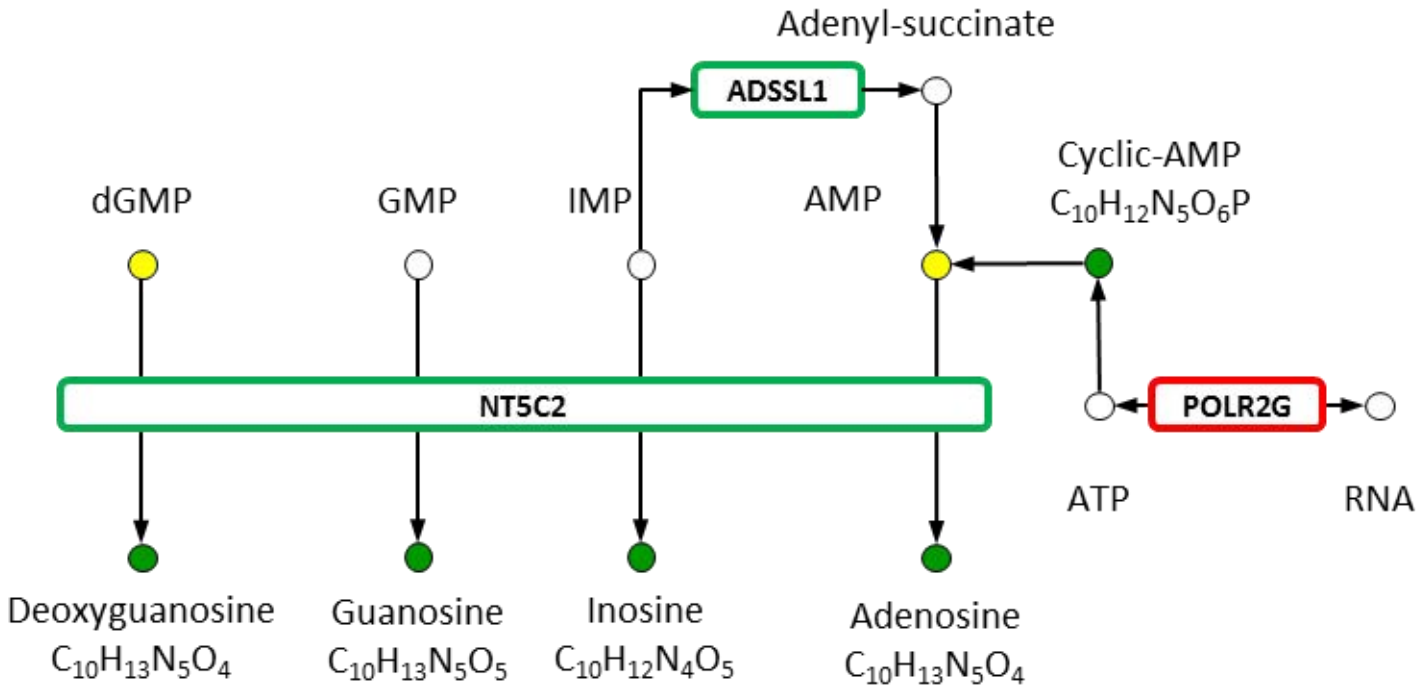

Figure 5.1: Map of the key interactions between significantly changing putative metabolites and gene-products in the purine metabolism pathway. Circles represent metabolites which are not-detected (white), putatively annotated but unchanged in intensity (yellow) or putatively annotated significantly elevated in intensity (green) with directional arrows indicating inter-conversions between metabolites. Oblongs represent gene products that catalyse reactions between metabolites and are either significantly up- (green) or down- regulated.

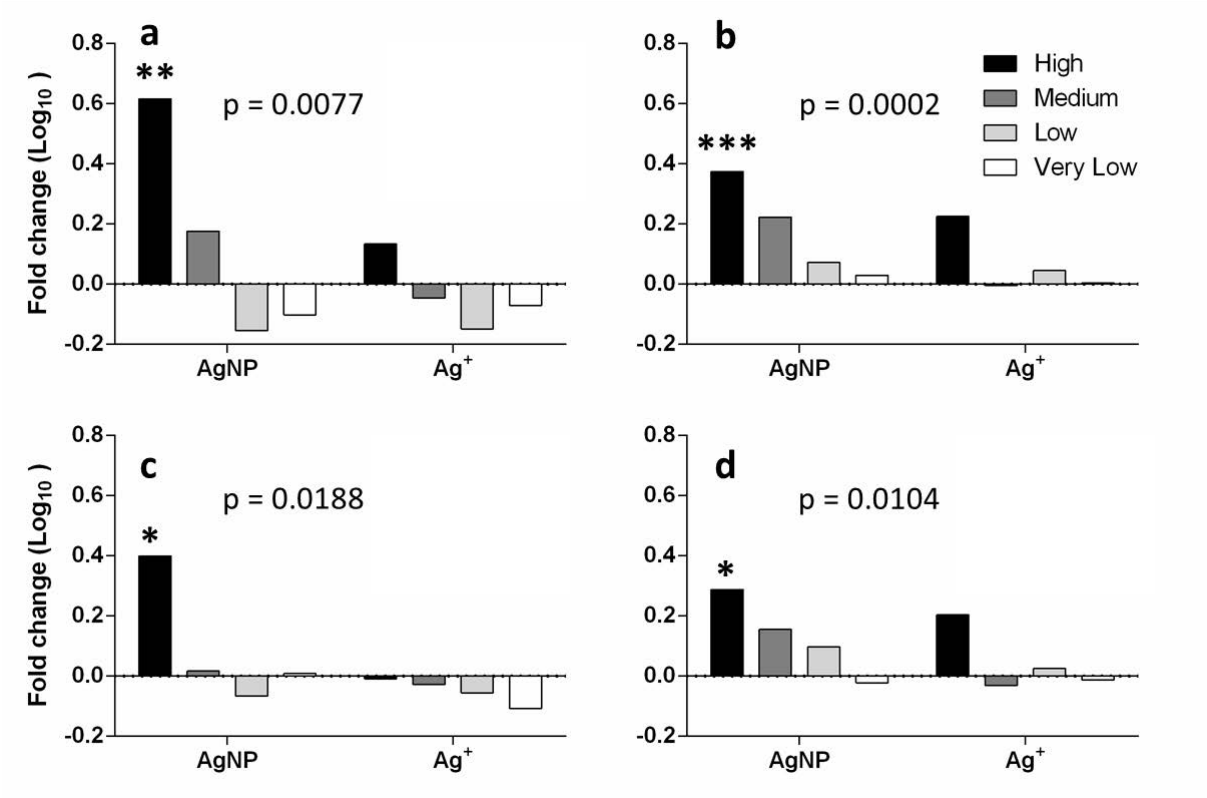

Figure 5.2: Fold changes of the peaks corresponding to the putative IDs of inosine (a), guanosine (b), cAMP (c) and adenosine/deoxyguanosine (d) relative to the combined control in response to varying concentrations of AgNP and Ag^+. Mean relative fold changes have been Log_{10} transformed. P-values were generated following a 1-way ANOVA and stars have been placed over those groups that changed significantly compared to the combined control. Analysis by 2-way ANOVA indicated no significant difference between AgNPs and dissolved Ag.

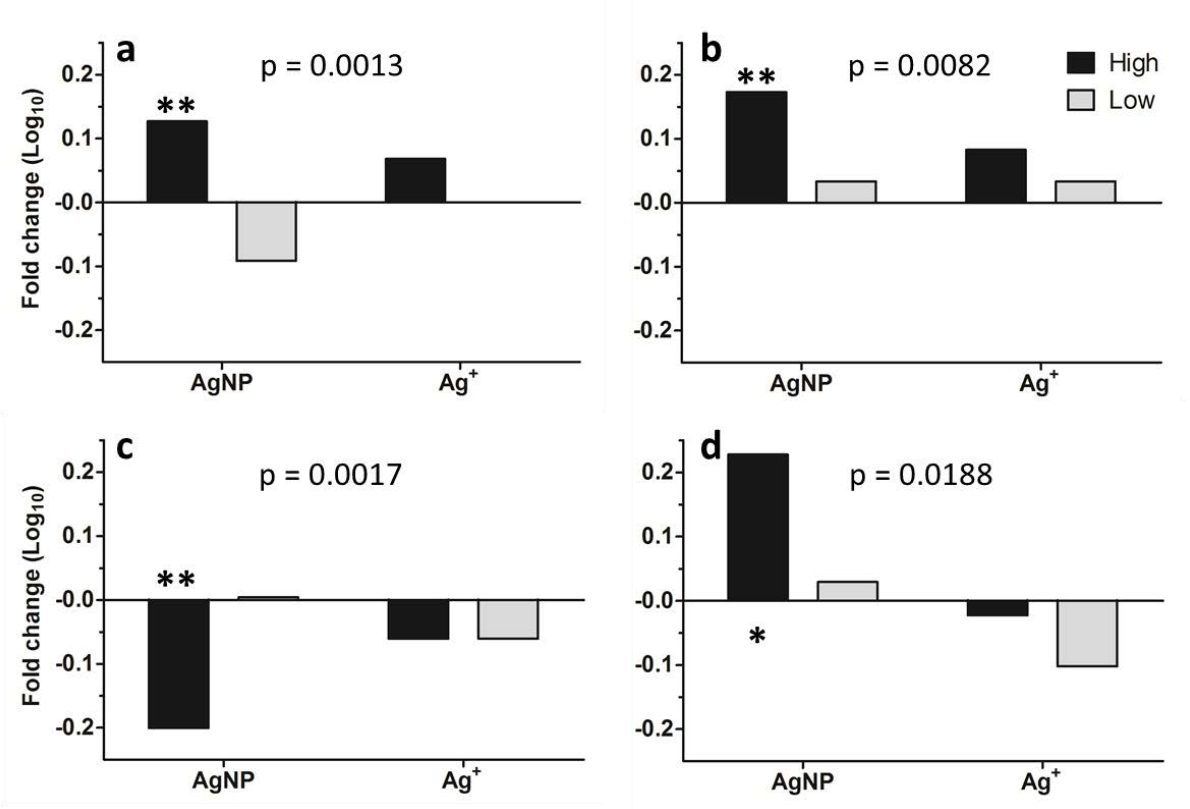

Figure 5.3: Fold changes of microarray gene spots for ADSSL1 (a), NT5C2 (b), POLR2G (c) and PAPSS2 (d) relative to the combined control in response to High and low concentration AgNP and Ag^+ exposure. Mean relative fold change values have ben Log_{10} transformed. P-values were generated following a 1-way ANOVA and stars have been placed over those groups that changed significantly compared to the combined control. Analysis by 2-way ANOVA indicated no significant difference between AgNPs and dissolved Ag.

5.3.4 Attempted confirmation of perturbed gene regulation by qPCR

RT-qPCR was used to confirm the perturbations of the four genes with predicted functions within the KEGG purine metabolism pathway measured to be significantly changing by DNA microarray. During validation, the primers designed for DM02745 (PAPSS2) did not produce a product so were excluded from RT-qPCR. Additionally the primers designed for DM00720 were chosen over DM00042 due better alignment of the product sequence with the target gene (ADSSL1). The remaining primers were successfully validated and found to amplify the correct targets as described above (section 5.2.7). All target genes measured in the test control and exposure groups showed relatively small error between technical replicates but large variation between biological replicates. As a result, when the different control and exposure conditions were measured by qPCR and compared by ANOVA, target-gene expression was not found to be significantly different (Figure 5.4).

.

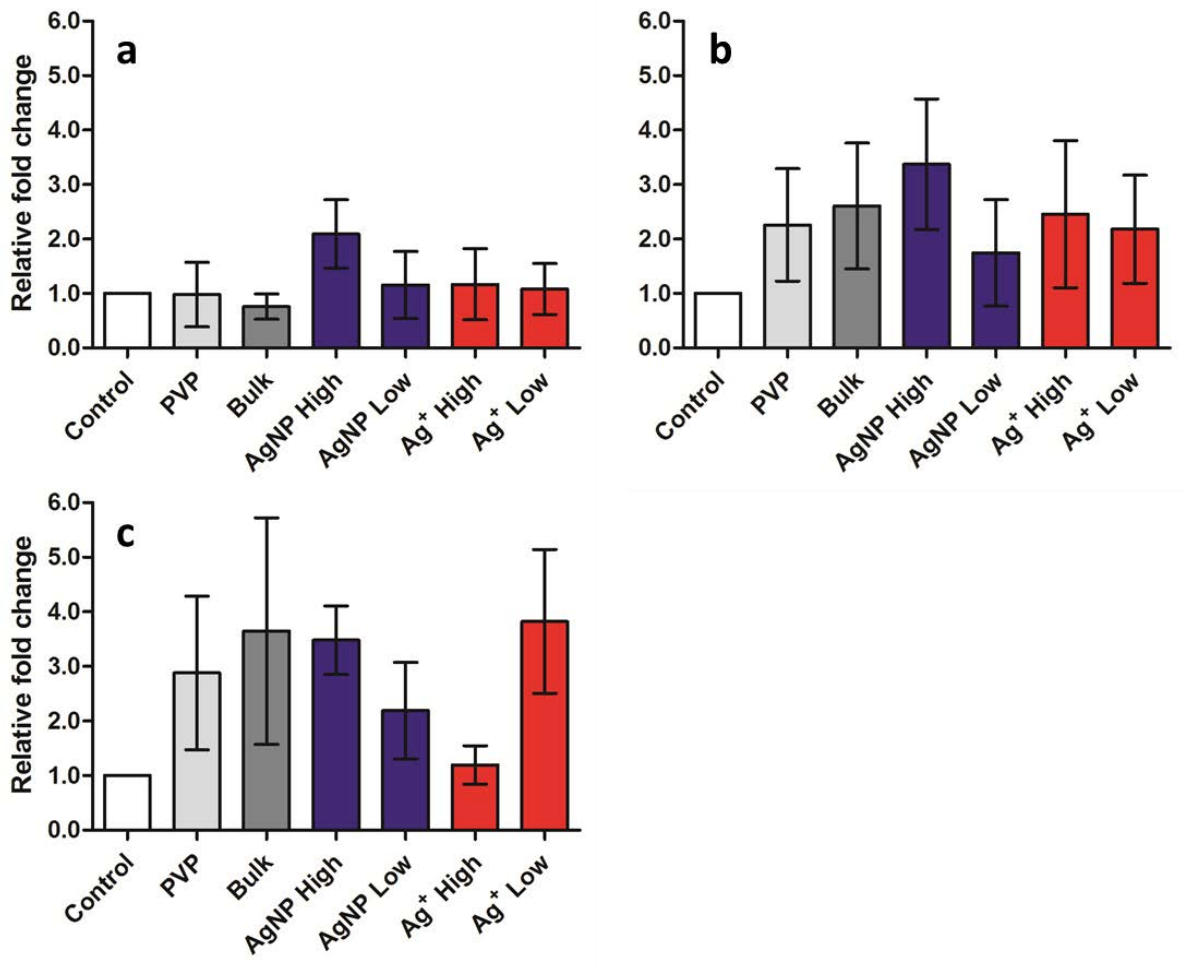

Figure 5.4 The mean ± SEM relative fold changes of ADSSL1 (a), NT5C2 (b) and POLR2G (c) expression following exposure to AgNP, Ag^{+} and control conditions. Relative fold change was determined by the Pfaffl method. Expression levels were not found to alter significantly in any exposure or control condition.

5.3.5 Identification of inosine and guanosine by MS/MS fragmentation

As stated earlier, the empirical formulae and KEGG Compound names assigned by MI-Pack are putative annotations, and may not reflect the true identity of m/z peaks involved. To comprehensively identify peaks of interest they can be isolated and fragmented using MS/MS. The fragmentation pattern of the isolated peaks can then be compared with pure metabolite standards to confirm their identity. It was only possible to successfully isolate two of the four target peaks; 267.07334 *m/z* and 282.08422 *m/z* corresponding to the putative KEGG IDs of inosine and guanosine respectively. Upon fragmentation of 267.07334 *m/z* (Figure 5.5) and 282.08422 *m/z* (Figure 5.6) the main fragments observed were at 134.9 *m/z* and 150.0 *m/z* respectively which are the approximate *m/z* values of deprotonated ($[M-H]^-$) hypoxanthine and guanine (Stentoft et al., 2014). This purports to a neutral loss of approximately 132 Da, corresponding to loss of a deoxyribose sugar in both instances (Stentoft et al., 2014). Subsequent isolation and fragmentation of the ion at 134.9 m/z, yielded two additional peaks at 91.9 *m/z* and 108.0 *m/z* (Figure 5.5) which have been reported previously as corresponding to the loss of –HCNO and –HCN respectively from hypoxanthine (Struck-Lewicka et al., 2014). Further fragmentation of 150.0 *m/z* produced an additional peak at 133.0 *m/z* (Figure 5.6) potentially corresponding to the neutral loss of NH_3 from the guanine structure (Struck-Lewicka et al., 2014).

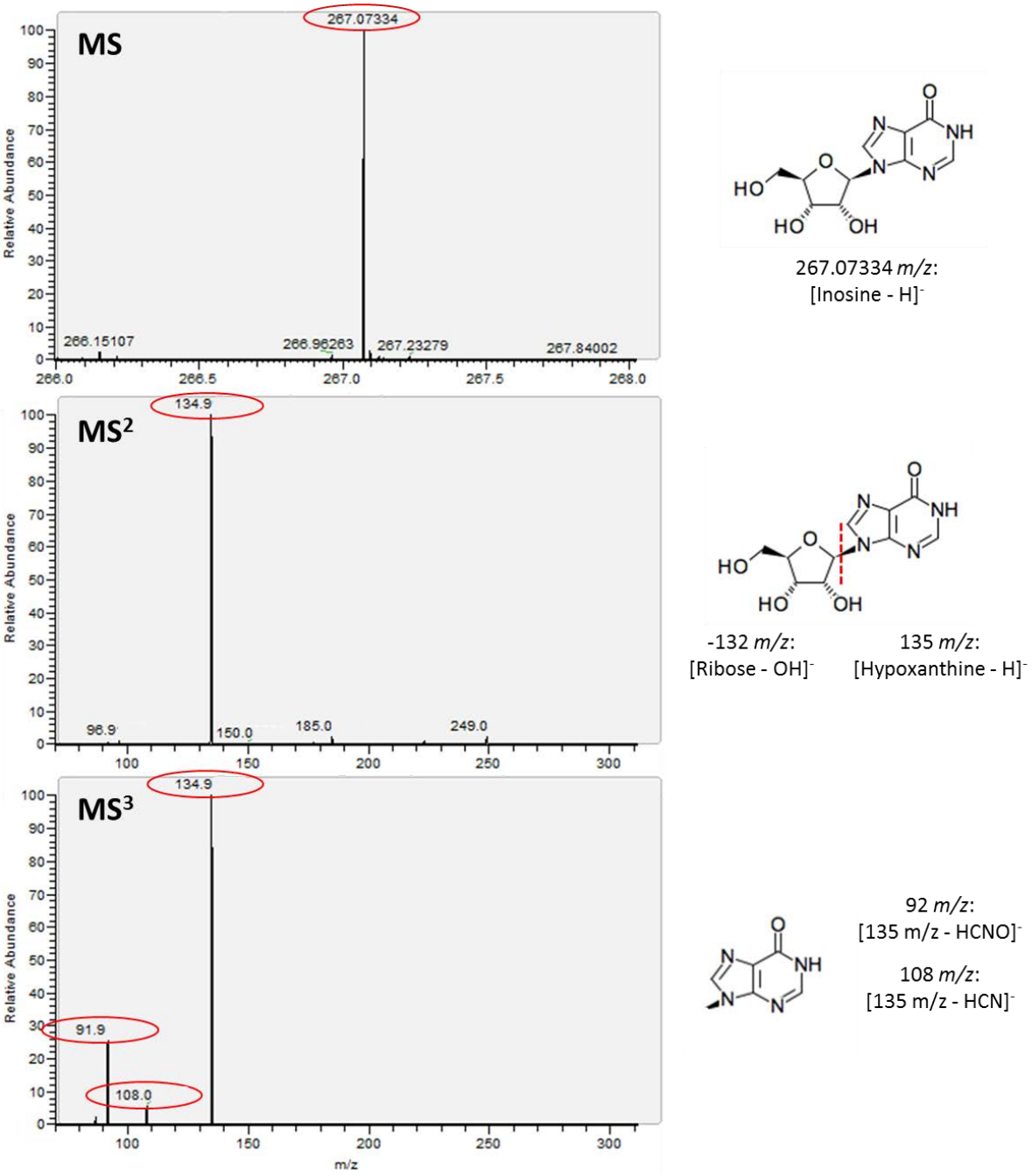

Figure 5.5: The fragmentation pattern of an isolated precursor ion at 267.07334 *m/z*. Shown above is the isolated parent peak (MS), the initial fragments (MS^2), and the fragments produce upon fragmentation of the main MS^2 fragment (MS^3).

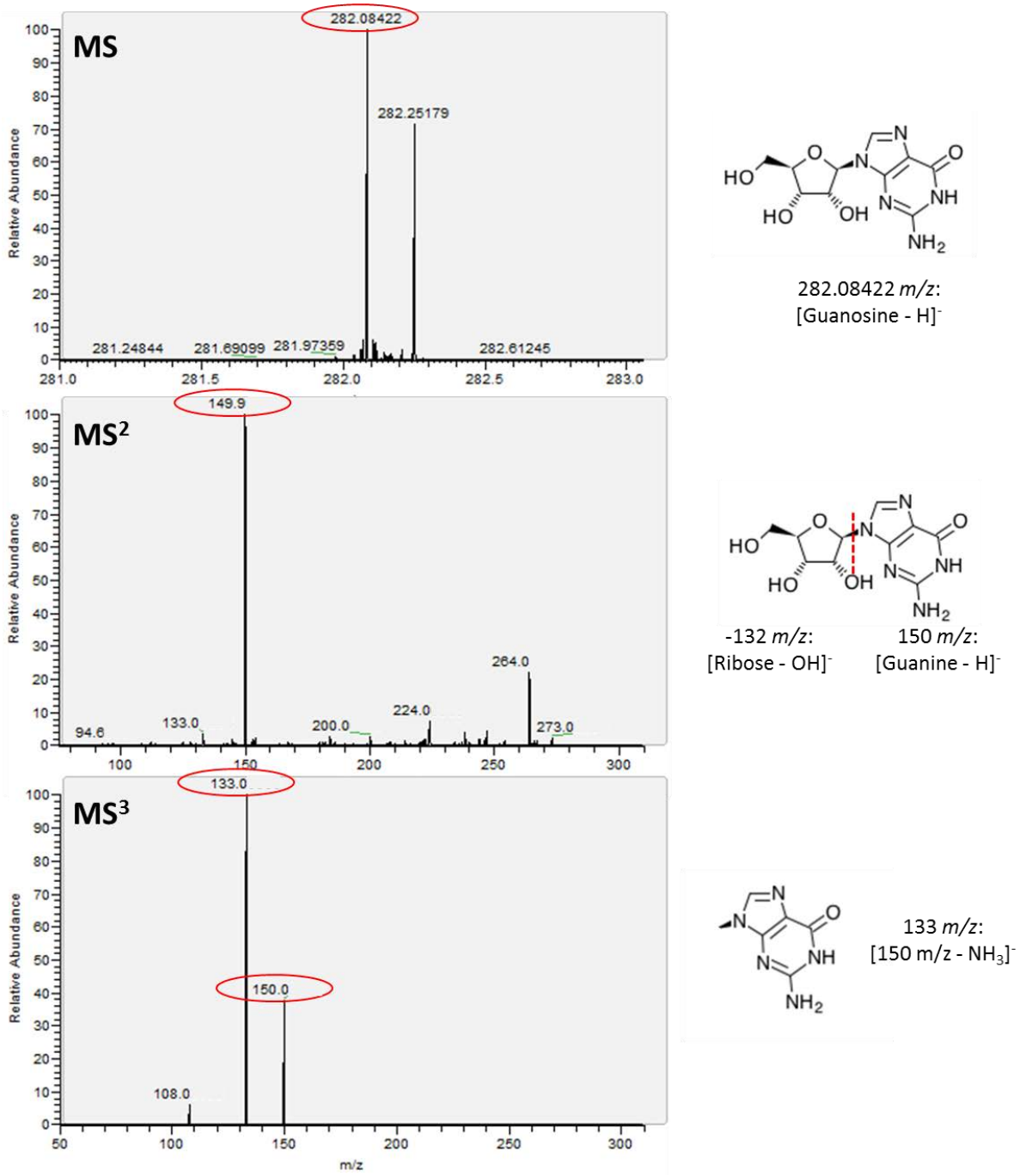

Figure 5.6: The fragmentation pattern of an isolated precursor ion at 282.08422 *m/z*. Shown above is the isolated parent peak (MS), the initial fragments (MS^2), and the fragments produce upon fragmentation of the main MS^2 fragment (MS^3).

The similarities between the observed fragmentation patterns of these peaks to those previously reported from purified standards (Struck-Lewicka et al., 2014; Stentoft et al., 2014) heavily suggests that *m/z* 267.07334 and 282.08422 correspond to the $[M-H]^-$ ions of inosine and guanosine respectively. As stated above, the peaks corresponding to these two compounds, and to the putative identities of cAMP, adenosine and deoxyguanosine, are within the top 50 PC3 loadings values generated in the previous chapter. This emphasizes the importance of these compounds in the response induced by AgNP exposure, with inosine ranked as the most important variable in the entire model.

Guanosine is a precursor for the synthesis of GTP; the substrate for G-protein coupled receptors. As seen from ORA (Table 5.7), downstream G-protein coupled receptor signalling pathways appeared to be affected following AgNP exposure. Related to this, the putative metabolite cAMP, seen to increase significantly in response to AgNP exposure, is an important second messenger molecule.

Both inosine and guanosine are ribonucleosides and as such are involved in the synthesis of RNA. Guanosine is used in the synthesis of messenger, ribosomal and transfer RNA whereas inosine is involved in the biosynthesis of some tRNA molecules (Elliott and Trewyn, 1984). Their elevated production in response to AgNP and Ag^+ exposure could simply be the result of increased transcription and translation of proteins involved in the response to toxicant exposure. The inhibition of RNA polymerase by AgNP has been previously observed; Wang and colleagues demonstrated that exposure of erythroid progenitor cells to AgNP resulted in the inhibition of RNA polymerase activity and RNA transcription through the direct binding of AgNPs to the enzyme (Wang et al., 2013). This could explain the significant increase in inosine and guanosine with respect to combined control groups; inhibition of RNA polymerase could indirectly result in an accumulation of these metabolites due to reduced RNA synthesis.

Alternatively inosine, guanosine and also adenosine have been previously reported to act as cyto-protective compounds by combating oxidative stress (Jurkowitz et al., 1998; Módis et al., 2009; Li et al., 2011; Cipriani et al., 2014). These compounds have been suggested to have both anti-oxidant properties and induce the expression of DNA repair genes and the production of antioxidants (Gudkov et al., 2006; Dal-Cim et al., 2012). It is therefore possible that the increased production of inosine and guanosine is the result of AgNP or Ag^+ induced oxidative stress.

5.4 Conclusions

The work presented in this chapter represents the first attempt to identify the molecular response of *D. magna* to AgNP and Ag^+ exposure using a combination of metabolomics and transcriptomics techniques. In the previous chapter, microarray gene-spots and m/z peaks that changed significantly in intensity were shortlisted, giving a list of the most important variables in the molecular response to AgNP and Ag^+ exposure. Here, those features were successfully assigned putative identities, and pathway analysis was applied to identify molecular pathways which had been putatively perturbed. Through use of IMPaLA, ORA was simultaneously applied to the transcriptomics and metabolomics shortlists to statistically integrate both levels of observation. The results of this analysis showed perturbation of genes and metabolites involved in the metabolism of lipids and fatty acids, the transport of small organic compounds, the metabolism of carbohydrates, G-protein coupled receptor signalling and the metabolism of purines. Further investigation of these pathways showed substantial interaction between the components on the purine metabolism pathway, with one enzyme in particular (NT5C2) being responsible for the production of 4 putative compounds. Due to the large variation of gene-expression between biological replicates, confirmation of significantly

altered expression for these genes by PCR was not successful. However, MS/MS fragmentation gave greater confidence in the identity of *m/z* 267.07334 and *m/z* 282.08422 as the purine nucleosides inosine and guanosine respectively. The remaining significant peaks in this pathway could not be successfully isolated.

These two metabolites and the putative compounds adenosine and cAMP are within the top 50 PC3 loadings of the metabolomics PCA model produced in the last chapter. This indicates that these compounds play an important role in the metabolic response of *D. magna* to AgNP and Ag^{+} exposure. Exactly what role these two compounds play cannot be identified by this study, but both compounds are involved in the synthesis of RNA and have also been reported to have properties that protect cells from oxidative stress (Jurkowitz et al., 1998; Módis et al., 2009). The latter role links with mechanisms of AgNP (AshaRani et al., 2009; Chairuangkitti et al., 2013) and Ag^{+} (Yoshimaru et al., 2006; Cortese-Krott et al., 2009) toxicity suggested in the literature involving the induction of oxidative stress. It could be possible that the production of these compounds is increased for their signalling roles in an effort to increase production of DNA damage repair and antioxidant enzymes (Dal-Cim et al., 2012). However, it is possible the significant increase in these two metabolites is the result of RNA polymerase inhibition, which is consistent with previously published findings (Wang et al., 2013). In summary these two compounds represent good targets for future work investigating the mechanism of AgNP-induced toxicity.

Chapter 6: Exploring the role of reactive oxygen species and oxidative stress in Ag toxicity to *D. magna*

6.1 Introduction

Reactive oxygen species (ROS) are a group of short-lived chemically reactive oxygen-containing molecules which include the superoxide radical ($^{\cdot}O_2^-$), hydroxyl radical ($^{\cdot}OH$), hydrogen peroxide (H_2O_2) and singlet oxygen ($^1O_2$) (He et al., 2011). ROS are produced naturally within mitochondria as a by-product of oxidative phosphorylation. During this process some electrons can "leak" from the electron transport chain and interact with oxygen leading to the formation of the superoxide radical ($^{\cdot}O_2^-$) (Campian et al., 2004). This process is relatively infrequent under normal physiological conditions, with only 1-3% of oxygen molecules within the mitochondria being converted into $^{\cdot}O_2^-$ (Boveris and Chance, 1973; He et al., 2011). Although $^{\cdot}O_2^-$ has a relatively low reactivity, its presence propagates the formation of other oxygen-containing radicals such as the hydroxyl radical ($^{\cdot}OH$) which possesses the highest reduction potential of all biologically relevant ROS (Fu et al., 2014).

Normally, the production of this highly reactive and damaging species is kept in check by endogenous antioxidant enzymes and molecules. The superoxide radical for example, is converted to hydrogen peroxide and molecular oxygen by the anti-oxidant enzyme superoxide dismutase (SOD) (Liochev and Fridovich, 2000). The resulting hydrogen peroxide is then readily converted into water and molecular oxygen by the enzyme catalase (Finkel and Holbrook, 2000). Antioxidants are small molecules which participate in redox reactions to remove ROS and prevent their propagation and interaction with cellular components. The most important antioxidant in eukaryotic cells is glutathione (GSH), a tripeptide comprised of glutamic acid, cysteine and glycine (γ-glutamylcysteinylglycine) which acts as a defence against ROS, reactive xenobiotics or other electrophiles such as Ag^+.

Glutathione can reduce ROS directly through the thiol group of its cysteine residue resulting in the removal of free ROS and the production of reduced glutathione (GSSG). Glutathione is regenerated through the enzyme glutathione reductase which produces two molecules of GSH from one molecule of GSSG. Glutathione can also sequester reactive species through the actions of glutathione-S-transferase (GST), which catalyses the conjugation of GSH to molecules such as such as peroxidised lipids and oxidises proteins (Strange et al., 2001). If the production of ROS becomes excessive, cellular anti-oxidant systems can become overwhelmed resulting in a state of oxidative stress (Finkel and Holbrook, 2000). Common consequences of oxidative stress include damage to DNA, the oxidation of polyunsaturated fatty acids in lipids (lipid peroxidation) and oxidation of amino acids in cellular proteins. This can result in genotoxicity and mutations, as well as membrane and enzyme dysfunction potentially leading to cytotoxicity and cell death.

Heavy metals induce the production of ROS through either the Fenton or Fenton-like reactions (**Equation 6.1**) or the Haber-Weiss reaction (**Equation 6.2**) whereby the metal catalyses the production of hydroxyl radicals from cellular hydrogen peroxide (Jomova and Valko, 2011; Fu et al., 2014).

Equation 6.1: The Fenton reaction

$$Ag^0 + H_2O_2 \rightarrow Ag^+ + \cdot OH + OH^-$$

Equation 6.2: The Haber-Weiss reaction

$$\cdot O_2^- + H_2O_2 \xrightarrow{Ag^0} O_2 + OH^- + \cdot OH$$

Ag is thought to induce the formation of ROS through a Fenton-like reaction such as that outlined in **Equation 6.1** resulting in the formation of Ag^+ from Ag^0 (He et al., 2011). The Ag^+ ion can then react with O_2 causing the formation $\cdot O_2^-$ and reformation of Ag^0. This Ag-

induced generation of ROS and oxidative stress has been measured *in vitro* and *in vivo* both directly, through the detection of ROS via fluorescence-based biochemical assays (De Matteis et al., 2015) and indirectly through measurement of down-stream effects such as DNA damage (Asharani et al., 2009; De Matteis et al., 2015), protein oxidation (Rainville et al., 2014) and the expression of antioxidant enzymes (Asharani et al., 2009; Poynton et al., 2012). *In vitro*, exposure to AgNPs has been shown to cause a significant increase in glutathione content and SOD activity within mouse hepatocytes (Arora et al., 2009). AgNP-induced genotoxicity has also been detected via the comet assay following exposures to human lung fibroblasts (AshaRani et al., 2009), human cervix carcinoma cells and human lung carcinoma cells (De Matteis et al., 2015). Heme-oxygenase-1 (HMOX) has also been measured to increase significantly in response to AgNP exposure by RT-qPCR (Asharani et al., 2009) in human lung fibroblasts. *In vivo*, the disruption of mitochondrial activity and oxidative phosphorylation has been observed following Ag exposure in *C. elegans* (Ahn et al., 2014), *D. magna* (Stensberg et al., 2013; Scanlan et al., 2013) and *D. rerio* (Aerle et al., 2013). The mitochondria are the principal location of oxygen within cells and as such are often the primary site of ROS generation (Finkel and Holbrook, 2000). The presence of AgNPs within these organelles is thought to result in an increased production of ROS that ultimately leads to the disruption of energy production (Asharani et al., 2009; Verano-Braga et al., 2014).

It is thought that exposure to Ag species induces oxidative stress in *D. magna*. Exposure to AgNP was found to result in an increase of protein carbonylation (Rainville et al., 2014) which the authors surmised as indicating protein oxidation caused by oxidative stress. However the same study indicated that exposure to AgNPs and $AgNO_3$ did not result in a significant change of GST, catalase or GAPDH activity, which are known enzymatic responses to excessive ROS production (Rainville et al., 2014). Targeted RT-qPCR also

failed to identify a significant increase in GST mRNA expression. However, AgNP and $AgNO_3$ exposed *D. magna* demonstrated a significant increase in the expression of a DNA repair gene (REV1) in response to exposure to $1/10^{th}$ of the LC_{50} and the LC_{25} of PVP-coated AgNPs over 24 h (Poynton et al., 2012). A ^{1}H NMR-based metabolomics investigation into the response of *D. magna* to AgNP and $AgNO_3$ exposure identified similar response profiles in the metabolome of animals exposed to both forms of Ag (Li et al., 2015a). The response included an increase in lactate and phosphocholine concentrations and a decrease in the concentrations of glucose and certain amino acids, which the authors surmised as being an indication of a disruption of energy metabolism and consequential oxidative stress (Li et al., 2015a). Whether or not oxidative stress is induced by Ag species in *D. magna* is therefore still a contested issue, it also remains unclear whether any previously detected indications of oxidative stress are the direct result of the presence of Ag, or an inevitable consequence of Ag-induced cell death.

In this chapter, *D. magna* neonates were exposed to the Low and Mid concentrations of AgNP and $AgNO_3$ used in Chapter 4, then subjected to targeted RT-qPCR analysis for three biomarkers of oxidative stress: GST, SOD and HMOX. The expression of MT (metallothionein) was also monitored as a positive control to confirm exposure and internalisation of Ag, as an increase in MT transcription and protein abundance is a well-documented response to both nanoparticle and dissolved Ag species exposure (see section 1.2). To confirm exposure to the intended concentrations of dissolved Ag and AgNP, the total silver concentration of each individual exposure was measured by ICP-MS. DLS was also used in an attempt to confirm the presence of particles in AgNP exposures, and absence of particles in $AgNO_3$ and control exposures. The aim of the work in this chapter was to test the hypothesis proposed in Chapter 5 (section 5.4), that the observed increase in adenosine and inosine production following Ag exposure is in response to oxidative stress. Particular

interest is given to HMOX, as its expression has been previously documented as being elevated in response to guanosine exposure (Quincozes-Santos et al., 2014).

6.2 Methods

6.2.1 AgNP and $AgNO_3$ toxicity exposures to *D. magna* neonates

PVP-coated AgNPs were prepared as outlined in section 2.3 and the final concentration was measured as 23.98 mg/l by ICP-MS using methods outlined below (section 6.2.3). This AgNP Master Stock was then diluted 10-fold through the addition of 2 ml of Master Stock to a total volume of 20 ml MilliQ water to produce the AgNP Spiking Stock. A Master Stock of $AgNO_3$ was prepared through the addition of 89.1 mg of $AgNO_3$ (Sigma Aldrich) to 200 ml MilliQ water giving a nominal concentration of 44.55 mg/l. A 1 in 20 dilution of this master stock, followed by two serial 1 in 10 dilutions was made to yield a Spiking Stock with a nominal concentration of 222.75 µg/l $AgNO_3$. The total Ag concentration of both the AgNP and $AgNO_3$ Master and Spiking Stocks was measured by ICP-MS using methods outlined in section 6.2.3. To initiate toxicant exposures, 10 neonates (<24 h old) were added using a plastic Pasteur pipette to 100 ml of media10 in 25 x 250 ml glass beakers. In groups of five, these vessels were spiked with either 100 µl or 200 µl of the AgNP or $AgNO_3$ spiking stock to produce the Low or High concentration exposures of AgNP or $AgNO_3$ respectively (nominal concentrations outlined in Table 6.1).

Table 6.1: The intended concentration of total silver within the Spiking Stocks and exposure vessels (µg/l)

	Total silver concentration (µg/l)		
	Spike stock (nominal)	Volume (µl) into 200ml	Nominal exposure conc.
AgNP Low	2398	100	1.18
AgNP Mid	2398	200	2.35
$AgNO_3$ Low	140	100	0.07
$AgNO_3$ Mid	140	200	0.14

A no-added silver control was created through the addition of 200 µl MilliQ water to five exposure vessels. Immediately following the addition of toxicant or MilliQ water, an additional 100 ml of media10 was added to each vessel to mix and to bring the final concentration to the intended nominal value (Table 6.1). Vessels were then covered with Clingfilm and left for 24 h in the environmental conditions outlined above (section 2.5). After 24 h, the exposures were terminated; the numbers of living and immobilised animals per exposure vessel were counted, then the remaining living neonates were removed onto gauze and transferred into a 2 ml Precellys homogenisation tube and flash-frozen in liquid nitrogen. Precellys tubes were then stored at -80°C until required for the extraction of RNA.

6.2.2 Dynamic light scattering (DLS)

Immediately after exposure initiation, 1ml aliquots of dosed exposure media from three, randomly selected vessels from the control, AgNP High and $AgNO_3$ High groups were transferred into a plastic cuvette for analysis by DLS. Particle size was measured using a Zetasizer 5000 (Malvern Instruments, UK) at 20°C following a 120 s period to allow for equilibration of temperature. The refractive index (0.54) and adsorption coefficient (3.99) for silver samples were used to create the standard operating procedure for analysis using Zetasizer software (Version 7.11, Malvern Instruments, UK).

The DLS technique shines a laser onto particles in suspension and determines their size from the fluctuations in the intensity of scattered light. In this study DLS was used to measure three parameters of particles within each solution: the z-average size (nm), the count rate and the polydispersity index. The z-average size represents the average hydrodynamic diameter of the particles in suspension; this value is most accurate with suspensions of spherical, monodisperse particles. The count rate (or photon count rate) is simply the number of detected photons which are reflected from the disperse particles. Particles with a particularly low count rate (for example <100) could be of too low a concentration for successful

analysis. The polydispersity index ranges from 0 to 1 and is an indication of the size-distribution of particles within the sample; a PDI greater than 0.7 is considered to have a very broad particle size distribution and is probably unsuitable for measurement by DLS (Malvern Instruments Ltd, 2011). Briefly, 5 replicate measurements were taken of each sample to allow the calculation of mean values for the 3 measured parameters. The mean and standard deviation for these parameters was calculated for the three biological replicates in each group and differences between groups were compared by a 1-way ANOVA using a Tukey-Kramer post-hoc test for multiple comparisons.

6.2.3 ICP-MS

After the exposure vessels were filled with dosed media, 500 µl of exposure water was removed into a 40 ml glass vial (acid-washed) and digested in an additional 500 µl concentrated, trace-metal grade HNO_3 overnight in preparation for ICP-MS analysis. Following digestion, samples were diluted to approximately 2 % (v/v) nitric acid through the addition of 16 ml MilliQ water. The total Ag concentration of each water sample was measured using an Agilent 7500ce with an Octopole Reaction system. Calibration was performed between 0 – 50 ppb of Ag using 0, 1, 5, 10, 20 and 50 ppb standards. Silver standards were prepared from a 1000 mg/l stock solution (VWR) in 2% nitric acid. A calibration graph of counts (number) against concentration (µg/l) gave a correlation coefficient (R^2) of 1.000. An average was taken from 4 technical replicate measurements (in ppb) for each sample of dosed media; these readings were then converted into a concentration (in µg/l) from the calibration graph. The limit of detection for silver on this instrument was 0.02 ppb. To investigate the potential interference of media10 within the samples with the measurement of dissolved total silver, two spike recovery tests were performed using aliquots of a control replicate after it had first been measured. The first test using a final spike concentration of 1 ppb gave a return reading of 1.05 ppb and the second using a final

concentration of 10 ppb gave a return reading of 10.07 ppb, indicating that the media component had no impact on the measurements.

6.2.4 Extraction of RNA

RNA extractions were performed using the Absolutely RNA minprep kit (Agilent) to manufacturer's instructions for animal tissue samples. Briefly, frozen animals (10 neonates per sample) were homogenised using a Precellys-24 ceramic bead-based homogeniser (Stretton Scientific Ltd., UK) in 250 µl of guanidine-thiocyanate containing lysis buffer for two 10 s bursts at 6400 rpm with a 15 s intermission. Homogenate was then transferred into a nuclease-free 1.5 ml microfuge tube containing a further 250 µl of 70% ethanol and vortex mixed. This mixture was then transferred to silica-based RNA-binding spin-columns and spun in a centrifuge for 60 s at 8000 rcf to allow RNA binding. The spin-columns were then washed with 600 µl of Low-salt buffer (60 s at 8000 rcf) and treated with DNase1 according to manufacturer's instructions. Once DNase treatment was completed the columns were washed with 600 µl High-salt buffer then 600 µl of Low-salt buffer (each for 60 s at 8000 rcf). Finally samples were washed with 300 µl Low salt buffer (8000 rcf for 2 minutes) and then dried by spinning (8000 rcf for 1 minute) without any additional buffer. Spin columns were transferred to a 1.5 ml nuclease-free microfuge tube and RNA was eluted using 30 µl of elution buffer (10 mM Tris-HCl (pH 7.5) and 0.1 mM EDTA). The quantity and quality of RNA was assessed using a spectrophotometer (NanoDrop 1000, Thermo Scientific, Waltham, MA) with an analysis constant of 40 for RNA.

6.2.5 Synthesis of cDNA

Prior to primer validation and RT-qPCR, cDNA was synthesised using a Tetro cDNA synthesis kit (Bioline Reagents Limited, London, UK) according to manufacturer's instructions. RNA was first incubated with a mix of random hexamers (1 µl) for 2 minutes at 65 °C to denature template RNA. Due to the relatively low yields of RNA extracted from

samples, the maximum available volume of 12 µl was used for cDNA synthesis. Once incubation was completed, 5x RT Buffer (4 µl), a 10 mM dNTP mix (1 µl), Ribosafe RNase inhibitor (1 µl), and 1 µl Tetro reverse transcriptase (200 units/µl) was added to each tube. Each reaction was incubated using a thermocycler (Eppendorf Mastercycler Gradient; Eppendorf, Cambridge, UK) according to the temperature cycle outlined below (Table 6.2). The concentration of cDNA was measured after synthesis using a Nanodrop spectrophotometer (NanoDrop 1000, Thermo Scientific, Waltham, MA), with an analysis constant of 33 for single-stranded DNA, and stored at -20°C prior to analysis by RT-qPCR.

Table 6.2: The temperature cycle for synthesis of cDNA using Tetro reverse transcriptase

Temperature	Duration	Notes
25 °C	10 min	Annealing
42 °C	90 min	cDNA synthesis
70 °C	15 min	Denaturation

6.2.6 Primer design

Validated forward and reverse primers for five *D. magna* target genes (sequences outlined in Table 6.3) were ordered from and synthesised by Integrated DNA Technologies (IDT, Belgium).

Table 6.3: qPCR primer sequences and target information.

Gene Name	Genbank ID	Direction	Primer Efficiency	Primer Sequence (5' to 3')
Actin	CAB72313.2	Forward Reverse	94.8 %	GGTATGTGCAAGGCTGGATT GGTGTGGTGCCAGATCTTTT
Heme-oxygenase-1	EFX85559.1	Forward Reverse	98.6 %	TATGGAGCACAATGGCTTGA GGATTTGACCTCCCGAAAAT
Superoxide dismutase	EFX79040.1	Forward Reverse	N/A	GTAAGGGTGGGCATGAACTG ATCTGCCAACATAAATGCCATA
Glutathione-S-Transferase	EFX81636.1	Forward Reverse	97.9 %	ACATGGCCGGAGTAGACATC GTCAATGACTGCACGTTGCT
Metallothionein	DV437826.1	Forward Reverse	94.7 %	ACGTGGAGAAACGGTCAGAG ACAAATGCAAGCGGAATTTT

6.2.7 RT-qPCR

Approximately 100 ng of cDNA from each sample was mixed with a final concentration of 1 µM forward and reverse primers and 10 µl of SensiFAST SYBR Lo-ROX mix (Bioline Reagents Limited, London, UK) and made to a total volume of 20 µl per individual reaction. Each biological sample was plated in triplicate on a 96-well PCR plate (Agilent Technologies). A separate plate was used for each of the selected genes with a functioning pair of primers including 4 x $\log_{10}$-fold dilutions of template cDNA as a concentration curve, a non-template control and a non-reverse-transcriptase control which utilised template RNA instead of cDNA. Forward and reverse primers for the *D. magna* Actin gene were utilised as a reference gene. Each plate was scanned for SYBR Green 1 intensity on an AriaMx RT-PCR machine and AriaMx PC analysis software (Agilent technologies) using a 2 minute, 95C

hot start, a 3-step amplification cycle (Table 6.4). Melt-profile analysis was plotted for each sample to ensure only a single product was amplified and primer dimers were not formed.

Table 6.4: RT-qPCR temperature cycle. Each stage proceeds in order from top to bottom with the middle three stages repeated (in order) 39 times before melt-curve determination

Temperature (°C)	Duration	No. cycles	
95	2 min	1	Hot start
95	5 s	40	3-step amplification
60	10 s		
72	5 s		
95	30 s	1	Melt curve
65	30 s	1	
95	30 s	1	

The amplification efficiencies of the reference and target genes were not equal (**Table 6.3**); therefore the Pfaffl method (Pfaffl, 2001) was used to calculate relative expression levels of target genes. The Pfaffl method allows relative quantification of the expression of a target gene in comparison to a reference gene (often called a housekeeping gene) and follows the equation outlined in Equation 5.1. Briefly, the quantification cycle (C_q) of treated samples was subtracted from the average background C_q taken from control samples to produce a ΔC_q for both the target and reference genes. The primer efficiency value for the target gene raised to the power of its ΔCq is then divided by the primer efficiency value for the reference gene raised to the power of its ΔC_q. The result is a relative fold change of a target gene in treated samples compared to control samples normalised by a reference gene. Differences between groups were compared by a 1-way ANOVA using a Tukey-Kramer post-hoc test for multiple comparisons. Any set of technical replicates with a standard deviation greater than 2 was considered unreliable and as such was removed from statistical analysis.

Equation 6.3: The Pfaffl method for relative quantification and calculation of the relative expression ratio (*R*). Where *E* represents the amplification efficiency of the target or reference gene and ΔCq is the Cq deviation of control – sample of the target of reference gene.

$$R = \frac{(E_{\text{target}})^{\Delta Cq_{\text{target}}(control-sample)}}{(E_{\text{reference}})^{\Delta Cq_{\text{ref}}(control-sample)}}$$

6.3 Results and Discussion

6.3.1 Characterisation of dosed exposure media using DLS and ICP-MS

On preparation of the dosed exposure media, samples were taken for characterisation by DLS and ICP-MS. DLS was used to characterise the size and presence of Ag particles within dosed media and to confirm the presence of particles in AgNP exposures as well as the absence of particles in $AgNO_3$ and control exposures. ICP-MS was selected for its high sensitivity and was used to determine the total Ag concentration within each exposure beaker in order to confirm that animals were exposed to the intended concentration of Ag.

Low levels of large polydisperse particles were detected in every sample including the no-added silver control. The z-average particle sizes were measured to be 976.00 ± 407.4 nm in control samples, 722.20 ± 22.37 nm in the AgNP High group and 994.47 ± 371.09 nm in $AgNO_3$ High group (Figure 6.1 A). All samples gave similarly large PDI values; 0.6 ± 0.1, 0.7 ± 0.1 and 0.6 ± 0.2 for the control, AgNP High and $AgNO_3$ High groups respectively (Figure 6.1 B). The final measured parameter, the average photon count rate, was low in each group; 138.83 ± 84.28 nm, 79.12 ± 16.25 nm and 146.00 ± 95.17 for the control, AgNP and $AgNO_3$ groups respectively (Figure 6.1 C). Following statistical analysis by 1-way ANOVA, it was determined that there were no statistically significant differences between mean values for particle size ($p = 0.5396$), PDI ($p = 0.4895$) or count rate ($p = 0.5167$).

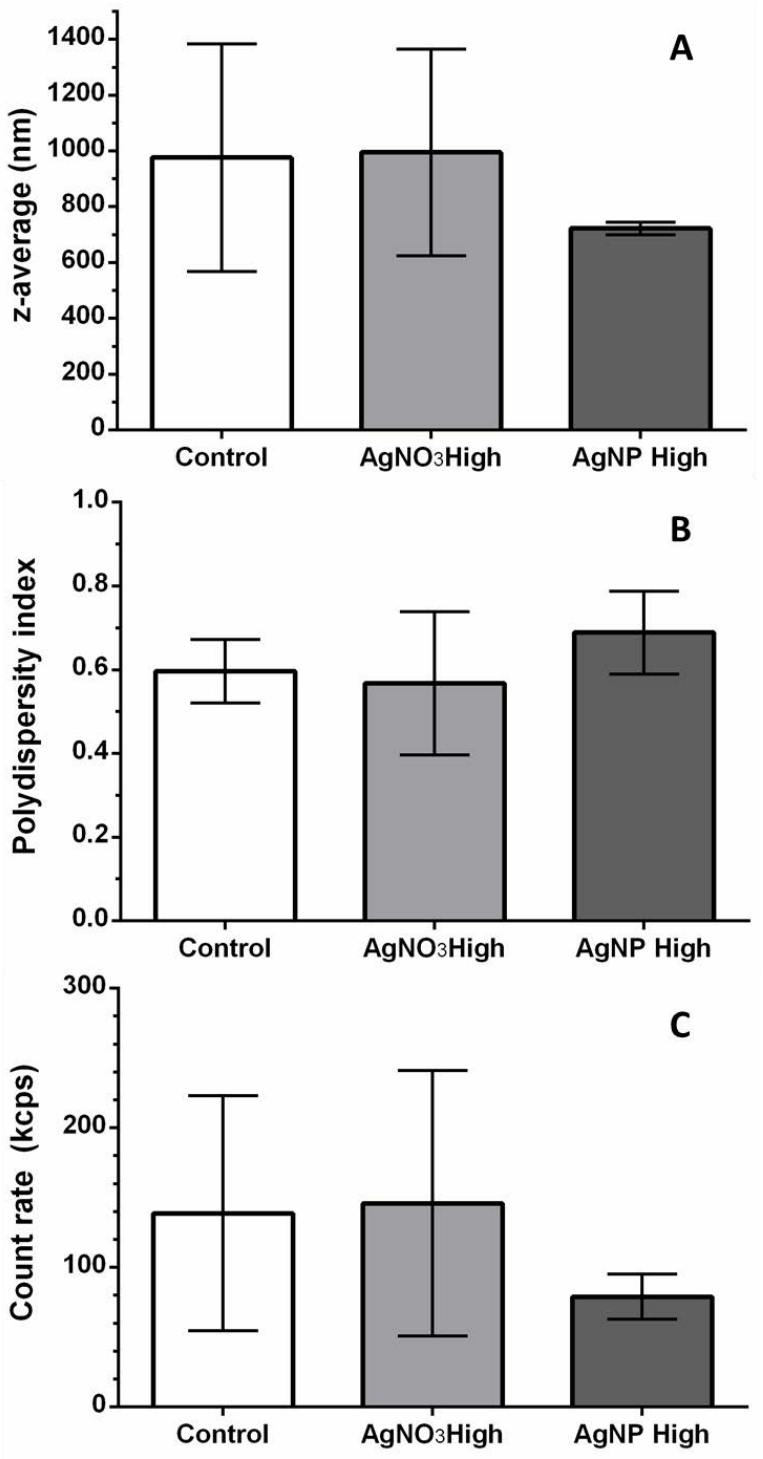

Figure 6.1: Characterisation of particles within control, $AgNO_3$ and AgNP exposure media by DLS. Depicted are the mean z-average particle size (A), the mean polydispersity index (B) and the mean photon count rate (C). Error bars represent the standard deviation (n = 3), differences between each of the three parameters were deemed as not significant following a 1-way ANOVA and Tukey-Kramer post hoc test.

The concentration of total Ag within dosed exposure media and spiking stocks was measured by ICP-MS following digestion with HNO_3. The mean total silver concentration of the AgNP Low and AgNP Mid groups were measured to be 1.24 ± 0.05 µg/l and 2.29 ± 0.11 µg/l respectively which are both within 10 % of their respective nominal concentrations of 1.18 µg/l and 2.35 µg/l (Table 6.5). Despite the increased sensitivity of ICP-MS compared to other techniques such as GF-AAS and ICP-OES, the concentration of total silver within the $AgNO_3$ Low and Mid groups was below the limit of detection following dilution to 2 % HNO_3, and as such could not be measured directly (Table 6.5). However, the concentration of $AgNO_3$ spiking solution was measured to be 129 µg/l which, assuming accurate dilutions, would equate to a total silver concentration of 0.06 µg/l and 0.13 µg/l for the $AgNO_3$ Low and $AgNO_3$ High groups. The total silver concentrations for the AgNP groups measured directly from spiked-media and the concentration values for dissolved silver groups derived from the $AgNO_3$ spiking stocks will be taken as the actual concentrations; all of which are within 10 % of the intended nominal concentrations (Table 6.5).

Table 6.5: The average measured concentrations of total Ag within AgNP exposure media with standard deviation (n = 5) for each group compared to the intended nominal concentrations. The control samples gave results below the < 0.02 µg/l detection limit of the instrument. The concentration of $AgNO_3$ dosed media have been derived from the measured concentration of the $AgNO_3$ spiking stock, as the true concentration was below the detection limit of the instrument.

	Total silver concentration (µg/l)		
	Nominal	Measured (mean)	Standard deviation
Control	0.00	< 0.02	N/A
AgNP Low	1.18	1.24	0.05
AgNP Mid	2.35	2.29	0.11
$AgNO_3$ Low	0.07	0.06	N/A
$AgNO_3$ Mid	0.14	0.13	N/A

Across all three parameters measured by DLS, there were no significant differences in particle content between the control and highest concentration $AgNO_3$ and AgNP exposures. The large average polydispersity indices measured for all three groups as well as the low photon count rates give an indication that the samples are not suitable for measurement by DLS (Malvern Instruments Ltd, 2011). However, the apparent detection of large polydisperse particles could be caused by the genuine presence of particles within all groups. These particles could be common to all three groups or different for each group. For example, particles detected in the AgNP high group could be the result of particle aggregation between the PVP-AgNPs present within the media. Particles detected in the $AgNO_3$ exposure may be the precipitation of insoluble AgCl formed by the reaction of Ag^+ with Cl^- present within media10. Finally, particles present within the control group could be small dust particles or natural organic matter transferred into the media with the animals. Alternatively, the readings could be an artefact of the exposure medium, induced by light scattered by the dissolved salts present within media10 and not by dissolved or nanoparticle silver. Regardless, the absence of significant differences between the three measured parameters indicates that DLS cannot distinguish between the particles present within the AgNP High group and the control group. As such it is apparent that DLS is an inappropriate technique to use at such low concentrations of Ag within media10 to confirm the presence or absence of particles. A more appropriate method may be the use of an imaging technique such as confocal microscopy or TEM to directly visualise the presence or absence of particles or aggregates in exposure media.

The results of ICP-MS analysis confirm the presence of Ag within spiked exposure media. The successful measurement of spike-recovery tests (Section 6.2.3) indicated that measurements of Ag-spiked samples returning values less than the limit of detection are not the result of interaction between the Ag and the exposure media. Therefore particles that are

present within the AgNP High group are likely either to be of too low a concentration to accurately detect by DLS, as suggested by the low photon count rate, or are potentially masked by the presence of naturally occurring particles common to all exposure groups.

6.3.2 Targeted analysis of antioxidant enzyme expression by RT-qPCR

Following a 24 h exposure period, no neonates were immobilised in the control, $AgNO_3$ Low and $AgNO_3$ High groups. Both concentrations of AgNP exposure induced neonate immobilisation; the lowest concentration induced partial immobilisation (44 % of the total starting population) whereas the highest concentration induced total immobilisation of the starting population, resulting in that group's removal from the study (see Appendix Table 9.5). Surviving neonates from the AgNP Low group were still collected for extraction of RNA and analysis by RT-qPCR alongside the other remaining three groups.

During analysis, no amplification was observed for reactions using primers for superoxide dismutase (SOD). SYBR green melt-curve data for each sample showed a complete absence of product; this remained true even with the highest amount of template used in the concentration curve, suggesting the primers for this target gene were not viable. As such, the expression of this particular target gene was not measured as was originally intended. The primers for the remaining three target genes; glutathione-S-transferase (GST), metallothionein (MT) and heme-oxygenase 1 (HMOX), were viable and measurement of their expression was successful (Figure 6.2). During synthesis of cDNA, one replicate of the $AgNO_3$ Low group yielded 10 fold less cDNA than all other replicates. As such there was an insufficient quantity for qPCR of this sample, reducing the replicate number for $AgNO_3$ Low to four for all three target genes. Equally, 2 biological replicates in the MT analysis (one from AgNP Low and one from $AgNO_3$ Mid) and one from HMOX analysis ($AgNO_3$ Mid) were excluded from statistical analyses for having standard deviations amongst technical replicates greater than 2.0. Following $\log_{10}$ transformation, the fold-change of GST and

HMOX relative to control expression was deemed as statistically insignificant between all groups by 1-way ANOVA and Tukey-Kramer post-hoc test ($p = 0.7674$ and $p = 0.7913$ respectively). Metallothionein expression however was seen to increase significantly relative to control ($p = 0.0287$) upon exposure to the lowest concentration of AgNP (1.24 µg/l) (Figure 6.2). The change in expression upon exposure to 0.06 and 0.13 µg/l $AgNO_3$ was not significant relative to control samples.

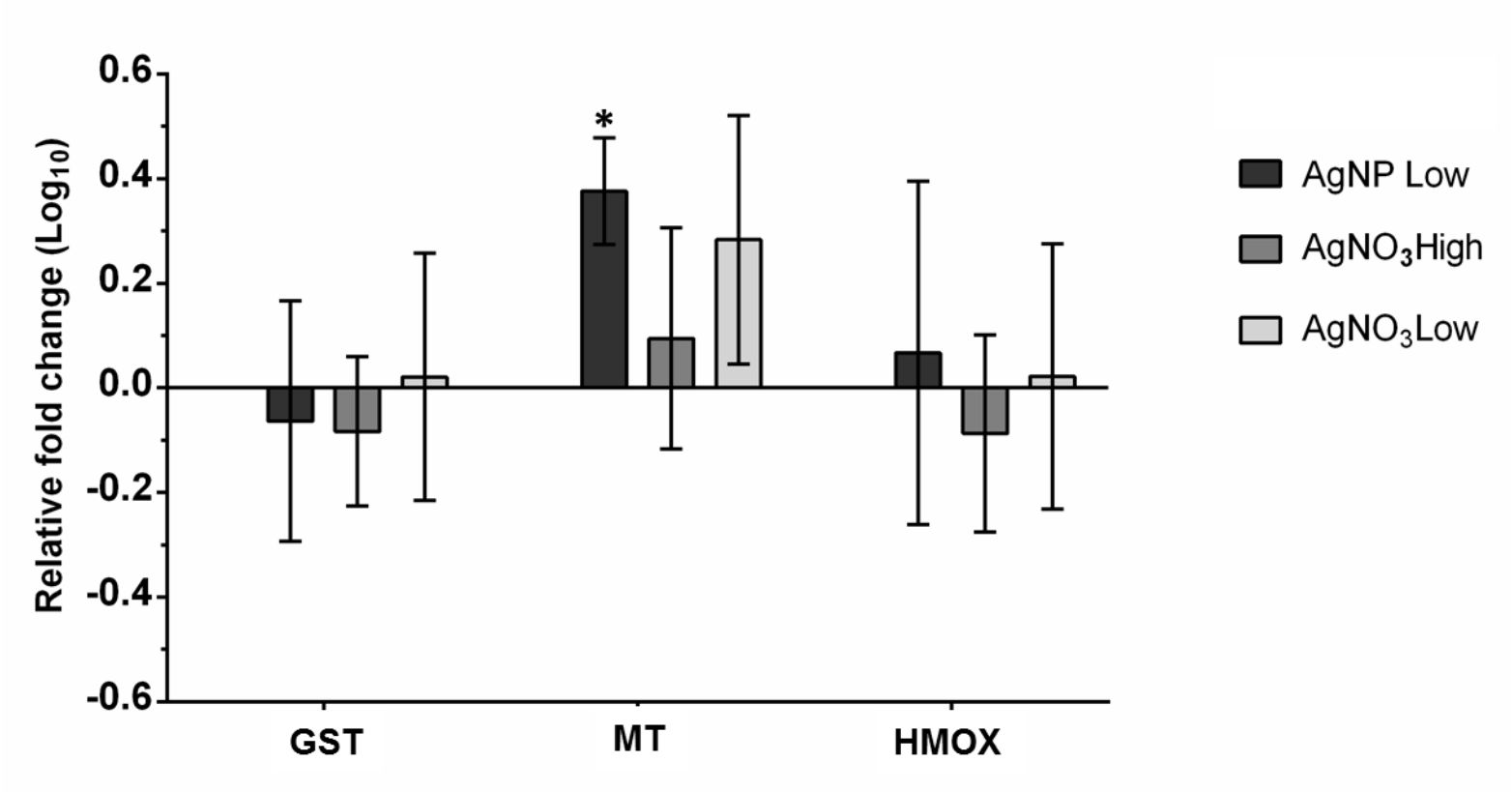

Figure 6.2: Relative gene expression of glutathione-S-transferase (GST), metallothionein (MT) and heme-oxygenase 1 (HMOX) in *D. magna* following exposure to 1.19 µg/l of AgNP (AgNP Low), 0.06 µg/l and 0.13 µg/l of $AgNO_3$ ($AgNO_3$ Low and $AgNO_3$ High respectively). Relative fold changes calculated by the Pfaffl method have been log_{10} transformed prior to analysis ANOVA. Error bars represent the standard deviation of each group (n = 3 for AgNP Low, n = 4 for $AgNO_3$ Low and n = 4 for $AgNO_3$). The * denotes a significant increase in MT expression relative to the control group (p = 0.0287).

The significant increase in MT expression observed here conforms to previously reported results in *D. magna* (Poynton et al., 2012; Rainville et al., 2014) and other *in vivo* models (Ferguson et al., 1996; Chae et al., 2009; Meyer et al., 2010; García-Alonso et al., 2011; Yang et al., 2012; Johari et al., 2015). This result suggests the successful internalisation of Ag into *D. magna* cells upon exposure to AgNP. MT expression will be increased in response to the presence of Ag within these cells in order to sequester Ag and Ag^{+} and remove from the cell. The mean relative expression of MT in animals exposed to $AgNO_3$ was increased when compared to control animals but deemed not to be significant following a 1-way ANOVA (Figure 6.2). This result was unexpected as increased MT expression and activity is a well-documented response to dissolved Ag exposure (Poynton et al., 2012; Rainville et al., 2014; De Matteis et al., 2015; Arai et al., 2015). It should be noted that the error on both mean values was large (Figure 6.2) and the non-significant result may simply be caused by insufficient biological replicates and therefore be a false negative. However in 2012, Poynton et al. also saw a significant increase in the transcription of MT in response to commercial PVP-coated AgNPs (8.14 µg/l, 35 nm core diameter), a result which again was not reciprocated upon exposure to 0.16 µg/l or 0.32 µg/l $AgNO_3$. (Poynton et al., 2012).

The expression of both GST and HMOX was also observed to not change significantly following exposure to both AgNPs and $AgNO_3$. The role of GST in *D. magna* response to Ag exposure has been measured previously by RT-qPCR (Poynton et al., 2012) and through measurement of GST enzyme activity (Rainville et al., 2014). In both instances GST was also seen to not increase significantly in response to Ag silver exposure. This is in spite of evidence of oxidative stress being identified in the latter study (Rainville et al., 2014). Despite being part of the response of certain cell lines to Ag exposure (Asharani et al., 2009) HMOX expression does not appear to be a part of the response to Ag exposure

in *D. magna* (Figure 6.2). The lack of response observed from these two biomarkers of oxidative stress suggests that this state is not induced by exposure to dissolved or nanoparticle Ag. However, Ag-induced oxidative stress has been observed across multiple bacterial (Lok et al., 2007; Choi and Hu, 2008; Hwang et al., 2008; Park et al., 2009) and eukaryotic (Arora et al., 2009; Asharani et al., 2009; Domingos et al., 2009; Chairuangkitti et al., 2013) cell lines as well as in multiple model organisms (Chae et al., 2009; Meyer et al., 2010; García-Alonso et al., 2011; Yang et al., 2012; Johari et al., 2015). It is therefore more likely that if oxidative stress is induced in *D. magna*, as has been reported (Poynton et al., 2012; Rainville et al., 2014; Li et al., 2015a), GST and HOX transcription plays no part in the response mechanism.

6.4 Conclusions

The targeted RT-qPCR conducted in this study suggests that although Ag is successfully internalised, transcription of GST and HMOX are not involved in the response of *D. magna* to Ag exposure. Despite the observation that two well-defined biomarkers of cellular oxidative stress do not increase significantly in response to Ag exposure, the result of this work does not categorically confirm that ROS generation plays no part in Ag toxicity. The production of ROS by AgNP has been observed in many previous publications, either through the direct catalysis of H_2O_2 degradation (He et al., 2011), direct measurement of ROS production *in vitro* (Asharani et al., 2009; De Matteis et al., 2015), or analysis of the damaging consequences of oxidative stress across multiple model organisms (Chae et al., 2009; Meyer et al., 2010; García-Alonso et al., 2011; Yang et al., 2012; Johari et al., 2015). The presence of ROS was not measured directly within this study so it is still possible, as reported by previous publications, that Ag that is internalised within the cells of *D. magna* induces the formation of ROS. MT is known to respond to the presence of ROS, so it is possible that the significant increase of MT in this chapter is

instead in response to ROS generation and not solely the presence of Ag within the organism's cells. However with the other target genes in this chapter (HOX and GST) remaining unresponsive to Ag exposure, it seems more likely that the significant response of MT is metal-responsive and not in in response to oxidative stress.

One specific aim of this work was to investigate a hypothesis formed from the results of Chapter 5 (section 5.4) that an observed significant increase in two purine nucleosides was in response to oxidative stress. It had been previously documented that guanosine protects against oxidative damage through the induction of HMOX (Quincozes-Santos et al., 2014). The results from this chapter have shown that HMOX expression is not significantly altered following exposure to both AgNPs and $AgNO_3$. This means the observed significant increase in purine nucleoside concentration does not result in elevated HMOX expression, suggesting an alternate cause for their accumulation.

Chapter 7: General Discussion and future work

The aims set out at the start of this research (Section 1.5) were designed to investigate the unknown mechanism of AgNP toxicity in the freshwater crustacean *D. magna* using a dual-omics platform. The investigation took a non-targeted approach to help drive the formation of hypotheses concerning the molecular perturbations and responses induced by exposure to AgNP in comparison to $AgNO_3$. This approach would allow the comparison of the global molecular profiles of animals exposed to both forms of silver, allowing for the determination of the role of dissolution in AgNP toxicity, and the elucidation of their mechanisms of action. In addition, this thesis allowed the exploration of the possibility of using non-targeted omics analyses as part of nanoparticle risk assessment.

7.1 The role of dissolution in AgNP toxicity

Although the exact role of AgNP dissolution in toxicity is still unconfirmed, there is growing consensus among studies that would suggest a Trojan-horse like mechanism to be the most applicable to AgNP induced toxicity. The Trojan-horse mechanism hypothesis suggests AgNPs enact toxicity through the release of toxic Ag^+ ions following uptake of AgNP into the exposed cells or organisms. In *D. magna*, the presence of silver within whole-body digests of exposed animals has been previously measured by ICP-MS (Khan et al., 2015) and through use of radioisotopes (Zhao and Wang, 2012b). Secondary ion mass spectrometry imaging techniques have identified the presence of Ag within the lumen of the gut of AgNP-exposed animals which was seen to distribute into the surrounding tissues over time (Audinot et al., 2013). ICP-MS measurements in Chapter 4 (section 4.3.4) supported this literature base by indicating a significantly greater concentration of silver within AgNP exposed animals than those exposed to theoretical concentration of the dissolved Ag fraction of AgNP exposures on its own. This result

potentially indicated the delivery of greater internal concentrations of dissolved silver than would be if AgNPs only dissolved externally to the animals.

What has not been observed in the *in vivo* investigations mentioned above is the relative proportions of the nanoparticle and dissolved species of the measured total Ag within exposed *D. magna*. These proportions of Ag speciation would help towards showing that AgNPs are adsorbed within *D. magna* then dissolve internally into Ag^+, showing that aspect of the Trojan-horse hypothesis to be possible. This type of investigation has been examined *in vitro*, leading to the detection of AgNPs within endo-lysosomal structures (Greulich et al., 2011; Arai et al., 2015; De Matteis et al., 2015) and the time-dependent release of Ag^+ following exposure to the acidic environment of these structures (De Matteis et al., 2015). These observations indicate, at least *in vitro*, that the Trojan-horse mechanism, in terms of uptake and dissolution, is possible.

The relative proportion of AgNP and dissolved Ag within AgNP-exposed *D. magna* could be investigated through use of a combination of separation and measurement techniques as have been implemented previously on *D. magna* exposure media (Shen et al., 2015). The ICP-MS analysis of acid-digested *D. magna* exposed to AgNPs and $AgNO_3$ presented in Chapter 4 could be taken further through additional determination of the internal concentration of total dissolved Ag by ICP-MS of acid-digested animals following centrifugal ultrafiltration using a 30-kDa filter (Shen et al., 2015). The respective internal AgNP concentration would be the resulting difference between these two total measurements. Combination of these techniques with visualisation techniques such as TEM or SIMS would be necessary to aid interpretation of whether any observed dissolution would occur within the lumen of the gut or in the surrounding tissues.

What is still lacking from the literature, both *in vitro* and *in vivo*, is evidence of which of the many forms of Ag is directly responsible for Ag-induced toxicity. The work in Chapter 4 of this thesis adds to this body of literature, identifying similar molecular profiles induced by both AgNP and dissolved Ag, which would agree with the hypothesis that AgNPs induce toxicity through the internal or intracellular release of dissolved Ag. This work suggests the involvement of dissolved Ag in AgNP toxicity. Also observed was a significant difference in the magnitude of the perturbations induced by AgNPs and $AgNO_3$, which is a potential indication that the nanoparticle fraction has an additional affect. Measurement of total Ag body burden in *D. magna* neonates exposed to AgNPs and the respective dissolved Ag fraction alone showed a significantly elevated body burden in AgNP-exposed animals. This potentially indicates the adsorption and possible ingestion of AgNPs into the organism. Targeted RT-qPCR for the expression of metallothionein indicated a significant increase in the gene's expression following exposure to the highest concentration of AgNP (Section 6.3.2). In the work described in Chapter 6, this gene was targeted as a positive control for successful Ag cellular uptake, as MT expression and activity is known to increase in response to Ag exposure to sequester and remove the Ag from the cells This, coupled with the observation that both species of Ag induce similar overall molecular responses, potentially indicates presence of Ag with *D. magna* cells. This would be consistent with previously published findings in *D. magna* (Zhao and Wang, 2012b; Stensberg et al., 2013), and *in vitro* (Park et al., 2010; Wang et al., 2013) which conclude that AgNPs work through a Trojan-horse type mechanism by acting as a vehicle for the delivery of the toxic Ag^+ ion following cellular uptake.

It is probable that the observed difference in magnitude between molecular profiles induced by AgNP and $AgNO_3$ exposure is due to differences in the sites of absorption and subsequent distribution of these forms of Ag. The relationship between total Ag exposure

concentration and the resulting body burden in *D. magna* potentially indicated a higher rate of uptake when animals were exposed to $AgNO_3$ compared to AgNPs (section 4.3.4). This is not unexpected, as dissolved Ag is known to be more bioavailable than AgNPs due to its more rapid method of cellular uptake. It is possible however that this potential difference in uptake rate is the result of the different species of Ag targeting different sites. It has been shown previously that dissolved Ag are absorbed by *D. magna* through the site of gaseous exchange (Bianchini and Wood, 2003), and that AgNPs are thought to enter the organism through the digestive tract (Zhao and Wang, 2010; Audinot et al., 2013). An obvious direction in which to take this line of investigation further is through the use of imaging techniques to identify and compared these sites of AgNP and dissolved Ag absorption. Micro-proton induced X-ray emission (MicroPIXE) has been used previously to observe and quantify the distribution of AgNPs ingested by the woodlouse *Pocellio scaber* (Tkalec et al., 2011). An alternative technique would be SIMS imaging, which has been used previously to visualise AgNPs, TiO_2 NPs and SiO_2 NPs within *D. magna*, identifying the presence of AgNPs in the lumen of the digestive tract (Audinot et al., 2013). Exposures identical to those outlined in Chapter 4 would allow the comparison of the distribution of silver following AgNP exposure, or exposure to the dissolved Ag fraction alone.

7.2 The molecular response of *D. magna* to Ag exposure

The background knowledge of the molecular perturbations induced by AgNPs is comparatively low. AgNPs along with other nanomaterials therefore represent an ideal opportunity to utilise omics-technologies for a non-targeted approach to determining their mechanism of toxicity. Some studies to date have focused on biochemical interactions known to be perturbed by Ag^+; such as disruption of Na^+ transport (Stensberg et al., 2013), mitochondrial disruption (Almofti et al., 2003; Stensberg et al., 2013; Ahn et al., 2014) and

the formation of ROS with the subsequent induction of oxidative stress (Park et al., 2009; Hsiao et al., 2015). This strategy, while a sensible start point, potentially provides only a narrow scope on the molecular mechanism, leaving potential novel changes undiscovered. Many omics investigations into AgNP toxicity have also centred their conclusions on the mechanisms mentioned above (Poynton et al., 2012; Aerle et al., 2013; Rainville et al., 2014; Verano-Braga et al., 2014; Li et al., 2015a; 2015b; Carrola et al., 2015), but several have identified other components or pathways involved in the toxic response to AgNPs that were previously unrecognised (Hadrup et al., 2012; Aerle et al., 2013; Verano-Braga et al., 2014).

A quantitative proteomics investigation identified up-regulation of serine/threonine protein kinase (PAK), mitogen-activated protein kinase (MAPK) and protein phosphatase 2A (PP2A) subunits following exposure of human colon carcinoma cells to 100 nm citrate-coated AgNPs (Verano-Braga et al., 2014). PAK and MAPK are both involved in signalling cascades that result in caspase-dependent and caspase-independent apoptosis respectively, and PP2A is involved in the regulation of the cell cycle. This study also implied an increase in degradation of proteins by the ubiquitin-proteasome system, possibly damage proteins, followed by the synthesis of replacement proteins (Verano-Braga et al., 2014). In addition to concluding that both AgNPs and dissolved silver impact oxidative phosphorylation and mitochondrial activity, Van Aerle et al. (2013) identified significant down-regulation of proteasome subunit beta type-1 and up-regulation of ribosomal protein S6 modification-like protein B, the authors suggested that together these alterations imply an increased level of protein turnover due to oxidative damage (Aerle et al., 2013). An NMR-based metabolomics study in rats measured an increased excretion of uric acid and allantoin in urine following AgNP exposure, suggesting a disruption of purine metabolism (Hadrup et al., 2012).

In Chapter 5, pathway analyses of the Ag-exposed *D. magna* identified perturbations in transcription pathways involved in G-protein coupled receptor (GPCR) signalling and signalling cascades involving MAP kinases, nerve growth factor, neurotrophin and Rho-GTPases. This supports previous observations of MAPK up-regulation in AgNP-exposed human colon carcinoma cells (Verano-Braga et al., 2014). GPCRs initiate cellular signalling cascades through MAPKs that result in the regulation of genes involved in cell growth and differentiation, as well as inflammation and apoptosis. The pathways involved in the metabolism of dietary sugars as well as purines and amino-sugars and nucleotide sugars were identified as being perturbed, potentially indicating the disruption of energy production that has been repeatedly reported following AgNP exposure. The hypothesis-generating ability of omics-technologies highlighted these pathways as potential candidates for further investigation.

Integrated pathway analysis indicated the metabolic and transcriptional perturbations of components within the purine metabolism pathway to be the most interconnected in comparison to other impacted pathways. This was therefore chosen as the next line of investigation within Chapter 5. The purine nucleosides inosine and guanosine were identified as increasing significantly in *D. magna* in response to Ag exposure. A previous NMR-based metabolomics study in rats measured an increased excretion of uric acid and allantoin in urine following AgNP exposure, suggesting a disruption in the metabolism of purine nucleosides (Hadrup et al., 2012). Besides this study, there have been few others to focus on or identify this metabolic pathway in the AgNP response. The exact cause of this increased production is unknown but seems unlikely to be in response to oxidative stress as investigated in Chapter 6. Increasing guanosine production has been observed previously to indirectly combat oxidative stress through stimulation of Heme-oxygenase1 (Quincozes-Santos et al., 2014). RT-qPCR performed as part of Chapter 6 showed no

significant change in the expression of HMOX or GST, two markers of oxidative stress, following exposure of *D. magna* to AgNPs and $AgNO_3$. The transcription (Poynton et al., 2012) and enzyme activity (Rainville et al., 2014) of GST in *D. magna* has been measured to be unchanged in response to AgNP exposure before, as have the activities of other well-characterised markers of oxidative stress such as catalase and GAPDH (Rainville et al., 2014). These results disprove the hypothesis proposed at the conclusion of Chapter 5 that the observed increase in guanosine content is in response to Ag-induced oxidative stress ultimately resulting in the stimulation of HMOX activity.

The production of ROS and induction of oxidative stress by AgNP is becoming a well-established mechanism in mammalian cell lines and some model organisms, though the evidence for oxidative stress in *D. magna* is somewhat conflicting and contradictory. Oxidative stress has been suggested as a mechanism of AgNP toxicity in *D. magna* before, but the direct measurement of Ag-induced ROS has only been attempted very recently (Ulm et al., 2015). The result of this measurement was unclear, with no significant production of ROS observed, though the author surmised that this may be the result of the significant increase in GSH production observed alongside the ROS assay (Ulm et al., 2015). It could be possible that the observed increased production of GSH may be in response to the presence of Ag^+ rather than ROS, as GSH non-specifically sequesters electrophiles which include heavy metals. Additionally, due to the relatively low EC_{50} of Ag species, any measurements of oxidative stress may not be caused directly by Ag, but potentially as a by-product of Ag-induced hypoxia or the latter stages of cell death. It may be the case that in *D. magna*, oxidative stress is not a primary mechanism of Ag toxicity; if ROS are generated they may be dealt with through species specific enzymes which are currently unknown.

It is also possible that the enzymes targeted in Chapter 6 might be involved in the response to Ag exposure, but that no significant transcriptional change was seen after a 24 h exposure. It could be that the transcriptional response of these enzymes occurs rapidly and the altered transcription is missed 24 h after exposure. A time-course would be required to rule out any transcriptional response from GST & HMOX entirely. Additional enzymes to investigate would be catalase and SOD using alternative primers. Transcriptomics analyses give no indication of protein activity and production, only the level of transcription of their corresponding genes. Quantitative measurement of the presence and activity of these enzymes would give a more direct indication of their roles in the response of *D. magna* to Ag exposure.

It is possible that the significant increase in purine nucleosides observed in Chapter 5 are not elevated as a result of increased anabolism, but rather decreased catabolism. For example, many of these metabolites are involved in the production of nucleoside triphosphates through oxidative phosphorylation, a process which has been seen to be inhibited by Ag exposure (Li et al., 2015a; Carrola et al., 2015). These purine nucleosides are all ultimately involved in the synthesis of RNA by RNA polymerase, which is inhibited directly through the actions of AgNPs (Wang et al., 2013). A disruption of purine metabolism has also been indicated before in rats (Hadrup et al., 2012) suggesting that this particular response to Ag exposure may be conserved across multiple species, making it a potential biomarker for screening in other organisms.

To investigate this mechanism further, a targeted approach by LC-MS could be used to accurately quantify the production of inosine and guanosine as well as other putative purine nucleosides which could not be isolated by FT-ICR MS. Coupled with ICP-MS analysis of the same samples, the production of these metabolites could be correlated with respect to silver body-burden, thus cementing their role in the MoA of AgNP toxicity. To

test the hypothesis that AgNP and $AgNO_3$ exposure does not lead to excessive ROS production in *D. magna*, the presence of ROS could be measured directly through use of fluorescence-based assays as previously used *in vitro* (Chairuangkitti et al., 2013) and in *D. magna* (Ma et al., 2012). This assay would need the use of a comparative positive control for ROS production such as H_2O_2 for interpretation of results. The hypothesis stated by Wang and colleagues (Wang et al., 2013) could be investigated further through measurement of the expression and activity of RNA polymerase II. Correlation of this activity over time with the concentration of purine nucleosides measured by LC-MS would go further to confirming this mechanism of toxicity in *D. magna*.

7.3 The use of omics-technologies in nanoparticle risk assessment

Due to a relative absence of background knowledge with regards to the molecular changes they induce, nanomaterials represent an ideal opportunity to utilise the high-throughput, non-targeted approach of omics technologies for the investigation of mechanisms of toxicity. This approach allows the capture of the entire molecular response providing a solid basis of knowledge from which to create hypotheses and direct further testing.

This approach may result in the discovery in molecular perturbations that would go potentially unnoticed by the traditional hypothesis-driven research. As discussed in section 1.3.5, there are previous omics investigations into AgNP toxicity which have discovered significant perturbations that are not traditionally associated with the toxicity of dissolved Ag. The observations made in this thesis that Ag exposure results in an accumulation of purine nucleosides that is not likely to be related to oxidative stress is another example of the power of omics in molecular toxicity investigations. Although the exact cause of the significant increase in guanosine and inosine requires further investigation, these two metabolites have been highlighted as potential markers of Ag

exposure in *D. magna*. An ideal biomarker is considered to be a molecule that is indicative of early toxicant exposure that can be detected in individual organisms and used to predict population-level effects. A true success story of biomarkers in regulatory ecotoxicology includes the discovery of vitellogenin as a biomarker of feminisation of male fish following exposure to oestrogen-like compounds (Jobling et al. 1998). Understanding of the exact mechanism of inosine and guanosine elevation following Ag exposure will be required to cement these two metabolites as specific markers of Ag exposure, as opposed to non-specific markers common to multiple mechanisms of toxicity.

Although useful for mechanistic investigations and the potential identification of biomarkers, the routine application of omics technologies, as they stand, to environmental risk assessment of new chemicals is an unlikely prospect. In order for it to become a reality there are several technological obstacles that need to be surpassed. Firstly, a major limitation of microarray transcriptomics is that they require a fully sequenced and annotated genome for effective use in toxicogenomics. For example, the *D. magna* microarray used in Chapter 4 only covers just under half of the total *D. magna* genome; 15,000 genes compared to approximately 31,000 genes (Colbourne et al., 2011). This means that over half the genome remains unmeasured, which could include genes that alter significantly and uniquely in expression following toxicant exposure to either AgNP or $AgNO_3$. Microarray transcriptomics, therefore, are not readily accessible for use with non-model organisms. This particular limitation could potentially be overcome through the use of the relatively new technology of RNA sequencing (RNA-seq). This technique converts extracted RNA into a library of cDNA fragments which are sequenced in a high-throughput manner (Wang et al 2009). A major advantage to this technique is that it is not limited to the detection of transcripts that correspond to existing sequenced genomes, and can therefore be used in non-model organisms.

Despite the increased sensitivity of FT-ICR MS compared to other metabolomics techniques, many important naturally low-level metabolites may go undetected due to the relatively low available biomass obtained from *D. magna* neonates. These limitations, though unavoidable, mean that the possibility of an independant AgNP-toxicity mechanism cannot be entirely ruled out, though from the data presented in Chapter 4 and the literature discussed above (section 1.2.3) the observations made in this thesis support the Trojan-horse mechanism. Untargeted, direct infusion FT-ICR metabolomics allows for the detection of 1000's of metabolites from biological samples. However, the major limitation of this and all available metabolomics technologies is the subsequent identification of these metabolites which remains a labour-intensive step (Dunn et al., 2012). For example, there are a number of biological metabolites which have the same molecular mass and potentially the same empirical formulae. Currently it is difficult to discriminate between metabolites, making biological interpretation of some metabolic profiles difficult. There have been developments in the automatic annotation of detected metabolites in recent years (Weber and Viant, 2010; Xia et al., 2012) though there is still a lack of metabolite information present in online libraries available for automated searches (Dunn et al., 2012).

Despite the limitations in the available technologies, the high throughput analytical methods present an opportunity in obtaining large quantities of toxicology data with relatively low input. They also, as has been demonstrated in this thesis, can provide unique insights into mechanisms of toxicity.

7.4 Concluding remarks

The data collected in this thesis suggests that although ultimately AgNP toxicity towards *D. magna* is most likely induced by released Ag ions, there is a potential "nanostructure-dependant biological activity" (Oberdörster et al., 2005a) relating to the Trojan-horse mechanism. In a regulatory context this data could potentially be used in the argument for separate regulatory framework for AgNPs. Ultimately however, it is suggested from this work that the mechanisms of AgNP and $AgNO_3$ toxicity are unlikely to be so different to warrant different levels of regulation.

Chapter 8: References

Ackermann, M. and Strimmer, K. (2009) A general modular framework for gene set enrichment analysis. *BMC bioinformatics*, 10: 47–66

Adam, N., Schmitt, C., Galceran, J., Companys, E., Vakurov, A., Wallace, R., Knapen, D., Blust, R. (2014) The chronic toxicity of ZnO nanoparticles and $ZnCl_2$ to *Daphnia magna* and the use of different methods to assess nanoparticle aggregation and dissolution. *Nanotoxicology*, 8 (7): 709–17

Adams, N. and Kramer, J. (1998) Reactivity of Ag^+ ion with thiol ligands in the presence of iron sulfide. *Environmental Toxicology and Chemistry*, 17 (4): 625–629

Aerle, R., Lange, A., Moorhouse, A., Paszkiewicz, K., Ball, K., Johnston, B., de-Bastos, E., Booth, T., Tyler, C., Santos, E. (2013) Molecular mechanisms of toxicity of silver nanoparticles in zebrafish embryos. *Environmental Science & Technology*, 47: 8005–8014

Ahn, J.-M., Eom, H.-J., Yang, X., Meyer, J., Choi, J. (2014) Comparative toxicity of silver nanoparticles on oxidative stress and DNA damage in the nematode, *Caenorhabditis elegans*. *Chemosphere*, 108: 343–52

Allen, H., Impellitteri, C., Macke, D., Heckman, D., Poynton, H., Lazorchak, J., Govindaswamy, S., Roose, D., Nadagouda, M. (2010) Effects from filtration, capping agents, and presence/absence of food on the toxicity of silver nanoparticles to *Daphnia magna*. *Environmental Toxicology and Chemistry*, 29 (12): 2742–50

Allwood, J. and Goodacre, R. (2010) An introduction to liquid chromatography-mass spectrometry instrumentation applied in plant metabolomic analyses. *Phytochemical Analysis* : PCA, 21 (1): 33–47

Almofti, M., Ichikawa, T., Yamashita, K., Terada, H., Shinohara, Y. (2003) Silver ion induces a cyclosporine A-insensitive permeability transition in rat liver mitochondria and release of apoptogenic cytochrome c. *Journal of Biochemistry*, 134 (1): 43–49

Altshuler, I., Demiri, B., Xu, S., Constantin, A., Yan, N., Cristescu, M. (2011) An integrated multi-disciplinary approach for studying multiple stressors in freshwater ecosystems: *Daphnia* as a model organism. *Integrative and Comparative Biology*, 51 (4): 623–33

Antczak, P., Jo, H., Woo, S., Scanlan, L., Poynton, H., Loguinov, A., Chan, S., Falciani, F., Vulpe, C. (2013) Molecular toxicity identification evaluation (mTIE) approach predicts chemical exposure in *Daphnia magna*. *Environmental Science and Technology*, 47 (20): 11747–11756

Arai, Y., Miyayama, T. and Hirano, S. (2015) Difference in the toxicity mechanism between ion and nanoparticle forms of silver in the mouse lung and in macrophages. *Toxicology*, 328: 84–92

Arakawa, H., Neault, J. and Tajmir-Riahi, H. (2001) Silver(I) complexes with DNA and RNA studied by Fourier transform infrared spectroscopy and capillary electrophoresis. *Biophysical Journal*, 81 (3): 1580–1587

Arora, S., Jain, J., Rajwade, J., Paknikar, K. (2009) Interactions of silver nanoparticles with primary mouse fibroblasts and liver cells. *Toxicology and Applied Pharmacology*, 236 (3): 310–8

Asghari, S., Johari, S., Lee, J., Kim, Y., Jeon, Y., Choi, H., Moon, M., Yu, I. (2012) Toxicity of various silver nanoparticles compared to silver ions in *Daphnia magna*. *Journal of Nanobiotechnology*, 10: 14

Asharani, P, Hande, M., and Valiyaveettil, S. (2009a) Anti-proliferative activity of silver nanoparticles. *BMC Cell Biology*, 10: 65

Asharani, P. V, Mun, G., Hande, M., Valiyaveettil, S. (2009b) Cytotoxicity and Genotoxicity of Silver., *ACS Nano*, 3 (2): 279–290

Audinot, J., Georgantzopoulou, A., Piret, J., Gutleb, A., Dowsett, D., Migeon, H., Hoffmann, L. (2013) Identification and localization of nanoparticles in tissues by mass spectrometry. *Surface and Interface Analysis*, 45 (1): 230–233

Baalousha, M. and Lead, J. (2012) Rationalizing nanomaterial sizes measured by atomic force microscopy, flow field-flow fractionation, and dynamic light scattering: sample preparation, polydispersity, and particle structure. *Environmental Science & Technology*, 46 (11): 6134–6142

Badawy, A., Luxton, T., Silva, R., Scheckel, K., Suidan, M., Tolaymat, T. (2010) Impact of environmental conditions (pH, ionic strength, and electrolyte type) on the surface charge and aggregation of silver nanoparticles suspensions. *Environmental Science & Technology*, 44 (4): 1260–1266

Behra, R., Sigg, L., Clift, M., Herzog, F., Minghetti, M., Johnston, B., Petri-Fink, A. Rothen-Rutishauser, B. (2013) Bioavailability of silver nanoparticles and ions: from a chemical and biochemical perspective. *Journal of The Royal Society Interface*, *10*(87),.

Bekyarova, E., Fornasiero, P., Kaspar, J., Graziani, M. (1998) CO oxidation on Pd/CeO_2-ZrO_2 *Catalysis Today*., 45: 179–183

Benjamini, Y. and Hochberg, Y. (1995) Controlling the false discovery rate: a practical and powerful approach to multiple testing. *Journal of the Royal Statistical Society. Series B* 57 (1): 289–300

Benn, T. and Westerhoff, P. (2008) Nanoparticle Silver Released into Water from Commercially Available Sock Fabrics. *Environmental Science & Technology*, 42 (11): 4133–4139

Bhabra, G., Sood, A., Fisher, B., Cartwright, L., Saunders, M., Evans, W., Surprenant, A., Lopez-Castejon, G., Mann, S., Davis, S., Hails, L., Ingham, E., Verkade, P., Lane, J., Heesom, K., Newson, R., Case, C.(2009) Nanoparticles can cause DNA damage across a cellular barrier. *Nature Nanotechnology*, 4 (12): 876–83

Bianchini, A. and Wood, C. (2003) Mechanism of acute silver toxicity in *Daphnia magna*. *Environmental Toxicology and Chemistry*, 22 (6): 1361–1367

Bianchini, A. and Wood, C. (2008) Does sulfide or water hardness protect against chronic silver toxicity in *Daphnia magna*? A critical assessment of the acute-to-chronic toxicity ratio for silver. *Ecotoxicology and Environmental Safety*, 71 (1): 32–40

Bleeker, E., Jong, W., Geertsma, R., Groenewold, E., Heugens, E., Koer-Jacquemijns, M., Meent, D., Popma, J., Rietveld, A., Wijnhoven, S., Cassee, F., Oomen, A. (2013) Considerations on the EU definition of a nanomaterial: science to support policy making. *Regulatory Toxicology and Pharmacology* : RTP, 65 (1): 119–25

Bouhifd, M., Hartung, T., Hogberg, H., Kleensang, A., Zhao, L. (2013) Review: toxicometabolomics. *Journal of Applied Toxicology*, 33 (12): 1365–83

Boveris, A. and Chance, B. (1973) The mitochondrial generation of hydrogen peroxide. General properties and effect of hyperbaric oxygen. *The Biochemical Journal*, 134 (3): 707–16

Bradford, A., Handy, R., Readman, J., Atfield, A., Muhling, M. (2009) Impact of silver nanoparticle contamination on the genetic diversity of natural bacterial assemblages in estuarine sediments. *Environmental Science and Technology*, 43 (12): 4530–4536

Bragg, P. and Rainnie, D. (1974) The effect of silver ions on the respiratory chain of *Escherichia coli*. *Canadian Journal of Microbiology*, 20 (6): 883–9

British Standards Institution (2007) Terminology for nanomaterials. PAS 136:2007. Text, p. 16

Bruins, A. (1998) Mechanistic aspects of electrospray ionization. *Journal of Chromatography A*, 794 (1-2): 345–357

Bunescu, A., Garric, J., Vollat, B., Canet-Soulas, E., Graveron-Demilly, D., Fauvelle, F. (2010) *In vivo* proton HR-MAS NMR metabolic profile of the freshwater cladoceran *Daphnia magna*. *Molecular bioSystems*, 6 (1): 121–5

Bury, N. and Wood, C., 1999. Mechanism of branchial apical silver uptake by rainbow trout is via the proton-coupled Na^+ channel. *American Journal of Physiology-Regulatory, Integrative and Comparative Physiology*,*277*(5), pp.R1385-R1391.

Campian, J., Qian, M., Gao, X., Eaton, J. (2004) Oxygen tolerance and coupling of mitochondrial electron transport. *Journal of Biological Chemistry*, 279 (45): 46580–46587

Campos, B., Garcia-Reyero, N., Rivetti, C., Escalon, L., Habib, T., Tauler, R., Tsakovski, S., Pina, B., Barata, C. (2013) Identification of metabolic pathways in *Daphnia magna* explaining hormetic effects of selective serotonin reuptake inhibitors and 4-nonylphenol using transcriptomic and phenotypic responses. *Environmental Science & Technology*, 47 (16): 9434–43

Carrola, J., Bastos, V., Ferreira de Oliveira, J. , Oliveira, H., Santos, C., Gil, A., Duarte, I. (2015) Insights into the impact of silver nanoparticles on human keratinocytes metabolism through NMR metabolomics. *Archives of Biochemistry and Biophysics*, pp. 1–9

Cavill, R., Kamburov, A., Ellis, J., Athersuch, T., Blagrove, M., Herwig, R., Ebbels, T., Keun, H. (2011) Consensus-phenotype integration of transcriptomic and metabolomic data implies a role for metabolism in the chemosensitivity of tumour cells. *PLoS Computational Biology*, 7 (3): e1001113

Chae, Y., Pham, C., Lee, J., Bae, E., Yi, J., Gu, M. (2009) Evaluation of the toxic impact of silver nanoparticles on Japanese medaka (*Oryzias latipes*). *Aquatic Toxicology*, 94 (4): 320–7

Chairuangkitti, P., Lawanprasert, S., Roytrakul, S., Aueviriyavit, S., Phummiratch, D., Kulthong, K., Chanvorachote, P., Maniratanachote, R. (2013) Silver nanoparticles induce toxicity in A549 cells via ROS-dependent and ROS-independent pathways. *Toxicology in Vitro*, 27 (1): 330–8

Chaloupka, K., Malam, Y. and Seifalian, A. (2010) Nanosilver as a new generation of nanoproduct in biomedical applications. *Trends in Biotechnology*, 28 (11): 580–588

Chambers, C., Proctor, C. and Kabler, P. (1962) Bactericidal effect of low concentrations of silver. *American Water Works Association*, 54 (2): 208–216

Chaudhry, Q., Scotter, M., Blackburn, J., Ross, B., Boxall, A., Castle, L., Aitken, R., Watkins, R. (2008) Applications and implications of nanotechnologies for the food sector. *Food Additives & Contaminants*. 25 (3): 241–58

Chen, X. and Schluesener, H. (2008) Nanosilver: A nanoproduct in medical application. *Toxicology Letters*, 176 (1): 1–12

Chladek, G., Mertas, A., Barszczewska-Rybarek, I., Nalewajek, T., Zmudzki, J., Krol, W., Lukaszczyk, J. (2011) Antifungal activity of denture soft lining material modified by silver nanoparticles-a pilot study. *International Journal of Molecular Sciences*, 12 (7): 4735–44

Choi, O. and Hu, Z. (2008) Size dependent and reactive oxygen species related nanosilver toxicity to nitrifying bacteria. *Environmental Science & Technology*, 42 (12): 4583–4588

Christian, P., Von der Kammer, F., Baalousha, M.,Hofmann, T. (2008) Nanoparticles: structure, properties, preparation and behaviour in environmental media. *Ecotoxicology*, 17 (5): 326–43

Cipriani, S., Bakshi, R. and Schwarzschild, M. (2014) Protection by inosine in a cellular model of Parkinson's disease. *Neuroscience*, 274: 242–9

Colbourne, J., Pfrender, M. and Gilbert, D. (2011) The ecoresponsive genome of *Daphnia pulex*. *Scienc*e, 331 (6017): 555–561

Colbourne, J., Singan, V.. and Gilbert, D. (2005) wFleaBase: the *Daphnia* genome database. *BMC Bioinformatics*, 6 (1): 45

Comfort, K., Maurer, E. and Hussain, S. (2014) Slow release of ions from internalized silver nanoparticles modifies the epidermal growth factor signalling response. Colloids and Surfaces B: *Biointerfaces*, 123: 136–142

Comisarow, M. and Melka, J. (1979) Error estimates for finite zero-filling in Fourier transform spectrometry. *Analytical Chemistry*, 51 (13): 2198–2203

Cortese-Krott, M., Münchow, M., Pirev, E., Heßner, F., Bozkut, A., Uciechowski, P., Pallua, N., Kroncke, K., Suschek, C. (2009) Silver ions induce oxidative stress and

intracellular zinc release in human skin fibroblasts. *Free Radical Biology and Medicine*, 47 (11): 1570–7

Couvreur, P. (2013) Nanoparticles in drug delivery: past, present and future. *Advanced Drug Delivery Reviews*, 65 (1): 21–3

Dal-Cim, T., Molz, S., Egea, J., Parada, E., Romero, A., Budni, J., Martin de Saavedra, M., Barrio, L., Tasca, C., López, M. (2012) Guanosine protects human neuroblastoma SH-SY5Y cells against mitochondrial oxidative stress by inducing heme oxigenase-1 via PI3K/Akt/GSK-3β pathway. *Neurochemistry International*, 61 (3): 397–404

David, R., Dakic, V., Williams, T., Winter, M., Chipman, J. (2011) Transcriptional responses in neonate and adult *Daphnia magna* in relation to relative susceptibility to genotoxicants. *Aquatic Toxicology*, 104 (3-4): 192–204

Dettmer, K., Aronov, P. and Hammock, B. (2007) Mass spectrometry-based metabolomics. *Mass Spectrometry Reviews*, 26 (1): 51–78

Dieterle, F., Ross, A., Schlotterbeck, G., Senn, H. (2006) Probabilistic quotient normalization as robust method to account for dilution of complex biological mixtures. Application in ^{1}H NMR metabonomics. *Analytical Chemistry*, 78 (13): 4281–90

Domingos, R., Baalousha, M., Ju-Nam, Y., Reid, M., Tufenkji, N., Lead, J., Leppard, G., Wilkinson, K. (2009) Characterizing manufactured nanoparticles in the environment: multimethod determination of particle sizes. *Environmental Science & Technology*, 43 (19): 7277–7284

Donaldson, K., Stone, V., Tran, C., Kreyling, W., Borm, P. (2004) Nanotoxicology. *Occupational and Environmental Medicine*, 61 (9): 727–8

Dunn, W., Erban, A., Weber, R., Creek, D., Brown, M., Breitling, R., Hankemeier, T., Goodacre, R., Neumann, S., Kopka, J., Viant, M. (2012) Mass appeal: metabolite identification in mass spectrometry-focused untargeted metabolomics. *Metabolomics*, 9 (S1): 44–66

Ebert, D. (2005) Ecology, epidemiology and evolution of parasitism in *Daphnia*. Bethesda (MD): *National Center for Biotechnology Information*

Elliott, M. and Trewyn, R. (1984) Inosine biosynthesis in transfer RNA by an enzymatic insertion of hypoxanthine. *The Journal of Biological Chemistry*, 259 (4): 2407–10

Erickson, R., Brooke, L., Kahl, M.., Venter, F., Harting, S., Markee, T., Spehar, R. (1998) Effects of laboratory test conditions on the toxicity of silver to aquatic organisms. *Enviromental Toxicology and Chemistry*, 17 (4): 572–578

EU, (2011). Commission recommendation of 18 October 2011 on the definition of nanomaterial (2011/696/EU). *Official Journal of the European Union, L* 275, 38–40.

Fabrega, J., Luoma, S., Tyler, C., Galloway, T., Lead, J. (2011) Silver nanoparticles: behaviour and effects in the aquatic environment. *Environment International*, 37 (2): 517–531

Ferguson, E., Leach, D. and Hogstrand, C. (1996) August. Metallothionein protects against silver blockage of the Na+/K+-ATPase. *Proceedings of the fourth International Conference, Transport, Fate and Effects of Silver in the Environment* (pp. 191-200). Madison, WI: University of Wisconsin-Madison.

Fiehn, O. (2002) Metabolomics--the link between genotypes and phenotypes. *Plant Molecular Biology*, 48 (1-2): 155–71

Finkel, T. and Holbrook, N. (2000) Oxidants, oxidative stress and the biology of ageing. *Nature*, 408 (6809): 239–247

Flicek, P., Amode, M., Barrell, D., Beal, K., Billis, K., Brent, S., Varvalho-Silva, D., Clapham, P., Coates, G., Fitzgerald, S., Gil, L., Giron, C., Gordon, L., Hourlier, T., Hunt, S., Johnson, N., Juettemann, T., Kahari, A., Keenan, S., Kulesha, E., Martin, F., Maurel, T., McLaren, W., Murphy, D., Nag, R., Overduin, B., Pignatelli, M., Pritchard, B., Pritchard, E., Riat, H., Ruffier, M., Sheppard, D., Taylor, K., Thormann, A., Trevanion, S., Vullo, A., Wilder, S., Wilson, M., Zadissa, A., Aken, B., Birney, E., Cunningham, F., Harrow, J., Herrero, J., Hubbard, T., Kinsella, R., Muffato, M., Parker, A., Spudich, G., Yates, A., Zerbino, D., Searle, S. (2014) Ensembl 2014. *Nucleic Acids Research*, 42 (Database issue): D749–55

Fu, P., Xia, Q., Hwang, H.-M., Ray, P., Yu, H. (2014) Mechanisms of nanotoxicity: generation of reactive oxygen species. *Journal of Food and Drug Analysis*, 22 (1): 64–75

Gaiser, B., Biswas, A., Rosenkranz, P., Jepson, M., Lead, J., Stone, V., Tyler, C., Fernandes, T. (2011) Effects of silver and cerium dioxide micro-and nano-sized particles on *Daphnia magna*. *Journal of Environmental Monitoring*, 13 (5): 1227–1235

García-Alonso, J., Khan, F., Misra, S., Turmaine, M., Smith, B., Rainbow, P., Luoma, S., Valsami-Jones, E. (2011) Cellular internalization of silver nanoparticles in gut epithelia of the estuarine polychaete *Nereis diversicolor*. *Environmental Science & Technology*, 45 (10): 4630–6

Garcia-Reyero, N., Poynton, H., Kennedy, A., Guan, X., Escalon, B., Chang, B., Varshavsky, J., Loguinov, A., Vulpe, C., Perkins, E. (2009) Biomarker discovery and

transcriptomic responses in *Daphnia magna* exposed to munitions constituents. *Environmental Science & Technology*, 43 (11): 4188–93

Geiser, M., Rothen-Rutishauser, B., Kapp, N., Schurch, S., Kreyling, W., Schulz, H., Semmler, M., Hof, V., Heyder, J., Gehr, P. (2005) Ultrafine particles cross cellular membranes by nonphagocytic mechanisms in lungs and in cultured cells. *Environmental Health Perspectives*, 113 (11): 1555–1560

Geranio, L., Heuberger, M. and Nowack, B. (2009) The behavior of silver nanotextiles during washing. *Environmental Science & Technology*, 43 (21): 8113–8118

Gottschalk, F., Sun, T. and Nowack, B. (2013) Environmental concentrations of engineered nanomaterials: Review of modelling and analytical studies. *Environmental Pollution*, 181: 287–300

Götz, S., García-Gómez, J.., Terol, J., Williams, T., Nagaraj, S., Nueda, M., Robles, M., Talon, M., Dopazo, J., Conesa, A. (2008) High-throughput functional annotation and data mining with the Blast2GO suite. *Nucleic Acids Research*, 36 (10): 3420–35

Greulich, C., Diendorf, J., Simon, T., Eggeler, G., Epple, M., Koller, M. (2011) Uptake and intracellular distribution of silver nanoparticles in human mesenchymal stem cells. *Acta Biomaterialia*, 7 (1): 347–354

Groh, K., Dalkvist, T., Piccapietra, F., Behra, R., Suter, M., Schirmer, K. (2014) Critical influence of chloride ions on silver ion-mediated acute toxicity of silver nanoparticles to zebrafish embryos. *Nanotoxicology*, 5390: 1–11

Gudkov, S. , Shtarkman, I., Smirnova, V., Chernikov, A., Bruskov, V. (2006) Guanosine and inosine as natural antioxidants and radioprotectors for mice exposed to lethal doses of γ-radiation. *Biochemistry, Biophysics, and Molecular Biology* 407 (1): 47–50

De Gusseme, B., Hennebel, T., Christiaens, E., Saveyn, H., Verbeken, K., Fitts, J., Boon, N., Verstraete, W. (2011) Virus disinfection in water by biogenic silver immobilized in polyvinylidene fluoride membranes. *Water Research*, 45 (4): 1856–64

Hadrup, N., Lam, H., Loeschner, K., Mortensen, A., Larsen, E., Frandsen, H. (2012) Nanoparticulate silver increases uric acid and allantoin excretion in rats, as identified by metabolomics. *Journal of Applied Toxicology*, 32 (11): 929–33

He, D., Jones, A., Garg, S., Pham, N., Waite, T. (2011) Silver nanoparticle− reactive oxygen species interactions: application of a charging− discharging model. *The Journal of Physical Chemistry C*, 115: 5461–5468

Heckmann, L.-H., Sibly, R., Connon, R., Hooper, H., Hutchinson, T., Maund, S., Hill, C., Bouetard, A., Callaghan, A. (2008) Systems biology meets stress ecology: linking molecular and organismal stress responses in *Daphnia magna. Genome Biology*, 9 (2): R40

Hogstrand, C. and Wood, C. (1998) Toward a better understanding of the bioavailability, physiology, and toxicity of silver in fish: Implications for water quality criteria. *Environmental Toxicology and Chemistry*, 17 (4): 547–561

Hoheisel, S., Diamond, S. and Mount, D. (2012) Comparison of nanosilver and ionic silver toxicity in *Daphnia magna* and *Pimephales promelas*. *Environmental Toxicology and Chemistry*, 31 (11): 2557–63

Horbach, G., Van Den Brule, S., Magkoufopoulou, C., Vietti, G., Papoutsi, D., Leyns, L., Kirsch-Volders, M. (2014) The safety of nanomaterials: translation from academic research to industrial and regulatory applications. *Journal of Translational Toxicology*, 1 (1): 40–45

Hrydziuszko, O. and Viant, M. (2011) Missing values in mass spectrometry based metabolomics: an undervalued step in the data processing pipeline. *Metabolomics*, 8 (S1): 161–174

Hsiao, I.-L., Hsieh, Y.-K., Wang, C.-F., Chen, I.-C., Huang, Y.-J.. (2015) Trojan-horse mechanism in the cellular uptake of silver nanoparticles verified by direct intra- and extracellular silver speciation analysis. *Enviromental Science and Technology*, 49 (6): 3813–21

Huang, D., Sherman, B. and Lempicki, R. (2009) Systematic and integrative analysis of large gene lists using DAVID bioinformatics resources. *Nature Protocols*, 4: 44–57

Hwang, E., Lee, J., Chae, Y., Kim, Y., Kim, B., Sang, B.-I., Gu, M. (2008) Analysis of the toxic mode of action of silver nanoparticles using stress-specific bioluminescent bacteria. *Small*, 4 (6): 746–750

ISO, Nanotechnologies – Terminology and definitions for nano-objects – Nanoparticle, nanofibre and nanoplate. *International Organisation for Standardisation (ISO)*, Genève, Switserland, 2008.

Jiang, J., Oberdörster, G. and Biswas, P. (2008) Characterization of size, surface charge, and agglomeration state of nanoparticle dispersions for toxicological studies. Journal of *Nanoparticle Research*, 11 (1): 77–89

Johari, S., Kalbassi, M., Lee, S., Dong, M., Yu, I. (2015) Silver nanoparticles affects the expression of biomarker genes mRNA in rainbow trout (*Oncorhynchus mykiss*). *Comparative Clinical Pathology*

Johnson, A., Bowes, M., Crossley, A., Jarvie, H., Jurkschat, K., Jurgens, M., Lawlor, A., Park, B., Rowland, P., Spurgeon, D., Svensden, C., Thompson, I., Barnes, R., Williams,

R., Xu, N. (2011) An assessment of the fate, behaviour and environmental risk associated with sunscreen TiO_2 nanoparticles in UK field scenarios. *Science of the Total Environment*, 409 (13): 2503–10

Jomova, K. and Valko, M. (2011) Advances in metal-induced oxidative stress and human disease. *Toxicology*, 283 (2-3): 65–87

Jung, W., Koo, H., Kim, K., Shin, S., Kim, S., Park, Y. (2008) Antibacterial activity and mechanism of action of the silver ion in *Staphylococcus aureus* and *Escherichia coli*. *Applied and Environmental Microbiology*, 74 (7): 2171–2178

Jurkowitz, M., Litsky, M., Browning, M., Hohl, C. (1998) Adenosine, inosine, and guanosine protect glial cells during glucose deprivation and mitochondrial inhibition: correlation between protection and ATP preservation. *Journal of Neurochemistry*, 71 (2): 535–48

Kaegi, R., Sinnet, B., Zuleeg, S., Hagendorfer, H., Mueller, E., Vonbank, R., Boller, M., Burkhardt, M. (2010) Release of silver nanoparticles from outdoor facades. *Environmental Pollution*, 158 (9): 2900–2905

Kamburov, A., Cavill, R., Ebbels, T., Herwig, R., Keun, H. (2011) Integrated pathway-level analysis of transcriptomics and metabolomics data with IMPaLA. *Bioinformatics*, 27 (20): 2917–8

Keating, K. and Dagbusan, B. (1984) Effect of selenium deficiency on cuticle integrity in the Cladocera (Crustacea). *Proceedings of the National Academy of Sciences of the United States of America*, 81 (11): 3433–7

Kennedy, A., Hull, M., Bednar, A., Goss, J., Gunter, J., Bouldin, J., Vikesland, P., Steevens, J. (2010) Fractionating nanosilver: importance for determining toxicity to aquatic test organisms. *Environmental Science & Technology*, 44 (24): 9571–9577

Keun, H. (2006) Metabonomic modeling of drug toxicity. *Pharmacology & Therapeutics*, 109 (1-2): 92–106

Khan, F., Kennaway, G., Croteau, M.-N., Dybowska, A., Smith, B., Nogueira, A., Rainbow, P., Luoma, S., Valsami-Jones, E. (2014) *In vivo* retention of ingested Au NPs by *Daphnia magna*: no evidence for trans-epithelial alimentary uptake. *Chemosphere*, 100: 97–104

Khan, F., Paul, K., Dybowska, A., Valsami-Jones, E., Lead, J., Stone, V., Fernandes, T. (2015) Accumulation dynamics and acute toxicity of silver nanoparticles to *Daphnia magna* and *Lumbriculus variegatus*: Implications for metal modelling approaches. *Environmental Science & Technology*, pp. 4389–4397

Khatri, P., Sirota, M. and Butte, A. (2012) Ten years of pathway analysis: current approaches and outstanding challenges. *PLoS Computational Biology*, 8 (2): e1002375

Kim, J., Kim, S. and Lee, S. (2011) Differentiation of the toxicities of silver nanoparticles and silver ions to the Japanese medaka (*Oryzias latipes*) and the cladoceran *Daphnia magna*. *Nanotoxicology*, 5 (2): 208–14

Kind, T. and Fiehn, O. (2006) Metabolomic database annotations via query of elemental compositions: mass accuracy is insufficient even at less than 1 ppm. *BMC Bioinformatics*, 7: 234

Kirwan, J., Weber, R., Broadhurst, D., Viant, M. (2014) Direct infusion mass spectrometry metabolomics dataset: a benchmark for data processing and quality control. *Scientific Data*, 1: 1–13

Kreyling, W., Semmler-Behnke, M. and Chaudhry, Q. (2010) A complementary definition of nanomaterial. *Nano Today*, 5 (3): 165–168

Lampert, W. (2011) *Daphnia*: Development of a Model Organism in Ecology and Evolution.

Le, T.-H., Lim, E.-S., Hong, N.-H., Lee, S.-K., Shim, Y., Hwang, J., Kim, Y.-H., Min, J. (2013) Proteomic analysis in *Daphnia magna* exposed to As(III), As(V) and Cd heavy metals and their binary mixtures for screening potential biomarkers. *Chemosphere*, 93 (10): 2341–8

Leblanc, G., Mastone, J., Paradice, A., Wilson, B., Haines Jr, B. Robillard, K., (1984). The influence of speciation on the toxicity of silver to fathead minnow (*Pimephales promelas*). *Environmental Toxicology and Chemistry*, *3*(1), pp.37-46.

Lenz, E. and Wilson, I. (2007) Analytical strategies in metabonomics. *Journal of Proteome Research*, 6 (2): 443–58

Li, H., Yan, Z., Zhu, J., Yang, J., He, J. (2011) Neuroprotective effects of resveratrol on ischemic injury mediated by improving brain energy metabolism and alleviating oxidative stress in rats. *Neuropharmacology*, 60 (2-3): 252–8

Li, L., Wu, H., Ji, C., Gestel, C., Allen, H., Peijnenburg, W. (2015a) A metabolomic study on the responses of *Daphnia magna* exposed to silver nitrate and coated silver nanoparticles. *Ecotoxicology and Environmental Safety*, 119: 66–73

Li, L., Wu, H., Peijnenburg, W., Gestel, C. (2015b) Both released silver ions and particulate Ag contribute to the toxicity of AgNPs to earthworm *Eisenia fetida*. *Nanotoxicology*, 9 (6): 792–801

Liau, S., Read, D., Pugh, W., Furr, J., Russell, A. (1997) Interaction of silver nitrate with readily identifiable groups: relationship to the antibacterial action of silver ions. *Letters in Applied Microbiology*, 25 (4): 279–83

Liochev, S. and Fridovich, I. (2000) Copper- and zinc-containing superoxide dismutase can act as a superoxide reductase and a superoxide oxidase. *The Journal of Biological Chemistry*, 275 (49): 38482–5

Lok, C.-N., Ho, C.-M., Chen, R., He, Q.-Y., Yu, W.-Y., Sun, H., Kwong-Hang, P., Chiu, J.-F., Che, C.-M. (2007) Silver nanoparticles: partial oxidation and antibacterial activities. *Journal of Biological Inorganic Chemistry*, 12 (4): 527–34

Lubick, N. (2008) Nanosilver toxicity: ions, nanoparticlessor both. *Environmental Science & Technology*, 42 (23): 8959–8964

Luoma, S. (2008) Silver nanotechnologies and the environment. *The Project on Emerging Nanotechnologies Report*, (15)

Ma, H., Brennan, A. and Diamond, S. (2012) Photocatalytic reactive oxygen species production and phototoxicity of titanium dioxide nanoparticles are dependent on the solar ultraviolet radiation spectrum. *Environmental Toxicology and Chemistry*, 31 (9): 2099–107

Malvern Instruments Ltd (2011) Inform white paper dynamic light scattering. *Malvern Guides*, pp. 1–6

Martins, J., Oliva Teles, L. and Vasconcelos, V. (2007) Assays with *Daphnia magna* and *Danio rerio* as alert systems in aquatic toxicology. *Environment International*, 33 (3): 414–25

De Matteis, V., Malvindi, M., Galeone, A., Brunetti, V., Luca, E., Kote, S., Kshirsagar, P., Sabella, S., Bardi, G., Pompa, P. (2015) Negligible particle-specific toxicity mechanism of silver nanoparticles: The role of Ag^{+} ion release in the cytosol. *Nanomedicine: Nanotechnology, Biology and Medicine*, 11 (3): 731–739

McQuillan, J. and Shaw, A.. (2014) Differential gene regulation in the Ag nanoparticle and Ag^{+}-induced silver stress response in *Escherichia coli*: A full transcriptomic profile. *Nanotoxicology*, 5390 (I): 1–8

Meyer, J., Lord, C., Yang, X., Turner, E., Badireddy, A., Marinakos, S., Chilkoti, A., Wiesner, M., Auffan, M. (2010) Intracellular uptake and associated toxicity of silver nanoparticles in *Caenorhabditis elegans*. *Aquatic Toxicology*, 100 (2): 140–50

Mijnendonckx, K., Leys, N., Mahillon, J., Silver, S., Houdt, R. (2013) Antimicrobial silver: uses, toxicity and potential for resistance. *Biometals*, 26 (4): 609–21

Módis, K., Gero, D., Nagy, N., Szoleczky, P., Toth, Z., Szabo, C. (2009) Cytoprotective effects of adenosine and inosine in an in vitro model of acute tubular necrosis. *British Journal of Pharmacology*, 158 (6): 1565–78

Moore, M. (2006) Do nanoparticles present ecotoxicological risks for the health of the aquatic environment? *Environment International*, 32 (8): 967–76

Morgan, I., Henryb, P. and Wood, C. (1997) The mechanism of acute silver nitrate toxicity in freshwater rainbow trout (*Oncorhynchus mykiss*) is inhibition of gill Na^{+} and Cl^{-} transport. *Aquatic Toxicology*, 38: 145–163

Mueller, N. and Nowack, B. (2008) Exposure modeling of engineered nanoparticles in the environment. *Environmental Science & Technology*, 42 (12): 4447–53

Nagato, E., D'eon, J., Lankadurai, B., Poirier, D., Reiner, E., Simpson, A., Simpson, M. (2013) ^{1}H NMR-based metabolomics investigation of *Daphnia magna* responses to sub-lethal exposure to arsenic, copper and lithium. *Chemosphere*, 93 (2): 331–7

Nam, H., Kwon, S., Chung, H., Lee, S.-Y., Kwon, S.-H., Jeon, H., Kim, Y., Park, J., Kim, J., Her, S., Oh, Y.-K., Kwon, I., Kim, K., Jeong, S. (2009) Cellular uptake mechanism and intracellular fate of hydrophobically modified glycol chitosan nanoparticles. *Journal of Controlled Release*, 135 (3): 259–267

Newton, K., Puppala, H., Kitchens, C., Colvin, V., Klaine, S. (2013) Silver nanoparticle toxicity to *Daphnia magna* is a function of dissolved silver concentration. *Environmental Toxicology and Chemistry*, 32 (10): 2356–64

Nguyen, D., Arpat, B., Wang, N., Carroll, R. (2002) DNA microarray experiments: biological and technological aspects. *Biometrics*, 58 (4): 701–17

Notter, D. a., Mitrano, D. and Nowack, B. (2014) Are nanosized or dissolved metals more toxic in the environment? A meta-analysis. *Environmental Toxicology and Chemistry*, 33 (12): 2733–2739

Nowack, B., Krug, H. and Height, M. (2011) 120 Years of nanosilver history: Implications for policy makers. *Environmental Science & Technology*, 45 (4): 1177–83

Nuwaysir, E., Bittner, M., Trent, J., Barret, C., Afshari, C. (1999) Microarrays and toxicology: the advent of toxicogenomics. *Molecular Carcinogenesis*, 24 (3): 153–9

Oberdörster, G., Maynard, A., Donaldson, K., Castranova, V., Fitzpatrick, J., Ausman, K., Carter, J., Karn, B., Kreyling, W., Lai, D., Olin, S., Monterio-Riviere, N., Warheit, D., Yang, H. (2005a) Principles for characterizing the potential human health effects from exposure to nanomaterials: elements of a screening strategy. *Particle and Fibre Toxicology*, 2 (1): 8

Oberdörster, G., Oberdörster, E. and Oberdörster, J. (2005b) Nanotoxicology: an emerging discipline evolving from studies of ultrafine particles. *Environmental Health Perspectives*, 113 (7): 823–839

OECD (2004), Test No. 202: *Daphnia* sp. Acute Immobilisation Test, OECD Guidelines for the Testing of Chemicals, Section 2, OECD Publishing, Paris.

Otte, K., Fröhlich, T., Arnold, G., Laforsch, C. (2014) Proteomic analysis of *Daphnia magna* hints at molecular pathways involved in defensive plastic responses. *BMC Genomics*, 15: 306

Park, E.-J., Yi, J., Kim, Y., Choi, K., Park, K. (2010) Silver nanoparticles induce cytotoxicity by a Trojan-horse type mechanism. *Toxicology in Vitro*, 24 (3): 872–8

Park, H.-J., Kim, J., Kim, J., Lee, J.-H., Hahn, J.-S., Gu, M., Yoon, J. (2009) Silver-ion-mediated reactive oxygen species generation affecting bactericidal activity. *Water Research*, 43 (4): 1027–1032

Parkin, I. and Palgrave, R. (2005) Self-cleaning coatings. *Journal of Materials Chemistry*, 15 (17): 1689

Parsons, H., Ekman, D., Collette, T., Viant, M. (2009) Spectral relative standard deviation: a practical benchmark in metabolomics. *The Analyst*, 134 (3): 478–85

Parsons, H., Ludwig, C., Günther, U., Viant, M. (2007) Improved classification accuracy in 1- and 2-dimensional NMR metabolomics data using the variance stabilising generalised logarithm transformation. *BMC Bioinformatics*, 8: 234

Payne, T., Southam, A., Arvanitis, T., Viant, M. (2009) A signal filtering method for improved quantification and noise discrimination in fourier transform ion cyclotron resonance mass spectrometry-based metabolomics data. *Journal of the American Society for Mass Spectrometry*, 20 (6): 1087–95

Pfaffl, M.W. (2001) A new mathematical model for relative quantification in real-time RT-PCR. *Nucleic Acids Research*, 29 (9): e45

Piccapietra, F. (2012) Colloidal stability of silver nanoparticles and their interactions with the alga *Chlamydomonas reinhardtii* (Doctoral dissertation, Diss., Eidgenössische Technische Hochschule ETH Zürich, Nr. 20365, 2012).

Piña, B. and Barata, C. (2011) A genomic and ecotoxicological perspective of DNA array studies in aquatic environmental risk assessment. *Aquatic Toxicology*, 105 (3-4 Suppl): 40–9

Poynton, H.C., Lazorchak, J.M., Impellitteri, C. a, et al. (2011a) Differential gene expression in Daphnia magna suggests distinct modes of action and bioavailability for ZnO nanoparticles and Zn ions. *Environmental Science & Technology*, 45 (2): 762–8

Poynton, H., Lazorchak, J., Impellitteri, C., Smith, M., Rogers, K., Patra, M., Hammer, K., Allen, H., Vulpe, C. (2012) Toxicogenomic responses of nanotoxicity in *Daphnia magna* exposed to silver nitrate and coated silver nanoparticles. *Environmental Science & Technology*, 46 (11): 6288–96

Poynton, H., Taylor, N., Hicks, J., Colson, K., Chan, S., Clark, C., Scanlan, L., Loguinov, A., Vulpe, C., Viant, M. (2011b) Metabolomics of microliter hemolymph samples enables an improved understanding of the combined metabolic and transcriptional responses of *Daphnia magna* to cadmium. *Environmental Science & Technology*, 45 (8): 3710–7

Purcell, T. and Peters, J. (1998) Sources of silver in the environment. *Environmental Toxicology and Chemistry*, 17 (4): 539–546

Quincozes-Santos, A., Bobermin, L., Souza, D., Bellaver, B., Goncalves, C.-A., Souza, D. (2014) Guanosine protects C6 astroglial cells against azide-induced oxidative damage: A putative role of heme oxygenase 1. *Journal of Neurochemistry*, 130 (1): 61–74

Rai, M., Yadav, A. and Gade, A. (2009) Silver nanoparticles as a new generation of antimicrobials. *Biotechnology Advances*, 27 (1): 76–83

Rai, M., Deshmukh, S., Ingle, P., Gade, A. (2012) Silver nanoparticles: the powerful nanoweapon against multidrug-resistant bacteria. *Journal of Applied Microbiology*, 112 (5): 841–52

Rainville, L.-C., Carolan, D., Varela, A., Doyle, H., Sheehan, D. (2014) Proteomic evaluation of citrate-coated silver nanoparticles toxicity in *Daphnia magna*. *The Analyst*, 139 (7): 1678–86

Ratte, H. (1999) Bioaccumulation and toxicity of silver compounds: A review. *Environmental Toxicology and Chemistry*, 18 (1): 89–108

Ribeiro, F., Gallego-Urrea, J., Jurkschat, K., Crossley, A., Hassellov, M., Taylor, C., Soares, A., Loureiro, S. (2014) Silver nanoparticles and silver nitrate induce high toxicity to *Pseudokirchneriella subcapitata, Daphnia magna* and *Danio rerio*. *The Science of the Total Environment*, 466-467: 232–41

Rivetti, C., Campos, B., Faria, M., Catala, N., Malik, A., Munoz, I., Tauler, R., Soares, A., Osorio, V., Perez, S., Gorga, M., Petrovic, M., Mastroianni, N., Alda, M., Masia, A., Campo, J., Pico, Y., Guasc, H., Barcelo, D., Barata, C. (2014) Transcriptomic, biochemical and individual markers in transplanted *Daphnia magna* to characterize impacts in the field. *The Science of the Total Environment*

Robertson, D. (2005) Metabonomics in toxicology: A review. *Toxicological Sciences*, 85 (2): 809–822

Robertson, D., Reily, M. and Baker, J. (2007) Metabonomics in pharmaceutical discovery and development. *Journal of Proteome Research*, 6 (2): 526–39

Rogers, J., Parkinson, C., Choi, Y., Speshock, J., Hussain, S. (2008) A preliminary assessment of silver nanoparticle inhibition of monkeypox virus plaque formation. *Nanoscale Research Letters*, 3 (4): 129–133

Römer, I., Gavin, A., White, T., Merrifield, R., Chipman, J., Viant, M., Lead, J. (2013) The critical importance of defined media conditions in *Daphnia magna* nanotoxicity studies. *Toxicology Letters,* 223 (1): 103–8

Römer, I., White, T., Baalousha, M., Chipman, K., Viant, M., Lead, J. (2011) Aggregation and dispersion of silver nanoparticles in exposure media for aquatic toxicity tests. *Journal of Chromatography. A*, 1218 (27): 4226–33

Roy, I. and Vij, N. (2010) Nanodelivery in airway diseases: challenges and therapeutic applications. *Nanomedicine : Nanotechnology, Biology, and Medicine*, 6 (2): 237–44

Rozen, S. and Skaletsky, H. (1999) Primer3 on the WWW for general users and for biologist programmers. *Bioinformatics Methods and Protocols*

Russell, A. and Hugo, W. (1994) Antimicrobial activity and action of silver. *Progress in medicinal chemistry*, *31*, p.351.

Ryman-Rasmussen, J., Cesta, M., Brody, A., Shipley-Phillips, J., Everitt, J., Tewksbury, E., Moss, O., Wong, B., Dodd, D., Andersen, M., Bonner, J. (2009) Inhaled carbon nanotubes reach the subpleural tissue in mice. *Nature Nanotechnology*, 4 (11): 747–51

Sangster, T., Major, H., Plumb, R., Wilson, A., Wilson, I. (2006) A pragmatic and readily implemented quality control strategy for HPLC-MS and GC-MS-based metabonomic analysis. *The Analyst*, 131 (10): 1075–1078

Scanlan, L., Reed, R., Loguinov, A., Antczak, P., Tagmount, A., Aloni, S., Nowinski, D., Luong, P., Tran, C., Karunaratne, N., Pham, D., Lin, X., Falciani, F., Higging, C., Ranville, J., Vulpe, C., Gilbert, B. (2013) Silver nanowire exposure results in internalization and toxicity to *Daphnia magna*. *ACS Nano*, 7 (12): 10681–94

SCENIHR, Opinion on the scientific basis for the definition of the term ‘‘nanomaterial’’. Scientific Committee on Emerging and Newly Identified Health Risks (SCENIHR), *European Commission Brussels*, Belgium, 2010

Schirmer, K., Fischer, B., Madureira, D., Pillai, S. (2010) Transcriptomics in ecotoxicology. *Analytical and Bioanalytical Chemistry*, 397 (3): 917–23

Scown, T., Santos, E., Johnston, B., Gaiser, B., Baalousha, M., Mitov, S., Lead, J., Stone, V., Fernandes, T., Jepson, M., Aerle, R., Tyler, C. (2010) Effects of aqueous exposure to silver nanoparticles of different sizes in rainbow trout. *Toxicological Sciences*, 115 (2): 521–34

Seaton, A., Tran, L., Aitken, R., Donaldson, K. (2010) Nanoparticles, human health hazard and regulation. *Journal of the Royal Society, Interface*, 7 Suppl 1 (September 2009): S119–29

Shen, M.-H., Zhou, X.-X., Yang, X.-Y., Chao, J.-B., Liu, R., Liu, J.-F. (2015) Exposure medium: key in identifying free Ag^{+} as the exclusive species of silver nanoparticles with acute toxicity to *Daphnia magna*. *Scientific Reports*, 5: 9674

Skjolding, L., Kern, K., Hjorth, R., Hartmann, N., Overgaard, S., Ma, G., Veinot, J., Baun, A. (2014) Uptake and depuration of gold nanoparticles in *Daphnia magna. Ecotoxicology*, 23 (7): 1172–83

Southam, A., Payne, T., Cooper, H., Arvanitis, T., Viant, M. (2007) Dynamic range and mass accuracy of wide-scan direct infusion nanoelectrospray fourier transform ion cyclotron resonance mass spectrometry-based metabolomics increased by the spectral stitching method. *Analytical Chemistry*, 79 (12): 4595–4602

Stebounova, L., Guio, E. and Grassian, V. (2011) Silver nanoparticles in simulated biological media: A study of aggregation, sedimentation, and dissolution. *Journal of Nanoparticle Research*, 13 (1): 233–244

Stensberg, M., Madangopal, R., Yale, G., Wei, W., Ochoa-Acuna, H., Wei, A. Mclamore, E., Rickus, J., Porterfield, D., Sepulveda, M. (2013) Silver nanoparticle-specific mitotoxicity in *Daphnia magna. Nanotoxicology*, (April): 1–10

Stentoft, C., Vestergaard, M., Løvendahl, P., Kristensen, N., Moorby, J., Jensen, S. (2014) Simultaneous quantification of purine and pyrimidine bases, nucleosides and their degradation products in bovine blood plasma by high performance liquid chromatography tandem mass spectrometry. *Journal of Chromatography*. A, 1356: 197–210

Stevenson, A., Bea, D., Civit, S., Contera, S., Cerveto, A., Trigueros, S. (2012) Three strategies to stabilise nearly monodispersed silver nanoparticles in aqueous solution. *Nanoscale Research Letters*, 7 (1): 151

Strange, R., Spiteri, M., Ramachandran, S., Fryer, A. (2001) Glutathione-S-transferase family of enzymes. *Mutation Research*, 482 (1-2): 21–26

Struck-Lewicka, W., Kaliszan, R. and Markuszewski, M. (2014) Analysis of urinary nucleosides as potential cancer markers determined using LC-MS technique. *Journal of Pharmaceutical and Biomedical Analysis*

Tatarazako, N. and Oda, S. (2007) The water flea *Daphnia magna* (*Crustacea, Cladocera*) as a test species for screening and evaluation of chemicals with endocrine disrupting effects on crustaceans. *Ecotoxicology*, 16 (1): 197–203

Taylor, N., Weber, R., Southam, A., Payne, T., Hrydziuszko, O., Arvanitis, T., Viant, M. (2009) A new approach to toxicity testing in *Daphnia magna*: application of high throughput FT-ICR mass spectrometry metabolomics. *Metabolomics*, 5 (1): 44–58

Taylor, N., Weber, R., White, T., Viant, M. (2010) Discriminating between different acute chemical toxicities via changes in the daphnid metabolome. *Toxicological Sciences*, 118 (1): 307–17

Tejamaya, M., Römer, I., Merrifield, R., Lead, J. (2012) Stability of citrate, PVP, and PEG coated silver nanoparticles in ecotoxicology media. *Environmental Science & Technology*, 46 (13): 7011–7017

Tkalec, Ž., Drobne, D., Vogel-Mikuš, K., Pongrac, P., Regvar, M., Strus, J., Pelicon, P., Vavpetic, P., Grlj, N., Remskar, M. (2011) Micro-PIXE study of Ag in digestive glands of

a nano-Ag fed arthropod (Porcellio scaber, Isopoda, Crustacea). *Nuclear Instruments and Methods in Physics Research B*, 269 (20): 2286–2291

Ulm, L., Krivohlavek, A., Jurašin, D., Ljubojevic, M., Sinko, G., Crnkovic, T., Zuntar, I., Sikic, S., Vrcek, I., (2015) Response of biochemical biomarkers in the aquatic crustacean *Daphnia magna* exposed to silver nanoparticles. *Environmental Science and Pollution Research*

Vance, M., Kuiken, T., Vejerano, E., McGinnis, S., Hochella, M., Rejeski, D., Hull, M. (2015) Nanotechnology in the real world: Redeveloping the nanomaterial consumer products inventory. *Beilstein Journal of Nanotechnology*, 6 (October 2013): 1769–1780

Verano-Braga, T., Miethling-Graff, R., Wojdyla, K., Rogowska-Wrzesinska, A., Brewer, J., Erdmann, H., Kjeldsen, F. (2014) Insights into the cellular response triggered by silver nanoparticles using quantitative proteomics. *ACS Nano*, 8 (3): 2161–75

Viant, M. (2008) Recent developments in environmental metabolomics. *Molecular BioSystems*, 4 (10): 980–6

Viant, M. (2009) Applications of metabolomics to the environmental sciences. *Metabolomics*, 5 (1): 1–2

Viant, M., Bearden, D., Bundy, J., Burton, I., Collette, T., Ekman, D., Ezernieks, V., Karakach, T., Lin, C., Rochfort, S., De Ropp, J., Teng, Q., Tjeerdema, R., Walter, J., Wu, H. (2009) International NMR-based environmental metabolomics intercomparison exercise. *Environmental Science & Technology*, 43 (1): 219–25

Viant, M. and Sommer, U. (2012) Mass spectrometry based environmental metabolomics: a primer and review. *Metabolomics*, 9 (S1): 144–158

Wang, Z., Liu, S., Ma, J., Qu, G., Wang, X., Yu, S., He, J., Liu, J., Xia, T., Jiang, G.-B. (2013) Silver nanoparticles induced RNA polymerase-silver binding and RNA transcription inhibition in erythroid progenitor cells. *ACS Nano*, 7 (5): 4171–86

Wardak, A., Gorman, M., Swami, N., Rejeski, D. (2007) Environmental regulation of nanotechnology and the TSCA. *IEEE Technology and Society Magazine*, 26 (2): 48–56

Watanabe, H., Takahashi, E., Nakamura, Y., Oda, S., Tatarazako, N., Iguchi, T. (2007) Development of a *Daphnia magna* DNA microarray for evaluating the toxicity of environmental chemicals. *Environmental Toxicology and Chemistry*, 26 (4): 669–76

Weber, R., Southam, A., Sommer, U., Viant, M. (2011) Characterization of isotopic abundance measurements in high resolution FT-ICR and Orbitrap mass spectra for improved confidence of metabolite identification. *Analytical Chemistry*, 83 (10): 3737–3743

Weber, R. and Viant, M. (2010) MI-Pack: Increased confidence of metabolite identification in mass spectra by integrating accurate masses and metabolic pathways. *Chemometrics and Intelligent Laboratory Systems*, 104 (1): 75–82

White, T. (2013) Assessing toxicity in *Daphnia magna* : an oxidative lipidomic approach. Doctoral thesis, University of Birmingham.

Williams, T., Turan, N., Diab, A., Wu, H., Mackenzie, C., Bartie, K., Hrydziuszko, O., Lyons, B., Stentiford, G., Herbert, J., Abraham, J., Katsiadaki, I., Leaver, M., Taggart, J., George, S., Viant, M., Chipman, K., Falciani, F. (2011) Towards a system level understanding of non-model organisms sampled from the environment: a network biology approach. *PLoS Computational Biology*, 7 (8): e1002126

Wise, B., Gallagher, N., Bro, R., Shaver, J., Windig, W. and Koch, R. (2007) PLS Toolbox 4.0. *Eigenvector Research Incorporated*, *3905*.

Wood, C. (1999) Physiology and modeling of mechanisms of silver uptake and toxicity in fish. *Environmental Toxicology and Chemistry*, 18 (1): 71–83

Wu, H., Southam, A., Hines, A., Viant, M. (2008) High-throughput tissue extraction protocol for NMR- and MS-based metabolomics. *Analytical Biochemistry*, 372 (2): 204–12

Xia, J., Mandal, R., Sinelnikov, I., Broadhurst, D., Wishart, D. (2012) MetaboAnalyst 2.0--a comprehensive server for metabolomic data analysis. *Nucleic Acids Research*, 40 (Web Server issue): W127–33

Xia, J. and Wishart, D. (2010) MetPA: a web-based metabolomics tool for pathway analysis and visualization. *Bioinformatics,* 26 (18): 2342–4

Yang, X., Gondikas, A., Marinakos, S., Auffan, M., Liu, J., Hsu-Kim, H., Meyer, J. (2012) Mechanism of silver nanoparticle toxicity is dependent on dissolved silver and surface coating in *Caenorhabditis elegans*. *Environmental Science & Technology*, 46 (2): 1119–27

Yoshimaru, T., Suzuki, Y., Inoue, T., Niide, O., Ra, C. (2006) Silver activates mast cells through reactive oxygen species production and a thiol-sensitive store-independent Ca^{2+} influx. *Free Radical Biology and Medicine*, 40 (11): 1949–1959

Yudkin, J. (1937) The effect of silver ions on some enzymes of *Bacterium coli*. *Enzymologia*, 2: 161–170

Zhao, C.-M. and Wang, W.-X. (2010) Biokinetic uptake and efflux of silver nanoparticles in *Daphnia magna*. *Environmental Science & Technology*, 44 (19): 7699–704

Zhao, C.-M. and Wang, W.-X. (2011) Comparison of acute and chronic toxicity of silver nanoparticles and silver nitrate to *Daphnia magna*. *Environmental Toxicology and Chemistry*, 30 (4): 885–92

Zhao, C.-M. and Wang, W.-X. (2012a) Importance of surface coatings and soluble silver in silver nanoparticles toxicity to *Daphnia magna*. *Nanotoxicology*, 6 (4): 361–70

Zhao, C.-M. and Wang, W.-X. (2012b) Size-dependent uptake of silver nanoparticles in *Daphnia magna*. *Environmental Science & Technology*, 46 (20): 11345–51

Zhao, C.-M. and Wang, W.-X. (2013) Regulation of sodium and calcium in *Daphnia magna* exposed to silver nanoparticles. *Environmental Toxicology and Chemistry*, 32 (4): 913–9

Zhao, F., Zhao, Y., Liu, Y., Chang, X., Chen, C., Zhao, Y. (2011) Cellular uptake, intracellular trafficking, and cytotoxicity of nanomaterials. *Small*, 7 (10): 1322–1337

Chapter 9: Appendix

9.1 Mean measured total Ag concentrations following separation of dissolved Ag and AgNP

Data in this section is relevant to data reported in Chapter 3, Section 3.3.3.

Table 9.1: Mean total Ag concentrations ± SD following separation of AgNP suspensions into the dissolved and nanoparticle fractions by ultracentrifugation at 0 h, 24 h and 48 h after initial dispersal. A two-way ANOVA with Sidak's comparison test determined that total silver concentration was significantly different ($p<0.0001$) between the dissolved and nanoparticle fractions, but did not change significantly over time ($p=0.2101$).

	Total Ag conc. (µg/l)		
Time point (h)	**0**	**24**	**48**
Dissolved Ag	2.51 ± 0.42	2.15 ± 0.19	1.96 ± 0.13
AgNP	0.28 ± 0.14	0.46 ± 0.22	0.29 ± 0.15

Table 9.2: Mean total Ag concentrations ± SD following separation of AgNP suspensions into the dissolved and nanoparticle fractions by ultrafiltration at 0 h, 24 h and 48 h after initial dispersal. A two-way ANOVA with Sidak's comparison test determined that total silver concentration was significantly different ($p<0.0001$) between the dissolved and nanoparticle fractions, and the AgNP fraction only was deemed to change significantly over time ($p=0.0089$).

	Total Ag conc. (µg/l)		
Time point (h)	**0**	**24**	**48**
Dissolved Ag	0.15 ± 0.04	0.19 ± 0.11	0.26 ± 0.23
AgNP	3.52 ± 0.19	3.07 ± 0.1	2.70 ± 0.18

9.2 Lists of m/z peaks and putative IDs used for calibration in negative ion mode

Table 9.3: List of *m/z* values and putative annotation used for calibration of *D. magna* polar MS spectra in negative ion mode reported in Chapter 4.

Empirical Formula	Ion form	*m/z*
$C_3H_6O_3$	$[M+Cl]^-$	125.0010
H_3O_4P	$[M+Cl]^-$	132.9463
H_3O_4P	$[M+(^{37}Cl)]^-$	134.9434
$C_6H_{14}N_4O_2$	$[M-H]^-$	173.1045
$C_5H_{10}O_5$	$[M+Hac-H]^-$	209.0669
$C_6H_{14}N_4O_2$	$[M+Cl]^-$	209.0814
$C_6H_{13}NO_5$	$[M+Cl]^-$	214.0489
$C_6H_{12}O_6$	$[M+Cl]^-$	215.0330
$C_{18}H_{32}O_{16}$	$[M+Cl]^-$	539.1387
$C_{18}H_{32}O_{16}$	$[M+(^{37}Cl)]^-$	541.1358

9.3 Mortality data for sub-lethal toxicity exposures

Table 9.4: Number of mortalities occurring in each treatment group over the 24 h exposure period prior to transcriptomics and metabolomic analyses in Chapter 4.

Treatment group	Nominal total Ag conc. (µg/l)	Neonates per replicate	Replicates	Total neonates per treatment	Total mortalities per treatment	Remaining replicates
Untreated control	0.00	30	6	180	0	6
PVP control	0.00	30	6	180	0	6
Bulk silver control	4.70	30	6	180	0	6
AgNP High	4.70	30	8	240	106	4
AgNP Mid	2.35	30	6	180	21	5
AgNP Low	1.18	30	6	180	0	6
AgNP V Low	0.59	30	6	180	0	6
Ag High	0.28	30	6	180	0	6
Ag Mid	0.14	30	6	180	0	6
Ag Low	0.07	30	6	180	0	6
Ag V Low	0.04	30	6	180	0	6
Ag Filtrate	-	30	6	180	0	6

Table 9.5: Number of mortalities occurring in each treatment group over the 24 h exposure period prior to RTt-qPCR analysis in Chapter 6.

Treatment group	Nominal total Ag conc. (µg/l)	Neonates per replicate	Replicates	Total neonates per treatment	Total mortalities per treatment	Remaining replicates
Untreated control	0	10	5	50	0	5
AgNP Mid	2.35	10	5	50	50	0
AgNP Low	1.18	10	5	50	22	3
Ag Mid	0.14	10	5	50	0	5
Ag Low	0.07	10	5	50	0	5

9.4 Tables of annotated variables that change significantly in intensity in response to AgNP and Ag^{+} exposure

Table 9.6: List of significantly changing gene-spots with putative human analogue Ensembl gene IDs reported in Chapter 5. P-values are included after correcting for the multiple-testing hypothesis. FC AgNP refers to the fold increase as calculated for the AgNP High group.

Observed	Statistics		Ensemble: Human Orthologues		
Gene ID	P-value	FC AgNP High	Human Ensembl gene code	Human Symbol	Putative Human Function
DM00071	0.00000	3.4743	ENSG00000109971	HSPA8	heat shock 70kDa protein 8
DM01384	0.00000	0.4075	ENSG00000159640	ACE	angiotensin I converting enzyme (peptidyl-dipeptidase A) 1
DM03092	0.00001	6.5768	ENSG00000064703	DDX20	DEAD (Asp-Glu-Ala-Asp) box polypeptide 20
DM02355	0.00001	3.9502	ENSG00000157326	DHRS4	dehydrogenase/reductase (SDR family) member 4
DM04280	0.00001	0.6873	ENSG00000100902	PSMA6	proteasome (prosome, macropain) subunit, alpha type, 6
DM05899	0.00001	0.2121	ENSG00000119471	HSDL2	hydroxysteroid dehydrogenase like 2
DM01056	0.00001	3.1685	ENSG00000155016	CYP2U1	cytochrome P450, family 2, subfamily U, polypeptide 1
DM02516	0.00002	0.4515	ENSG00000067167	TRAM1	translocation associated membrane protein 1
DM04714	0.00002	2.9871	ENSG00000003436	TFPI	tissue factor pathway inhibitor (lipoprotein-associated coagulation inhibitor)
DM12060	0.00002	0.5487	ENSG00000185420	SMYD3	SET and MYND domain containing 3
DM01303	0.00002	0.4776	ENSG00000187546	AGMO	alkylglycerol monooxygenase
DM03602	0.00003	0.6865	ENSG00000108479	GALK1	galactokinase 1
DM12557	0.00003	0.6622	ENSG00000167740	CYB5D2	cytochrome b5 domain containing 2
DM02250	0.00003	0.6092	ENSG00000178537	SLC25A20	solute carrier family 25 (carnitine/acylcarnitine translocase), member 20

DM02371	0.00003	0.3549	ENSG00000161544	CYGB	cytoglobin
DM03493	0.00003	1.7435	ENSG00000174684	B3GNT1	UDP-GlcNAc:betaGal beta-1,3-N-acetylglucosaminyltransferase 1
DM01371	0.00003	0.6477	ENSG00000205323	SARNP	SAP domain containing ribonucleoprotein
DM06641	0.00004	2.8733	ENSG00000003436	TFPI	tissue factor pathway inhibitor (lipoprotein-associated coagulation inhibitor)
DM05885	0.00004	0.6029	ENSG00000182551	ADI1	acireductone dioxygenase 1
DM03367	0.00005	1.4806	ENSG00000103647	CORO2B	coronin, actin binding protein, 2B
DM10805	0.00007	0.7180	ENSG00000157326	DHRS4	dehydrogenase/reductase (SDR family) member 4
DM00456	0.00007	2.3591	ENSG00000115758	ODC1	ornithine decarboxylase 1
DM00027	0.00007	0.5642	ENSG00000071894	CPSF1	cleavage and polyadenylation specific factor 1, 160kDa
DM03119	0.00007	1.5733	ENSG00000166140	ZFYVE19	zinc finger, FYVE domain containing 19
DM05446	0.00007	0.5743	ENSG00000136783	NIPSNAP3A	nipsnap homolog 3A (C. elegans)
DM01260	0.00008	1.9029	ENSG00000134250	NOTCH2	notch 2
DM02432	0.00010	3.0783	ENSG00000003436	TFPI	tissue factor pathway inhibitor (lipoprotein-associated coagulation inhibitor)
DM05927	0.00010	1.5919	ENSG00000151458	ANKRD50	ankyrin repeat domain 50
DM05852	0.00011	1.7372	ENSG00000138764	CCNG2	cyclin G2
DM02266	0.00012	0.5420	ENSG00000142606	MMEL1	membrane metallo-endopeptidase-like 1
DM04755	0.00012	0.6413	ENSG00000137486	ARRB1	arrestin, beta 1
DM11586	0.00013	0.6439	ENSG00000242485	MRPL20	mitochondrial ribosomal protein L20
DM05408	0.00013	0.2412	ENSG00000075035	WSCD2	WSC domain containing 2
DM00376	0.00022	2.4874	ENSG00000115159	GPD2	glycerol-3-phosphate dehydrogenase 2 (mitochondrial)
DM09960	0.00025	1.5097	ENSG00000132669	RIN2	Ras and Rab interactor 2
DM02468	0.00025	0.6631	ENSG00000094841	UPRT	uracil phosphoribosyltransferase (FUR1) homolog (S. cerevisiae)

DM02494	0.00026	0.7962	ENSG00000149177	PTPRJ	protein tyrosine phosphatase, receptor type, J
DM11264	0.00026	0.6574	ENSG00000111713	GYS2	glycogen synthase 2 (liver)
DM02335	0.00027	0.6839	ENSG00000254772	EEF1G	eukaryotic translation elongation factor 1 gamma
DM00069	0.00029	1.7820	ENSG00000145284	SCD5	stearoyl-CoA desaturase 5
DM04140	0.00035	0.6427	ENSG00000099991	CABIN1	calcineurin binding protein 1
DM03961	0.00040	3.9691	ENSG00000115758	ODC1	ornithine decarboxylase 1
DM00952	0.00043	1.9785	ENSG00000133063	CHIT1	chitinase 1 (chitotriosidase)
DM05995	0.00046	3.5313	ENSG00000115758	ODC1	ornithine decarboxylase 1
DM03816	0.00048	1.8132	ENSG00000164684	ZNF704	zinc finger protein 704
DM00562	0.00055	0.3695	ENSG00000175550	DRAP1	DR1-associated protein 1 (negative cofactor 2 alpha)
DM02393	0.00057	3.8465	ENSG00000109971	HSPA8	heat shock 70kDa protein 8
DM09969	0.00057	0.6957	ENSG00000100243	CYB5R3	cytochrome b5 reductase 3
DM11923	0.00057	0.4722	ENSG00000128274	A4GALT	alpha 1,4-galactosyltransferase
DM01236	0.00069	2.0997	ENSG00000133063	CHIT1	chitinase 1 (chitotriosidase)
DM02379	0.00069	0.7852	ENSG00000108591	DRG2	developmentally regulated GTP binding protein 2
DM04460	0.00071	1.7384	ENSG00000163629	PTPN13	protein tyrosine phosphatase, non-receptor type 13 (APO-1/CD95 (Fas)-associated phosphatase)
DM04081	0.00071	0.2714	ENSG00000167972	ABCA3	ATP-binding cassette, sub-family A (ABC1), member 3
DM15042	0.00072	0.6538	ENSG00000183077	AFMID	arylformamidase
DM02966	0.00072	0.7871	ENSG00000259494	MRPL46	mitochondrial ribosomal protein L46
DM03524	0.00080	0.7412	ENSG00000189091	SF3B3	splicing factor 3b, subunit 3, 130kDa
DM01093	0.00092	0.6413	ENSG00000072042	RDH11	retinol dehydrogenase 11 (all-trans/9-cis/11-cis)
DM14267	0.00092	2.0238	ENSG00000134398	ERN2	endoplasmic reticulum to nucleus signaling 2
DM00345	0.00100	1.6183	ENSG00000198650	TAT	tyrosine aminotransferase
DM02147	0.00101	0.6576	ENSG00000066926	FECH	ferrochelatase
DM09632	0.00108	1.8781	ENSG00000031823	RANBP3	RAN binding protein 3
DM12494	0.00118	2.7924	ENSG00000105321	CCDC9	coiled-coil domain containing 9

DM00720	0.00130	1.3355	ENSG00000185100	ADSSL1	adenylosuccinate synthase like 1
DM02970	0.00137	0.3504	ENSG00000189058	APOD	apolipoprotein D
DM08384	0.00137	3.5998	ENSG00000174469	CNTNAP2	contactin associated protein-like 2
DM14638	0.00142	0.6788	ENSG00000172922	RNASEH2C	ribonuclease H2, subunit C
DM12851	0.00143	0.7374	ENSG00000131795	RBM8A	RNA binding motif protein 8A
DM00035	0.00150	0.2480	ENSG00000033050	ABCF2	ATP-binding cassette, sub-family F (GCN20), member 2
DM08209	0.00150	1.8361	ENSG00000115159	GPD2	glycerol-3-phosphate dehydrogenase 2 (mitochondrial)
DM01101	0.00154	1.4681	ENSG00000167972	ABCA3	ATP-binding cassette, sub-family A (ABC1), member 3
DM01736	0.00154	0.8078	ENSG00000136238	RAC1	ras-related C3 botulinum toxin substrate 1 (rho family, small GTP binding protein Rac1)
DM07379	0.00156	0.5620	ENSG00000113369	ARRDC3	arrestin domain containing 3
DM00278	0.00167	0.6331	ENSG00000168002	POLR2G	polymerase (RNA) II (DNA directed) polypeptide G
DM01270	0.00185	3.7642	ENSG00000115758	ODC1	ornithine decarboxylase 1
DM01416	0.00188	0.7152	ENSG00000105323	HNRNPUL1	heterogeneous nuclear ribonucleoprotein U-like 1
DM05158	0.00192	0.7594	ENSG00000184719	RNLS	renalase, FAD-dependent amine oxidase
DM11181	0.00192	1.4593	ENSG00000142459	EVI5L	ecotropic viral integration site 5-like
DM05670	0.00205	1.4628	ENSG00000110172	CHORDC1	cysteine and histidine-rich domain (CHORD) containing 1
DM01911	0.00206	2.6526	ENSG00000003436	TFPI	tissue factor pathway inhibitor (lipoprotein-associated coagulation inhibitor)
DM06071	0.00219	2.4197	ENSG00000161011	SQSTM1	sequestosome 1
DM00320	0.00222	1.3789	ENSG00000124766	SOX4	SRY (sex determining region Y)-box 4
DM09628	0.00222	1.7530	ENSG00000198355	PIM3	pim-3 oncogene
DM02562	0.00250	1.6677	ENSG00000163399	ATP1A1	ATPase, Na+/K+ transporting, alpha 1 polypeptide
DM03699	0.00250	1.3408	ENSG00000078098	FAP	fibroblast activation protein, alpha

DM05812	0.00250	2.2108	ENSG00000167107	ACSF2	acyl-CoA synthetase family member 2
DM09238	0.00250	3.6838	ENSG00000116690	PRG4	proteoglycan 4
DM06700	0.00251	1.4004	ENSG00000198355	PIM3	pim-3 oncogene
DM06034	0.00257	0.5968	ENSG00000187021	PNLIPRP1	pancreatic lipase-related protein 1
DM03922	0.00268	0.5584	ENSG00000133884	DPF2	D4, zinc and double PHD fingers family 2
DM08519	0.00268	0.3507	ENSG00000186897	C1QL4	complement component 1, q subcomponent-like 4
DM02678	0.00284	0.7231	ENSG00000167553	TUBA1C	tubulin, alpha 1c
DM14232	0.00303	0.6694	ENSG00000136783	NIPSNAP3A	nipsnap homolog 3A (C. elegans)
DM00310	0.00318	0.6772	ENSG00000143870	PDIA6	protein disulfide isomerase family A, member 6
DM06413	0.00323	1.5949	ENSG00000171916	LGALS9C	lectin, galactoside-binding, soluble, 9C
DM12561	0.00328	0.6833	ENSG00000177830	CHID1	chitinase domain containing 1
DM01880	0.00341	1.8506	ENSG00000111405	ENDOU	endonuclease, polyU-specific
DM05671	0.00352	2.2624	ENSG00000115159	GPD2	glycerol-3-phosphate dehydrogenase 2 (mitochondrial)
DM02765	0.00355	0.7735	ENSG00000116171	SCP2	sterol carrier protein 2
DM05908	0.00367	0.6004	ENSG00000137413	TAF8	TAF8 RNA polymerase II, TATA box binding protein (TBP)-associated factor, 43kDa
DM01420	0.00371	0.8060	ENSG00000109736	MFSD10	major facilitator superfamily domain containing 10
DM12081	0.00387	0.4370	ENSG00000146416	AIG1	androgen-induced 1
DM04939	0.00388	2.1361	ENSG00000145284	SCD5	stearoyl-CoA desaturase 5
DM04096	0.00414	0.7541	ENSG00000128918	ALDH1A2	aldehyde dehydrogenase 1 family, member A2
DM00781	0.00417	1.2590	ENSG00000129991	TNNI3	troponin I type 3 (cardiac)
DM07815	0.00421	0.5645	ENSG00000198721	ECI2	enoyl-CoA delta isomerase 2
DM01388	0.00424	0.8393	ENSG00000198876	DCAF12	DDB1 and CUL4 associated factor 12
DM03781	0.00436	0.6683	ENSG00000115593	SMYD1	SET and MYND domain containing 1
DM00602	0.00452	1.2076	ENSG00000123933	MXD4	MAX dimerization protein 4

DM05074	0.00454	0.6283	ENSG00000106392	C1GALT1	core 1 synthase, glycoprotein-N-acetylgalactosamine 3-beta-galactosyltransferase, 1
DM09447	0.00454	1.4681	ENSG00000139970	RTN1	reticulon 1
DM10991	0.00459	3.3813	ENSG00000100003	SEC14L2	SEC14-like 2 (S. cerevisiae)
DM02885	0.00473	3.7623	ENSG00000134716	CYP2J2	cytochrome P450, family 2, subfamily J, polypeptide 2
DM05652	0.00486	0.3468	ENSG00000166321	NUDT13	nudix (nucleoside diphosphate linked moiety X)-type motif 13
DM09366	0.00508	1.4645	ENSG00000141568	FOXK2	forkhead box K2
DM12655	0.00513	5.1607	ENSG00000158457	TSPAN33	tetraspanin 33
DM00273	0.00521	0.5957	ENSG00000196367	TRRAP	transformation/transcription domain-associated protein
DM03467	0.00536	0.6592	ENSG00000185630	PBX1	pre-B-cell leukemia homeobox 1
DM10733	0.00537	0.8482	ENSG00000144021	CIAO1	cytosolic iron-sulfur protein assembly 1
DM05824	0.00538	3.3987	ENSG00000166579	NDEL1	nudE nuclear distribution E homolog (A. nidulans)-like 1
DM03365	0.00577	1.7260	ENSG00000134597	RBMX2	RNA binding motif protein, X-linked 2
DM00183	0.00587	0.8556	ENSG00000174611	KY	kyphoscoliosis peptidase
DM04796	0.00630	0.7763	ENSG00000105323	HNRNPUL1	heterogeneous nuclear ribonucleoprotein U-like 1
DM03103	0.00631	0.6805	ENSG00000131368	MRPS25	mitochondrial ribosomal protein S25
DM06307	0.00643	0.6628	ENSG00000103275	UBE2I	ubiquitin-conjugating enzyme E2I
DM05946	0.00648	0.5949	ENSG00000146070	PLA2G7	phospholipase A2, group VII (platelet-activating factor acetylhydrolase, plasma)
DM05988	0.00648	0.7258	ENSG00000067829	IDH3G	isocitrate dehydrogenase 3 (NAD+) gamma
DM04366	0.00651	1.7302	ENSG00000155016	CYP2U1	cytochrome P450, family 2, subfamily U, polypeptide 1
DM03797	0.00670	0.5019	ENSG00000184674	GSTT1	glutathione S-transferase theta 1
DM01908	0.00756	2.8001	ENSG00000185432	METTL7A	methyltransferase like 7A
DM00756	0.00773	1.7984	ENSG00000183569	SERHL2	serine hydrolase-like 2

DM09398	0.00776	0.3835	ENSG00000065000	AP3D1	adaptor-related protein complex 3, delta 1 subunit
DM02669	0.00783	0.7745	ENSG00000105664	COMP	cartilage oligomeric matrix protein
DM03384	0.00789	0.6022	ENSG00000155189	AGPAT5	1-acylglycerol-3-phosphate O-acyltransferase 5
DM03709	0.00801	1.7615	ENSG00000226589	VARS	valyl-tRNA synthetase
DM01455	0.00807	0.6682	ENSG00000004700	RECQL	RecQ protein-like (DNA helicase Q1-like)
DM00040	0.00808	0.6637	ENSG00000104774	MAN2B1	mannosidase, alpha, class 2B, member 1
DM00814	0.00822	1.4942	ENSG00000076685	NT5C2	5'-nucleotidase, cytosolic II
DM03658	0.00843	6.4938	ENSG00000164344	KLKB1	kallikrein B, plasma (Fletcher factor) 1
DM01074	0.00851	1.7454	ENSG00000197763	TXNRD3	thioredoxin reductase 3
DM00339	0.00852	0.7378	ENSG00000198947	DMD	dystrophin
DM03428	0.00857	2.4011	ENSG00000119396	RAB14	RAB14, member RAS oncogene family
DM03819	0.00857	2.0453	ENSG00000100003	SEC14L2	SEC14-like 2 (S. cerevisiae)
DM06039	0.00895	0.5742	ENSG00000108784	NAGLU	N-acetylglucosaminidase, alpha
DM00614	0.00904	0.7319	ENSG00000168872	DDX19A	DEAD (Asp-Glu-Ala-Asp) box polypeptide 19A
DM01731	0.00930	1.8245	ENSG00000198886	MT-ND4	mitochondrially encoded NADH dehydrogenase 4
DM05720	0.00930	0.2438	ENSG00000112077	RHAG	Rh-associated glycoprotein
DM02909	0.00934	0.7466	ENSG00000132485	ZRANB2	zinc finger, RAN-binding domain containing 2
DM03081	0.00941	1.3132	ENSG00000115828	QPCT	glutaminyl-peptide cyclotransferase
DM05126	0.00941	0.5954	ENSG00000160282	FTCD	formiminotransferase cyclodeaminase
DM03475	0.00944	0.5008	ENSG00000115875	SRSF7	serine/arginine-rich splicing factor 7
DM08925	0.00974	0.6897	ENSG00000142655	PEX14	peroxisomal biogenesis factor 14
DM02019	0.00988	0.3276	ENSG00000120053	GOT1	glutamic-oxaloacetic transaminase 1, soluble (aspartate aminotransferase 1)
DM05560	0.01010	0.7534	ENSG00000108797	CNTNAP1	contactin associated protein 1
DM02525	0.01050	0.7949	ENSG00000184270	HIST2H2AB	histone cluster 2, H2ab

DM05163	0.01070	1.8849	ENSG00000178445	GLDC	glycine dehydrogenase (decarboxylating)
DM12100	0.01100	1.6479	ENSG00000072310	SREBF1	sterol regulatory element binding transcription factor 1
DM11844	0.01110	0.8117	ENSG00000100815	TRIP11	thyroid hormone receptor interactor 11
DM00943	0.01120	1.5845	ENSG00000110047	EHD1	EH-domain containing 1
DM05392	0.01120	3.5749	ENSG00000167107	ACSF2	acyl-CoA synthetase family member 2
DM06233	0.01120	0.7756	ENSG00000162928	PEX13	peroxisomal biogenesis factor 13
DM05985	0.01140	2.0461	ENSG00000167671	UBXN6	UBX domain protein 6
DM05947	0.01150	0.1584	ENSG00000130508	PXDN	peroxidasin homolog (Drosophila)
DM11143	0.01200	1.3378	ENSG00000171603	CLSTN1	calsyntenin 1
DM02065	0.01210	1.2674	ENSG00000044574	HSPA5	heat shock 70kDa protein 5 (glucose-regulated protein, 78kDa)
DM00032	0.01280	1.3250	ENSG00000084110	HAL	histidine ammonia-lyase
DM03339	0.01310	0.7243	ENSG00000124098	FAM210B	family with sequence similarity 210, member B
DM00992	0.01340	2.6057	ENSG00000163982	OTOP1	otopetrin 1
DM00259	0.01370	4.1704	ENSG00000158552	ZFAND2B	zinc finger, AN1-type domain 2B
DM09286	0.01410	1.7400	ENSG00000151726	ACSL1	acyl-CoA synthetase long-chain family member 1
DM00547	0.01440	2.3924	ENSG00000178896	EXOSC4	exosome component 4
DM01392	0.01440	0.3464	ENSG00000133063	CHIT1	chitinase 1 (chitotriosidase)
DM04518	0.01440	3.6908	ENSG00000175567	UCP2	uncoupling protein 2 (mitochondrial, proton carrier)
DM04572	0.01440	0.7092	ENSG00000126777	KTN1	kinectin 1 (kinesin receptor)
DM00569	0.01450	2.3902	ENSG00000065526	SPEN	spen homolog, transcriptional regulator (Drosophila)
DM03695	0.01470	2.7305	ENSG00000130856	ZNF236	zinc finger protein 236
DM09474	0.01500	1.5888	ENSG00000092295	TGM1	transglutaminase 1 (K polypeptide epidermal type I, protein-glutamine-gamma-glutamyltransferase)

DM00617	0.01510	1.1574	ENSG00000091664	SLC17A6	solute carrier family 17 (sodium-dependent inorganic phosphate cotransporter), member 6
DM03451	0.01510	0.6833	ENSG00000030582	GRN	granulin
DM01960	0.01520	3.2948	ENSG00000109971	HSPA8	heat shock 70kDa protein 8
DM00744	0.01560	0.7250	ENSG00000077097	TOP2B	topoisomerase (DNA) II beta 180kDa
DM02429	0.01580	2.1818	ENSG00000151692	RNF144A	ring finger protein 144A
DM08720	0.01580	0.6490	ENSG00000160200	CBS	cystathionine-beta-synthase
DM05292	0.01600	0.6014	ENSG00000147485	PXDNL	peroxidasin homolog (Drosophila)-like
DM05304	0.01600	0.8035	ENSG00000103091	WDR59	WD repeat domain 59
DM10155	0.01600	1.2110	ENSG00000118263	KLF7	Kruppel-like factor 7 (ubiquitous)
DM05806	0.01610	0.3293	ENSG00000105404	RABAC1	Rab acceptor 1 (prenylated)
DM01520	0.01620	0.5384	ENSG00000143933	CALM2	calmodulin 2 (phosphorylase kinase, delta)
DM01477	0.01670	0.8266	ENSG00000108852	MPP2	membrane protein, palmitoylated 2 (MAGUK p55 subfamily member 2)
DM04687	0.01680	1.2811	ENSG00000165591	FAAH2	fatty acid amide hydrolase 2
DM14363	0.01710	0.7894	ENSG00000203837	PNLIPRP3	pancreatic lipase-related protein 3
DM00674	0.01730	0.8392	ENSG00000111596	CNOT2	CCR4-NOT transcription complex, subunit 2
DM03815	0.01740	0.5297	ENSG00000064651	SLC12A2	solute carrier family 12 (sodium/potassium/chloride transporters), member 2
DM00530	0.01750	0.7300	ENSG00000147082	CCNB3	cyclin B3
DM01805	0.01750	0.7357	ENSG00000213619	NDUFS3	NADH dehydrogenase (ubiquinone) Fe-S protein 3, 30kDa (NADH-coenzyme Q reductase)
DM10996	0.01750	0.5632	ENSG00000140395	WDR61	WD repeat domain 61
DM05804	0.01830	2.2211	ENSG00000149554	CHEK1	checkpoint kinase 1
DM03096	0.01860	1.4295	ENSG00000241685	ARPC1A	actin related protein 2/3 complex, subunit 1A, 41kDa
DM02745	0.01880	1.6944	ENSG00000198682	PAPSS2	3'-phosphoadenosine 5'-phosphosulfate synthase 2
DM01821	0.01970	1.2436	ENSG00000138279	ANXA7	annexin A7

DM01875	0.02000	1.3462	ENSG00000151726	ACSL1	acyl-CoA synthetase long-chain family member 1
DM02090	0.02030	0.7083	ENSG00000115042	FAHD2A	fumarylacetoacetate hydrolase domain containing 2A
DM01347	0.02050	1.1305	ENSG00000213614	HEXA	hexosaminidase A (alpha polypeptide)
DM11028	0.02050	0.7818	LRG_75	IRAK4	interleukin-1 receptor-associated kinase 4
DM02091	0.02090	1.3297	ENSG00000182149	IST1	increased sodium tolerance 1 homolog (yeast)
DM05080	0.02110	1.4501	ENSG00000165985	C1QL3	complement component 1, q subcomponent-like 3
DM00759	0.02120	1.2840	ENSG00000105220	GPI	glucose-6-phosphate isomerase
DM10960	0.02130	5.4013	ENSG00000186212	SOWAHB	sosondowah ankyrin repeat domain family member B
DM01820	0.02150	0.6506	ENSG00000166311	SMPD1	sphingomyelin phosphodiesterase 1, acid lysosomal
DM04083	0.02150	0.7963	ENSG00000173566	NUDT18	nudix (nucleoside diphosphate linked moiety X)-type motif 18
DM06245	0.02150	1.6354	ENSG00000142606	MMEL1	membrane metallo-endopeptidase-like 1
DM01624	0.02180	1.4893	ENSG00000168036	CTNNB1	catenin (cadherin-associated protein), beta 1, 88kDa
DM02684	0.02180	1.1872	ENSG00000100116	GCAT	glycine C-acetyltransferase
DM12738	0.02180	0.7614	ENSG00000013573	DDX11	DEAD/H (Asp-Glu-Ala-Asp/His) box helicase 11
DM04913	0.02200	1.4767	ENSG00000135407	AVIL	advillin
DM01030	0.02230	1.1823	ENSG00000114790	ARHGEF26	Rho guanine nucleotide exchange factor (GEF) 26
DM00546	0.02250	0.6590	ENSG00000156413	FUT6	fucosyltransferase 6 (alpha (1,3) fucosyltransferase)
DM10721	0.02280	0.6726	ENSG00000144848	ATG3	autophagy related 3
DM00702	0.02300	0.5463	ENSG00000130508	PXDN	peroxidasin homolog (Drosophila)
DM06133	0.02300	0.5579	ENSG00000184674	GSTT1	glutathione S-transferase theta 1

DM00525	0.02360	0.8154	ENSG00000146426	TIAM2	T-cell lymphoma invasion and metastasis 2
DM00864	0.02360	0.5624	ENSG00000197894	ADH5	alcohol dehydrogenase 5 (class III), chi polypeptide
DM09002	0.02370	0.6354	ENSG00000116213	WRAP73	WD repeat containing, antisense to TP73
DM13877	0.02370	0.8008	ENSG00000168259	DNAJC7	DnaJ (Hsp40) homolog, subfamily C, member 7
DM05449	0.02390	5.2312	ENSG00000197601	FAR1	fatty acyl CoA reductase 1
DM01979	0.02430	1.3491	ENSG00000137968	SLC44A5	solute carrier family 44, member 5
DM12852	0.02430	1.8929	ENSG00000130508	PXDN	peroxidasin homolog (Drosophila)
DM06151	0.02490	0.4107	ENSG00000100241	SBF1	SET binding factor 1
DM06053	0.02500	0.6146	ENSG00000140526	ABHD2	abhydrolase domain containing 2
DM02027	0.02530	0.7880	ENSG00000103187	COTL1	coactosin-like 1 (Dictyostelium)
DM11602	0.02530	0.5966	ENSG00000090273	NUDC	nuclear distribution C homolog (A. nidulans)
DM03430	0.02540	4.0099	ENSG00000175567	UCP2	uncoupling protein 2 (mitochondrial, proton carrier)
DM06999	0.02540	0.7439	ENSG00000076201	PTPN23	protein tyrosine phosphatase, non-receptor type 23
DM02224	0.02570	0.7344	ENSG00000072163	LIMS2	LIM and senescent cell antigen-like domains 2
DM01291	0.02580	0.6272	ENSG00000072315	TRPC5	transient receptor potential cation channel, subfamily C, member 5
DM08804	0.02600	0.6633	ENSG00000108829	LRRC59	leucine rich repeat containing 59
DM03652	0.02610	0.3232	ENSG00000125454	SLC25A19	solute carrier family 25 (mitochondrial thiamine pyrophosphate carrier), member 19
DM08435	0.02610	0.7020	ENSG00000108561	C1QBP	complement component 1, q subcomponent binding protein
DM00977	0.02670	1.1959	ENSG00000187391	MAGI2	membrane associated guanylate kinase, WW and PDZ domain containing 2
DM10506	0.02690	2.0427	ENSG00000164181	ELOVL7	ELOVL fatty acid elongase 7
DM04007	0.02710	0.5360	ENSG00000109790	KLHL5	kelch-like family member 5

DM02114	0.02760	0.5015	ENSG00000174100	MRPL45	mitochondrial ribosomal protein L45
DM05601	0.02760	0.5002	ENSG00000124120	TTPAL	tocopherol (alpha) transfer protein-like
DM10942	0.02790	1.5663	ENSG00000164494	PDSS2	prenyl (decaprenyl) diphosphate synthase, subunit 2
DM08652	0.02800	2.3691	ENSG00000100906	NFKBIA	nuclear factor of kappa light polypeptide gene enhancer in B-cells inhibitor, alpha
DM04383	0.02820	0.4924	ENSG00000114520	SNX4	sorting nexin 4
DM12203	0.02850	0.7146	ENSG00000134216	CHIA	chitinase, acidic
DM00611	0.02870	0.6816	ENSG00000112357	PEX7	peroxisomal biogenesis factor 7
DM01818	0.02910	1.1943	ENSG00000163041	H3F3A	H3 histone, family 3A
DM02257	0.02910	0.6360	ENSG00000225830	ERCC6	excision repair cross-complementing rodent repair deficiency, complementation group 6
DM02922	0.03030	1.3361	ENSG00000129151	BBOX1	butyrobetaine (gamma), 2-oxoglutarate dioxygenase (gamma-butyrobetaine hydroxylase) 1
DM10005	0.03090	0.5078	ENSG00000099901	RANBP1	RAN binding protein 1
DM01395	0.03100	0.8492	ENSG00000113460	BRIX1	BRX1, biogenesis of ribosomes, homolog (S. cerevisiae)
DM12306	0.03110	1.3932	ENSG00000167107	ACSF2	acyl-CoA synthetase family member 2
DM04392	0.03150	0.8824	ENSG00000126561	STAT5A	signal transducer and activator of transcription 5A
DM11804	0.03190	0.5956	ENSG00000148335	NTMT1	N-terminal Xaa-Pro-Lys N-methyltransferase 1
DM03205	0.03220	2.5635	ENSG00000101333	PLCB4	phospholipase C, beta 4
DM05399	0.03240	1.2646	ENSG00000166825	ANPEP	alanyl (membrane) aminopeptidase
DM01354	0.03280	1.0180	ENSG00000134255	CEPT1	choline/ethanolamine phosphotransferase 1
DM04942	0.03280	0.6358	ENSG00000196116	TDRD7	tudor domain containing 7
DM00825	0.03330	0.7612	ENSG00000176658	MYO1D	myosin ID
DM02522	0.03330	1.2194	ENSG00000173812	EIF1	eukaryotic translation initiation factor 1
DM04056	0.03360	0.6679	ENSG00000196547	MAN2A2	mannosidase, alpha, class 2A,

					member 2
DM11370	0.03360	3.2553	ENSG00000175115	PACS1	phosphofurin acidic cluster sorting protein 1
DM01693	0.03390	0.6056	ENSG00000109971	HSPA8	heat shock 70kDa protein 8
DM07156	0.03430	0.7771	ENSG00000131018	SYNE1	spectrin repeat containing, nuclear envelope 1
DM02259	0.03480	0.2481	ENSG00000161544	CYGB	cytoglobin
DM05007	0.03480	0.8308	ENSG00000188603	CLN3	ceroid-lipofuscinosis, neuronal 3
DM04586	0.03520	1.9758	ENSG00000006652	IFRD1	interferon-related developmental regulator 1
DM13920	0.03530	4.0838	ENSG00000129151	BBOX1	butyrobetaine (gamma), 2-oxoglutarate dioxygenase (gamma-butyrobetaine hydroxylase) 1
DM05006	0.03570	2.5752	ENSG00000107290	SETX	senataxin
DM02416	0.03580	0.5340	ENSG00000080819	CPOX	coproporphyrinogen oxidase
DM04009	0.03630	0.7202	ENSG00000099797	TECR	trans-2,3-enoyl-CoA reductase
DM12865	0.03630	3.2559	ENSG00000038219	BOD1L1	biorientation of chromosomes in cell division 1-like 1
DM06954	0.03670	0.8743	ENSG00000100644	HIF1A	hypoxia inducible factor 1, alpha subunit (basic helix-loop-helix transcription factor)
DM12393	0.03670	0.3965	ENSG00000115839	RAB3GAP1	RAB3 GTPase activating protein subunit 1 (catalytic)
DM01522	0.03710	0.6450	ENSG00000168522	FNTA	farnesyltransferase, CAAX box, alpha
DM05043	0.03710	2.0267	ENSG00000154646	TMPRSS15	transmembrane protease, serine 15
DM01837	0.03760	0.5948	ENSG00000109971	HSPA8	heat shock 70kDa protein 8
DM03456	0.03830	0.1695	ENSG00000136856	SLC2A8	solute carrier family 2 (facilitated glucose transporter), member 8
DM00042	0.03860	1.1277	ENSG00000185100	ADSSL1	adenylosuccinate synthase like 1
DM05418	0.03870	1.9117	ENSG00000001084	GCLC	glutamate-cysteine ligase, catalytic subunit
DM11223	0.03870	1.7351	ENSG00000072803	FBXW11	F-box and WD repeat domain containing 11
DM10263	0.03880	1.1620	ENSG00000100003	SEC14L2	SEC14-like 2 (S. cerevisiae)

DM12082	0.03880	1.7198	ENSG00000130508	PXDN	peroxidasin homolog (Drosophila)
DM13482	0.03900	2.1348	ENSG00000067533	RRP15	ribosomal RNA processing 15 homolog (S. cerevisiae)
DM01049	0.03970	0.7165	ENSG00000162613	FUBP1	far upstream element (FUSE) binding protein 1
DM08668	0.04000	1.7412	ENSG00000088826	SMOX	spermine oxidase
DM01024	0.04060	1.1780	ENSG00000145819	ARHGAP26	Rho GTPase activating protein 26
DM09085	0.04070	1.6929	ENSG00000164181	ELOVL7	ELOVL fatty acid elongase 7
DM00260	0.04090	2.1557	ENSG00000142168	SOD1	superoxide dismutase 1, soluble
DM02382	0.04110	0.7867	ENSG00000111058	ACSS3	acyl-CoA synthetase short-chain family member 3
DM03031	0.04140	2.0241	ENSG00000162813	BPNT1	3'(2'), 5'-bisphosphate nucleotidase 1
DM07644	0.04140	0.7879	ENSG00000062716	VMP1	vacuole membrane protein 1
DM01043	0.04190	1.4569	ENSG00000173542	MOB1B	MOB kinase activator 1B
DM00597	0.04220	1.9817	ENSG00000178445	GLDC	glycine dehydrogenase (decarboxylating)
DM00728	0.04220	0.7212	ENSG00000175193	PARL	presenilin associated, rhomboid-like
DM00234	0.04310	0.8052	ENSG00000122545	39326	septin 7
DM05727	0.04380	2.2515	ENSG00000125772	GPCPD1	glycerophosphocholine phosphodiesterase GDE1 homolog (S. cerevisiae)
DM00340	0.04420	0.6613	ENSG00000100836	PABPN1	poly(A) binding protein, nuclear 1
DM01110	0.04420	3.6811	ENSG00000132437	DDC	dopa decarboxylase (aromatic L-amino acid decarboxylase)
DM12380	0.04460	0.9633	ENSG00000151092	NGLY1	N-glycanase 1
DM11440	0.04490	0.8970	ENSG00000140474	ULK3	unc-51-like kinase 3 (C. elegans)
DM06069	0.04510	1.7856	ENSG00000127314	RAP1B	RAP1B, member of RAS oncogene family
DM01168	0.04520	0.7934	ENSG00000100321	SYNGR1	synaptogyrin 1
DM09437	0.04520	1.4785	ENSG00000185100	ADSSL1	adenylosuccinate synthase like 1
DM11378	0.04530	0.7715	ENSG00000072422	RHOBTB1	Rho-related BTB domain containing 1
DM05084	0.04540	0.7196	ENSG00000091136	LAMB1	laminin, beta 1
DM07213	0.04590	0.8237	ENSG00000135862	LAMC1	laminin, gamma 1 (formerly LAMB2)
DM00469	0.04720	0.2671	ENSG00000161544	CYGB	cytoglobin

DM04850	0.04780	0.7455	ENSG00000116260	QSOX1	quiescin Q6 sulfhydryl oxidase 1
DM00780	0.04830	0.7994	ENSG00000120063	GNA13	guanine nucleotide binding protein (G protein), alpha 13
DM00932	0.04880	0.7501	ENSG00000183044	ABAT	4-aminobutyrate aminotransferase
DM03407	0.04890	0.8409	ENSG00000104969	SGTA	small glutamine-rich tetratricopeptide repeat (TPR)-containing, alpha

Table 9.7: List of significantly changing *m/z* peaks and their putative empirical formulae and KEGG names reported in Chapter 5. P-values are included after correcting for the multiple testing hypothesis. FC AgNP refers to the fold increase as calculated for the AgNP High group.

Observed	Statistics			Identification				
m/z	Adj. P-values	FC AgNP High	Loads Rank	Empirical formula	Ion form	Neutral mass (Da)	Mass error	KEGG Compound Names
127.0167	0.001	0.813	761	$C_4H_{10}O_2$	$[M+K-2H]^-$	90.0681	-0.29	['(R,R)-Butane-2,3-diol', '(S,S)-Butane-2,3-diol']
127.0167	0.001	0.813	761	$C_3H_8O_3$	$[M+Cl]^-$	92.0473	-0.76	['Glycerol']
129.0137	0.007	0.740	862	$C_3H_8O_3$	$[M+(^{37}Cl)]^-$	92.0473	-0.75	['Glycerol']
161.0456	0.015	1.744	339	$C_4H_6O_3$	$[M+Hac-H]^-$	102.0317	0.57	['(S)-Methylmalonate semialdehyde', '2-Oxobutanoate', 'Acetoacetate', 'Succinate semialdehyde']
193.0872	0.030	1.560	259	$C_9H_{10}O$	$[M+Hac-H]^-$	134.0732	0.89	['Phenylacetone']
161.0456	0.015	1.744	339	$C_6H_{10}O_5$	$[M-H]^-$	162.0528	0.57	['(2R,3S)-2,3-Dimethylmalate', '(R)-2-Ethylmalate', '(R)-3,3-Dimethylmalate', '(S)-2-(Hydroxymethyl)glutarate', '1,5-Anhydro-D-fructose', '2-Dehydro-3-deoxy-D-fuconate', '2-Dehydro-3-deoxy-L-fuconate', '2-Dehydro-3-deoxy-L-rhamnonate', 'L-Fucono-1,5-lactone', 'L-Rhamnono-1,4-lactone']
239.0774	0.000	4.523	14	$C_6H_{12}O_6$	$[M+Hac-H]^-$	180.0634	0.65	['D-Fructose', 'D-Fuconate', 'D-Galactose', 'D-Glucose', 'D-Mannose', 'D-Sorbose', 'D-Tagatose', 'L-Fuconate', 'L-Rhamnonate', 'L-Sorbose', 'alpha-D-Glucose', 'beta-D-Glucose', 'myo-Inositol']
249.0803	0.007	0.630	1185	$C_8H_{14}O_3S$	$[M+Hac-H]^-$	190.0664	0.28	['2-Oxo-7-methylthioheptanoic acid']

239.0328	0.008	1.282	539	$C_{12}H_{10}O_4$	$[M+Na-2H]^-$	218.0579	0.8	['4-Methylumbelliferyl acetate']
277.1115	0.007	0.775	1127	$C_{10}H_{18}O_3S$	$[M+Hac-H]^-$	218.0977	0	['2-Oxo-9-methylthiononanoic acid']
261.1077	0.000	1.300	750	$C_{13}H_{20}O_3$	$[M+(^{37}Cl)]^-$	224.1412	0.05	['(6S,9R)-Vomifoliol']
263.0092	0.000	1.865	135	$C_6H_{13}O_7P$	$[M+Cl]^-$	228.0399	-0.36	['(R)-4-Phosphopantoate', '(R)-5-Phosphomevalonate']
261.0968	0.000	1.342	746	$C_{10}H_{16}N_4O_3$	$[M+Na-2H]^-$	240.1222	-0.42	['Homocarnosine', 'N(alpha)-gamma-L-Glutamylhistamine', 'beta-Alanyl-N(pi)-methyl-L-histidine']
243.0624	0.025	1.531	133	$C_9H_{12}N_2O_6$	$[M-H]^-$	244.0695	0.45	['Uridine']
249.0803	0.007	0.630	1185	$C_{10}H_{18}O_5S$	$[M-H]^-$	250.0875	0.28	['2-(5-Methylthio)pentylmalic acid', '3-(5-Methylthio)pentylmalic acid']
266.0895	0.010	1.939	49	$C_{10}H_{13}N_5O_4$	$[M-H]^-$	267.0968	0.23	['Adenosine', 'Deoxyguanosine']
267.0735	0.008	4.127	1	$C_{10}H_{12}N_4O_5$	$[M-H]^-$	268.0808	0.17	['Inosine']
333.0591	0.001	1.711	157	$C_7H_{15}O_9P$	$[M+Hac-H]^-$	274.0454	-0.29	['1-Deoxy-D-altro-heptulose 7-phosphate']
274.0391	0.000	1.759	203	$C_{10}H_{13}NO_6S$	$[M-H]^-$	275.0464	0.06	['L-Tyrosine methyl ester 4-sulfate']
277.1115	0.007	0.775	1127	$C_{12}H_{22}O_5S$	$[M-H]^-$	278.1188	0	['2-(7-Methylthio)heptylmalic acid', '3-(7-Methylthio)heptylmalic acid']
277.2173	0.019	1.929	46	$C_{18}H_{30}O_2$	$[M-H]^-$	278.2246	-0.01	['(9Z,12Z,15Z)-Octadecatrienoic acid']
282.0844	0.000	2.373	44	$C_{10}H_{13}N_5O_5$	$[M-H]^-$	283.0917	-0.01	['Guanosine']
324.1582	0.006	1.150	457	$C_{15}H_{29}NO_4$	$[M+K-2H]^-$	287.2097	-0.08	['L-Octanoylcarnitine']
329.1063	0.023	0.652	1253	$C_{19}H_{20}N_2O$	$[M+K-2H]^-$	292.1576	0.46	['Cinchonidinone', 'Cinchoninone']
349.0765	0.004	4.522	5	$C_{12}H_{16}N_4O_7$	$[M+Na-2H]^-$	328.1019	-0.34	['7-Hydroxy-6-methyl-8-ribityl lumazine']
328.0451	0.019	2.513	27	$C_{10}H_{12}N_5O6P$	$[M-H]^-$	329.0525	-0.45	["2',3-Cyclic AMP", "3',5-Cyclic AMP"]
333.0591	0.001	1.711	157	$C_9H_{19}O_11P$	$[M-H]^-$	334.0665	-0.29	['2-(alpha-D-Galactosyl)-sn-glycerol 3-phosphate', '2-(beta-D-Glucosyl)-sn-glycerol 3-phosphate', "alpha-D-Galactosyl-(1,1')-sn-glycerol 3-phosphate", 'sn-glycero-3-Phospho-1-inositol']

395.0420	0.006	1.463	314	$C_{14}H_{19}N_2O_7P$	$[M+K-2H]^-$	358.0930	0.89	['N1-(5-Phospho-alpha-D-ribosyl)-5,6-dimethylbenzimidazole']
483.1833	0.000	1.779	213	$C_{16}H_{28}N_2O_{11}$	$[M+Hac-H]^-$	424.1693	0.26	['Chitobiose']
530.0613	0.000	2.554	112	$C_{15}H_{23}N_5O_{10}P_2$	$[M+Cl]^-$	495.0920	-0.29	['Isopentenyladenosine-5-diphosphate']
563.1831	0.000	4.086	10	$C_{18}H_{32}O_{16}$	$[M+Hac-H]^-$	504.1690	0.44	['Cellotriose', 'D-Gal alpha 1->6D-Gal alpha 1->6D-Glucose', 'Raffinose']